EFFECT OF POLYURETHANE COATING AND NANOMATERIAL REINFORCEMENT ON STRUCTURE AND PERFORMANCE OF UHMWPE FILAMENTS AND FABRICS

by

SHUANGYAN WU

(Under the Direction of Gajanan S. Bhat)

ABSTRACT

Ultra-high-molecular-weight polyethylene (UHMWPE) fiber is widely used for flexible ballistic products due to it high specific strength and modulus. However, with the emergence of advanced ammunition and firearms, materials with enhanced mechanical properties are always in great demand. This research aims to develop environmentally friendly approaches for fabricating nanocomposite coated UHMWPE filament yarns/fabrics. Waterborne polyurethanes (WPU) and inorganic fullerene-like tungsten disulfide (IF-WS_2) nanoparticles were used. Graphene nanoplatelets (GNPs) were later added for comparison.

A study conducted to understand the effects of dispersion medium and coating composition on PU/IF-WS_2/UHMWPE yarns, shows water and water/ethanol mixture are suitable for preparing the nanofluids and uniform coating. Improved mechanical properties and additional matrix-related failure mechanisms are observed for coated samples. Continuous yarn coating contributes to higher efficiency and better yarn alignment than individual coating. Additionally, thermoset PU leads to higher sample wash durability than thermoplastic PU. Also, plasma pretreatment (PT) induces

functional groups (-OH, C=O, C-O) on the fiber surface and improves sample performance and durability.

Part of this study focused on the PT and PU/IF-WS_2 coating on woven fabrics. The PT lowers fabric water contact angle from 105.2° to 81.1° and greatly strengthens coated fabrics, with up to 73%, 137%, 694%, and 757% higher toughness, elongation, storage modulus, and loss modulus over neat fabrics, respectively. Up to 98.8% of the coating is retained after washing. Increasing PU amount and curing temperature improves wash durability but decreases toughness. IF-WS_2 and stabilizer amounts show significant effects on yarn toughness. The optimal conditions are 1% solid IF-WS_2, 10% PU, 5% stabilizer, and 120℃ for curing.

Then, PU/nanofiller films were prepared with varying amounts of IF-WS_2 or GNPs to study the mechanisms. Adding water-based IF-WS_2 enhances film performance due to its reinforcing effect and uniform distribution, whereas GNPs decrease film properties due to their negative impact on film formation.

Herein, a thorough study on the effects of various critical parameters on formed composites is presented. The developed materials achieved vastly improved mechanical, viscoelastic, and energy absorption performance based on the same weight, therefore are highly promising for lightweight and flexible body armor and anti-impact uses.

INDEX WORDS: UHMWPE, Waterborne polyurethanes, IF-WS_2, Coating, Nanocomposites

EFFECT OF POLYURETHANE COATING AND NANOMATERIAL REINFORCEMENT ON STRUCTURE AND PERFORMANCE OF UHMWPE FILAMENTS AND FABRICS

by

SHUANGYAN WU

B.Sc., Jiangnan University, China, 2014

M.Sc., Jiangnan University, China, 2017

A Dissertation Submitted to the Graduate Faculty of The University of Georgia in Partial Fulfillment of the Requirements for the Degree

DOCTOR OF PHILOSOPHY

ATHENS, GEORGIA

2022

EFFECT OF POLYURETHANE COATING AND NANOMATERIAL REINFORCEMENT ON STRUCTURE AND PERFORMANCE OF UHMWPE FILAMENTS AND FABRICS

by

SHUANGYAN WU

Major Professor:	Gajanan S. Bhat
Committee:	Suraj Sharma
	Sergiy Minko
	Jason Locklin
	Sudhagar Mani

Electronic Version Approved:

Ron Walcott
Vice Provost for Graduate Education and Dean of the Graduate School
The University of Georgia
August 2022

ACKNOWLEDGEMENTS

I would like to express my deepest gratitude to my supervisors, Dr. Gajanan S. Bhat, for his invaluable guidance, tremendous support, encouragement, and patience during my PhD study.

I would also like to thank my committee members: Dr. Suraj Sharma, Dr. Sergiy Minko, Dr. Jason Locklin, Dr. Sudhagar Mani for their expert guidance, suggestions, and help for providing instruments and lab use.

I'm thankful to Dr. Abhyuday Mandal for his guidance in experimental design and Dr. Eric Formo from GEM for guiding sample testing. I also appreciate all the help and support from TMI faculty and staff. The support from Honeywell, Lubrizol, and Nanotech Industrial Solutions for providing UHMWPE filaments & woven fabrics, PU dispersions, IF-WS_2 additive, and rheology modifier is acknowledged.

My gratitude extends to Talon Scott Shaw, Aysiah R Gibbs, Yuta D Hagiya, Partha Sikdar, Anuradhi Liyanapathiranage, Avik Kumar Dhar, Md Mazbah Uddin, Smriti Rai, and Brianna Blevins for their great help and suggestions during this work. And I deeply appreciate my parents and sister for their endless support and care. Lastly, special thanks go to my husband, Kyle Rebstock, for his tremendous support, encouragement, and understanding.

Table of Contents

Page

CHAPTER 1

Introduction

Ultra-high-molecular-weight polyethylene (UHMWPE) fiber is a high-performance fiber invented by DSM company in the 1960s. It has linear molecular chains with high polymerization degree, and outstanding mechanical and physical properties such as high tensile strength, high Young's modulus, and extremely low density (0.97 g/cm^3), which are highly favored for high-performance, lightweight, and flexible products [1][2][3]. Due to its exceptional properties, UHMWPE fiber has been widely used in protective gears such as personal armors, vehicle armors, and cut-resistant gloves. In civil applications, it has been increasingly used for high-performance products such as climbing equipment, sails, and automotive winching.

1.1. Problem

Commercial UHMWPE fibers such as Spectra® and Dyneema® have been used in protective garments, particularly, soft body armors to provide basic ballistic protection. However, due to the development of more advanced firearms and ammunition, UHMWPE fiber-based materials with enhanced mechanical and energy absorption performances are always in great demand. To modify its performance while maintaining its lightweight, a common approach is applying nanocomposite coatings with polymer matrices and nanomaterials. In which, the high elasticity of polymer matrix and high modulus of nanomaterials can be incorporated with the fiber characteristics. However, conventional polymer matrices use organic solvents as dispersion mediums, which contribute to a higher volatile organic compounds (VOCs) release, increasing the

environmental pollution and health risk for operators. Meanwhile, dispersing inorganic nanoparticles in aqueous environment is a well-known challenge considering the lack of hydrophilic/polar groups on most nanomaterials. The distribution uniformity of nanoparticle plays an important role in the nano reinforcement effect on fiber materials. Additionally, UHMWPE fiber (-(C_2H_4-)$_n$-) has no polar groups in its molecular structure, thus it is chemically inert. Along with its smooth fiber surface, UHMWPE fiber shows low interfacial adhesion with polymer matrices. This may affect the fabrication of UHMWPE polymer composites and limit their performances.

1.2. Approaches to Solve the Problem

To enhance the mechanical and energy absorption performances of UHMWPE fiber, its fiber-based nanocomposites are fabricated with waterborne polyurethane (PU) matrices and inorganic fullerene-like tungsten disulfide (IF-WS_2) nanoparticles. Graphene nanoplatelets (GNPs) are also included for comparison. Polyurethane is commonly formed by the reaction between a polyol and a diisocyanate, the structures of both components can be tailored to obtain desired properties for versatile applications such as coating, paints, adhesives, and sealants. Different from conventional organic solvent-based PU material, waterborne PU can be stably dispersed in water or water/solvent mixed mediums. This leads to less volatile or toxic solvent release providing a more environmentally friendly approach for fabricating UHMWPE polymer nanocomposites. To stabilize the IF-WS_2 nanoparticles in waterborne PU, approaches including using water/ethanol mixed mediums and adding rheology modifiers have been studied due to the high stability of IF-WS_2 in ethanol and the anti-setting function of the rheology modifiers. To improve the surface reactivity of UHMWPE fibers, plasma pre-treatment is adopted on the fibers due to its high

effectivity, high efficiency, good treating accuracy, reduced damage to treated materials, and easy-to-process advantages. Induced oxygen based polar groups and improved wettability for the UHMWPE materials are expected.

1.3. Rationale

Fiber-based composites are preferred to metal or ceramic materials in various applications including ballistic materials due to their low density, high flexibility, and high mechanical properties. In anti-ballistic applications, fiber based composite materials are expected to stop bullets from penetrating, and absorb the kinetic energy through mechanisms including surface damage, yarn deformation, matrix cracking, material deformation, delamination, etc. Thus, the desired properties for ballistic composites include high elastic modulus, good tensile strength, high elongation at break, and low density [4]. Toughness, the area under the stress-strain curve, is related to both tensile strength and elongation at break. When developing fiber-based nanocomposites, various factors may affect their mechanical properties including matrix type, matrix concentration, nanofiller type, nanofiller concentration, fiber/matrix adhesion, fabrication method, fabrication parameters, etc.

Waterborne PU elastomers possesses high flexibility, high elasticity, good abrasion resistance, and good chemical resistance, which make them promising matrix candidates for enhancing the strain to failure (2.8%~3.5%) of UHMWPE fiber [5]. During preparation, water can be applied as the main medium for PU dispersion instead of organic solvents that may be harmful to the environment, operators, and product users. PU can also function as a medium and binder in the nanocomposite system for dispersing nanoparticles on UHMWPE fibers. Due to the hydrophobic and chemical inert properties of most nanoparticles, evenly dispersing these

nanoparticles on fiber materials with sufficient fiber/nanoparticle bonding becomes a challenge. In the literature, two main methods have been recorded for this issue: nanoparticle modification and polymer matrix application. In contrast to the approach of modifying nanoparticles with polar groups (e.g., graphene to graphene oxide (GO)), the polymer matrix approach involves mixing nanoparticles in water- or organic solvent- based polymer dispersions which shows higher adhesion to polymeric fibers. It is more commonly used due to its high effectivity and easy-to-process advantages. Meanwhile PU failure mechanisms such as matrix delamination, debonding, and cracking may lead to higher toughness/energy absorption for composite materials.

IF-WS_2 nanoparticles are composed of non-carbon elements and have a fullerene-like close-caged structure. This unique nano structure endows it with high elasticity, high stiffness, and great shock absorbing ability, which are beneficial for reinforcing UHMWPE fibers for improved strength and energy absorption applications [6]. Researchers have applied IF-WS_2 into polymer matrices to improve their enhanced mechanical, thermal, or tribology properties. Besides, recent studies suggested that incorporating fullerene C_{60} nanoparticles onto thermoplastic PU nonwoven fabrics could largely improve their dynamic mechanical properties. The C_{60} nanoparticles showed better reinforcing effect than other nanomaterials including graphite, nanoclay, polyhedral oligomeric silsesquioxane (POSS), and INT-WS_2 [7]. Due to the similar spherical structure and excellent mechanical properties of IF-WS_2, it was thought that IF-WS_2 could also strengthen PU films and PU incorporated UHMWPE fibers. In the cost and safety aspects, IF-WS_2 is commonly used as lubrication additive due to its ultra-low friction, it is less reactive and flammable than C_{60}, and much cheaper than carbon-based nanomaterials. Moreover, from the same work, it was also indicated that graphite composed of many layers of graphene contributed to the second-highest damping improvement to the target PU nonwovens. Therefore, graphene nanoplatelet (GNP),

which has extremely large surface area (e.g., 750m^2/g), high ultimate strength, and good elastic modulus was also included in chapters 6 and 7. Its effects are compared with that of IF-WS_2 nanoparticles.

To improve the surface reactivity of UHMWPE fibers, different attempts have been reported such as plasma treatment, chemical treatment, surface itching, and grafting. Most approaches could induce oxygen-containing groups to fiber surface. However, they also caused micro pits and dents on fiber surface largely reducing fiber mechanical properties. In commercial applications, plasma treatment is commonly used due to its simplicity, high efficiency, and limited material damage through accurate treatment control.

For high performance applications such as ballistic garments, protective gloves, sails, and hiking equipment, the material weight and flexibility are critical for the final product. For instance, in soft body armors, multilayered fabrics are used to provide sufficient protection, composite products with heavy weight and low flexibility may largely limit the mobility of users and reduce their comfort. Therefore, to achieve low weight addition and even distribution of nanofiller/matrix, dip coating method is commonly used due to its ease of processing.

In some research, the reinforcement of IF-WS_2 or GO nanoparticles on p-aramid fabrics have been studied, using solvent-based polymer matrices such as poly (vinyl butyral), and the fabricated nanocomposites showed improved mechanical and anti-impact performances [6][8][9]. However, the effects of waterborne PU and IF-WS_2/GNP on the structure and performance of UHMWPE yarns and fabrics have not been investigated. The development of flexible UHMWPE nanocomposites is rarely reported. To fill the research gap, this investigation is significant. Through this work, the effects of waterborne PU matrix and nanomaterials on UHMWPE yarns and fabrics are studied in terms of their mechanical properties, energy-to-break, viscoelasticity,

coating wash durability, material structure, and surface morphologies. The fabrication parameters are optimized, and the mechanisms of property enhancements are investigated. The results obtained in this research can provide reference to future research and development of flexible and lightweight UHMWPE nanocomposites with enhanced mechanical properties, tensile energy absorption, and viscoelastic properties.

1.4. Hypothesis

It is hypothesized that fabricated UHMWPE/nanoparticles/polyurethane nanocomposites will have higher mechanical, tensile energy absorption, and viscoelastic properties compared to the neat UHMWPE yarns or fabrics.

1.5. Objectives

In this project, the aim was to develop lightweight UHMWPE fiber/fabric-based nanocomposites with enhanced mechanical properties (maximum load, elongation at break, toughness), improved viscoelastic properties (storage modulus, loss modulus), and high wash durability, which can be potentially used for ballistic garments and energy absorption materials.

The specific objectives were to:

- Develop feasible nanocomposite coating methods for UHMWPE filament yarns as well as UHMWPE woven fabrics
- Study the effects of dispersion medium, PU amount, and IF-WS_2 amount, on the structure, mechanical properties, and failure mechanisms of individually coated UHMWPE yarns
- Study the effect of plasma pre-treatment and PU/IF-WS_2 continuous coating on UHMWPE yarns and fabrics

- Optimize the fabrication parameters for PU/nanofiller (IF-WS_2 and GNPs) coated UHMWPE yarns based on their mechanical properties and coating wash durability
- Study the failure mechanisms and structural parameters of PU/nanofiller (IF-WS_2 and GNPs) films

1.6. Reference

[1] YAVAŞ MO, AVCI A, ŞIMŞIR M, AKDEMIR A. Ballistic Performance of Kevlar49/ UHMW-PEHB26 Hybrid Layered-Composite. Uluslararası Muhendis Arastirma ve Gelistirme Derg 2015. https://doi.org/10.29137/umagd.379789.

[2] Karahan M, Ulcay Y, Eren R, Karahan N, Kaynak G. Investigation into the Tensile Properties of Stitched and Unstitched Woven Aramid/Vinyl Ester Composites. Text Res J 2010. https://doi.org/10.1177/0040517509346441.

[3] Zhang YD, Wang YL, Huang Y, Wan YZ. Preparation and properties of three-dimensional braided UHMWPE fiber reinforced PMMA composites. J Reinf Plast Compos 2006. https://doi.org/10.1177/0731684406068400.

[4] Abtew MA, Boussu F, Bruniaux P, Loghin C, Cristian I. Ballistic impact mechanisms – A review on textiles and fibre-reinforced composites impact responses. Compos Struct 2019;223. https://doi.org/10.1016/j.compstruct.2019.110966.

[5] Zhang Z, Yan L, He Z, Ma J, Wang H. Study on the blast resistance of concrete beams reinforced with ultra-high-molecular-weight polyethylene (UHMWPE) fibers. IOP Conf. Ser. Mater. Sci. Eng., 2020. https://doi.org/10.1088/1757-899X/780/4/042023.

[6] Simić DM, Stojanović DB, Brzić SJ, Totovski L, Uskoković PS, Aleksić RR. Aramid hybrid composite laminates reinforced with inorganic fullerene-like tungsten disulfide nanoparticles. Compos Part B Eng 2017. https://doi.org/10.1016/j.compositesb.2017.05.002.

[7] Fogle JG. Processing , Structure , and Properties of Nanoparticle Reinforced Nonwoven Sandwich Composites 2013.

[8] Simić DM, Stojanović DB, Dimić M, Mišković K, Marjanović M, Burzić Z, et al. Impact resistant hybrid composites reinforced with inorganic nanoparticles and nanotubes of WS2. Compos Part B Eng 2019. https://doi.org/10.1016/j.compositesb.2019.107222.

[9] da Silva AO, Weber RP, Monteiro SN, Lima AM, Faria GS, da Silva WO, et al. Effect of graphene oxide coating on the ballistic performance of aramid fabric. J Mater Res Technol 2019:1–12. https://doi.org/10.1016/j.jmrt.2019.12.058.

CHAPTER 2

Literature Review[1]

Ever since the invention of high-performance synthetic fibers, fiber materials with excellent strength-to-weight ratio, modulus, and flexibility have been used in various protective and high-performance applications such as defense, aerospace, anti-impact, and automotive. UHMWPE fiber (e.g., Spectra®, Dyneema®) is one of the most commonly used fibers in armor systems due to their high specific tensile strength, Young's modulus, impact resistance, and chemical resistance properties. Research shows fiber materials with higher strength, modulus, and strain to failure exhibit faster propagation of transverse wave and better energy dissipation ability. Other types of fibers such as para-aramid, glass fiber, carbon fiber, high-modulus polypropylene (HMPP), and natural fibers have also been reported for ballistic material applications [1][2][3]. However, UHMWPE fibers show the best comprehensive properties including high mechanical properties, extremely low density, and high stability to environmental factors such as UV light and moisture. Nanotechnology, which is defined as the manipulation of materials in the nanoscale (at least one dimension <100nm), has attracted considerable interest in tailoring mechanical properties and energy dissipation capability of fiber and fabric materials. Various research was conducted to incorporate nanomaterials in the development of high strength and anti-impact materials,

[1] Wu, S. Y., Sikdar, P., & Bhat, G. S. (2022). *Defence Technology*. https://doi.org/10.1016/j.dt.2022.06.007. (Some part of this chapter).
Reprinted here with permission of the publisher.

promising results were reported [4][5][6][7]. With their nano size and large surface-area-to-volume ratio, nanomaterials possess outstanding mechanical and shock absorption properties. In the literature, nanotechnologies involving nanofibers, nanomaterials, and nanocomposites have been adopted for fabricating materials with enhanced anti-impact and mechanical performance [8]. Nanomaterials including carbon nanotubes (CNTs), graphene, nanoclay, etc. can be incorporated into fabric substrates or/and polymer matrices as reinforcing nanofillers for diversified composite applications. The performances of these nanocomposites are affected by various nanofiller factors such as its size, shape, alignment, distribution uniformity, and concentration. Owing to their high mechanical and thermal properties, nanomaterial reinforced composites have been studied in vast end uses such as ballistic, anti-impact, biomedical, and food package materials [9]. Different fabrication methods can be used for fiber nanocomposites depending on their composite forms such as polymer/nanofiller composites, flexible fabric/nanofiller composites, and fabric/nanofiller/polymer composites [10–12]. Due to the emergence of more powerful firearms and ammunition, developing fiber-based nanocomposites with high flexibility and enhanced mechanical performances is in great demand for soft armor application. In this chapter, high-performance UHMWPE fibers will be introduced, the comparison of mechanical properties between various fibers will be presented. Waterborne elastomeric polyurethane will be discussed as a polymer matrix, while nanotechnologies involving nanomaterials, nanocomposites, and nanocomposite fabrication will be reviewed. Also included are some characterization methods used for evaluating mechanical properties, viscoelastic performance, chemical structure, etc. for materials.

2.1. Ultra-high-molecular-weight polyethylene fibers

Ultra-high-molecular-weight polyethylene is a subset of the thermoplastic polyethylene that has the chemical formula of $-(C_2H_4)_n-$, the polymerization degree (n) of UHMWPE can reach as many as 200,000 [13][14]. Compared with high-density polyethylene (HDPE), which has a molecular weight of up to 200,000 g/mol, UHMWPE has a much higher average molecular weight up to 6 million g/mol with its extremely long chains [13]. During stress or impact actions, the long molecular chains transfer force efficiently to the molecular backbone through strong intermolecular interactions, which gives UHMWPE fibers excellent energy absorption capability and extremely high impact strength [14]. Besides, UHMWPE fiber possesses exceptional physical and mechanical properties including very low density, high specific strength, and high stiffness [15][16][17]. The physical and mechanical properties for UHMWPE and other fiber materials used in ballistic materials are presented in Table 2.1 and Figure 2.1. In general, fiber materials with high mechanical properties and low density are preferred for lightweight protective gears and high-performance products, while other factors such as cost, stiffness, and shatter resistance are also considered. UHMWPE shows great and balanced properties including low density (lower than all fibers listed) and high specific tensile strength & modulus (higher than all except carbon fiber). Carbon fiber shows better specific tensile and modulus than UHMWPE fibers, however, it is stiff, brittle, and prone to vibration and shattering resulting in insufficient damping property, which largely limits its application. Polyhydroquinone-diimidazopyridine (PIPD) fiber also shows excellent tensile strength and modulus, but it is susceptible to ultraviolet light exposure and high moisture, which lead to its degradation and property reduction [18]. With the high mechanical properties and low density, UHMWPE fibers are widely used for bullet-resistant, anti-impact, and high strength products [19][14][20] [21][22].

Table 2.1. Mechanic properties of some high-performance fibers used in ballistic applications [1][23][24].

Fiber Types	Fiber Categories	Density (g/cm3)	Tensile strength (GPa)	Tensile Modulus (GPa)	Strain to Failure (%)
Silk fiber	Silkworm silk	1.32	0.5	5	15
	Spider silk	1.32	1.3	22	40
Nylon	Nylon 6	1.14	0.5	3	18-26
Glass	S-Glass	2.48	4.4	90	5.7
	E-Glass	2.63	3.5	68.5	4.0
Carbon Fibers	Standard	1.77	3.65	33.5	1.5
	Celion	1.8	4.0	230	1.8
	Aksaca	1.78	4.2	240	1.8
Para-Aramid	Technora, Teijin	1.39	3.0	70	4.4
	Twaron, Teijin	1.45	3.1	121	2.0
	Kevlar 29, DuPont	1.44	2.97	70	4.2
	Kevlar 129, DuPont	1.44	3.39	96	3.5
	Kevlar 49, DuPont	1.44	2.97	113	2.6
	Kevlar KM2, DuPont	1.44	3.3	70	4.0
UHMWPE	Spectra 900, Honeywell	0.97	2.4	73	2.8
	Spectra 1000, Honeywell	0.97	2.83	103	2.8
	Spectra 2000, Honeywell	0.97	3.34	124	3.0
	Dyneema, Toyoba/DSM	0.97	2.6	87	3.5
Aromatic Polyester	Vectran	1.47	3.2	91	3.0
PIPD	M5 Fiber (Goal)	1.7	9.5	450	2.0-2.5
	M5 Fiber (Conservative)	1.7	8.5	300	2.5

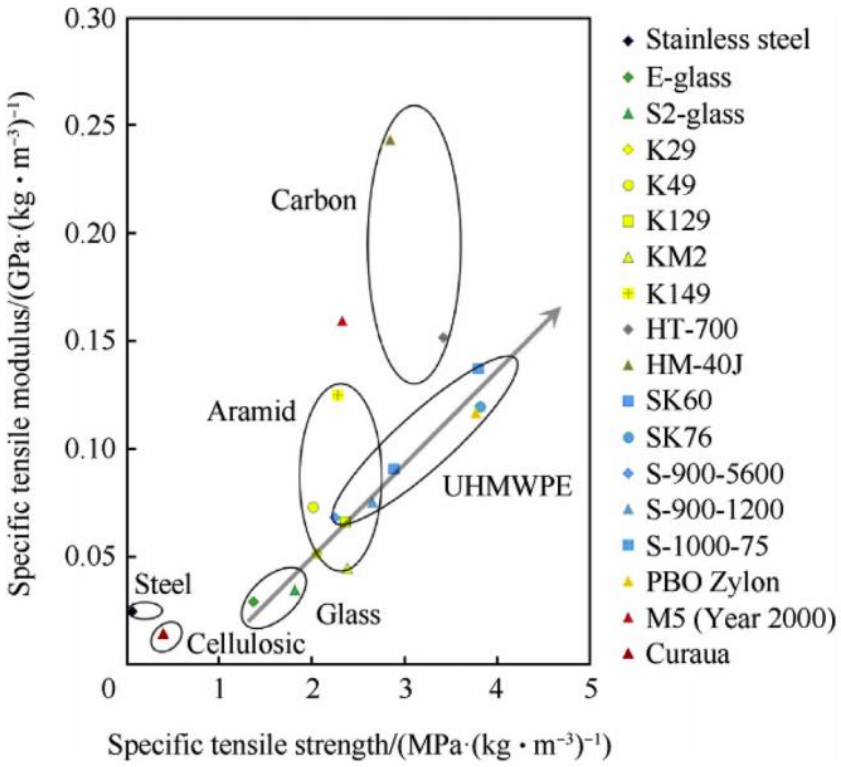

Figure 2.1. Distribution of specific tensile and specific modulus of main fiber materials used in ballistic applications.

2.2. Surface modification of UHMWPE fibers

UHMWPE fiber shows poor interfacial adhesion with polymer matrices, which largely limits the performances of its polymer composites. The low interfacial adhesion of UHMWPE fiber is due to two main reasons. First, with no polar groups in the molecular structure, linear polyethylene is chemically inert. Second, it is known that isotropic polyethylene has a low surface energy of 33 mJ/m^2 [25]. This drawback lowers the interlaminar shear strength of UHMWPE fiber/polymer matrix composites, weakens their properties, causes difficulty for their fabrication, and limits the application of UHMWPE fiber in polymer composites [26]. To improve UHMWPE fiber wettability and enhance its fiber/matrix adhesion, surface modification of UHMWPE fibers has been adopted by researchers using various methods. The common approach is using chemical

or physical treatments, such as chemical etching [27][28], plasma treatment [29][30][31][32][33][34], irradiation treatment [35][36][37][38], UV initiated graft [39] and corona discharge treatment [40]. In addition, matrix modification by adding nanofillers was also reported to improve fiber/matrix interfacial bonding, however, the addition of nanofillers may affect the matrix curing property [41]. Among these approaches, plasma treatment is commonly used due to its ease to apply and limited fiber strength damage. Through plasma treatment, surface etching and chemical reactions can be induced by free radical reactions and bond breakage caused by ions or photons in order to improve the UHMWPE surface adhesion [30]. For example, Yim et al. studied the impact of atmospheric pressure dielectric barrier discharge (DBD) plasma on UHMWPE fibers. In this study, several variables including treatment times, gases, and gas flow rates were manipulated. The chemical composition and roughness of the treated fiber surface were detected [42]. The results indicated an increase in both surface roughness and oxygen-containing groups (hydroxyl, carbonyl, and carboxyl) on the treated fiber surface. These results were confirmed with other studies reporting the impact of plasma treatments on UHMWPE fibers [43][33]. The presence of oxygen-containing groups improves fiber wettability and rough fiber surfaces contribute to mechanical interlocking at the fiber-matrix interface. Together, these effects may improve UHMWPE/polymer matrix interfacial adhesion through both mechanical interlocking and chemical bonding [43][33]. Moreover, in another research, Lin et al. modified UHMWPE fiber surface with plasma treatment and chemical agents, then UHMWPE fiber/Epoxy composites were fabricated using the prepreg-compression molding method. The characterizations on fiber chemical structure, surface morphology, and tensile strength were conducted, the results indicated that both fiber modification methods improved the interfacial adhesion of the final composites, slightly increased their tensile strength but decreased their tensile elongation. The

plasma and chemical treatments roughened the fibers' surfaces by introducing micro pits and corrugated protuberance, respectively[44].

2.3. Nanomaterials

Nanotechnology (or "nanotech") is the science, technology, and engineering conducted to manipulate matter on a nanoscale (1-100nm for at least one dimension) [45]. It allows controlling and understanding nanomaterials at the most fundamental level involving individual atoms and molecules [46]. According to the overall geometry, nanomaterials can be divided into 0D (e.g. fullerenes, C60), 1D (e.g. carbon nanotubes, CNTs), 2D (e.g. graphene nanoplatelets, GNPs) and 3D (e.g. graphite) [47]. The structures of these four examples are shown in Figure 2.2. It is well-known that nanomaterials have extremely high surface-area-to-volume ratios and outstanding energy absorption abilities. Nanomaterials such as tungsten disulfide (WS_2), graphene, CNTs, nanoclay, and SiO_2 nanoparticles have been studied for improving the mechanical, impact resistance, and thermal properties of polymer matrices and fiber-based polymer composites [48].

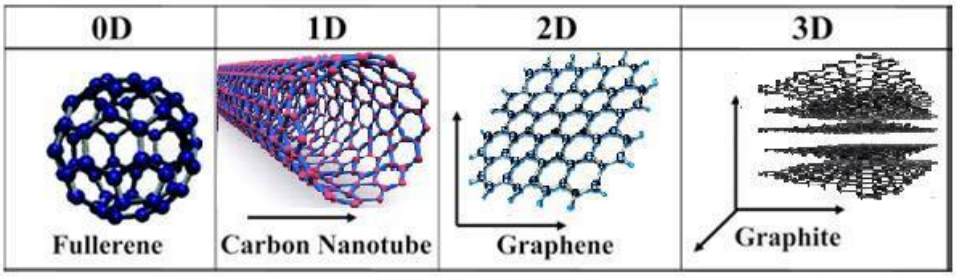

Figure 2.2. Structure examples of 0D (fullerene), 1D (carbon nanotube), 2D (graphene), and 3D (graphite) nanomaterials [49].

2.3.1. Tungsten disulfide

Tungsten disulfide, as a transition metal dichalcogenide, is one of the inorganic layered nanomaterials similar to molybdenum disulfide (MoS_2), it comprises 2D molecular sheets stacked

together [50]. The chemical structure of a single layer is shown in Figure 2.3. Analogous to fullerene and carbon nanotubes, tungsten disulfide can be grouped into two types based on how the molecular sheets are folded, which are inorganic fullerene-like tungsten disulfide (IF-WS_2) and inorganic nanotubes of tungsten disulfide (INT-WS_2). Between these two types, IF-WS_2 has a fullerene-like spherical and closed structure in nanoscale. It shows high chemical stability, ultra-low friction, high elasticity, high stiffness, good compressive strength, and excellent shock absorbing ability (survive under pressure up to 25 GPa, temperature 1000 °C) due to its inorganic WS_2 components and fullerene-like nanostructure [51][52]. These excellent properties and low cost make it a promising and practical material for fiber-based nanocomposite applications as a reinforcing nanofiller. In some literature, the applications of WS_2 as nano components in high strength, anti-ballistic, and energy absorption composites have been reported [53][54][55]. For example, the impact of IF-WS_2 on the mechanical and viscoelastic properties of aramid/phenolic/poly(vinyl butyral)(PVB) composites was studied previously. The results indicated that adding 1 wt% or 2 wt% of IF-WS_2 nanoparticles could improve mechanical properties (higher tan δ peak and larger areas under the stress-strain curves), and enhance impact resistance of the composites [51]. Later on, incorporating INT-WS_2 was also found to improve the impact resistance of the hybrid composite [54]. The TEM images of IF-WS_2 and INT-WS_2 are shown in Figure 2.4. Figure 2.5 shows the SEM images of IF-WS_2, INT-WS_2, their corresponding aramid fabric/PVB composites, and the control composite without WS_2. Also included in this figure are the energy-dispersive X-ray spectroscopy (EDS) mapping images of IF-WS_2 and INT-WS_2 reinforced aramid fabric/PVB composites.

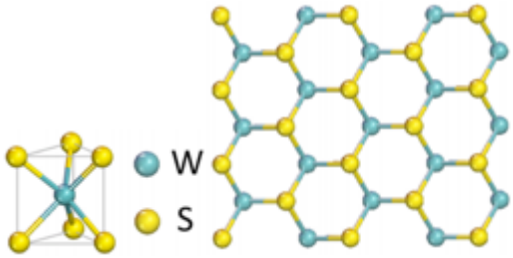

Figure 2.3. Crystal structure of single-layer tungsten disulfide [56].

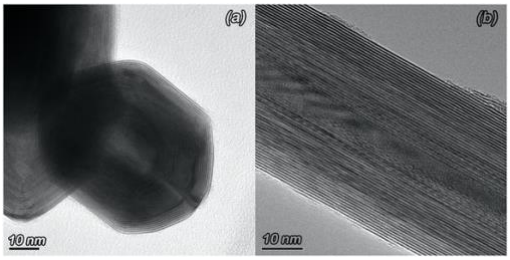

Figure 2.4. Transmission electron microscope images of (a) IF-WS_2 and (b) INT-WS_2 [54].

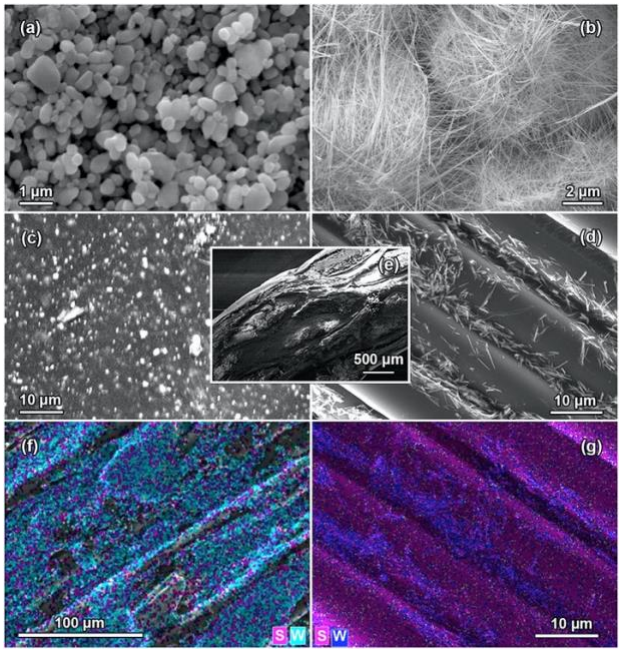

Figure 2.5. Scanning electron microscopy images of (a) IF-WS_2, (b) INT-WS_2, (c) aramid fabric/ PVB/IF-WS_2 composite, (d) aramid fabric/PVB/INT-WS_2 composite, and (e) aramid fabric/PVB control composite (center). EDS mapping images of (f) aramid fabric/PVB/IF-WS_2 and (g) aramid fabric/PVB/INT-WS_2 composites with elements S and W [54].

2.3.2. Graphene

Graphene, the first 2D nanomaterial discovered only over a decade ago, is a single layer of carbon atoms that are arranged in a hexagonal lattice [57][58]. It has a thickness of one carbon atom (~0.335nm). Due to its sp2 hybridized bonds, symmetrical plane structure, and strong covalent bonding, graphene possesses unique properties including high ultimate strength (130 GPa), high elastic modulus (1 TPa), large specific surface area (2630 m^2/g), good thermal conductivity (5000W/mK) [9]. With these properties, graphene and its derivatives such as multilayer graphene, graphene nanoplatelets and graphene oxide have been explored in high-performance nanocomposites applications [59][60][61][62]. The chemical structures of graphene and graphene oxide are shown in Figure 2.6.

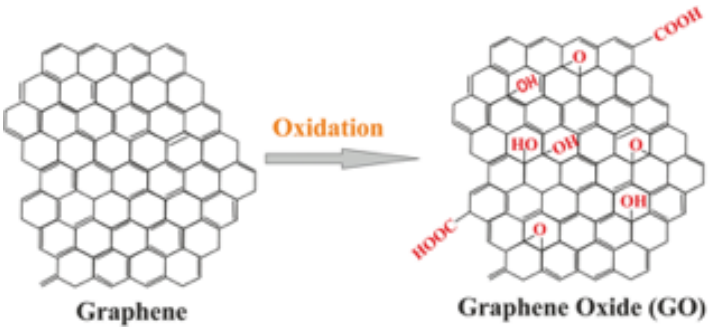

Figure 2.6. Chemical structures and conversions of graphene and graphene oxide [63].

In recent study, nanoparticle-formed graphene laminates were inserted in between Kevlar-29 fiber layers as a reinforcement component, and this new approach was found to significantly improve the ballistic performance of the Kevlar material. With 10 graphene laminates inserted, the total deformation of the vest materials after ballistic tests reduced and their stability increased [64]. Graphene oxide, which has various oxygen-containing groups such as carboxyl, hydroxyl, and epoxy groups, shows better chemical reactivity with polymer fiber surface and easier handling property with its amphiphilic structure compared to graphene [65]. In the literature, graphene oxide

coatings on different fibers (e.g. aramid and natural curaua fibers) using several approaches (deposition-filtration, immersing in GO dispersion) have been reported [11][66][65]. The images of untreated Twaron® fabric, GO treated fabric through filtration and it after manipulation are presented in Figure 2.7. Based on the ballistic tests, Twaron® fabric coated with GO through twice filtration had 50% higher energy absorption than the plain fabric, and all three samples formed cone shapes during ballistic events as shown in Figure 2.8 [11]. Similarly, the influences of incorporating GNPs into glass fiber /epoxy, polypropylene, or epoxy on the mechanical properties of the materials were also investigated in several papers, it was found that adding GNPs could improve tensile strength, Young's modulus, fracture toughness, ductility and/or energy absorption capacity of fabricated materials to different contents [67][68][69].

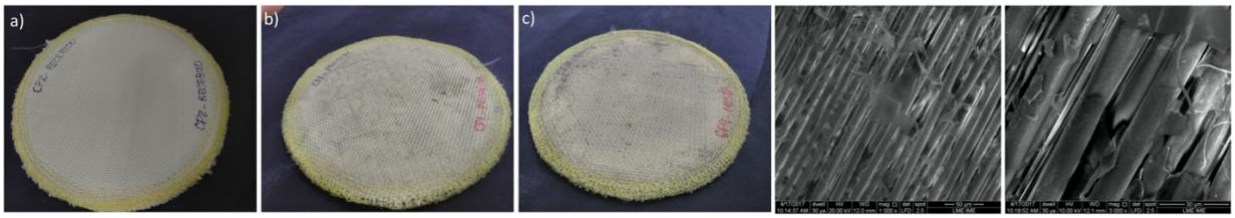

(A) (B)

Figure 2.7. (A) Images of aramid-based specimens. a) untreated, b) GO treated (1 filtration), c) GO treated (2 filtrations); (B) SEM of GO treated aramid after manual manipulation (1000× and 3000×) [11].

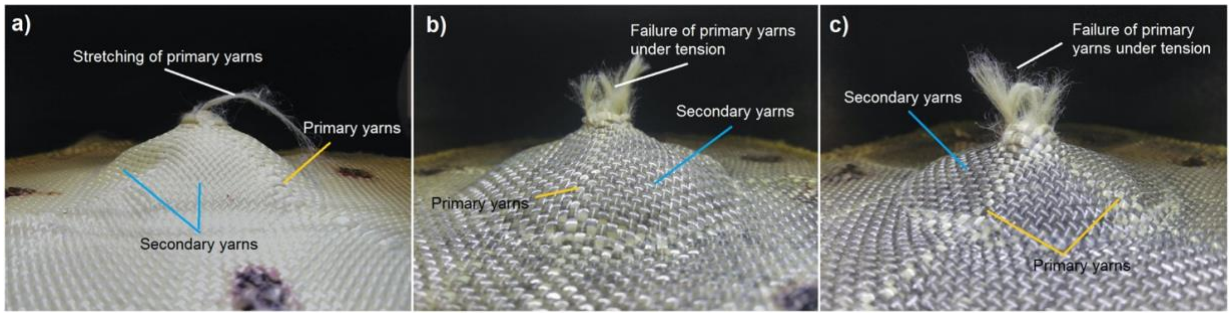

Figure 2.8. Images of the aramid samples after ballistic tests: a) untreated, b) GO treated (1 filtration), c) GO treated (2 filtrations) [11].

2.4. Polymer matrices

Different types of polymers can be used to fabricate polymer matrix composites and nanocomposites for desired properties. These polymers can be thermoplastic or thermoset polymers based on their deformation ability with heat. They can also be divided into elastomeric and non-elastomeric polymers based on the existence of polymer elasticity.

2.4.1. Thermoplastic polymer

Thermoplastic polymers are polymers that can be softened and melted when heat applied, they can be reprocessed with heat or solvents. Unlike thermoset polymers which contain permanent covalent bond crosslinks, thermoplastic polymers form weaker physical crosslinks between molecular chains through different types of bonds such as intermolecular interactions, hydrogen bonds, and van der Waals forces. These physically formed crosslinks can be easily destroyed under heat, and reform when cooling down, this contributes to the softening and reforming abilities of thermoplastic polymers at elevated temperatures. In textile-based anti-impact composites, several types of thermoplastic polymers have been explored as polymer matrices or binders including polyvinyl acetate (PVA) [70], polypropylene (PP) [71][72][73], high-density polyethylene (HDPE), polycarbonate, etc. For instance, Ignatova et al. studied the effect of thermoplastic PVA coating on the ballistic impact response of Twaron® fabrics. The surface morphology of the coated fabric is shown in Figure 2.9. The images of deformed fabrics after high-velocity impact tests with different velocities are presented in Figure 2.10. The results suggested that compared to the neat 5-layers fabric panels, the ballistic limit of the PVA/Twaron® composites with the same number of fabric layers could increase by almost twice. Besides, the plasticine indentation tests indicated the indentation depth of coated fabrics (5%-6% coating add-on) reduced up to three times compared to the neat fabrics [70].

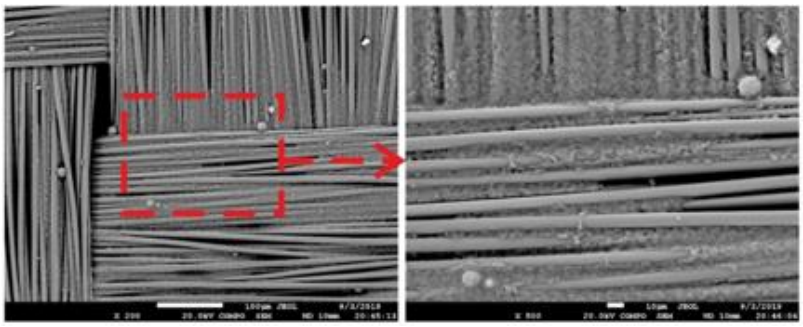

Figure 2.9. Surface morphologies of the PVA coated Twaron® fabric [70].

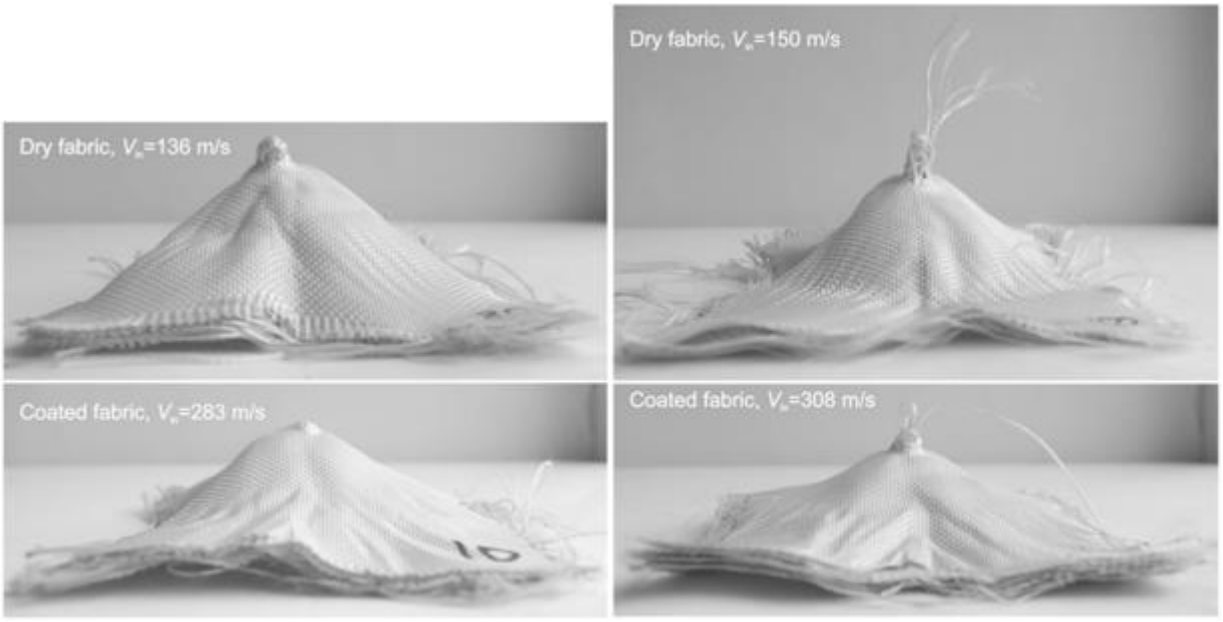

(a) (b)

Figure 2.10. The images of deformed dry fabric and PVA coated fabric after ballistic tests. (1) impacting velocity slightly below the ballistic limits; (b) impacting velocity slightly higher than the ballistic limits [70].

2.4.2. Thermoset polymers

Thermoset polymers are polymers that cannot be remelted to liquid forms or remolded when heated after they are initially formed and cured. Instead, they directly degrade without entering a fluid phase at a high temperature. During their curing processes, crosslinking reactions can be initiated by different factors such as crosslinking agents, catalysts, heat, change in pH and pressure, then covalent bonds form between the molecular chains leading to three-dimensional

network structures. The formed chemical crosslinks, which restrict the sliding of molecular chains, are hard to destroy with heat or solvents. This contributes to the permanent solid forms of thermoset polymers and their excellent thermal stability and chemical resistance. The molecular structures of thermoplastic and thermoset resins are presented in Figure 2.11. In ballistic materials, several thermoset polymers were investigated including epoxy (non-elastomer) [5][74][75], vinyl esters [76][77], phenolic resins[78][79], and polyesters [80]. For instance, Domun et al. used thermoset epoxy polymer (EP) to fabricate stiff glass fiber/ nanomaterial composite laminates for perforated and unperforated ballistic tests. 4 different types of nanomaterials including CNTs, GNPs, boron nitride nanosheets (BNNS) /CNTs, and boron nitride nanotubes (BNNT) /GNPs were incorporated. Figure 2.12 shows the images of the composite laminates after non-perforated ballistic tests. The results revealed that the last nanomaterial incorporated epoxy/glass fiber nanocomposites achieved the best incident velocity reduction, which is 18.1% higher than it of the neat epoxy/glass fiber composites [5]. Similarly, images of vinyl ester incorporated glass fiber- or carbon fiber-based composites after impact tests can be found in Figure 2.13.

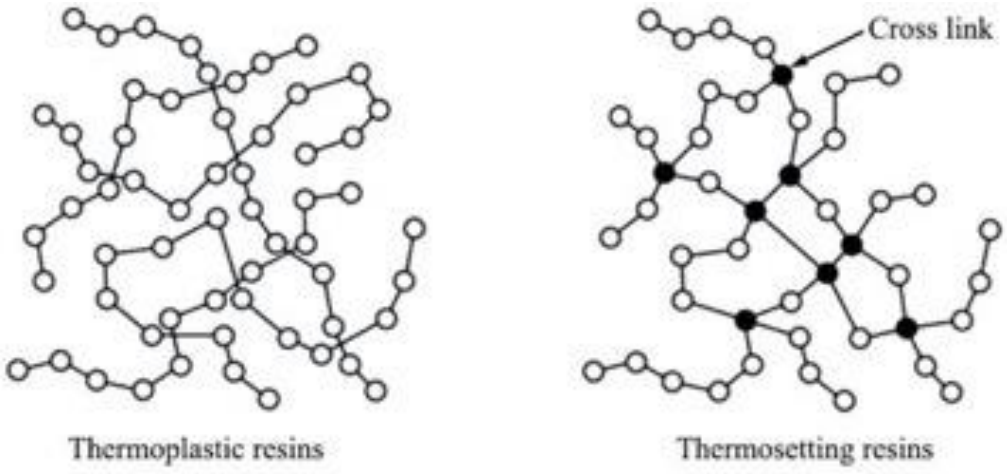

Figure 2.11. The molecular structures of thermoplastic and thermoset resins [81].

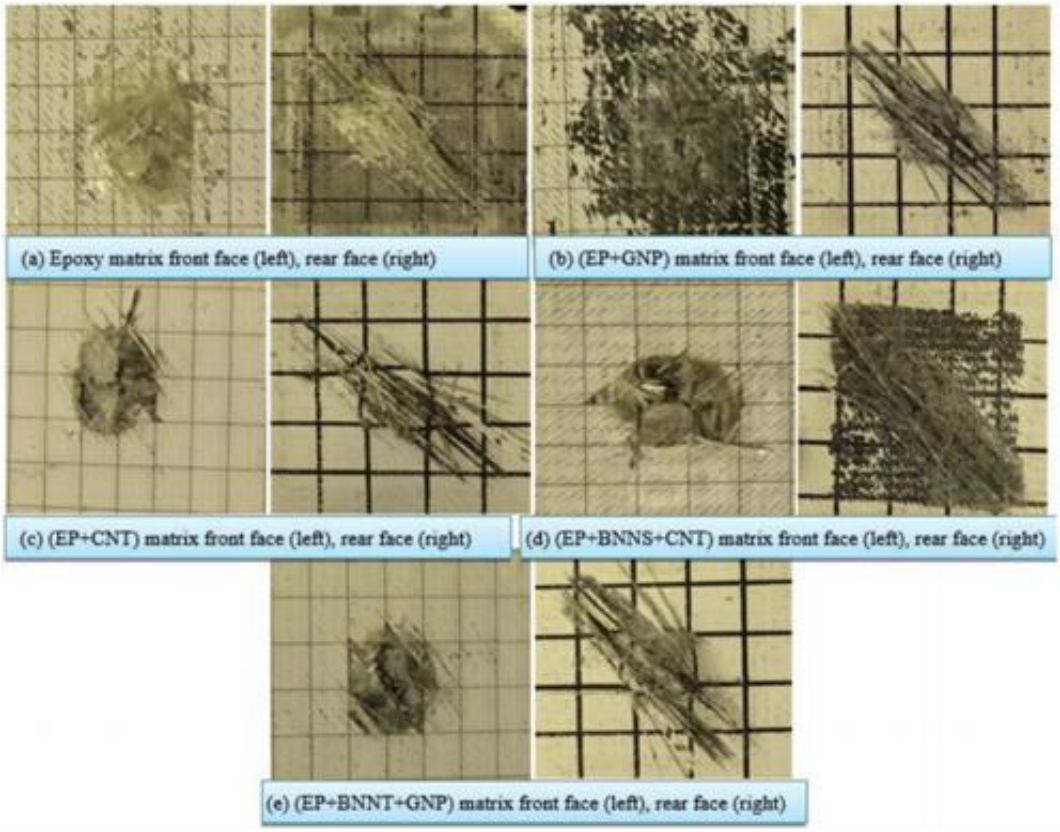

Figure 2.12**.** Images of the stiff glass fiber/epoxy composite laminates incorporated with varying nanomaterials after non-perforated ballistic tests. (a) only EP (epoxy polymer) used; (b) EP + GNP; (c) EP + CNT; (d) EP + BNNS (boron nitride nanosheets) + CNT; (e) EP + BNNT (boron nitride nanotubes) +GNP [5].

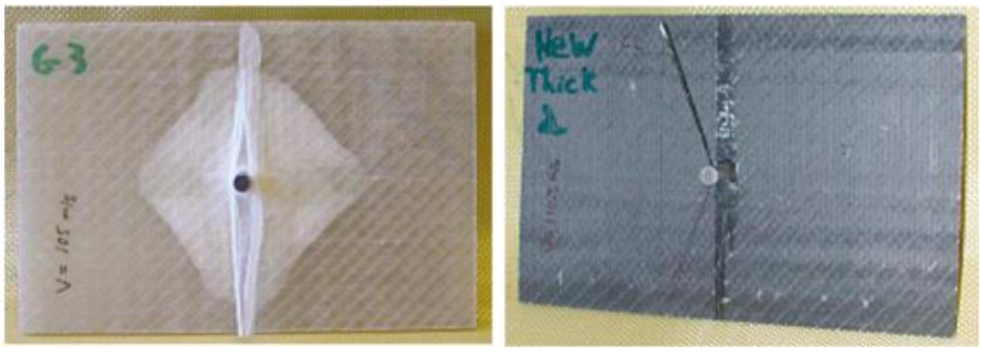

Figure 2.13. The images of the samples partially penetrated by the projectiles. (a) Glass/ vinyl esters panel. (b) Carbon/ vinyl esters panel [76].

2.4.3. Elastomers

Elastomers, or elastic polymers, are a particular group of polymers that are rubbery and extensible with high yield strain and low Young's modulus [82]. Elastomers are mostly thermoset

polymers with chemical crosslinks, but thermoplastic elastomers with physic crosslinks are also available. At the molecular level, elastomers normally have long and loosely cross-linked molecular chains with weak intermolecular forces, and they are amorphous above their glass transition temperatures (T_g) which allows significant polymer molecular motions. With their glass transition temperatures well below ambient temperatures, they behave as rubbers at room temperature. Elastomer's structure characteristics allow elastomer molecules to straighten out from the original coiled form along the force direction when stress is applied. And when the stress is removed, the molecules return to their random coil arrangements due to chemical or physical crosslink restriction (Figure 2.14). And at the macroscopic level, elastomers can be pulled and stretched to a certain extent, and recover their original shapes once released. Elastomers are viscoelastic showing both viscosity and elasticity. They are usually made of elements of carbon, hydrogen, and oxygen, or silicon. Some common elastomers are natural rubbers, polyurethanes, polybutadiene, silicone, and neoprene. Among these, polyurethane products are extensively used for elastic coating on wood, ceramic, metal, and textiles with soft textures. In this research, elastomeric polymers (thermoplastic or thermoset) are preferred for developing flexible composite materials.

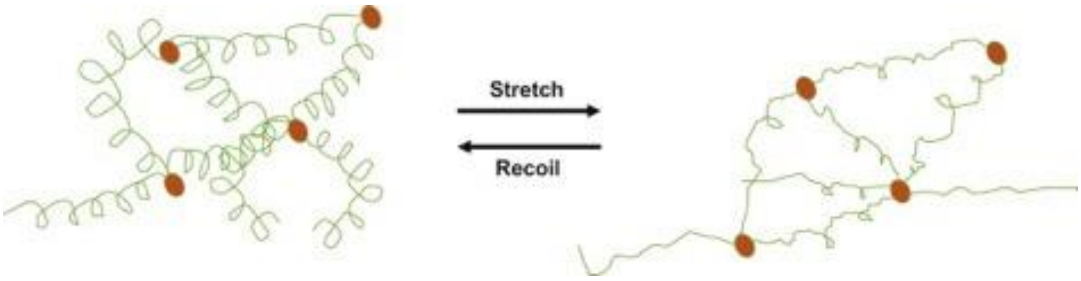

Figure 2.14. Elastomer structure [83].

2.4.4. Polyurethane elastomer

Polyurethane (PU) elastomers are synthetic resins that contain urethane (carbamate) (-NHCOO-) linkages connecting the organic units. At the formation level, they are copolymers commonly formed by the reactions between polyols and diisocyanates. The general chemical reaction of polyurethane is shown in Figure 2.15. While most polyurethane elastomers are thermoset, there are also some thermoplastic polyurethanes. In thermoset PU elastomers, chemical crosslinks through covalent bonds and low intermolecular interaction allow the sliding of molecular chains under stress and the recovery after removing the force. While in thermoplastic PU elastomers, hydrogen bonding and hard domain formation act as physical crosslinks to prevent permanent molecular motion and contribute to polymer reversible deformation. In the molecular structure of a thermoplastic PU, two segments are usually identified, soft and hard, the soft segment comprises long and flexible polyol, while the hard segment comes from rigid isocyanate. Because of the rigidity of hard segments and hydrogen bonds between hard segments, they form hard domains (or crystalline) functioning as physical crosslinks [84]. And soft segments form the soft phase (or amorphous). Figure 2.16 presents the molecular and bulk structures of polyurethane. In general, soft segments give elasticity and softness to the elastomers when stretched under stress, while the chemical or physical crosslink sections contribute to rigidity and toughness. A larger number of soft segments and a lower crosslinking density lead to a softer and more elastic polyurethane. Moreover, the properties of PU can also be affected by the types of isocyanates and polyol. For instance, polyurethanes made of polyester polyol, polyether polyol, polycarbonate polyol, and polyamide polyol may show varying properties.

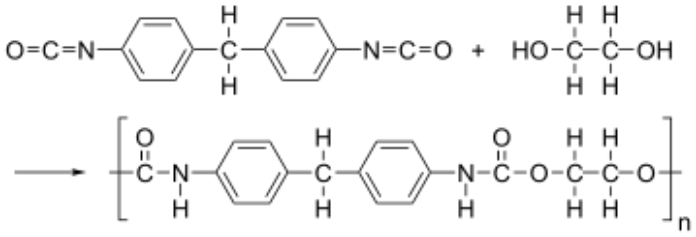

Figure 2.15. General chemical reaction of a polyol and a diisocyanate (Adapted from https://en.wikipedia.org/wiki/Polyurethane).

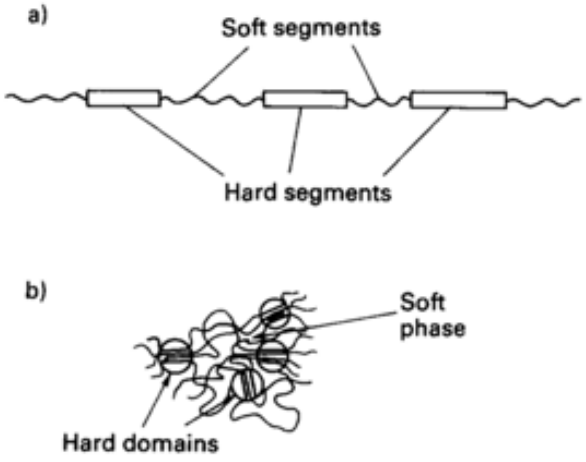

Figure 2.16. The schematic of PU molecular structure. (a) Soft and hard segments (b) Relaxed structure [84].

Overall, polyurethane elastomer is versatile. It possesses exceptionally balanced properties including high elasticity, superb flexibility, good abrasion resistance, good tear strength, good chemical and UV resistance, and a wide range of hardness [85]. Different from conventional thermoset polymers that are likely to become brittle when their stiffness increases, thermoset PU elastomers resist fracture, remain elastic, and possess great toughness even with very hard formulations. Because of their tailorable properties with different isocyanate types, polyol types, and soft to hard segment ratios, PU elastomers are used in many applications including leathers, coatings, paints, films, adhesives, foams, etc [86][85][87][88]. Due to its property combination of both high elasticity of rubber and excellent toughness/durability of metal, PU elastomer is also one of the most commonly used elastomeric polymers in several engineered products [89].

Compared with conventional polyurethane elastomers, waterborne PU elastomers use water as the primary solvent instead of organic solvents. With the environmental regulation to reduce the discharge of volatile organic components (VOCs) and their negative impact on the environment, coating formulas with organic solvents are gradually replaced by waterborne polymers [90]. In a WPU dispersion, polyurethane particles are uniformly dispersed in an aqueous environment forming a binary colloidal system. The process of making PU emulsion (with no NCO groups but with PU segments) usually involves (1) producing of urethane prepolymer with carboxyl groups using polyisocyanate, polymeric polyols, modifier containing a carboxyl group, (2) neutralizing the carboxyl group in water, (3) emulsifying the prepolymer in water using high speed stirring, and (4) chain extension with an amine chain extender [91]. These produced waterborne PUs are non-toxic and cause less pollution to nature, therefore have been widely utilized in coating and adhesion for textile, paper, wood, and glass fibers [90].

2.5. Nanocomposites

Composites are materials comprising at least two phases with different chemical and physical properties, and all phases are integrated to form a solid material with properties distinct from either component [92]. Similar to the origins of the Stone Age, Bronze Age, and Iron Age, our modern time can be defined as the Composite Age because of the extensive use and research of composites in areas such as ballistic materials, aerospace, biomedical, food packaging, and cosmetic products [9]. Similarly, nanocomposites are composites that have at least one dimension of one phase in the nanoscale (<100 nm) [8]. With the emergence of various nanomaterials with excellent properties, nanocomposites have become highly promising materials for numerous fields including ballistic protective garments, biomaterials, coating materials, biomedical engineering,

etc [23]. In body armor application, fiber-based polymer composites occupy the major portion of composites due to their high strength-to-weight ratio, high stiffness, high corrosion resistance, enhanced energy absorption, and design flexibility [9]. Apart from fiber-based polymer nanocomposites, polymer nanocomposites that have no textiles involved were also reported in the literature for bullet-proof materials. With similar dispersing methods used for fiber-based polymer nanocomposites, nanomaterials in polymer nanocomposites can be mixed with polymer dispersions to form composite nanofluids for applications such as shear thickening fluids (STFs) or rigid anti-impact materials after solidification. In addition, fabric-based nanocomposites have also been explored in some papers, these nanocomposites were made with fabric substrates and nanoparticles, no polymer matrices were involved. In the preparation processes, nanofiller/water or nanofiller/solvent dispersions were directly distributed on target fabrics, and nanoparticles were fixed on fabrics through formed chemical bonds or physical attraction after evaporating water or solvents [11][93].

2.5.1. Fiber-based polymer nanocomposites

Fiber-reinforced nanocomposites usually comprise three parts: (1) textile fibers in different forms, (2) nanofillers, and (3) polymer matrices. The mechanical performance, energy absorption capability, morphology, and structure of final nanocomposites depend on the selection of all three components and the fabrication process.

First of all, textile fibers can be incorporated as textile reinforcing components or substrates in the form of fibers, yarns, or fabrics. As reviewed before, high-performance fibers (e.g. UHMWPE, para-aramid, glass fibers, and carbon fibers.) are commonly utilized for lightweight body armors and anti-impact protective materials due to their high strength-to-weight ratio, high flexibility, low cost, etc [1]. Textiles in varying structures and forms such as fibers, 2D woven

fabric (e.g. plain weave, basket weave, and triaxial weave), 2D nonwoven fabric, unidirectional laminates, cross-ply laminates, 3D woven fabrics, and knitted fabrics have been used to develop either soft or rigid materials for personal, vehicle and equipment ballistic protection [1][94][95]. The sketches of some 2D and 3D weave structures of fabrics are shown in Figure 2.17. During the impact process on a layer of fabric, most of the kinetic energy from the projectile will be absorbed by primary and secondary fibers through fiber strain and breakage. And the total energy absorption capacity and ballistic resistance of fabricated composites can be affected by various textile factors such as fiber types, fiber weight ratios in composites, fabric structures, and fabric thicknesses [48].

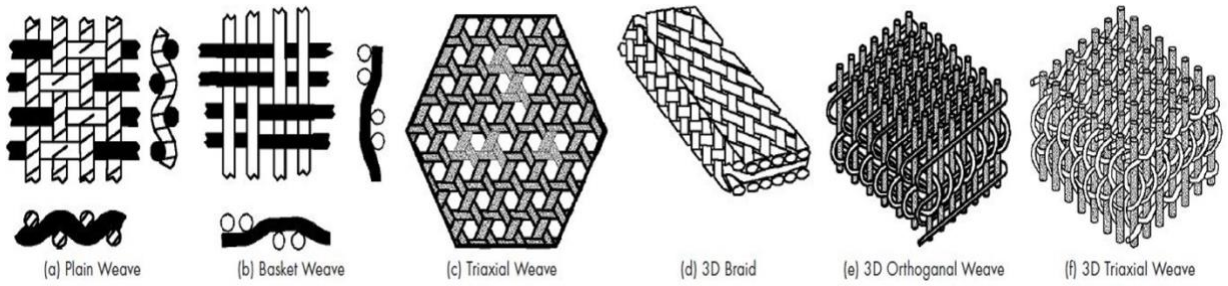

Figure 2.17. Different 2D (a,b,c) and 3D (d,e,f) fabric structures [1].

Secondly, nanofillers are dispersed on fabric textiles for nano-reinforcement. As mentioned before, nanomaterials such as WS_2, graphene, nanoclay, CNTs are commonly used as reinforcing nanofillers for developing high strength and anti-impact composites. According to reported fabrication processes of fiber-reinforced polymer nanocomposites, nanofillers were often mixed in polymeric matrices to form uniform fluids. Compared with neat composites, nanocomposites can achieve higher tensile strength, modulus, toughness, and energy absorption capacity when suitable nanofillers and fabrication methods are applied [96]. The mechanical and ballistic performances of nanocomposites can be impacted by nanofiller factors such as nanofiller type, size, shape, addition amount, and distribution uniformity in polymer matrices.

At last, the polymer matrices can be either thermoplastic or thermoset polymers. In fiber-based polymer nanocomposites, apart from their primary property contribution, polymers may also function as binders to incorporate textile components with selected nanofillers and evenly distribute nanoparticles. Polymer matrices have three primary functions, which are (1) improving mechanical performance by bonding the fibers together in position and dissipating the impact or stress energy into individual fibers [97], (2) increasing the energy absorption capacity of polymer composites through matrix fracture, delamination and debonding processes [98], and (3) protecting the composites from environmental elements that may cause property damage such as ultra-violet light and high moisture [99][100][101].

2.5.2. Fiber-based polymer nanocomposite fabrication

To apply nanotechnology and incorporate nanomaterials with fiber substrates, different fabrication methods have been reported. The fabrication process for most fiber-based polymer nanocomposites can be divided into 3 main parts, (1) preparation of nanofiller-matrix dispersions, (2) incorporating nanofiller mixtures with textile substrates, and (3) designing layered architectures for nanocomposites.

To utilize nanomaterials and achieve high property enhancement for nanocomposites, the major challenge during the preparation is to obtain uniform dispersions of nanofillers in the polymer matrices since most nanofillers (e.g., graphene, CNTs) are hydrophobic and chemically inert, which leads to their low stability within polymer matrices. To prepare uniform nanofiller-matrix mixtures and avoid agglomeration of nanofillers, two main approaches have been reported, which are functionalizing nanofillers and optimizing mixing process. Functionalizing nanofiller aims to improve its reactivity and surficial affinity, treatments such as chemical reaction with agents and plasma surface modification can be applied to nanofillers [6][102][103][9]. Through

these treatments, some nanofillers can be grafted with functional groups (e.g. -COOH, -OH) that can react and bond with some polymer matrices, while in some cases, defects can be introduced onto nanofiller surfaces. In the second approach, a proper mixing process may also be selected to prepare homogeneous nanofiller-matrix dispersions. Important mixing factors including but not limited to the solvent type, viscosities of the solvent and matrix, mixing method, and mixing time may be considered. For the mixing method, ultra-sonication (using a probe sonicator or ultrasonic bath) has been utilized in many works [104][105], other methods such as mechanical mixing (using stirrer blades), magnetic-heat stirring (using a magnetic stirring and heating system), and three roll shear mixing have also been used individually or combinedly to achieve uniform distributions of nanofillers in different polymer matrices [106][107][108][109][6]. For instance, A combined mixing process with ultrasonication, shear mixing, and mechanical mixing was applied to prepare the MWCNT/polyol modified epoxy resin in one published work, and the hot press fabrication method was adopted to make the E-glass/epoxy/MWCNT laminates. The corresponding process schematic is shown in Figure 2.18.

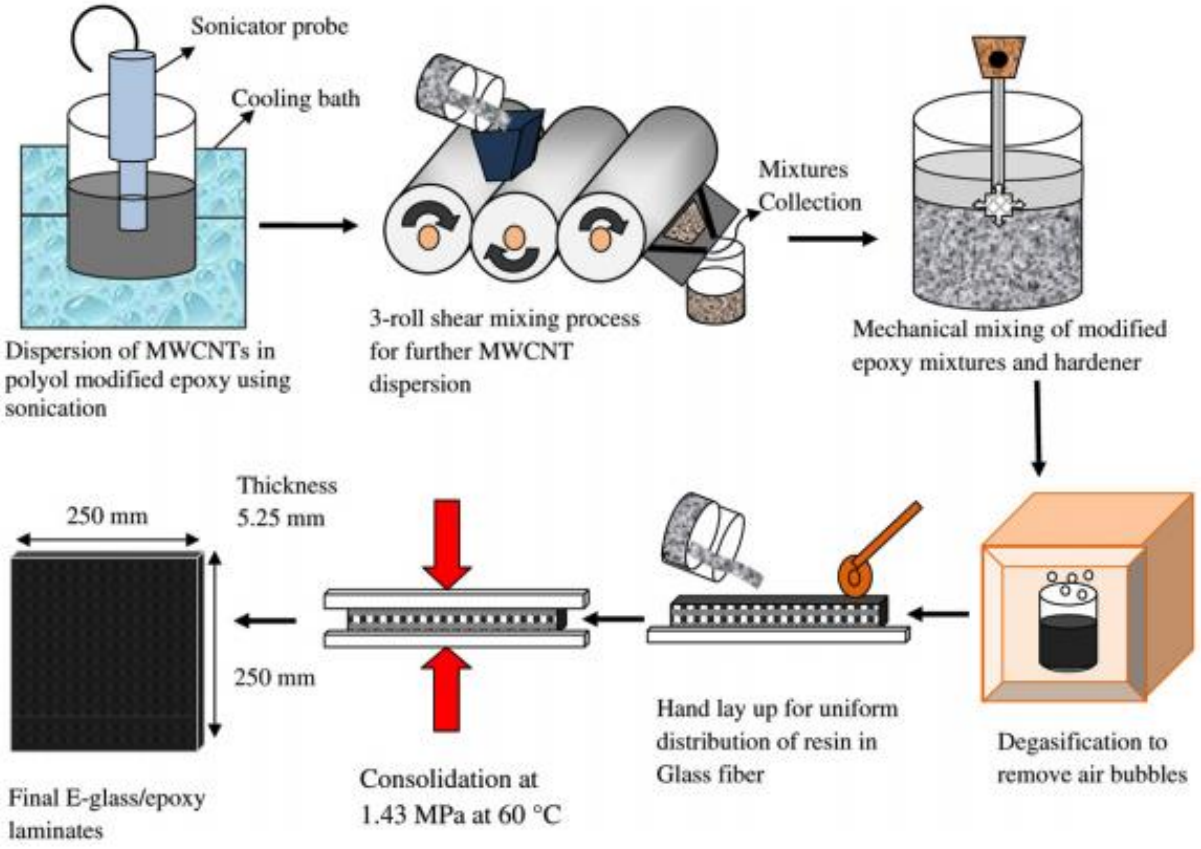

Figure 2.18. Schematic diagram of the fabrication process for E-glass/epoxy/MWCNT nanocomposites [6].

Dispersing nanofiller/polymer mixtures onto textile substrates to make flexible composite materials, as the second part, can be accomplished using various approaches. These approaches include (1) dip coating (with varying nipping pressures or dispersion concentrations for add-on control) [110][111], (2) impregnating coating assisted with ultrasonication [93], (3) spray coating method [23][112], etc. Normally, a drying process is followed after the fabrication step to remove water or solvents. Impregnating fabrics in polymer/nanomaterial mixtures is one of the easiest and most common fabrication methods for preparing flexible textile nanocomposites, while spray coating may provide a low-amount coating on fabric surface, however, it is challenging to obtain a uniform coating. Through these coating processes, nanomaterials can be incorporated with

selected fiber or fabric materials, and desirable properties such as good conductivity, high strength, shock absorption, and impact load dissipation ability for the materials may be achieved [113]. In previous research, spray coating was used to distribute SWCNT/ethanol solution on UHMWPE fabrics and fabricate fiber-based nanocomposites [112]. Other methods such as direct application and vacuum filtration of nanomaterials were also recorded for incorporating nanomaterials. In a previous paper, IF-WS_2 nanoparticle/PVB solution was directly applied on phenolic resin-coated aramid fabrics using a spatula, then the samples were dried in a vacuum oven to solidify the coated PVB solution into a film and the hydraulic press was applied to fabricate nanocomposite laminates [51]. Similarly, a vacuum filtration method has also been used to deposit the suspension of graphene oxide nanomaterials on aramid fabrics followed by a vacuum drying process to fabricate textile nanocomposite [11]. In addition, other fabrication methods such as hand lay-up [114], compression molding [115], vacuum-assisted resin transfer molding (VARTM) [116][117], prebuilding 3D nanofiller network [118] and three-dimensional (3D) printing [119][120] have also been used for fabricating mostly rigid ballistic composites [48].

In the last design phase, layered architectures of fabric laminates can be optimized based on different factors to enhance the ballistic properties of composite laminates. These main factors include (1) orientation arrangement of fabric layers (e.g. unidirectional or bidirectional) [121], (2) fabric components (e.g. sample type, hybrid) [122] and (3) stacking sequence of fabric layers [123]. Overall, nanocomposite laminates can be fabricated by applying polymer/nanofiller dispersions on individual fabrics and then forming laminates, or directly depositing nano dispersions on pre-arranged laminate structures. In summary, the energy absorption capability of fiber-reinforced polymer nanocomposites can be affected by various factors related to the fiber

substrate, polymer matrix, nanofiller component, and fabrication conditions as shown in Figure 2.19.

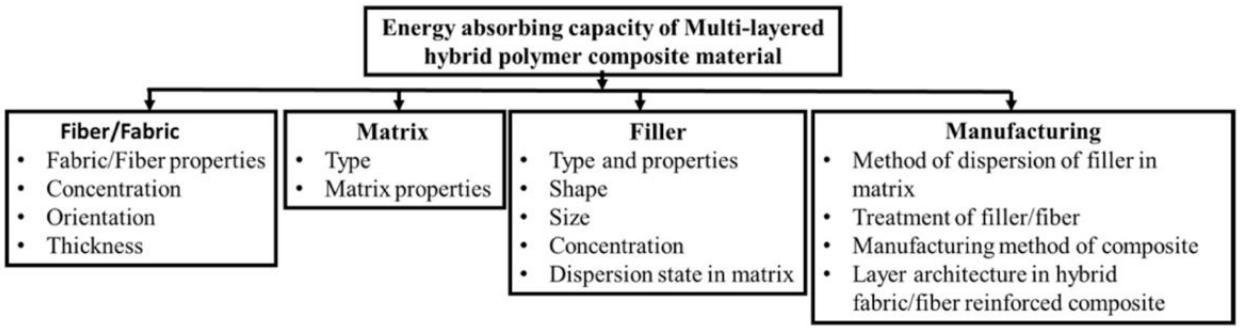

Figure 2.19. Factors affecting the performance of high-velocity impact-resistant fiber-based polymer nanocomposites [48].

2.6. Characterization

Performance evaluation is crucial for understanding the properties of bullet-proof materials, determining protection levels of the materials, and compare performances of different products. During in-service time and ballistic impact events, low-velocity and high-velocity impacts may happen to body armors and ballistic protective gears. To evaluate the mechanical properties and overall ballistic performances of ballistic materials, and products, various evaluation approaches including mechanical tests, high-velocity impact test, low-impact tests, and their combinations have been reported. However, in academic research, high-velocity ballistic tests may not be practical due to the lack of testing equipment, complexity of tests, high requirements for device setup, the demand for large test specimens, and high cost. Instead, other test methods such as tensile test and dynamic mechanical analysis are often used to study the related mechanical properties for target materials at early developing stage due to the facility availability, easy-to-conduct, and low-cost advantages. In the literature, stiffness and flexural strength, which are not

fundamental properties, but combined outcomes from three principal stresses including tensile, shear, and compressive stresses, were also used for ballistic materials [124][125][126]. Varying testing standards such as ASTM D5035, ASTM D3039, ASTM D3518, and ISO 527–4 were reported for tensile tests of woven fabrics or composite laminates, whereas evaluation standards such as ASTM D7264/D790 and D664/D3410 were used for flexural strength and compression strength tests of composites using three-point bending tests and universal testing machines (UTM), respectively [48][127][128][74].

2.6.1. Tensile Test

Through tensile strength tests, material properties such as ultimate tensile strength, elongation at break, and Young's modulus can be measured. These properties are essential for high-velocity impact materials. Besides, material toughness measures the total energy material absorbs per unit volume before rupture. It can be calculated using the area under the stress-strain curve obtained from tensile tests. However, for some materials, such as fibers and yarns, their cross-section areas and stress under load are difficult to measure and calculate due to their irregular cross-section shapes and pores between fibers. In this case, total tensile energy absorption, also called energy-to-break or work of rupture can be calculated with the integrated area under the load-elongation curve as shown in equation (2.1) and Figure 2.20. The total energy absorbed is expressed in the unit of joule (J). To compare different fiber or yarn materials, normalized energy-to-break or gravimetric toughness (J/g) can be calculated based on the fiber/yarn linear density (denier) and initial length (m) as shown in equation (2.2) [129].

$$Energy\ to\ break\ (J)\ =\ \int_0^{break} F \cdot dl \tag{2.1}$$

Where F is the load on the material, l is the material length.

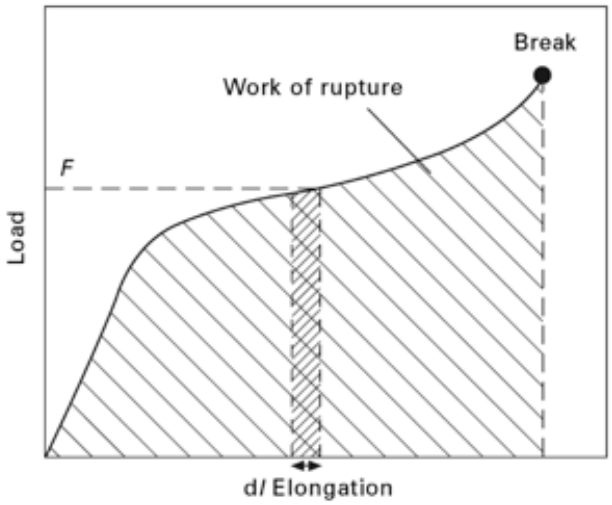

Figure 2.20. Work of rupture or tensile energy to break [129].

$$Normalized\ energy\ to\ break\ (J/g) = \frac{9000 \times Energy\ to\ break}{Linear\ density \times Intial\ length} \qquad (2.2)$$

2.6.2. Dynamic Mechanical Analysis

To study the viscoelastic properties (viscosity and elasticity) of polymer materials, DMA is commonly used as a vital and high-sensitivity technique. During the test, a sinusoidal force is applied to a material, the resulting deformation of the material at a certain temperature, frequency, or time is detected, and the responding time lag (phase angle) δ of the material behind the applied force is monitored (Figure 2.21). When a pure elastic material is tested, the material deforms instantaneously with the force resulting in the phase angle δ of 0. An increase phase angle corresponds to the increasing viscous behavior of the material. Then based on the phase lag δ, the corresponding stress (**σ**), strain (**ε**), storage modulus (**E'**), loss modulus (**E"**), and tan **δ** can be calculated using Equations (3) - (7), respectively. While storage modulus corresponds with the material's elasticity, stiffness, and ability to store energy, loss modulus reflects the material's viscosity and ability to dissipate energy through heat. Besides, the damping factor tan δ equals the ratio of loss modulus to storage modulus representing the damping coefficient of the tested

material. In DMA graphs, tan δ shows a similar trend to E'' but is independent of sample dimensions. Overall, through this test, the stiffness and damping properties of materials can be measured as a function of temperature, frequency, or time [130].

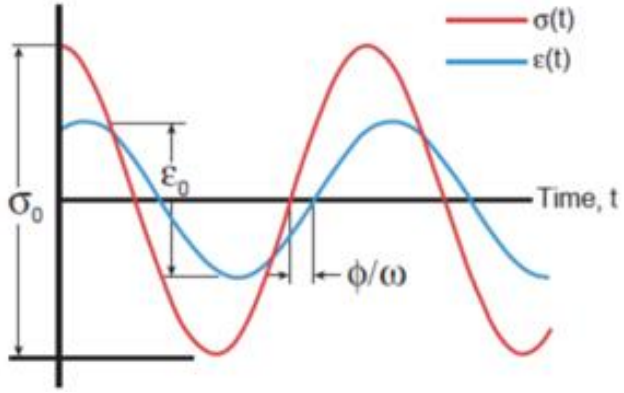

Figure 2.21. The phase lagging during sinusoidal cycle loading [130][131].

$$\sigma = \sigma_0 \sin \omega t \quad (3)$$

$$\varepsilon = \varepsilon_0 \sin(\omega t - \delta) \quad (4)$$

$$E' = \frac{\sigma_0 \cos\delta}{\varepsilon_0} \quad (5)$$

$$E'' = \frac{\sigma_0 \sin\delta}{\varepsilon_0} \quad (6)$$

$$\tan \delta = \frac{E''}{E'} \quad (7)$$

Where $\boldsymbol{\sigma_0}$ and $\boldsymbol{\varepsilon_0}$ are the maximum stress and strain respectively [130].

2.6.3. Other Characterizations

Apart from measuring the mechanical properties, other characterization methods such as differential scanning calorimetry (DSC), Fourier-transform infrared spectroscopy (FT-IR), scanning electron microscope (SEM), energy dispersive X-ray spectroscopy (EDX), and water contact angle can also be employed to study the heat flow/transition, chemical structure/functional groups, material microstructure/surface morphology, nanomaterial compositions/distribution, and wettability of the target material. By combining quantitative and qualitative characterizations, a

better understanding of the reinforcing and failure mechanisms of nanocomposite coated UHMWPE yarns and fabrics can be achieved.

2.7. Summary

In this project, the PU/nanofiller coating has been applied on UHMWPE filament yarns and fabrics for enhanced mechanical, viscoelastic and tensile energy absorption properties. The experimental content can be briefly summarized as the following.

- The UHMWPE filament yarns were individually coated using dip-coating method, proper mixing methods for PU/IF-WS_2 dispersion was explored. The effects of solvent type, water/ethanol solvent ratio, PU amount, and IF-WS_2 amount were studied. The failure mechanisms of the coated yarns were observed using SEM.
- UHMWPE yarns were plasma pre-treated, then several levels of PU/IF-WS_2 coating were applied on pre-treated UHMWPE yarns. The effect of plasma treatment on neat yarn was studied using FT-IR, tensile test, DMA test, and SEM. The effects of coating condition and plasma pre-treatment on the mechanical properties and wash durability of the composites were investigated.
- UHMWPE fabrics were plasma pre-treated and coated with PU/IF-WS_2 with varying compositions. FT-IR, water contact angle, tensile test, DMA, and SEM were utilized to understand the plasma treatment effect on the fabrics. Based on the mechanical properties, viscoelastic properties, and wash durability of the coated fabrics, the influences of coating conditions and plasma treatment were analyzed.
- Factorial designs were used to systematically study the impacts of fabrication parameters on mechanical properties and wash durability of PU/IF-WS_2/UHMWPE yarns. Fabrication parameters were screened and optimized. GNPs were incorporated into PU/UHMWPE

yarns with varying amounts. The performances of both optimized nanocomposite yarns were compared with those of the neat yarn.

- To understand the reinforcing mechanism of nanoparticles in the PU matrix, PU/nanofiller films were prepared using water-based casting method. Different nanofiller amounts for IF-WS_2 and GNPs were included. The film formation, mechanical properties, viscoelastic properties, surface morphology, and thermal transition of the PU and nanocomposite films were observed and studied.

2.8. References

[1] Abtew MA, Boussu F, Bruniaux P, Loghin C, Cristian I. Ballistic impact mechanisms – A review on textiles and fibre-reinforced composites impact responses. Compos Struct 2019;223. https://doi.org/10.1016/j.compstruct.2019.110966.

[2] Benzait Z, Trabzon L. A review of recent research on materials used in polymer–matrix composites for body armor application. J Compos Mater 2018. https://doi.org/10.1177/0021998318764002.

[3] Bhatnagar A. Lightweight ballistic composites: Military and law-enforcement applications. Light Ballist Compos Mil Law-Enforcement Appl 2006:1–429. https://doi.org/10.1533/9781845691554.

[4] Wisniewski A. Nanotechnology for Body Protection. Issues Armament Technol 2007;102:7–17.

[5] Domun N, Kaboglu C, Paton KR, Dear JP, Liu J, Blackman BRK, et al. Ballistic impact behaviour of glass fibre reinforced polymer composite with 1D/2D nanomodified epoxy matrices. Compos Part B Eng 2019. https://doi.org/10.1016/j.compositesb.2019.03.024.

[6] Rahman M, Hosur M, Zainuddin S, Vaidya U, Tauhid A, Kumar A, et al. Effects of amino-functionalized MWCNTs on ballistic impact performance of E-glass/epoxy composites using a spherical projectile. Int J Impact Eng 2013;57:108–18. https://doi.org/10.1016/j.ijimpeng.2013.01.011.

[7] Abu Talib AR, Abbud LH, Ali A, Mustapha F. Ballistic impact performance of Kevlar-29 and Al2O3 powder/epoxy targets under high velocity impact. Mater Des 2012;35:12–9. https://doi.org/10.1016/j.matdes.2011.08.045.

[8] Joshi M, Adak B. Advances in nanotechnology based functional, smart and intelligent textiles: A review. Compr. Nanosci. Nanotechnol., 2019. https://doi.org/10.1016/B978-0-12-803581-8.10471-0.

[9] Vidya, Mandal L, Verma B, Patel PK. Review on polymer nanocomposite for ballistic & aerospace applications. Mater Today Proc 2020. https://doi.org/10.1016/j.matpr.2020.02.652.

[10] Dewapriya MAN, Meguid SA. Comprehensive molecular dynamics studies of the ballistic resistance of multilayer graphene-polymer composite. Comput Mater Sci 2019. https://doi.org/10.1016/j.commatsci.2019.109171.

[11] da Silva AO, Weber RP, Monteiro SN, Lima AM, Faria GS, da Silva WO, et al. Effect of graphene oxide coating on the ballistic performance of aramid fabric. J Mater Res Technol 2019:1–12. https://doi.org/10.1016/j.jmrt.2019.12.058.

[12] Haro EE, Odeshi AG, Szpunar JA. The energy absorption behavior of hybrid composite laminates containing nano-fillers under ballistic impact. Int J Impact Eng 2016;96:11–22. https://doi.org/10.1016/j.ijimpeng.2016.05.012.

[13] Kurtz SM. The UHMWPE Handbook: Ultra-High Molecular Weight Polyethylene in Total Joint Replacement. 2004. https://doi.org/10.1016/B978-0-12-429851-4.X5000-1.

[14] Park SJ, Seo MK. Element and Processing. 2011. https://doi.org/10.1016/B978-0-12-375049-5.00006-2.

[15] Zhang D, Sun Y, Chen L, Zhang S, Pan N. Influence of fabric structure and thickness on the ballistic impact behavior of Ultrahigh molecular weight polyethylene composite laminate. Mater Des 2014;54:315–22. https://doi.org/10.1016/j.matdes.2013.08.074.

[16] Meng L, Li W, Ma R, Huang M, Wang J, Luo Y, et al. Long UHMWPE fibers reinforced rigid polyurethane composites: An investigation in mechanical properties. Eur Polym J 2018. https://doi.org/10.1016/j.eurpolymj.2018.05.021.

[17] Zhang TG, Satapathy SS, Vargas-Gonzalez LR, Walsh SM. Ballistic impact response of Ultra-High-Molecular-Weight Polyethylene (UHMWPE). Compos Struct 2015;133:191–201. https://doi.org/10.1016/j.compstruct.2015.06.081.

[18] Horrocks AR, Anand SC. Handbook of Technical Textiles: Second Edition. 2015. https://doi.org/10.1016/C2015-0-01011-5.

[19] Wang H, Hazell PJ, Shankar K, Morozov E V., Escobedo JP. Impact behaviour of Dyneema® fabric-reinforced composites with different resin matrices. Polym Test 2017;61:17–26. https://doi.org/10.1016/j.polymertesting.2017.04.026.

[20] Bhatnagar A. Lightweight Ballistic Composites: Military and Law-Enforcement Applications: Second Edition. 2016. https://doi.org/10.1016/C2014-0-03657-X.

[21] Sockalingam S, Chowdhury SC, Gillespie JW, Keefe M. Recent advances in modeling and experiments of Kevlar ballistic fibrils, fibers, yarns and flexible woven textile fabrics – a review. Text Res J 2017;87:984–1010. https://doi.org/10.1177/0040517516646039.

[22] Bandaru AK, Ahmad S, Bhatnagar N. Ballistic performance of hybrid thermoplastic composite armors reinforced with Kevlar and basalt fabrics. Compos Part A Appl Sci Manuf 2017;97:151–65. https://doi.org/10.1016/j.compositesa.2016.12.007.

[23] Benzait Z, Trabzon L. A review of recent research on materials used in polymer–matrix composites for body armor application. J Compos Mater 2018;52:3241–63. https://doi.org/10.1177/0021998318764002.

[24] Bilisik K. Two-dimensional (2D) fabrics and three-dimensional (3D) preforms for ballistic and stabbing protection: A review. Text Res J 2017. https://doi.org/10.1177/0040517516669075.

[25] Zheng Z, Tang X, Shi M, Zhou G. Surface Modification of Uitrahigh-Molecular-Weight Polyethylene Fibers. J Polym Sci Part B Polym Phys 2004. https://doi.org/10.1002/polb.10727.

[26] Zhang X, Wang Y, Lu C, Cheng S. Interfacial adhesion study on UHMWPE fiber-Reinforced composites. Polym Bull 2011. https://doi.org/10.1007/s00289-011-0491-2.

[27] Lin SP, Han JL, Yeh JT, Chang FC, Hsieh KH. Surface modification and physical properties of various UHMWPE-fiber-reinforced modified epoxy composites. J Appl Polym Sci 2007. https://doi.org/10.1002/app.25735.

[28] Silverstein MS, Breuer O, Dodiuk H. Surface modification of UHMWPE fibers. J Appl Polym Sci 1994. https://doi.org/10.1002/app.1994.070521213.

[29] Enomoto I, Mishima K, Kobayashi T, Soeda S. Functionalization of PE nonwoven fabric by plasma treatment to improve dyeing affinity. J Photopolym Sci Technol 2010. https://doi.org/10.2494/photopolymer.23.545.

[30] Teodoru S, Kusano Y, Rozlosnik N, Michelsen PK. Continuous plasma treatment of ultra-high-molecular-weight polyethylene (UHMWPE) fibres for adhesion improvement. Plasma Process. Polym., 2009. https://doi.org/10.1002/ppap.200930906.

[31] Oosterom R, Ahmed TJ, Poulis JA, Bersee HEN. Adhesion performance of UHMWPE after different surface modification techniques. Med Eng Phys 2006. https://doi.org/10.1016/j.medengphy.2005.07.009.

[32] Mercx FPM. Improved adhesive properties of high-modulus polyethylene structures: 3. Air- and ammonia-plasma treatment. Polymer (Guildf) 1994. https://doi.org/10.1016/0032-3861(94)90234-8.

[33] Tissington B, Pollard G, Ward IM. A study of the effects of oxygen plasma treatment on the adhesion behaviour of polyethylene fibres. Compos Sci Technol 1992. https://doi.org/10.1016/0266-3538(92)90011-Q.

[34] Moon SI, Jang J. The effect of the oxygen-plasma treatment of UHMWPE fiber on the transverse properties of UHMWPE-fiber/vinylester composites. Compos Sci Technol 1999. https://doi.org/10.1016/S0266-3538(98)00093-1.

[35] Sakurai K, Kondo Y, Miyazaki K, Okamoto T, Irie S, Sasaki T. Ultrahigh-molecular-weight-polyethylene-fiber surface treatment by electron-beam-irradiation-induced graft polymerization and its effect on adhesion in a styrene-butadiene rubber matrix. J Polym Sci Part B Polym Phys 2004. https://doi.org/10.1002/polb.20139.

[36] Martínez-Morlanes MJ, Castell P, Martínez-Nogués V, Martinez MT, Alonso PJ, Puértolas JA. Effects of gamma-irradiation on UHMWPE/MWNT nanocomposites. Compos Sci Technol 2011. https://doi.org/10.1016/j.compscitech.2010.11.013.

[37] Nevoralová M, Baldrian J, Pospíšil J, Chodák I, Horák Z. Structure modification of UHMWPE used for total joint replacements. J Biomed Mater Res - Part B Appl Biomater 2005. https://doi.org/10.1002/jbm.b.30317.

[38] Kondo Y, Miyazaki K, Yamaguchi Y, Sasaki T, Irie S, Sakurai K. Mechanical properties of fiber reinforced styrene-butadiene rubbers using surface-modified UHMWPE fibers under EB irradiation. Eur Polym J 2006. https://doi.org/10.1016/j.eurpolymj.2005.11.025.

[39] Wang J, Liang G, Zhao W, Lü S, Zhang Z. Studies on surface modification of UHMWPE fibers via UV initiated grafting. Appl Surf Sci 2006. https://doi.org/10.1016/j.apsusc.2005.12.165.

[40] Zheng Z, Wang X, Huang X, Shi M, Zhou G. Chemical modification combined with corona treatment of UHMWPE fibers and their adhesion to vinylester resin. J Adhes Sci Technol 2006. https://doi.org/10.1163/156856106777890626.

[41] Mohammadalipour M, Masoomi M, Ahmadi M, Kazemi Z. The effect of simultaneous fiber surface treatment and matrix modification on mechanical properties of unidirectional ultra-high molecular weight polyethylene fiber/epoxy/nanoclay nanocomposites. J Compos Mater 2018. https://doi.org/10.1177/0021998318755542.

[42] Yim JH, Ayan H, Pappas D, Vasilets VN, Fridman A, Palmese GR. Functionalization of polymers using n 2 pulsed dielectric barrier discharge, 2008. https://doi.org/10.1109/ppps.2007.4651910.

[43] Moon SI, Jang J. Factors affecting the interfacial adhesion of ultrahigh-modulus polyethylene fibre-vinylester composites using gas plasma treatment. J Mater Sci 1998. https://doi.org/10.1023/A:1013205918208.

[44] Yang Z, Peng H, Wang W, Liu T. Crystallization behavior of poly(ε-caprolactone)/layered double hydroxide nanocomposites. J Appl Polym Sci 2010;116:2658–67. https://doi.org/10.1002/app.

[45] Olawoyin R. Nanotechnology: The future of fire safety. Saf Sci 2018. https://doi.org/10.1016/j.ssci.2018.08.016.

[46] Al-Nemrawi NK, AbuAlSamen MM, Alzoubi KH. Awareness about nanotechnology and its applications in drug industry among pharmacy students. Curr Pharm Teach Learn 2019. https://doi.org/10.1016/j.cptl.2019.12.003.

[47] Tiwari JN, Tiwari RN, Kim KS. Zero-dimensional, one-dimensional, two-dimensional and three-dimensional nanostructured materials for advanced electrochemical energy devices. Prog Mater Sci 2012. https://doi.org/10.1016/j.pmatsci.2011.08.003.

[48] Clifton S, Thimmappa BHS, Selvam R, Shivamurthy B. Polymer nanocomposites for high-velocity impact applications-A review. Compos Commun 2020;17:72–86. https://doi.org/10.1016/j.coco.2019.11.013.

[49] Mohamed EF. Nanotechnology: Future of Environmental Air Pollution Control. Environ Manag Sustain Dev 2017;6:429. https://doi.org/10.5296/emsd.v6i2.12047.

[50] Goldman EB, Zak A, Tenne R, Kartvelishvily E, Levin-Zaidman S, Neumann Y, et al. Biocompatibility of tungsten disulfide inorganic nanotubes and fullerene-like nanoparticles with salivary gland cells. Tissue Eng - Part A 2015. https://doi.org/10.1089/ten.tea.2014.0163.

[51] Simić DM, Stojanović DB, Brzić SJ, Totovski L, Uskoković PS, Aleksić RR. Aramid hybrid composite laminates reinforced with inorganic fullerene-like tungsten disulfide nanoparticles. Compos Part B Eng 2017. https://doi.org/10.1016/j.compositesb.2017.05.002.

[52] Mojtabaei A, Otadi M, Goodarzi V, Khonakdar HA, Jafari SH, Reuter U, et al. Influence of fullerene-like tungsten disulfide (IF-WS2) nanoparticles on thermal and dynamic

mechanical properties of PP/EVA blends: Correlation with microstructure. Compos Part B Eng 2017. https://doi.org/10.1016/j.compositesb.2016.12.006.

[53] Volkova EI, Jones IA, Brooks R, Zhu Y, Bichoutskaia E. Meso-scale modelling of shock wave propagation in a SiC/Al nanocomposite reinforced with WS2-inorganic fullerene nanoparticles. Compos Struct 2013;96:601–5. https://doi.org/10.1016/j.compstruct.2012.08.039.

[54] Simić DM, Stojanović DB, Dimić M, Mišković K, Marjanović M, Burzić Z, et al. Impact resistant hybrid composites reinforced with inorganic nanoparticles and nanotubes of WS2. Compos Part B Eng 2019. https://doi.org/10.1016/j.compositesb.2019.107222.

[55] Naffakh M, Díez-Pascual AM, Marco C, Ellis GJ, Gómez-Fatou MA. Opportunities and challenges in the use of inorganic fullerene-like nanoparticles to produce advanced polymer nanocomposites. Prog Polym Sci 2013. https://doi.org/10.1016/j.progpolymsci.2013.04.001.

[56] Ye Y, Wong ZJ, Lu X, Ni X, Zhu H, Chen X, et al. Monolayer excitonic laser. Nat Photonics 2015. https://doi.org/10.1038/nphoton.2015.197.

[57] Akinwande D, Brennan CJ, Bunch JS, Egberts P, Felts JR, Gao H, et al. A review on mechanics and mechanical properties of 2D materials—Graphene and beyond. Extrem Mech Lett 2017. https://doi.org/10.1016/j.eml.2017.01.008.

[58] Gautam RK, Verma A. Electrocatalyst Materials for Oxygen Reduction Reaction in Microbial Fuel Cell. Microb. Electrochem. Technol., 2019. https://doi.org/10.1016/b978-0-444-64052-9.00018-2.

[59] Bizao RA, Machado LD, De Sousa JM, Pugno NM, Galvao DS. Scale effects on the ballistic penetration of graphene sheets. Sci Rep 2018. https://doi.org/10.1038/s41598-018-25050-2.

[60] Martirosyan KS, Zyskin M. Modeling and simulation of the elastic properties of kevlar reinforced by graphene. Graphene Sci Handb Size-Dependent Prop 2016:19–25. https://doi.org/10.1201/b19460-4.

[61] Lee C, Wei X, Kysar JW, Hone J. Measurement of the elastic properties and intrinsic strength of monolayer graphene. Science (80-) 2008. https://doi.org/10.1126/science.1157996.

[62] Meng Z, Han J, Qin X, Zhang Y, Balogun O, Keten S. Spalling-like failure by cylindrical projectiles deteriorates the ballistic performance of multi-layer graphene plates. Carbon N Y 2018. https://doi.org/10.1016/j.carbon.2017.10.068.

[63] Priyadarsini S, Mohanty S, Mukherjee S, Basu S, Mishra M. Graphene and graphene oxide as nanomaterials for medicine and biology application. J Nanostructure Chem 2018. https://doi.org/10.1007/s40097-018-0265-6.

[64] Vignesh S, Surendran R, Sekar T, Rajeswari B. Ballistic impact analysis of graphene nanosheets reinforced kevlar-29. Mater Today Proc 2020. https://doi.org/10.1016/j.matpr.2020.02.808.

[65] Costa UO, Nascimento LFC, Garcia JM, Monteiro SN, da Luz FS, Pinheiro WA, et al. Effect of graphene oxide coating on natural fiber composite for multilayered ballistic armor. Polymers (Basel) 2019. https://doi.org/10.3390/polym11081356.

[66] Zeng L, Liu X, Chen X, Soutis C. Surface Modification of Aramid Fibres with Graphene Oxide for Interface Improvement in Composites. Appl Compos Mater 2018. https://doi.org/10.1007/s10443-018-9718-9.

[67] Priya IIM, Vinayagam BK. Enhancement of bi-axial glass fibre reinforced polymer composite with graphene platelet nanopowder modifies epoxy resin. Adv Mech Eng 2018. https://doi.org/10.1177/1687814018793261.

[68] Liang JZ, Du Q, Tsui GCP, Tang CY. Tensile properties of graphene nano-platelets reinforced polypropylene composites. Compos Part B Eng 2016. https://doi.org/10.1016/j.compositesb.2016.04.011.

[69] Domun N, Hadavinia H, Zhang T, Liaghat G, Vahid S, Spacie C, et al. Improving the fracture toughness properties of epoxy using graphene nanoplatelets at low filler content. Nanocomposites 2017. https://doi.org/10.1080/20550324.2017.1365414.

[70] Ignatova A V., Kudryavtsev OA, Zhikharev M V. Influence of surface polymer coating on ballistic impact response of multi-layered fabric composites: Experimental and numerical study. Int J Impact Eng 2020. https://doi.org/10.1016/j.ijimpeng.2020.103654.

[71] Nayak N, Sivaraman P, Banerjee A, Madhu V, Dutta AL, Mishra VS, et al. Effect of matrix on the ballistic impact of aramid fabric composite laminates by armor piercing projectiles. Polym Compos 2012. https://doi.org/10.1002/pc.21259.

[72] Carrillo JG, Gamboa RA, Flores-Johnson EA, Gonzalez-Chi PI. Ballistic performance of thermoplastic composite laminates made from aramid woven fabric and polypropylene matrix. Polym Test 2012. https://doi.org/10.1016/j.polymertesting.2012.02.010.

[73] Bandaru AK, Chavan V V., Ahmad S, Alagirusamy R, Bhatnagar N. Ballistic impact response of Kevlar® reinforced thermoplastic composite armors. Int J Impact Eng 2016. https://doi.org/10.1016/j.ijimpeng.2015.10.014.

[74] Turner P, Liu T, Zeng X, Brown K. Three-dimensional woven carbon fibre polymer composite beams and plates under ballistic impact. Compos Struct 2018. https://doi.org/10.1016/j.compstruct.2017.10.091.

[75] Chatterjee VA, Verma SK, Bhattacharjee D, Biswas I, Neogi S. Manufacturing of dilatant fluid embodied Kevlar-Glass-hybrid-3D-fabric sandwich composite panels for the enhancement of ballistic impact resistance. Chem Eng J 2021. https://doi.org/10.1016/j.cej.2020.127102.

[76] Wonderly C, Grenestedt J, Fernlund G, Cěpus E. Comparison of mechanical properties of glass fiber/vinyl ester and carbon fiber/vinyl ester composites. Compos Part B Eng 2005. https://doi.org/10.1016/j.compositesb.2005.01.004.

[77] Mouritz AP. Ballistic impact and explosive blast resistance of stitched composites. Compos Part BEngineering 2001. https://doi.org/10.1016/S1359-8368(01)00015-4.

[78] Reddy PRS, Reddy TS, Madhu V, Gogia AK, Rao KV. Behavior of E-glass composite laminates under ballistic impact. Mater Des 2015. https://doi.org/10.1016/j.matdes.2015.06.094.

[79] Jordan JB, Naito CJ, Haque BZ. Quasi-static, low-velocity impact and ballistic impact behavior of plain weave E-glass/phenolic composites. J Compos Mater 2014. https://doi.org/10.1177/0021998313499952.

[80] Ali A, Adawiyah R, Rassiah K, Ng WK, Arifin F, Othman F, et al. Ballistic impact properties of woven bamboo- woven E-glass- unsaturated polyester hybrid composites. Def Technol 2019. https://doi.org/10.1016/j.dt.2018.09.001.

[81] Bergström J. Mechanics of Solid Polymers: Theory and Computational Modeling. 2015. https://doi.org/10.1016/C2013-0-15493-1.

[82] Panwar V, Pal K. Dynamic Mechanical Analysis of Clay-Polymer Nanocomposites. Clay-Polymer Nanocomposites, 2017. https://doi.org/10.1016/B978-0-323-46153-5.00012-4.

[83] Sastri VR. Materials Used in Medical Devices. Plast. Med. Devices, 2014. https://doi.org/10.1016/b978-1-4557-3201-2.00003-3.

[84] Petrović ZS, Ferguson J. Polyurethane elastomers. Prog Polym Sci 1991. https://doi.org/10.1016/0079-6700(91)90011-9.

[85] Gavgani JN, Adelnia H, Gudarzi MM. Intumescent flame retardant polyurethane/reduced graphene oxide composites with improved mechanical, thermal, and barrier properties. J Mater Sci 2014. https://doi.org/10.1007/s10853-013-7698-6.

[86] Joshi M, Adak B, Butola BS. Polyurethane nanocomposite based gas barrier films, membranes and coatings: A review on synthesis, characterization and potential applications. Prog Mater Sci 2018. https://doi.org/10.1016/j.pmatsci.2018.05.001.

[87] Zhai H, Euler A. Material challenges for lighter-than-air systems in high altitude applications. Collect. Tech. Pap. - AIAA 5th ATIO AIAA 16th Light. Syst. Technol. Conf. Balloon Syst. Conf., 2005. https://doi.org/10.2514/6.2005-7488.

[88] Mittal V. Elastomer clay nanocomposites for packaging. Adv Struct Mater 2011. https://doi.org/10.1007/978-3-642-15787-5_9.

[89] Wang X, Zhang J, Bao L, Yang W, Zhou F, Liu W. Enhancement of the ballistic performance of aramid fabric with polyurethane and shear thickening fluid. Mater Des 2020. https://doi.org/10.1016/j.matdes.2020.109015.

[90] Christopher G, Kulandainathan MA, Harichandran G. Biopolymers nanocomposite for material protection: Enhancement of corrosion protection using waterborne polyurethane nanocomposite coatings. Prog Org Coatings 2016. https://doi.org/10.1016/j.porgcoat.2016.05.012.

[91] Liu X, Hong W, Chen X. Continuous production of water-borne polyurethanes: A review. Polymers (Basel) 2020. https://doi.org/10.3390/polym12122875.

[92] İşmal ÖE, Paul R. Composite textiles in high-performance apparel. High-Performance Appar. Mater. Dev. Appl., 2017. https://doi.org/10.1016/B978-0-08-100904-8.00019-5.

[93] LaBarre ED, Calderon-Colon X, Morris M, Tiffany J, Wetzel E, Merkle A, et al. Effect of a carbon nanotube coating on friction and impact performance of Kevlar. J Mater Sci 2015. https://doi.org/10.1007/s10853-015-9088-8.

[94] Shanazari H, Liaghat GH, Hadavinia H, Aboutorabi A. Analytical investigation of high-velocity impact on hybrid unidirectional/woven composite panels. J Thermoplast Compos Mater 2017. https://doi.org/10.1177/0892705715604680.

[95] Martínez-Hergueta F, Ridruejo A, González C, Llorca J. Numerical simulation of the ballistic response of needle-punched nonwoven fabrics. Int J Solids Struct 2017.

https://doi.org/10.1016/j.ijsolstr.2016.11.031.

[96] Domun N, Hadavinia H, Zhang T, Sainsbury T, Liaghat GH, Vahid S. Improving the fracture toughness and the strength of epoxy using nanomaterials-a review of the current status. Nanoscale 2015. https://doi.org/10.1039/c5nr01354b.

[97] Wright WW. Kevlar aramid fiber. H. H. Yang. John Wiley & Sons, Chichester, 1993. pp. 200, price £39.95. ISBN 0-471-93765-7. Polym Int 1994. https://doi.org/10.1002/pi.1994.210330421.

[98] Naik NK, Shrirao P. Composite structures under ballistic impact. Compos Struct 2004. https://doi.org/10.1016/j.compstruct.2004.05.006.

[99] Bazhenov S. Dissipation of energy by bulletproof aramid fabric. J Mater Sci 1997. https://doi.org/10.1023/A:1018674528993.

[100] Liu X, Yu W, Pan N. Evaluation of high performance fabric under light irradiation. J Appl Polym Sci 2011. https://doi.org/10.1002/app.33200.

[101] Dobb MG, Robson RM, Roberts AH. The ultraviolet sensitivity of Kevlar 149 and Technora fibres. J Mater Sci 1993. https://doi.org/10.1007/BF01151257.

[102] Zhu Y, Bakis CE, Adair JH. Effects of carbon nanofiller functionalization and distribution on interlaminar fracture toughness of multi-scale reinforced polymer composites. Carbon N Y 2012. https://doi.org/10.1016/j.carbon.2011.11.001.

[103] Ma PC, Kim JK, Tang BZ. Effects of silane functionalization on the properties of carbon nanotube/epoxy nanocomposites. Compos Sci Technol 2007. https://doi.org/10.1016/j.compscitech.2007.05.006.

[104] Laurenzi S, Pastore R, Giannini G, Marchetti M. Experimental study of impact resistance in multi-walled carbon nanotube reinforced epoxy. Compos Struct 2013. https://doi.org/10.1016/j.compstruct.2012.12.002.

[105] Gibson J, McKee J, Freihofer G, Raghavan S, Gou J. Enhancement in ballistic performance of composite hard armor through carbon nanotubes. Int J Smart Nano Mater 2013. https://doi.org/10.1080/19475411.2013.870938.

[106] Pol MH, Liaghat GH, Hajiarazi F. Effect of nanoclay on ballistic behavior of woven fabric composites: Experimental investigation. J Compos Mater 2013. https://doi.org/10.1177/0021998312449768.

[107] Processing of Polymer Matrix Composites Containing CNTs. Carbon Nanotub. Reinf. Compos. CNR Polym. Sci. Technol., 2015. https://doi.org/10.1016/B978-1-4557-3195-4.00006-0.

[108] Agubra V, Owuor P, Hosur M. Influence of Nanoclay Dispersion Methods on the Mechanical Behavior of E-Glass/Epoxy Nanocomposites. Nanomaterials 2013. https://doi.org/10.3390/nano3030550.

[109] Taylor AC. Advances in nanoparticle reinforcement in structural adhesives. Adv. Struct. Adhes. Bond., 2010. https://doi.org/10.1533/9781845698058.1.151.

[110] Khodadadi A, Liaghat G, Vahid S, Sabet AR, Hadavinia H. Ballistic performance of Kevlar fabric impregnated with nanosilica/PEG shear thickening fluid. Compos Part B Eng 2019. https://doi.org/10.1016/j.compositesb.2018.12.121.

[111] Laha A, Majumdar A. Shear thickening fluids using silica-halloysite nanotubes to improve the impact resistance of p-aramid fabrics. Appl Clay Sci 2016. https://doi.org/10.1016/j.clay.2016.07.017.

[112] Khatiwada S, Armada CA, Barrera E V. Hypervelocity impact experiments on epoxy/ultra-high molecular weight polyethylene fiber composites reinforced with single-walled carbon nanotubes. Procedia Eng 2013;58:4–10. https://doi.org/10.1016/j.proeng.2013.05.003.

[113] Chinglenthoiba C, Ramkumar K, Shanmugaraja T, Sharma S. Study on Nanotechnology, Nanocoating and Nanomaterial. Int J Comput Aided Manuf 2017;3:17–25. https://doi.org/eISSN: 2456-642X.

[114] Barkoula NM, Alcock B, Cabrera NO, Peijs T. Flame-Retardancy Properties of Intumescent Ammonium Poly(Phosphate) and Mineral Filler Magnesium Hydroxide in Combination with Graphene. Polym Polym Compos 2008;16:101–13. https://doi.org/10.1002/pc.

[115] Gollins K, Delale F, Chiu J, Gursel A, Liaw B. Comparison of manufacturing techniques subject to high speed impact. ASME Int. Mech. Eng. Congr. Expo. Proc., 2014. https://doi.org/10.1115/IMECE2014-39677.

[116] Lin LY, Lee JH, Hong CE, Yoo GH, Advani SG. Preparation and characterization of layered silicate/glass fiber/epoxy hybrid nanocomposites via vacuum-assisted resin transfer molding (VARTM). Compos Sci Technol 2006. https://doi.org/10.1016/j.compscitech.2005.12.025.

[117] Kelkar AD, Tate JS, Chaphalkar P. Performance evaluation of VARTM manufactured textile composites for the aerospace and defense applications. Mater Sci Eng B Solid-State Mater Adv Technol 2006. https://doi.org/10.1016/j.mseb.2006.02.034.

[118] Zheng Y, Wang R, Dong X, Wu L, Zhang X. High Strength Conductive Polyamide 6 Nanocomposites Reinforced by Prebuilt Three-Dimensional Carbon Nanotube Networks. ACS Appl Mater Interfaces 2018. https://doi.org/10.1021/acsami.8b08944.

[119] Li Y, Zhong J, Wu L, Weng Z, Zheng L, Peng S, et al. High performance POSS filled nanocomposites prepared via UV-curing based on 3D stereolithography printing. Compos Part A Appl Sci Manuf 2019. https://doi.org/10.1016/j.compositesa.2018.11.024.

[120] Balla VK, Kate KH, Satyavolu J, Singh P, Tadimeti JGD. Additive manufacturing of natural fiber reinforced polymer composites: Processing and prospects. Compos Part B Eng 2019. https://doi.org/10.1016/j.compositesb.2019.106956.

[121] Mishra BP, Mishra D, Panda P, maharana A. An experimental investigation of the effects of reinforcement of graphene fillers on mechanical properties of bi-directional glass/epoxy composite. Mater Today Proc 2020. https://doi.org/10.1016/j.matpr.2020.03.154.

[122] Muhi RJ, Najim F, de Moura MFSF. The effect of hybridization on the GFRP behavior under high velocity impact. Compos Part B Eng 2009. https://doi.org/10.1016/j.compositesb.2009.08.002.

[123] Randjbaran E, Zahari R, Abdul Jalil NA, Abang Abdul Majid DL. Hybrid composite laminates reinforced with Kevlar/carbon/glass woven fabrics for ballistic impact testing. Sci World J 2014. https://doi.org/10.1155/2014/413753.

[124] Caminero MA, Rodríguez GP, Muñoz V. Effect of stacking sequence on Charpy impact and flexural damage behavior of composite laminates. Compos Struct 2016.

https://doi.org/10.1016/j.compstruct.2015.10.019.

[125] Gideon RK, Hu H, Wambua P, Gu B. Characterizations of basalt unsaturated polyester laminates under static three-point bending and low-velocity impact loadings. Polym Compos 2014. https://doi.org/10.1002/pc.22885.

[126] Pandey A, Muchhala D, Kumar R, S S, Venkat ANC, Mondal DP. Flexural deformation behavior of carbon fiber reinforced aluminium hybrid foam sandwich structure. Compos Part B Eng 2020. https://doi.org/10.1016/j.compositesb.2019.107729.

[127] Zulkifli F, Stolk J, Heisserer U, Yong ATM, Li Z, Hu XM. Strategic positioning of carbon fiber layers in an UHMwPE ballistic hybrid composite panel. Int J Impact Eng 2019. https://doi.org/10.1016/j.ijimpeng.2019.02.005.

[128] Afrouzian A, Movahhedi Aleni H, Liaghat G, Ahmadi H. Effect of nano-particles on the tensile, flexural and perforation properties of the glass/epoxy composites. J Reinf Plast Compos 2017. https://doi.org/10.1177/0731684417694753.

[129] Morton WE, Hearle JWS. Physical Properties of Textile Fibres: Fourth Edition. 2008. https://doi.org/10.1533/9781845694425.

[130] Fogle JG. Processing , Structure , and Properties of Nanoparticle Reinforced Nonwoven Sandwich Composites 2013.

[131] Menard K. An Introduction to Dynamic Mechanical Analysis. Dyn. Mech. Anal., 2008. https://doi.org/10.1201/9781420053135.ch1.

CHAPTER 3

Inorganic tungsten disulfide/waterborne polyurethane reinforced Spectra® fiber composites with improved mechanical and energy absorption properties[2]

[2] Wu. S. and Bhat, G. S. To be submitted to *Surface and Coatings Technology*.

Abstract

Fiber-based nanocomposites comprising high-performance fibers, nanomaterials, and polymer matrices play a significant role in bullet-resistant, anti-impact, aerospace, automotive, and construction applications. This research was conducted to determine the feasibility of incorporating tungsten disulfide (IF-WS_2)/waterborne-polyurethane (WPU) in varying water/ethanol mediums, and the effects of IF-WS_2/WPU impregnation on mechanical and energy absorption properties of ultra-high molecular weight polyethylene (UHMWPE) fibers. The tensile results indicate the maximum load, energy to break, and normalized energy to break increased by 28.8%, 29.1%, and 10.1% for 10 wt% WPU impregnated composites, and 26.5%, 44.9%, and 31.1% for the composites prepared with 2 wt% IF-WS_2/10 wt% WPU in water, respectively. Comparable improvements were observed for the composites optimized in water/ethanol mixture and ethanol mediums. However, WPU showed poor solubility in ethanol causing low distribution uniformity of IF-WS_2/WPU on UHMWPE fibers, which suggested pure ethanol was not a suitable dispersion medium for this application. The fiber failure mechanism for neat UHMWPE fibers showed fiber breakage, delamination, fibrillation, and splitting, while additional ductile breakage and matrix debonding were observed in WPU/IF-WS_2 reinforced specimens.

Keywords:

UHMWPE fiber, nanoparticles, waterborne polyurethane, mechanical properties, failure mechanism

3.1. Introduction

Nanomaterial and polymer matrix incorporated fiber-based composites have been extensively used in bullet-resistant and anti-impact areas such as body armors, aerospace, ballistic shields, and trauma plates [1][2][3]. This is due to their versatile properties and much higher strength-to-weight ratios compared to pure fibers and metal materials, which benefit the development of lightweight anti-ballistic materials for various end-uses. The properties of these nanocomposites are determined by various factors such as fiber properties, matrix type, matrix concentration, nanofiller type, nanofiller amount, and dispersion method [1][4]. Among common fiber materials, ultra-high molecular weight polyethylene (UHMWPE) fiber such as Spectra® or Dyneema® is one of the most promising high-performance fibers in personnel and vehicle ballistic protective applications [5][6][7]. This fiber possesses desired properties including extremely low density (0.97 g/cm^3), outstanding impact resistance, high specific toughness and tenacity, and good chemical resistance [7]–[10]. Polyurethane (PU) is a versatile class of elastomeric polymer formed with polyols and isocyanates [11]. Waterborne polyurethane (WPU), as the counterpart of solvent-borne PU (SPU), can be uniformly dispersed in an aqueous environment forming a binary colloidal system. By lowering volatile organic compound discharge, WPU leads to largely reduced environmental impact, thus it is often used as an alternative to conventional SPU [12][13]. Due to the existence of both “soft” (polyol) and “hard” (isocyanate) segments in its molecular structure, WPU confers well-balanced properties such as superb flexibility, high impact resistance, good abrasion resistance, and chemical resistance [14][15]. Therefore, WPU can be exploited in a wide range of commercial applications, for instance, corrosion protection, composite adhesives, elastomers, sealants, and leathers [16][17][18]. In this study, WPU is used as the polymer matrix

for fabricating soft fiber-based composites due to its high flexibility, good processability, high mechanical properties, and of course environmentally safer processing.

Inorganic tungsten disulfide (IF-WS_2) nanomaterial, commonly used as a lubricating additive, owns extremely low friction, high shock energy absorption (survives under pressure up to 25 GPa), good thermal stability (1000 °C), nontoxicity, biocompatibility, and superior cost-effective characteristics [19][20][21][22]. Due to these properties, IF-WS_2 nanomaterial has gained considerable attention in recent years. In early research, it has been utilized as an environmentally friendly reinforcing nanofiller in different polymer matrices to enhance their thermal, mechanical, impact resistance, or tribological properties [23][24][25]. IF-WS_2 incorporated composites can be used in applications including ballistic protection, automotive, aerospace, biomedical, etc [26][27]. Simić et.al studied the effect of IF-WS_2 on the thermo-mechanical and tribological properties of poly(vinyl butyral) (PVB) polymer. It was found that 1%-2% IF-WS_2 addition endowed the composite specimens increased glass transition temperature (T_g), elastic modulus, indentation hardness, and storage modulus, as well as reduced friction coefficient [26][28]. Similarly, Mojtabaei et al. investigated the influence of IF-WS_2 on the thermal properties of polypropylene/ethylene-vinyl acetate copolymer (PP/EVA) blends, the results indicated that IF-WS_2 addition improved the copolymer blend's thermal stability with higher melting/crystallization temperatures and lower degradation rate [29]. In a later publication, Simić et.al further explored the mechanical properties of PVB/WS_2 films and impact resistance of Kevlar®/IF-WS_2/PVB composites, and the results suggested that incorporating 3 wt% IF-WS_2 increased the maximum load, elongation, and tensile strength of the composite films. Meanwhile, adding IF-WS_2 enhanced the impact toughness and energy absorption function of certain Kevlar® fiber-reinforced polymer nanocomposites [30]. In most research involving IF-WS_2 nanofillers,

solvent-based polymer matrices such as PVB, phenolic resin, PP, EVA, and poly (phenylene sulfide) (PPS) have been reported [31][32][33][34]. From the published literature, it is evident that the combination of IF-WS_2 nanoparticles with WPU has not been explored. Furthermore, the influence of incorporating IF-WS_2/WPU on the mechanical and energy absorption properties of UHMWPE fibers has not been studied. Therefore, to fill the research gap, this work was conducted to investigate UHMWPE fiber-based flexible IF-WS_2/WPU composites. To find proper homogenization methods for preparing IF-WS_2/WPU nanofluids, varying dispersing mediums with water, ethanol, and water/ethanol mixture have been used. The effects of several component variables on the mechanical and energy absorption properties of the composites were investigated.

3.2. Materials and Methods

3.2.1. Materials

The UHMWPE yarn (Spectra® 1600, continuous untwisted multifilament) was supplied by Honeywell International Inc., USA. The physical and mechanical properties of the UHMWPE yarn are shown in Table 3.1. Waterborne PU dispersion Permax™ 202 (polyether polyol type; solid content = 41%; viscosity = 1 Pa·s) was obtained from Lubrizol Corp., USA. Inorganic fullerene-like tungsten disulfide (IF-WS_2) water-based dispersion (IW-4000; density: 1.44-1.80 g/cm^3) was obtained from Nanotech Industrial Solutions Inc., USA. The IF-WS_2 particles were reported to have a multi-layered spheric to ellipsoidal structure and an aspect ratio of 1-2.3 [29]. The particle diameter ranges from 20 nm to 80 nm (Figure 3.1), and the size of 20 measurements is 46 ± 15 nm on average.

Table 3.1. The physical properties of the UHMWPE yarns from the manufacturer.

Property	Linear density (denier)	Density (g/cm^3)	Filament number	Fiber Diameter (μm)
Spectra®-1600	1600	0.97	360	34

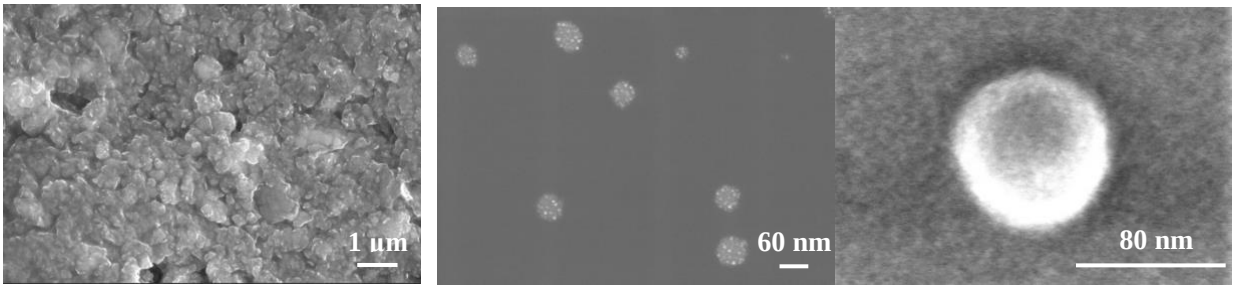

(a) (b) (c)

Figure 3.1. IF-WS_2 nanoparticle images: (a) Scanning Electron Microscopy (SEM); (b) Scanning transmission electron microscopy- high-angle annular dark-field (STEM-HAADF); (c) Scanning transmission electron microscopy-secondary electron (STEM-SE).

3.2.2. Sample preparation

In this research, diluted WPU dispersions and WPU/IF-WS_2 mixtures in different mediums (water, ethanol, water/ethanol) were prepared for Spectra® yarn coating. Deionized (DI) water was used for all samples in this work. To prepare WPU coating fluids, the WPU dispersion was added into the water according to the designed weight ratios, the WPU/water mixtures were then sonicated for 15 min using a Kendal ultrasonic bath. For WPU/IF-WS_2 dispersion preparation, the selected dispersing medium was weighed (and mixed manually when water/ethanol was used), then the required amounts of IF-WS_2 were added into the medium followed by ultrasonication of the mixture for 30 min. During sonication, the cap of the container (centrifuge tube or glass vial used here) was opened for 1-2 seconds after the first 15 min to release the generated heat from the dispersion and prevent WPU solidification due to excessive heating. After the initial sonication, a calculated amount of WPU dispersion was added to the prepared nanofluid, and homogenization

was continued with ultrasonication for another 30 min. Similarly, the container cap was removed for 1-2 seconds after the initial 15 min. Water in the ultrasonication bath was replaced with cool tap water every 30 min of operation so that the water temperature could be maintained in the range of 22.0°C - 25.2°C. For the preparation of WPU or WPU/IF-WS_2 incorporated Spectra® composites, Spectra® filament yarns (length of 30cm) were soaked in the dispersions for 1 min. After the impregnation, the yarns were air-dried at room temperature for 30 min and heated in an oven at 60°C overnight to evaporate complete amount of water and/or ethanol, during which, WPU and WPU/IF-WS_2 mixtures form solid films impregnating the yarns.

To check the effects of water and ethanol dispersing mediums on the stability of WPU/IF-WS_2 dispersions, three different WPU/IF-WS_2 mixtures (denoted as W, WE, and E) were first prepared using water, water/ethanol mixture, and ethanol mediums as shown in Table 3.2. Dispersion stability was visually evaluated regarding the appearance and amount of IF-WS_2 sediment in the samples as prepared, after 1 hour, 1 day, 8 days, and 14 days [35].

To produce Spectra®/WPU composites, WPU dispersions were prepared with 5 levels of WPU liquid amount in water: 5 wt%, 10 wt%, 20 wt%, 100 wt%, 200 wt% regarding the medium weight. WPU impregnated yarns were fabricated by the same procedure. Similarly, for making Spectra®/WPU/IF-WS_2 nanocomposites, varying WPU/IF-WS_2 nanofluids were prepared in water with seven levels of IF-WS_2 amount: 0 wt%, 0.25 wt%, 0.5 wt%, 1.0 wt%, 2.0 wt%, 4.0 wt%, 8.0 wt% with respect to the total weight of medium and WPU. In these nanofluids, the WPU amount was kept constant at 10 wt%. After preparing the dispersions, WPU/IF-WS_2 impregnated Spectra® yarns were produced for each combination.

Additionally, water and ethanol with different weight ratios: 1:5, 1:3, 1:1, 3:1, 5:1 were mixed and used as the dispersion mediums. Five homogeneous WPU/IF-WS_2 nanofluids were

prepared. in which, 10 wt% of WPU in water and 2 wt% of IF-WS_2 were added. Similarly, Spectra®/WPU/IF-WS_2 composites were produced with the nanofluids and Spectra® yarns. Furthermore, Spectra® composites were also fabricated with WPU/IF-WS_2 dispersions prepared in ethanol, which contain 2 wt% of IF-WS_2 and varying amounts of WPU: 0.33 wt%, 1.00 wt%, 1.67 wt%, 10 wt%.

Table 3.2. Components of the three WPU/IF-WS_2 dispersions prepared.

Sample code	W	WE	E
Dispersion medium	water	water: ethanol (1:1 wt%)	ethanol
WPU amount/ wt%		10	
IF-WS_2 amount/ wt%		3.6	

3.2.3. Characterization

3.2.3.1. Linear density

After the fabrication process, the mass of individual samples (length of 30cm) for neat Spectra® yarns, Spectra®/WPU yarns, and Spectra/WPU/IF-WS_2 yarns was measured using an electronic microbalance. The linear density, expressed in the unit of denier (g of 9000m), for each specimen was calculated using equation (3.1).

$$Linear\ density\ (\text{denier}) = \frac{Sample\ mass\ (g)}{Sample\ length\ (m)} \times 9000 \qquad (3.1)$$

3.2.3.2. Tensile Testing

The yarn tensile test was conducted according to ASTM standard 2256 standard using a universal tensile test machine Instron 4400R. Since the Spectra® fiber possesses extremely high tensile strength and smooth fiber surface, its yarn and fiber slippage during tensile tests has always been a major challenge for researchers to accurately measure its tensile strength [36][37]. In this

work, Capstan yarn grips shown in Figure 3.2 (a) were installed to reduce yarn slippage and jaw breaks for the untwisted Spectra® filament yarns during tensile tests [38][39]. The gauge length of 100mm and extension rate of 100mm/min were used. To further avoid slippage, each yarn (length of 300mm) was glued on two pieces of cardboards (size: 16mm × 29mm) using ELMER'S Washable Clear Glue as shown in Figure 3.2 (b) [40][41]. The glued yarns were left at room temperature overnight to completely dry. After which, the prepared specimens were tested. Maximum load (ML) and elongation at break were recorded.

From the tensile test data, the energy to break (EB) (J), also called total energy absorbed or work of rupture, of a sample was calculated by integrating the area under the force-elongation curve as shown in equation (3.2). And normalized energy to break (NEB) or gravimetric toughness (J/g) of a specimen was calculated using equation (3.3) [42]. At least 3 replicates were used, and the mean values are presented.

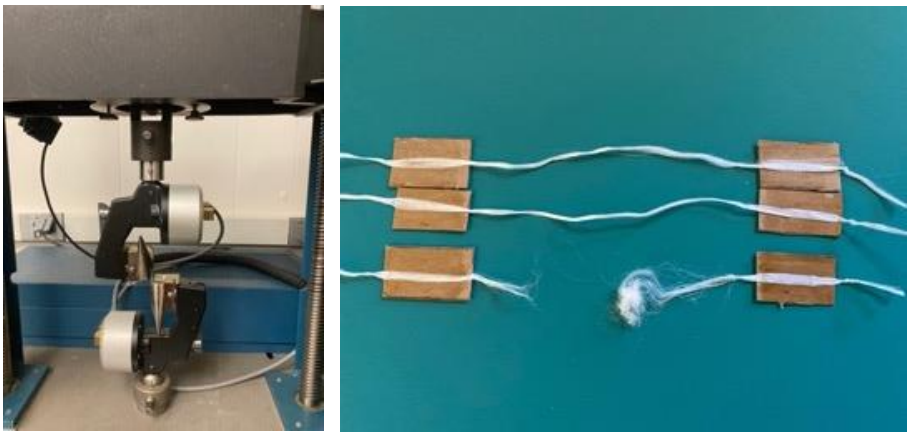

(a) (b)

Figure 3.2. Yarn tensile test: (a) the capstan grips used; (b) glued neat yarns and a neat yarn after the test.

$$EB(J) = \int_0^{l_{break}} F \cdot dl \tag{3.2}$$

Where F is the load on the material, l is the material length.

$$NEB\ (J/g) = \frac{9000 \times EB}{Linear\ density \times initial\ length} \quad (3.3)$$

3.2.3.3. Scanning Electron Microscopy (SEM) and Energy-dispersive X-ray spectroscopy (EDX)

The microscopic analysis of fiber surface morphology, material structure, WPU distribution on the fiber surface, and fiber failure mechanisms were performed using a Thermo Fisher Scientific Teneo FE-SEM. The samples were gold-coated before the SEM characterizations. The acceleration voltage of 5-10 kV and magnifications of ×500 and ×1000 was applied. The yarn morphology and fiber failure after the tensile test for the neat and impregnated specimens were observed using SEM. Along with the SEM instrument, an equipped EDX detector (150 mm Oxford XMaxN) was adopted to detect elements such as tungsten (W), sulfur (S), and oxygen (O), and map the distributions of these elements on impregnated yarns. From the mapping images, the distribution uniformity of IF-WS_2 nanoparticles and WPU on the specimens were evaluated [30].

3.3. Results and Discussion

3.3.1. IF-WS_2/WPU dispersion stability

To study the effects of water and ethanol related mediums on the stability of IF-WS_2 nanoparticles in WPU/medium dispersions, three WPU/IF-WS_2 mixtures were prepared. The dispersing mediums include water (W), ethanol (E), and water: ethanol wt%=1:1 (WE). Figure 3.3 shows the appearances of these suspensions after extended storage time: (a) as prepared, (b) 1 hour, (c) 1 day, (d) 8 days, and (e) 14 days. As seen in the images, the prepared WPU/IF-WS_2 dispersions showed color variation, which is attributed to the difference in distribution uniformity/stability of IF-WS_2 nanoparticles (yellow-brown color) in water, ethanol, and water/ethanol mixture, as well as the difference in PU (milk white) solubility in these three

mediums. All three dispersions were uniform in color and showed no nanoparticles on the bottom of the glass vials as prepared. Visible changes such as stratification or phase separation were not observed for their liquid phases even after 14 days. However, from the bottom of the glass containers, a very small amount of IF-WS_2 sediment was found in samples W and WE after 1 and 8 days, respectively. More sediment details are listed in Table 3.3. According to the table, the stability order of IF-WS_2 nanoparticles in W, WE, and E can be determined as E>WE>W. Meanwhile, based on the ease of dispersing WPU in the mediums and the amount of WPU settled in each specimen after 14 days which is not listed in the table, the order of WPU solubility in the three mediums can be considered as W>WE>E. Overall, IF-WS_2 nanoparticles showed good stability in all three mediums for 1 hour, which is adequate for completing the impregnation process for Spectra® yarns. Thus, these three medium systems were further explored for preparing Spectra®/WPU/IF-WS_2 nanocomposite. Process optimization with variables such as WPU amount, IF-WS_2 amount, or water: ethanol weight ratio was carried out in varying mediums.

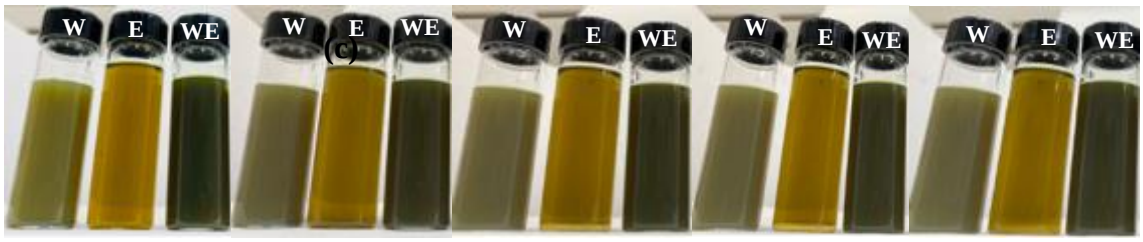

(a) (b) (c) (d) (e)

Figure 3.3. WPU/IF-WS_2 dispersions in different dispersing mediums (left to right: W-water; E-ethanol; WE-water/ethanol mixture with weight ratio=1:1): (a) as prepared; (b) after 1 hour; (c) after 1 day; (d) after 8 days; (e) after 14 days.

Table 3.3**.** Visual evaluation of WS_2 sediment amount for the prepared WPU/WS_2 dispersions after varying times.

	Sediment observed		
Sample	W	WE	E
As prepared	No	No	No
After 1 hour	No	No	No
After 1 day	very small amount	No	No
After 8 days	more	very small amount	No
After 14 days	more	more	No

3.3.2. Effects of WPU and IF-WS_2 amounts in water

To investigate the influence of WPU amount on the mechanical and energy absorption properties of Spectra®/WPU composites, 5 levels of WPU amount: 5 wt%, 10 wt%, 20 wt%, 100 wt%, 200 wt% were used with water, and corresponding Spectra®/WPU composites were fabricated. Figure 3.4 shows the tensile properties of neat and impregnated Spectra® yarns. Average values of their maximum load, energy to break, and normalized energy to break are presented. According to the one-way ANOVA analysis results (Table 3.4), the amount of WPU added significantly affected the ML, EB, and NEB of the fabricated composites at the confidence levels of 99.9%, 95%, and 99.9%, respectively. Their p-values are 0.0003, 0.0124, and <0.0001 in order. With a higher amount of WPU, the ML, EB, and NEB of the specimens exhibited a similar trend, that is initial increase up to 10%, followed by decrease with additional add on. With 10% WPU addition, the ML, EB, and NEB of the composites improved by 28.8%, 29.1%, and 10.1%, respectively, compared to that of neat Spectra® yarns. Among studied WPU amounts, elongation at break of the specimens was maintained in the range of 2.8%-3.5% with no significant difference.

Then seven nanocomposites were fabricated with varying levels of IF-WS_2 amounts: 0 wt%, 0.25 wt%, 0.50 wt%, 1 wt%, 2 wt%, 4 wt%, and 8 wt%. by impregnating individual yarns in the WPU (10 wt%)/IF-WS_2 mixtures. Tensile properties of the WPU and WPU/IF-WS_2

incorporated Spectra® composites are shown in Figure 3.5. The result from one-way ANOVA analysis shown in Table 3.5 reveals that, at a 95% confidence level, the IF-WS_2 addition amount significantly affects both maximum load and normalized energy to break of the Spectra® composites. The related p-values are 0.0240 and 0.0409, respectively. Increasing IF-WS_2 amount from 0% first leads to slight decrease in ML, EB, and NEB of the Spectra®/IF-WS_2/WPU composites, then slight increase at 1% and 2% IF-WS_2, followed by again small decreases at 4% and 8% IF-WS_2. This observed trend can be related to the balance between WPU and IF-WS_2 nanoparticle reinforcements. When the IF-WS_2 amount is low, the impregnated WPU matrix plays a major role in improving the energy absorption capability of the specimens. Adding a small amount of IF-WS_2 reduces the integrity of WPU films on fiber surface, negatively affecting the toughness of the WPU composites. With increasing IF-WS_2 amount (1% and 2%), the nanoparticle reinforcement can compensate for the integrity loss of WPU films resulting in higher overall tensile strength and toughness for the composites. Further increasing IF-WS_2 amount beyond 2 wt% may cause nanoparticle clusters on fiber surface. Besides, with a constant WPU amount, excess nanoparticles show poor adhesion to Spectra® filaments. Among the samples investigated, 2% of IF-WS_2 showed the highest EB and NEB enhancements. The ML, EB, and NEB of the Spectra®/IF-WS_2/WPU composites increased by 26.5%, 44.9%, and 31.1%, respectively, compared to that of neat yarns. It means, after normalization, with the same material weight, the total energy absorbed by the specimens before rupture improved by 31.1%. This is highly beneficial for developing lightweight and advanced energy absorption materials.

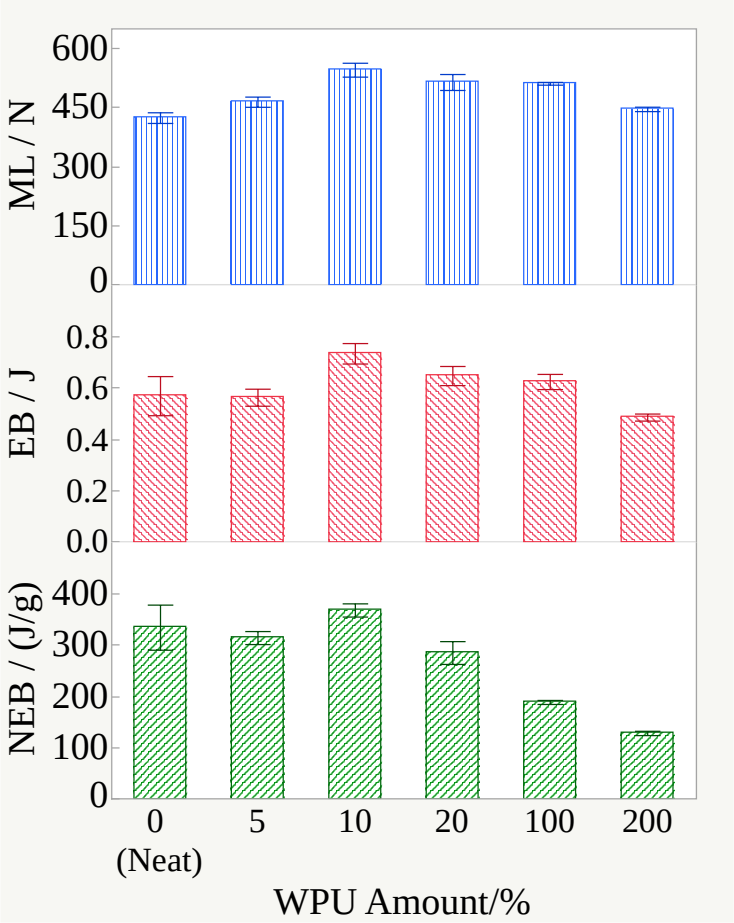

Figure 3.4. Tensile properties (mean and SE) of neat and WPU impregnated Spectra® yarns with different amounts of WPU used. (a) ML: maximum load; (b) EB: energy to break; (c) NEB: normalized energy to break.

Table 3.4. ANOVA table for the effect of WPU addition amount on maximum load, energy to break, and normalized energy to break of WPU impregnated Spectra® yarns.

Property	Source	DF	Sum of Squares	Mean Square	F Ratio	Prob > F
Maximum load	WPU amount	5	38011.335	7602.27	9.0998	0.0003
	Residual	16	13366.972	835.44		
	Total	21	51378.308			
Energy to break	WPU amount	5	0.13088909	0.026178	4.2055	0.0124
	Residual	16	0.09959452	0.006225		
	Total	21	0.23048360			
Normalized energy to break	WPU amount	5	140587.98	28117.6	19.5008	<.0001
	Residual	16	23069.91	1441.9		
	Total	21	163657.88			

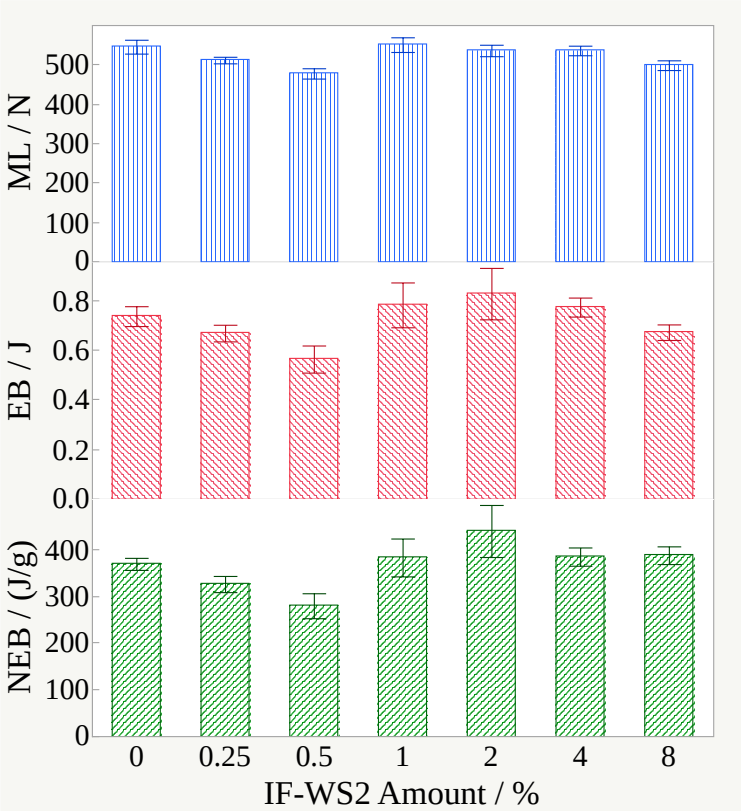

Figure 3.5. Tensile properties (mean and SE) of IF-WS_2/WPU impregnated Spectra® yarns with different IF-WS_2 amounts used. (a) ML: maximum load; (b) EB: energy to break; (c) NEB: normalized energy to break.

Table 3.5. ANOVA table for the effect of IF-WS_2 addition amount on maximum load and normalized energy to break of the Spectra®/IF-WS_2/WPU yarns.

	Source	DF	Sum of Squares	Mean Square	F Ratio	Prob > F
Maximum load	IF-WS_2 amount	6	14268.223	2378.04	3.3782	0.0240
	Residual	16	11262.908	703.93		
	Total	22	25531.131			
Normalized energy to break	IF-WS_2 amount	6	47003.307	7833.88	2.9109	0.0409
	Residual	16	43059.523	2691.22		
	Total	22	90062.830			

3.3.3. Effect of water/ethanol ratio in mixture medium

Water and ethanol mixtures with varying weight ratios (1:5, 1:3, 1:1, 3:1, and 5:1) were used as dispersing mediums to prepare (2 wt%) WS_2/ (10 wt%) WPU fluids. Adequate solubility and stability of WPU and IF-WS_2 nanoparticles in the mixed mediums were observed. Water and ethanol components in the mediums ensured the uniform distribution of WPU and IF-WS_2 nanoparticles, respectively. As water and ethanol are completely miscible, IF-WS_2 nanoparticles and WPU added can be mixed properly in prepared dispersions. The influence of water: ethanol weight ratio on the tensile properties of IF-WS_2/WPU impregnated yarns was studied. As listed in Table 3.6, the results depicted that, among the five water/ethanol weight ratios, the maximum average values for ML, EB, and NEB of the specimens were obtained at the weight ratio of 1:5. However, the one-way ANOVA analysis result suggested that the outcomes were not significantly different within the studied weight ratios, at a 95% confidence level. The p-values for these three properties were greater than 0.05. It means, within the designed range, the water: ethanol weight ratio in the mixture medium shows no significant effect on the studied tensile and energy absorption properties of the composites, when 10 wt% WPU and 2 wt% IF-WS_2 is used. Compared

to neat yarns, the ML, EB, and NEB of the WPU/IF-WS_2 reinforced Spectra® yarn improved up to 28.2%, 43.5%, and 35.3%, respectively.

Table 3.6. Tensile properties (mean and SE) of the neat and WPU/WS_2 impregnated yarns in various water/ethanol mediums.

Sample		Maximum load / N	Energy to break / J	Normalized energy to break / (J/g)
Water: ethanol weight ratio	1:5	542.46 ± 1.56	0.82 ± 0.00	452.63 ± 3.22
	1:3	506.36 ± 19.32	0.70 ± 0.09	366.88 ± 45.24
	1:1	513.33 ± 18.54	0.71 ± 0.06	374.47 ± 30.92
	3:1	512.66 ± 17.17	0.72 ± 0.06	366.21 ± 30.49
	5:1	515.40 ± 10.31	0.69 ± 0.05	354.75 ± 27.46
Neat yarn		423.20 ± 13.59	0.57 ± 0.08	334.53 ± 44.11

3.3.4. Effect of WPU amount in ethanol

In the stability comparison, IF-WS_2 nanoparticles showed uniform distribution and higher stability in ethanol compared to them in water and water/ethanol mediums. To explore whether adopting an ethanol medium can further strengthen the Spectra®/IF-WS_2/WPU composites, Spectra® yarns were impregnated with WPU/ (2%) IF-WS_2 fluids, in which pure ethanol medium was used. 3 levels of PU amount (0.33 wt%, 1.00 wt%, 1.67 wt%, 10 wt%) were used. Reduced amounts of WPU were chosen due to the low solubility of the WPU observed in ethanol. The average values for ML, EB, and NEB of the Spectra®/IF-WS_2/WPU specimens are plotted in Figure 3.6. At the WPU amounts of 1.67% and 10%, all three outcomes dropped to a varying degree. Through one-way ANOVA analysis, a significant effect of WPU amount was detected on normalized energy to break of fabricated composites at a 99% confidence level (Table 3.7). The obtained p-value is $0.0019 < 0.01$. With 1% WPU addition, promising comprehensive property

improvements were observed for the impregnated Spectra® samples, as the ML, EB, and NEB of the composite yarns increased by 26.1%, 45.3%, and 34.2%, respectively, compared to those of neat yarns.

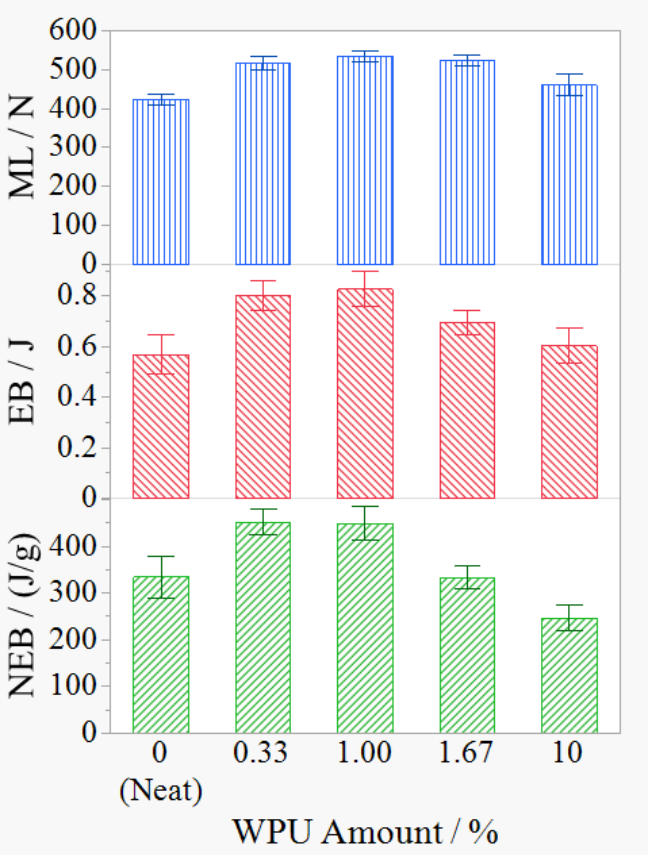

Figure 3.6. Tensile properties (mean and SE) of neat and WPU/IF-WS_2 impregnated yarns with varying WPU amounts in ethanol medium. (a) ML: maximum load; (b) EB: energy to break; (c) NEB: normalized energy to break.

Table 3.7. ANOVA table for the effect of WPU amount in ethanol on normalized energy to break of IF-WS_2/WPU impregnated Spectra®yarns.

Source	DF	Sum of Squares	Mean Square	F Ratio	Prob > F
IF-WS_2 amount	3	95636.54	31878.8	9.2575	0.0019
Residual	12	41322.99	3443.6		
Total	15	136959.53			

3.3.5. Surface morphology

To study the impact of WPU coating on the surface morphology of Spectra® yarns, SEM was used to observe the WPU yarnas impregnated with varying WPU dispersions. As shown in Figure 3.7, WPU were evenly distributed on prepared specimens, and no obvious WPU polymer clusters were observed. The dispersed WPU formed uniform and smooth films impregnating Spectra® filament surface after drying. Increasing WPU amount led to thicker polymer films with larger areas bonding a higher number of filaments. As analyzed in section 3.2, 10 wt% WPU addition resulted in better tensile and energy to break properties for the WPU/Spectra® composites than other WPU amounts studied. This is because when the PU amount is low, the Spectra® component plays a major role in the overall properties of the material. A higher WPU amount gives better adhesion bonding among the filaments, which turns the bundle of filaments into strongly united WPU/Spectra® threads as observed in SEM images. Thus, the WPU coating improves the load-carrying capability and energy absorption properties of the Spectra® yarns. However, compared to high-performance Spectra® yarns, WPU polymer material has much lower mechanical strength. When the WPU amount rises over the optimal amount (10 wt%), WPU property contribution to the composites based on the 'rule of mixture' surpasses the strength-enhancing effect due to WPU bonding [43]. This ultimately causes the decline of ML and EB of the composites. Along with additional WPU weight, the NEB capacity of the WPU/Spectra® composites is further reduced.

For Spectra®/IF-WS_2/WPU specimens, EDX was applied to map the distributions of IF-WS_2 nanoparticles and WPU polymer on the filaments. Three samples prepared with the following dispersions were tested: (a) 10 wt% WPU/ 2 wt% IF-WS_2 in water, (b) 10 wt% WPU/2 wt% IF-WS_2 in water/ethanol (1:5) mixture,and (c) 1 wt% WPU, 2 wt% IF-WS_2 in ethanol. Under these

three conditions, the fabricated composites achieved comparable tensile property and energy absorption enhancements. As shown in Figure 3.8, IF-WS_2 nanoparticle and WPU distributions on impregnated yarns were mapped according to the detected tungsten (W)/sulfur (S) and oxygen (O) atoms, respectively. From the images, the highest distribution uniformity for IF-WS_2 nanoparticles and WPU can be observed on specimen (a). The uniformity order of their distributions on the three samples can be evaluated as (a) > (b) > (c). This is attributed to the better dispersion ability of WPU polymer in water than in the other two medium systems, while IF-WS_2 particles also showed fair stability in water, as observed in section 3.1. With an increasing amount of ethanol in the medium, WPU dispersion ability decreases resulting in WPU aggregations and lower distribution uniformity of WPU on the filaments.

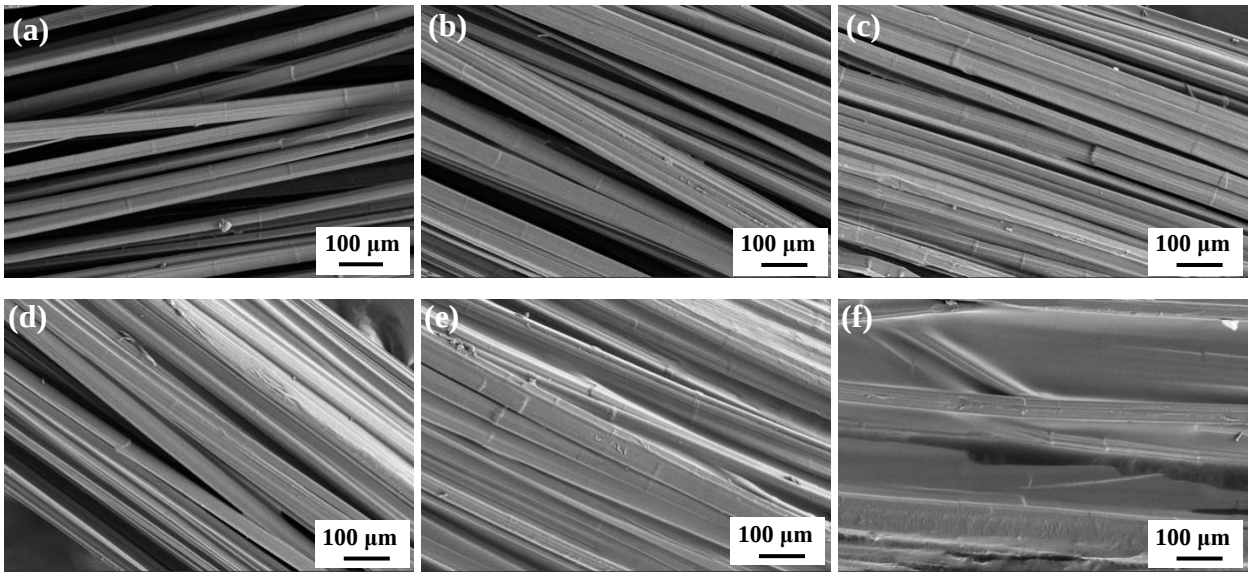

Figure 3.7. SEM images of WPU impregnated Spectra® yarns with varying WPU amounts. (a) 0 wt%, (b) 5 wt%, (c) 10 wt%, (d) 20 wt%, (e) 100 wt%, (f) 200 wt%.

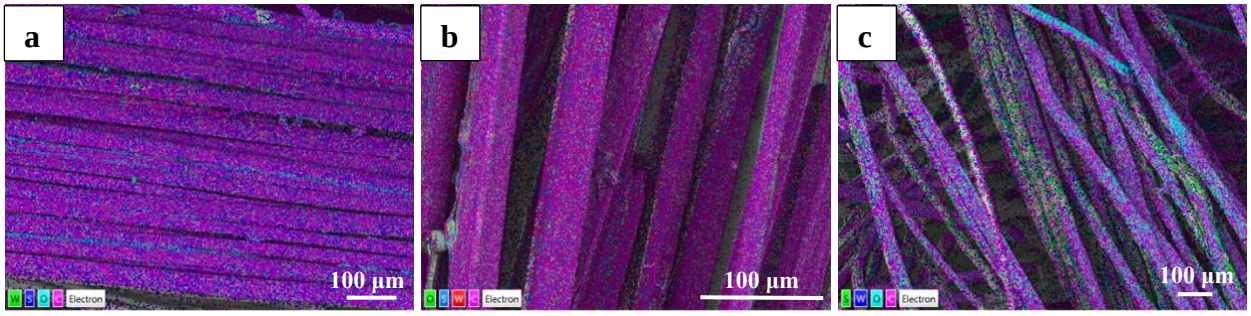

Figure 3.8. EDX images of elements C, O, S, and W for WPU/IF-WS_2 impregnated Spectra® yarns prepared in three dispersions: (a) 10 wt% WPU and 2 wt% IF-WS_2 in water. (b) 10 wt% WPU and 2 wt% IF-WS_2 in water/ethanol (1:5) mixture. (c) 1 wt% WPU and 2 wt% IF-WS_2 in ethanol.

3.3.6. Fiber failure mechanism

Fiber failure mechanisms of neat and IF-WS_2/WPU impregnated yarns were studied using SEM. After tensile tests, filament fractures of four specimens were observed, which included neat Spectra® yarn and three composite yarns prepared with 10 wt% WPU/2 wt% IF-WS_2 in water (S1), 10 wt% WPU/2 wt% IF-WS_2 in water/ethanol (1:5) mixture (S2), or 1 wt% WPU/2 wt% IF-WS_2 in ethanol (S3). As shown in Figure 3.9 (a-c), fibers in the neat yarn broke under tension mainly due to fiber breakage, splitting, delamination, and fibrillation. While additional failure mechanisms including ductile breakage and matrix/fiber debonding or adhesion failure were observed with S1 and S2 (Figure 3.9 (d-i)) [44]. Thus, apart from the energy absorption function of IF-WS_2 nanoparticles, additional WPU-involved failure mechanisms also contribute to the total energy to break increase for the composites [45]. In sample S3, more fiber breakage was spotted compared to the other two impregnated specimens due to its lower WPU addition (Figure 3.9 (j-l)). Overall, based on previous stability and EDX results, pure ethanol medium is not suitable for preparing WPU/IF-WS_2 fluids due to several limitations, which include the processing difficulty regarding dispersing WPU, low distribution uniformity of WPU/IF-WS_2 on Spectra® filaments, and ethanol's volatile property.

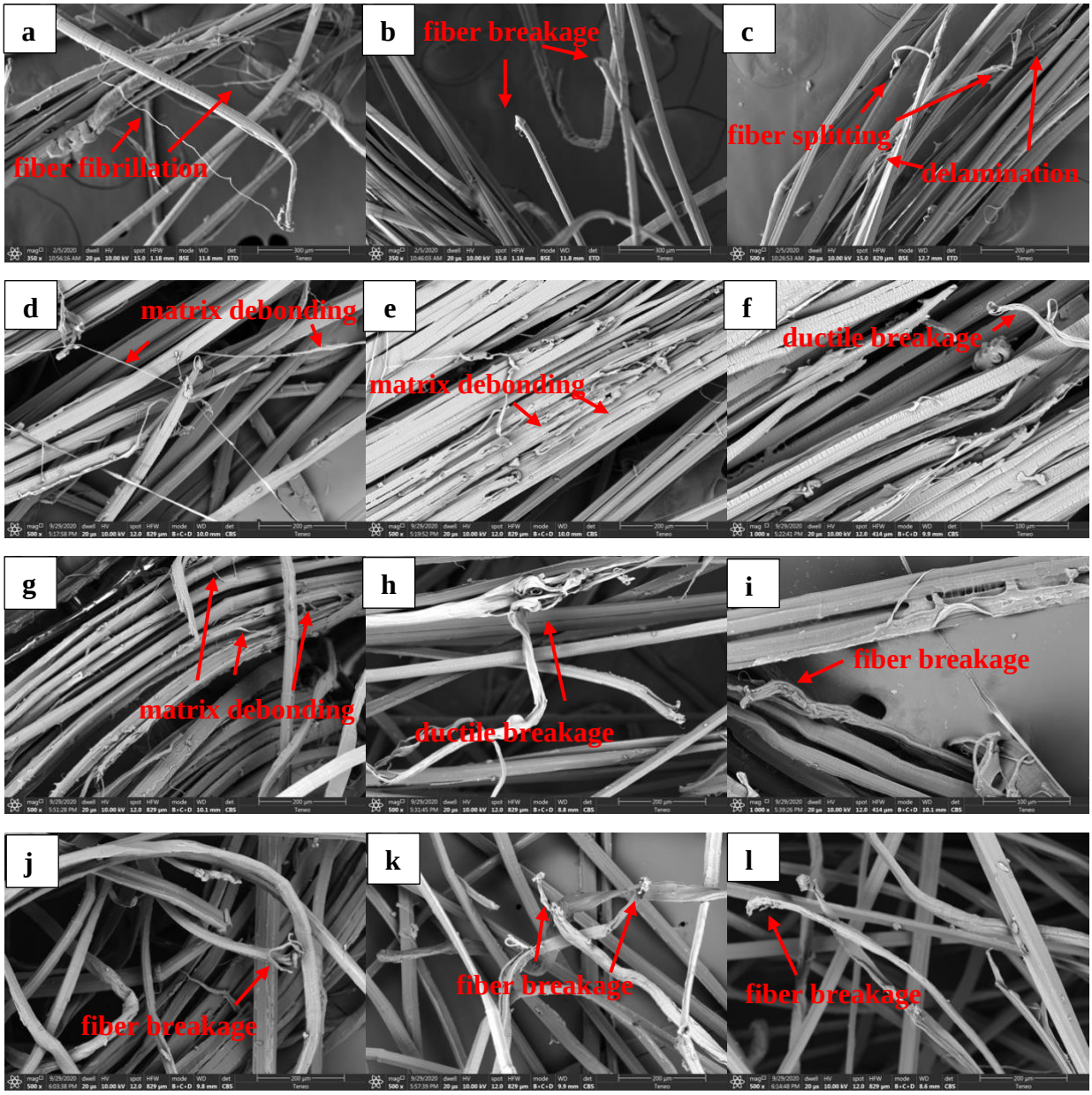

Figure 3.9. SEM images of fiber fracture for neat yarn and WPU/IF-WS_2 impregnated Spectra® yarns S1-S3. (a-c) Neat yarn. (d-f) S1, prepared with 10 wt% WPU/2 wt% IF-WS_2 in water; (g-i) S2, prepared with 10 wt% WPU/2 wt% IF-WS_2 in water/ethanol (1:5) mixture; (j-l) S3, prepared with 1 wt% WPU/2 wt% IF-WS_2 in ethanol.

3.4. Summary

Flexible Spectra®/IF-WS_2/WPU composites were fabricated through the impregnation method in this research. Three dispersion medium systems: water, water/ethanol mixture, and

ethanol were explored for preparing homogeneous IF-WS_2/WPU nanofluids. In all three mediums, IF-WS_2 nanoparticles showed high distribution uniformity with its stability order of ethanol >water/ethanol mixture >water. WPU solubility order was observed as water > water/ethanol > ethanol. The fabrication process in each system was optimized in terms of WPU amount, IF-WS_2 amount, or water/ethanol weight ratio. 10 wt% WPU in water was used for elastomeric coating on Spectra® yarns, which conferred a 28.8%, 29.1%, and 10.1% increase on the maximum load, energy to break, and normalized energy to break respectively for the impregnated yarns, compared to those of neat yarns. With an additional 2 wt% IF-WS_2 used in the dispersion (8.8 wt% WPU + 2.3 wt% IF-WS_2 on the yarn by calculation), the same properties of the Spectra®/IF-WS_2/WPU composites increased by 26.5%, 44.9%, and 31.1%, respectively. Using the other two medium systems, comparable property enhancements were obtained for the optimized composites.

The SEM and EDX images indicated that highest distribution uniformity of WPU and IF-WS_2 was achieved on the impregnated yarn using water medium followed by water/ethanol mixture, and then ethanol medium. Pure ethanol turned out to be an unsuitable dispersing medium for preparing IF-WS_2/WPU fluids due to the low solubility of WPU in ethanol, and its volatile nature, which result in poor coating uniformity on yarns. The two promising mediums: water and water/ethanol mixture can be further investigated for their impacts on the continuous fabrication of Spectra® yarn/WPU/IF-WS_2 composites. During tensile tests, neat yarns failed due to fiber breakage, splitting, delamination, and fibrillation, while WPU/IF-WS_2 impregnated yarns showed additional WPU/fiber adhesion failure and more ductile failure. Along with nanoparticle reinforcement, IF-WS_2/WPU/Spectra® composites achieved enhanced mechanical strength and energy absorption properties. With a 31.1%-35.3% increase in normalized energy absorption capacity, environmentally friendly components, and low processing cost advantages, the

developed materials can be further studied for advanced lightweight high-performance applications.

3.5. References

[1] S. Clifton, B. H. S. Thimmappa, R. Selvam, and B. Shivamurthy, "Polymer nanocomposites for high-velocity impact applications-A review," *Compos. Commun.*, vol. 17, no. August 2019, pp. 72–86, 2020.

[2] U. A. Shakil, S. Bin Abu Hassan, M. Y. Yahya, Mujiyono, and D. Nurhadiyanto, "A review of properties and fabrication techniques of fiber reinforced polymer nanocomposites subjected to simulated accidental ballistic impact," *Thin-Walled Structures*. 2021.

[3] E. J. Siochi and J. S. Harrison, "Structural nanocomposites for aerospace applications," *MRS Bull.*, 2015.

[4] B. A. Rozenberg and R. Tenne, "Polymer-assisted fabrication of nanoparticles and nanocomposites," *Progress in Polymer Science (Oxford)*. 2008.

[5] A. Bhatnagar, *Lightweight Ballistic Composites: Military and Law-Enforcement Applications: Second Edition*. 2016.

[6] S. Sockalingam, S. C. Chowdhury, J. W. Gillespie, and M. Keefe, "Recent advances in modeling and experiments of Kevlar ballistic fibrils, fibers, yarns and flexible woven textile fabrics – a review," *Text. Res. J.*, vol. 87, no. 8, pp. 984–1010, 2017.

[7] H. Wang, P. J. Hazell, K. Shankar, E. V. Morozov, and J. P. Escobedo, "Impact behaviour of Dyneema® fabric-reinforced composites with different resin matrices," *Polym. Test.*, vol. 61, pp. 17–26, 2017.

[8] M. A. Abtew, F. Boussu, P. Bruniaux, C. Loghin, and I. Cristian, "Ballistic impact mechanisms – A review on textiles and fibre-reinforced composites impact responses," *Compos. Struct.*, vol. 223, no. November 2018, 2019.

[9] T. G. Zhang, S. S. Satapathy, L. R. Vargas-Gonzalez, and S. M. Walsh, "Ballistic impact response of Ultra-High-Molecular-Weight Polyethylene (UHMWPE)," *Compos. Struct.*, vol. 133, pp. 191–201, 2015.

[10] L. H. Nguyen, S. Ryan, S. J. Cimpoeru, A. P. Mouritz, and A. C. Orifici, "The effect of target thickness on the ballistic performance of ultra high molecular weight polyethylene composite," *Int. J. Impact Eng.*, vol. 75, pp. 174–183, 2015.

[11] Z. S. Petrović and J. Ferguson, "Polyurethane elastomers," *Progress in Polymer Science*. 1991.

[12] G. Christopher, M. A. Kulandainathan, and G. Harichandran, "Biopolymers nanocomposite for material protection: Enhancement of corrosion protection using waterborne polyurethane nanocomposite coatings," *Prog. Org. Coatings*, 2016.

[13] J. Li, J. Cui, J. Yang, Y. Li, H. Qiu, and J. Yang, "Reinforcement of graphene and its derivatives on the anticorrosive properties of waterborne polyurethane coatings," *Compos. Sci. Technol.*, 2016.

[14] Q. Li *et al.*, "Polyurethane/polyphenylsilsequiloxane nanocomposite: From waterborne dispersions to coating films," *Prog. Org. Coatings*, 2018.

[15] J. N. Gavgani, H. Adelnia, and M. M. Gudarzi, "Intumescent flame retardant polyurethane/reduced graphene oxide composites with improved mechanical, thermal, and barrier properties," *J. Mater. Sci.*, 2014.

[16] Z. Liu *et al.*, "Solvent-free and self-catalysis synthesis and properties of waterborne polyurethane," *Polymer (Guildf).*, 2018.

[17] M. Joshi, B. Adak, and B. S. Butola, "Polyurethane nanocomposite based gas barrier films, membranes and coatings: A review on synthesis, characterization and potential applications," *Progress in Materials Science*. 2018.

[18] V. Mittal, "Elastomer clay nanocomposites for packaging," *Adv. Struct. Mater.*, 2011.

[19] M. Naffakh, A. M. Díez-Pascual, C. Marco, G. J. Ellis, and M. A. Gómez-Fatou, "Opportunities and challenges in the use of inorganic fullerene-like nanoparticles to produce advanced polymer nanocomposites," *Progress in Polymer Science*. 2013.

[20] Y. Q. Zhu *et al.*, "Shock-absorbing and failure mechanisms of WS2 and MoS 2 nanoparticles with fullerene-like structures under shock wave pressure," *J. Am. Chem. Soc.*, 2005.

[21] V. N. Bakunin, A. Y. Suslov, G. N. Kuzmina, and O. P. Parenago, "Synthesis and application of inorganic nanoparticles as lubricant components-a review," *J. Nanoparticle Res.*, 2004.

[22] A. S. Sethulekshmi, J. S. Jayan, A. Saritha, and K. Joseph, "Insights into the reinforcibility and multifarious role of WS2 in polymer matrix," *Journal of Alloys and Compounds*. 2021.

[23] M. Naffakh, A. M. Díez-Pascual, C. Marco, M. A. Gómez, and I. Jiménez, "Novel melt-processable poly(ether ether ketone)(PEEK)/inorganic fullerene-like WS2 nanoparticles for critical applications," *J. Phys. Chem. B*, 2010.

[24] F. Xu, C. Yan, Y. T. Shyng, H. Chang, Y. Xia, and Y. Zhu, "Ultra-toughened nylon 12 nanocomposites reinforced with IF-WS2," *Nanotechnology*, 2014.

[25] A. M. Díez-Pascual, M. Naffakh, C. Marco, and G. Ellis, "Rheological and tribological properties of carbon nanotube/thermoplastic nanocomposites incorporating inorganic fullerene-like WS2 nanoparticles," *J. Phys. Chem. B*, 2012.

[26] D. M. Simić, D. B. Stojanović, S. J. Brzić, L. Totovski, P. S. Uskoković, and R. R. Aleksić, "Aramid hybrid composite laminates reinforced with inorganic fullerene-like tungsten disulfide nanoparticles," *Compos. Part B Eng.*, 2017.

[27] M. Naffakh, C. Marco, M. A. Gómez, and I. Jiménez, "Novel melt-processable nylon-6/inorganic fullerene-like WS2 nanocomposites for critical applications," *Mater. Chem.*

Phys., 2011.

[28] D. Simić *et al.*, "Inorganic fullerene-like IF-WS2/PVB nanocomposites of improved thermo-mechanical and tribological properties," *Mater. Chem. Phys.*, 2016.

[29] A. Mojtabaei *et al.*, "Influence of fullerene-like tungsten disulfide (IF-WS2) nanoparticles on thermal and dynamic mechanical properties of PP/EVA blends: Correlation with microstructure," *Compos. Part B Eng.*, 2017.

[30] D. M. Simić *et al.*, "Impact resistant hybrid composites reinforced with inorganic nanoparticles and nanotubes of WS2," *Compos. Part B Eng.*, 2019.

[31] M. Naffakh, C. Marco, M. A. Gómez, J. Gómez-Herrero, and I. Jiménez, "Use of inorganic fullerene-like WS2 to produce new high-performance polyphenylene sulfide nanocomposites: Role of the nanoparticle concentration," *J. Phys. Chem. B*, 2009.

[32] M. Naffakh, Z. Martín, N. Fanegas, C. Marco, M. A. Gómez, and I. Jiménez, "Influence of inorganic fullerene-like WS2 nanoparticles on the thermal behavior of isotactic polypropylene," *J. Polym. Sci. Part B Polym. Phys.*, 2007.

[33] D. Haba, A. Hausberger, and A. J. Brunner, "Flaky and fullerene-like WS2 nanoparticles as tribologic and toughening additives for epoxy," in *Proceedings of the Institution of Mechanical Engineers, Part L: Journal of Materials: Design and Applications*, 2017.

[34] A. M. Díez-Pascual and M. Naffakh, "Mechanical and thermal behaviour of isotactic polypropylene reinforced with inorganic fullerene-like WS2 nanoparticles: Effect of filler loading and temperature," *Mater. Chem. Phys.*, 2013.

[35] S. U. Ilyas, S. Ridha, and F. A. Abdul Kareem, "Dispersion stability and surface tension of SDS-Stabilized saline nanofluids with graphene nanoplatelets," *Colloids Surfaces A Physicochem. Eng. Asp.*, 2020.

[36] B. Sanborn, A. M. DiLeonardi, and T. Weerasooriya, "Tensile Properties of Dyneema SK76 Single Fibers at Multiple Loading Rates Using a Direct Gripping Method," *J. Dyn. Behav. Mater.*, 2015.

[37] D. R. Jenket, A. E. Engelbrecht-Wiggans, A. L. Forster, and M. Al-Sheikhly, "A new method for tensile testing UHMMPE single fibers at high temperatures and strain-rates," *NISTIR 8265*, 2019.

[38] A. Fazal, "Polymer Fibre Composites: Investigation Into Performance Enhancement Through Viscoelastically Generated Pre-Stress," *Thesis*, 2014.

[39] V. B. C. Tan, X. S. Zeng, and V. P. W. Shim, "Characterization and constitutive modeling of aramid fibers at high strain rates," *Int. J. Impact Eng.*, 2008.

[40] C. Roiron, E. Lainé, J. C. Grandidier, D. Olivier, N. Garois, and C. Vix, "Study of the thermomechanical behavior of UHMWPE yarns under different loading paths," *Polym. Test.*, 2020.

[41] M. Hudspeth, X. Nie, and W. Chen, "Dynamic failure of Dyneema SK76 single fibers under biaxial shear/tension," *Polymer (Guildf).*, 2012.

[42] W. E. Morton and J. W. S. Hearle, *Physical Properties of Textile Fibres: Fourth Edition*. 2008.

[43] D. K. Y. Tam, S. Ruan, P. Gao, and T. Yu, "High-performance ballistic protection using polymer nanocomposites," in *Advances in Military Textiles and Personal Equipment*, 2012.

[44] F. D. C. Garcia Filho, M. S. Oliveira, A. C. Pereira, L. F. C. Nascimento, J. Ricardo Gomes Matheus, and S. N. Monteiro, "Ballistic behavior of epoxy matrix composites reinforced with piassava fiber against high energy ammunition," *J. Mater. Res. Technol.*, 2020.

[45] N. K. Naik and P. Shrirao, "Composite structures under ballistic impact," *Compos. Struct.*, 2004.

CHAPTER 4

Effect of plasma pre-treatment and polyurethane/IF-WS_2 nanocoating on mechanical and viscoelastic properties of UHMWPE yarns[3]

[3] Wu. S., Hagiya. Y. D., Bhat, G. S., and Rai. S. To be submitted to *Surface and Coatings Technology*.

Abstract

Ultra-high-molecular-weight polyethylene (UHMWPE) fiber is highly favored for fiber-based ballistic composites due to its high strength-to-weight ratio and flexibility. However, its poor adhesion to matrices largely limits its application in polymer composites. In this work, it was observed that applying plasma pre-treatment and then waterborne polyurethane (PU)/inorganic fullerene-like tungsten disulfide (IF-WS_2) nanoparticle coating could significantly increase the toughness, energy to break, and maximum load of UHMWPE fibers. The corresponding properties of the plasma pre-treated and coated fibers increase up to 31.6%, 50.9%, and 33.3%, respectively. In addition, high wash durability of the coating was obtained with up to 92% weight retention after washing. Optimum properties were observed for nanocomposite SA3 prepared using 15% PU (PUA type), 6% IF-WS_2, and water medium. Moreover, plasma pre-treatment which induced oxygen-containing functional groups on UHMWPE fibers, significantly improved the mechanical & viscoelastic properties and wash durability of the final UHMWPE/PUA/IF-WS_2 composites.

Keywords:

Plasma pre-treatment, UHMWPE fiber-based nanocomposite, mechanical properties, viscoelasticity, wash durability

4.1. Introduction

Ultra-high-molecular-weight polyethylene (UHMWPE) fibers possess a low density and exceptional mechanical properties: high Young's modulus, high tensile strength, great work to fracture, etc [1][2]. In recent years, it has attracted an increasing amount of interest in the application of fiber-based polymer composites for high-performance ballistic and impact-resistant products [3][4][5][6][7][8]. However, UHMWPE fiber exhibits poor interfacial adhesion to polymer matrices due to its smooth fiber surface, low surface energy, and inert chemical structure [9]. The poor fiber/polymer adhesion lowers the interlaminar shear strength of polymer composites and weakens their mechanical advantages, therefore, it largely restricts the application of the fibers in composites [10]. Various attempts have been made to modify UHMWPE fiber surface such as chemical etching [11][12], plasma treatment [13][14][15], irradiation treatment [16][17], UV initiated graft [18], and corona discharge [19][20]. Among these, plasma treatment is extensively used by researchers for its high efficiency and simplicity while limiting damage to target materials [21][22][23][24][25][26][27]. Huang et al. studied the impact of plasma treatment with argon on UHMWPE fibers, it was found to increase the micro crazes and water contact angle on the textile surface and enhanced the adhesive peel strength of the UHMWPE fibers [28].

Waterborne polyurethane (PU) has been documented for elastomeric coatings and fabrications of polymer composites for anti-corrosion and mechanical strength improvements [29][30][31][32]. Owing to its eco-friendly, easy-to-disperse, high elasticity, and excellent toughness benefits, waterborne PU has become a great polymer matrix candidate for developing nanofiller-reinforced high-strength composites [33][34][35]. Based on their heat deformation abilities, PU polymers can be divided into thermoset and thermoplastic PUs, the former crosslinks during the curing process forming molecular chain networks [36][37]. Inorganic fullerene-like

tungsten disulfide (IF-WS_2) possesses inorganic elements and a similar spherical structure as fullerene (C_{60}) on a nanoscale, which endows IF-WS_2 with high stiffness, good compressive strength, and excellent shock absorbing ability [38][39]. Due to its low cost and superior properties, IF-WS_2 has been used in research for making nanocomposites with improved mechanical properties and/or impact resistance [40][41][42][43]. With this being said, incorporating IF-WS_2/PU with UHMWPE fibers appears to be a promising approach to fabricate lightweight and flexible fiber-based nanocomposites. Of which enhanced mechanical properties, low environmental impact, and low cost are expected. Plasma pre-treatment of UHMWPE fibers was also thought to further strengthen the nanocomposites by increasing the interfacial bonding between UHMWPE fiber and PU matrix. However, in the literature, combining both plasma pre-treatment and PU/IF-WS_2 reinforcement to produce durable UHMWPE fiber-based nanocomposites has not been reported. Their effects on the mechanical and viscoelastic properties of UHMWPE fibers are yet to be studied.

In this work, the UHMWPE fibers were plasma pre-treated and then coated with several IF-WS_2/PU nanofluids using a continuous dip-coating method. Different amounts of IF-WS_2 and waterborne PU (thermoset or thermoplastic) were added to selected dispersion mediums to prepare the nanofluids. The effects of plasma treatment on the chemical structure and surface morphology of UHMWPE fibers were determined using ATR-FTIR and SEM techniques. The coating components were screened according to the viscoelastic, mechanical, and wash durability properties of the UHMWPE/PU/IF-WS_2 nanocomposites. Also investigated was the impact of plasma pre-treatment on the forementioned properties of the nanocomposites.

4.2. Materials and methods

4.2.1. Materials

The UHMWPE yarns (untwisted multifilament yarns, trade name: Spectra® 1600) were provided by Honeywell, USA. Their physical properties include linear density (measured) of 1557 denier, filament diameter of 34 μm, and filament number of 360. Two types of Aqueous PU dispersions were supplied by Lubrizol, USA. Table 4.1 shows their product information. Water-based IF-WS_2 additive was obtained from Nanotech Industrial Solutions, USA (trade name: IW-4000; particle size: 40-200nm as reported in the literature [39]; measured solid content: 48.8%).

Table 4.1. Product information for the two waterborne PU products used.

PU type	Trade name	Polyol type	Solid content /%	Self-Crosslinking
PUA	Aptalon™ M8100	polyamide polyol	37	Yes
PUB	Permax™ 202	Polyether polyol	41	No

4.2.2. Plasma pre-treatment and composite preparation

The continuous plasma treatment of Spectra® yarns was carried out by Pillar Technologies, Inc. The treatment was conducted with 80%N_2/20%O_2 gas using 700 Watts power. The yarns were treated with a moving speed of 6.1m/min.

The plasma-treated (PT) yarns were coated with different PU/IF-WS_2 mixtures (SA1-4, SB1-4) as described in Table 4.2. Several variables were selected for preparing the mixtures based on preliminary trials. These variables include PU type, PUA amount, PUB amount, IF-WS_2 amount, and type of solvent medium. A control specimen SA3-U was also fabricated with untreated Spectra® yarns. The weight-percentages of PU and IF-WS_2 were calculated based on

total liquid weight. A water/ethanol mixture was used as the dispersing medium to prepare the SA4 and SB4 composites, because of the high stability of IF-WS_2 nanoparticles in ethanol and the good dispersibility of PU products in water. Thus, the PU amounts for SA4 and SB4 were designed with respect to water weight. A designed amount of IF-WS_2 suspension was added to the prepared dispersion medium, and the mixture was sonicated in a Kendal ultrasonic bath for 30 min to prepare a homogeneous nanofluid. Then, corresponding amount of PUA or PUB was added to the mixture and sonicated for another 30 min. The cap of the container (centrifuge tube) was opened every 15 min for 1~2 seconds, and the water bath was replaced every 30 min during sonication to prevent PU from solidifying by heat generated during sonication.

Figure 4.1 illustrates the fabrication process for the Spectra®/PU/IF-WS_2 composites. Spectra® yarns were continuously coated with prepared PU/IF-WS_2 dispersions using a lab-assembled setup. A continuous yarn (plasma pre-treated or untreated) was stretched and oriented under tension, dip-coated with prepared PU/IF-WS_2 dispersions, nipped through two pressure rollers, pre-dried in the furnace, and wounded on a 3D printed rod attached directly to the DC motor. The nipping pressure between the rollers and the winding speed were kept constant. The measured temperature within the furnace tube was 196 ± 7°C. After continuous coating, each batch of composite yarn on the winding rod was transferred onto a hollow aluminum (Al) frame for its high heat resistance and even yarn spread. The wounded yarn on the frame was further dried (and cured for PUA) in a lab oven at 100°C (PUA) or 60°C (PUB) for 30 min. A good film formation of PUA requires higher drying and curing temperature for yarns impregnated with PUA/IF-WS_2. Otherwise, inconsistent, and brittle PUA films may form on Spectra® yarns, rather than uniform and durable films.

Table 4.2. The abbreviations and fabrication conditions of the Spectra® yarn/PU/IF-WS_2 composites.

Abbreviations	Yarn	PUA (wt%)	PUB (wt%)	WS_2 (wt%)	Medium
SA1	PT	10	-	2	W
SA2		15	-	2	W
SA3		15	-	6	W
SA4		15	-	2	WE
SB1		-	9	2	W
SB2		-	14	2	W
SB3		-	14	6	W
SB4		-	14	2	WE
SA3-U	UT	15	-	6	W

PT: plasma pre-treated; UT: untreated; W: water; WE: water/ethanol mixture (wt%): 1:5

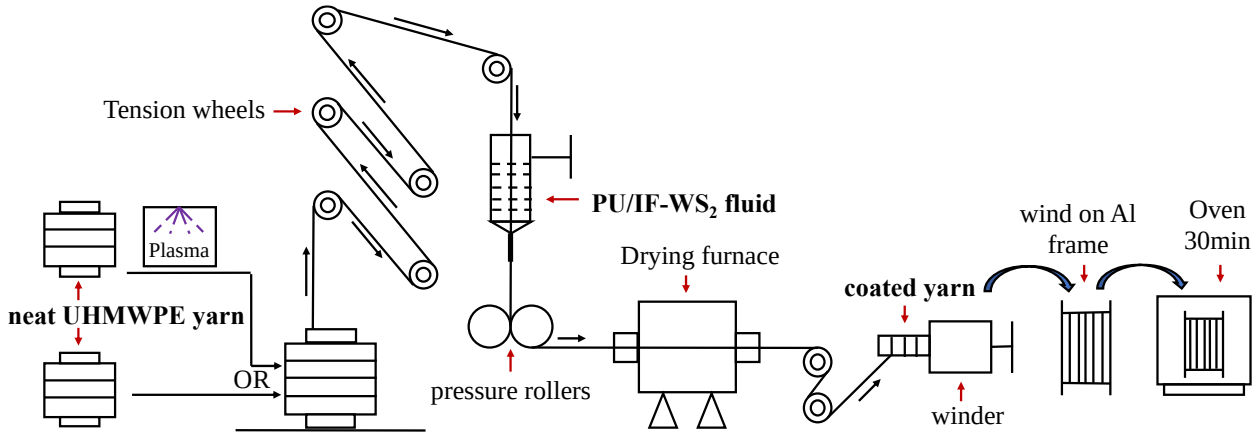

Figure 4.1. Illustration of the continuous yarn dip-coating process for Spectra®/PU/IF-WS_2 specimens.

4.2.3. Attenuated total reflectance-Fourier transform infrared spectroscopy

Infrared spectrums of absorbance for the neat and plasma treated yarns were obtained using an attenuated total reflectance-Fourier transform infrared (ATR-FTIR) spectrometer (ThermoFisher Nicolet 6700). The effect of plasma treatment on the chemical structure of Spectra®

fibers was studied. The spectrums range from 750 cm^{-1} to 4000 cm^{-1} and the scan number of 128 were applied. FTIR peaks on the spectrums were analyzed.

4.2.4. Scanning electron microscopy

Scanning electron microscopy (SEM) was performed on the neat and plasma treated yarns using a FE-SEM Thermo Fisher Teneo. Before testing, the specimens were coated with gold for electronic conductivity. The magnification was set at 500× and 2000× and the acceleration voltage of 5 kV was applied. The effect of plasma treatment on the surface morphology of the Spectra® fibers was observed.

4.2.5. Linear density and coating add-on percentage

10 neat yarns with length of 125cm were cut and weighed. The average sample weight was used to calculate the linear density, D (denier), of the neat yarn with Equation (4.1). 7 yarns with length of 30cm were cut from each of the coated yarns and weighted individually to estimate the add-on percentage of each sample with Equation (4.2). The add-on percentage for each coated yarn can be calculated by averaging the data from all sample replicates.

$$D = Linear\ density\ of\ neat\ yarn\ (denier) = \frac{average\ neat\ yarn\ weight}{neat\ yarn\ length} \times 9000 \quad (4.1)$$

$$Addon\ (\%) = \frac{sample\ weight\ after\ coating \times 9000 - D \times sample\ length}{D \times sample\ length} \times 100 \quad (4.2)$$

Where *D* is the average linear density of the neat yarn.

4.2.6. Dynamic mechanical analysis

A dynamic mechanical analysis (DMA) instrument (PerkinElmer DMA 8000) in tension mode with 0.005mm strain and 1.2 force multiplier was used to test the effects of plasma treatment and coatings on viscoelastic and dampening properties of Spectra® yarns. Neat yarns, PT yarns,

and PU/IF-WS2 coated yarns of 22mm length were tested. The test temperature increased from 30°C to 100°C at a heating rate of 3°C /min, while the frequency was at 1 Hz. The DMA data of the samples including storage modulus and loss modulus were analyzed.

4.2.7. Mechanical test

A tensile tester (Instron 4400R) was used to test the mechanical properties of neat, PT, and PU/IF-WS_2 coated yarns as per ASTM 2256 standard. To reduce yarn slippage during the test, capstan yarn grips were installed. Besides, both ends of the yarn were glued onto cardboard chips (dimension of 1.6 cm x 2.9 cm) with ELMER'S clear glue. The glued samples were dried overnight. For some glued samples, 12.5 full twists in 105 mm were applied between the cardboards to further increase the valid breaking rate of the yarns as directed in the standard. All samples were tested with a crosshead speed of 100mm/min and a gauge length of 100mm. The 'work of rupture' – total energy (J) to break – of individual yarns is obtained from the integrated area under the load-displacement curve. With that, the corresponding gravimetric yarn toughness (J/g) can be calculated using Equation (4.3) [44][45]. Overall, at least 3 replicates were tested, and the averages were compared.

$$Toughness\ (J/g) = \frac{energy\ to\ break}{Linear\ density \times initial\ length} \qquad (4.3)$$

4.2.8. Wash durability

To study the influences of PU type and coating components on the wash durability of the PU/IF-WS_2 coatings, the fabricated Spectra®/PU/IF-WS_2 yarns (length of 30 cm) were washed using an Atlas Launder-ometer as per AATCC Test Method 61 (condition No. 1A). The wash durability of the coating was evaluated based on its estimated weight retention percentage on the

target sample after standard washing. The calculation for the weight retention percentage of a sample is shown in equation (4.4).

$$Weight\ retention\ \% = \frac{weight\ after\ washing \times 9000 - D \times sample\ length}{weight\ before\ washing \times 9000 - D \times sample\ length} \times 100 \quad (4.4)$$

Where *D* is the average linear density (denier) of the neat yarn.

4.3. Results and discussion

4.3.1. Chemical structure

Figure 4.2 illustrates the FT-IR spectrums of the neat and plasma treated Spectra® yarns. From both spectrums, the characteristic peaks for UHMWPE fiber can be identified. The peaks at 2916 cm^{-1}, 2849 cm^{-1}, and 1473 cm^{-1} are assigned to symmetric stretching of CH_3, asymmetric stretching of CH_3, and bending vibration of CH_2, respectively [15]. After plasma treatment, new absorption peaks appear at 3250 cm^{-1} and 1720 cm^{-1}, which are attributed to O-H and C=O stretching vibrations, respectively. O-H bending between 1360~1370 cm^{-1} and C-O bonds between 1050~1310 cm^{-1} were also observed in the plasma treated sample [15][46]. Meanwhile, the peak at 1122 cm^{-1} shows significantly enhanced intensity in the PT specimen due to C-O stretching in secondary alcohol. These characteristic peaks indicate that new oxygen-containing polar groups (-OH, C=O, C-O) were introduced into the Spectra® yarn through plasma treatment [46][47].

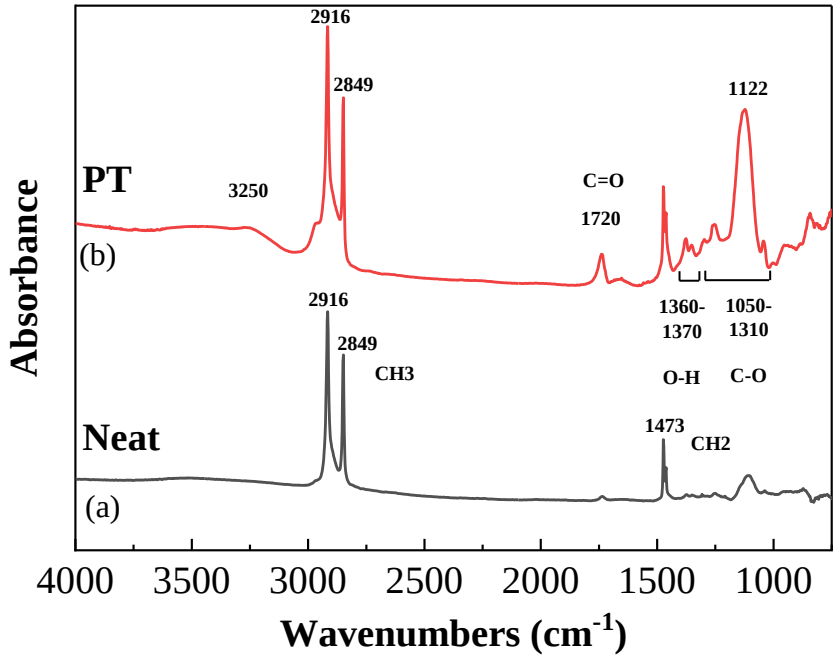

Figure 4.2. FT-IR spectrums of the Spectra® yarns: (a) neat; (b) plasma treated (PT).

4.3.2. Surface morphology

SEM was utilized to observe the surface morphologies on neat and PT Spectra® fibers and study the effect of plasma treatment. As shown in Figure 4.3 (a), neat Spectra® fibers show longitudinal striations and uneven surfaces formed from manufacturing. After surface modification using plasma treatment, no obvious surface morphological changes (e.g., etching pits, deepened gullies, cracks, or increased roughness) were shown on the fibers (Figure 4.3 (b)). This revealed that the plasma treating process was well-controlled to prevent severe fiber surface damage.

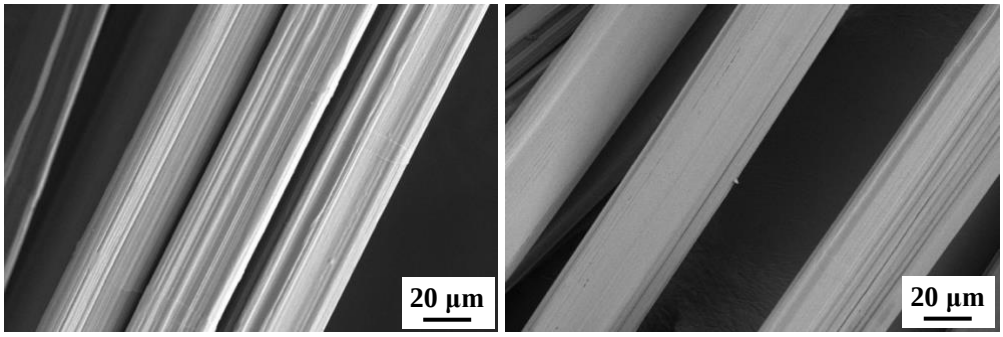

(a) (b)

Figure 4.3. SEM images of untwisted Spectra® filament yarns: (a) neat; (b) plasma treated.

4.3.3. Add-on percentage

After nanocomposite coating, the add-on percentages for different PT yarn/PU/IF-WS_2 specimens were measured. As shown in Table 4.3, the average add-on weight percentages for the PT treated and PU/IF-WS_2 coated samples (SA1-4, SB1-4) were maintained in a small range from 4.2% to 12.1%. According to the Anova test, at a 95% confidence level, the add-on amounts for SA1, SA2, SA4, SB1, SB2, and SB4 are not significantly different (F ratio: 2.239, p-value: 0.0714). With higher IF-WS_2 addition (6% over 2%), SA3 and SB3 showed small increases in their add-on percentages. The add-on amount for composite SA3-U increased slightly compared to its counterpart SA3 (α=0.05, Anova F ratio: 5.610, p-value: 0.0355). The toughness presented in this work was calculated based on specimen weight to directly compare the results from varying samples.

Table 4.3. The add-on percentages (mean and SE) for the PU/IF-WS_2 coated Spectra® yarns.

Samples	SA1	SA2	SA3	SA4	SB1	SB2	SB3	SB4	SA3-U
Add-on (%)	8.9 ± 1.6	7.7 ± 1.3	12.1 ± 1.4	4.6 ± 1.0	4.2 ± 1.0	5.5 ± 1.2	11.2 ± 1.8	4.9 ± 1.3	16.6 ± 1.3

4.3.4. Viscoelastic properties

DMA temperature sweeps (30°C-100°C) at 1Hz frequency were conducted on the plasma pre-treat/coated specimens involving PUA (SA1-4) and PUB (SB1-4). In addition, neat and PT Spectra® yarns were tested as controls. Figure 4.4 shows the dynamic mechanical behaviors (storage modulus, loss modulus and tan δ) of samples SA1-4, neat and PT yarns, while Figure 4.5 exhibits the SB1-4 samples and the controls. Both moduli of the samples showed an approximately linear decrease upon heating. This is due to the rising molecular kinetic energy and mobility, which lead to softening effect [48][49]. Meanwhile, tan δ of the samples, which is the ratio of the loss to the storage modulus, increases with higher temperature indicating the increased damping coefficient. As shown, both dynamic storage and loss moduli of the plasma treated sample decreased slightly, compared to those of the neat yarn. For composites SA1-SA4, the order of their storage modulus from highest to lowest is observed as SA1>SA2>SA3>SA4, while the tan δ (loss to storage modulus ratio) order shows the opposite as SA4>SA3>SA2>SA1. Specimens SA1, SA2, and SA3 showed improved storage and loss moduli in comparison with the neat or PT yarn and slightly decreased tan δ due to their high storage modulus. The improved storage modulus indicates enhanced elasticity and energy storage ability of the composite materials under stress, while the increased loss modulus reflects improvements in their viscosity and energy dissipation capability [50]. These enhancements are desired for use in ballistic and anti-impact applications. The poor viscoelastic property of SA-4 could be attributed to combined factors including the PU type, low PU addition amount, and water/ethanol medium used. Similarly, small improvements in storage modulus were noticed for composites SB1-SB4 compared with that of the PT yarn. Composites SB3 and SB4 exhibit higher loss modulus than neat and PT yarns, while samples SB1-SB2 show slightly improved loss modulus than the PT yarn. Tan δ of SB2-SB4 samples increase

to different degrees with the highest value from SB3 sample indicating their enhanced damping ratio. Both outcomes were collected at 30 °C from the PT yarn and tested composites. As listed in Table 4.4, all PT Spectra®/PU/IF-WS_2 composites, except SA4, show increased storage modulus (up to 51.9 %, SA1) and loss modulus (up to 53.2 %, SB3) in comparison to PT yarns.

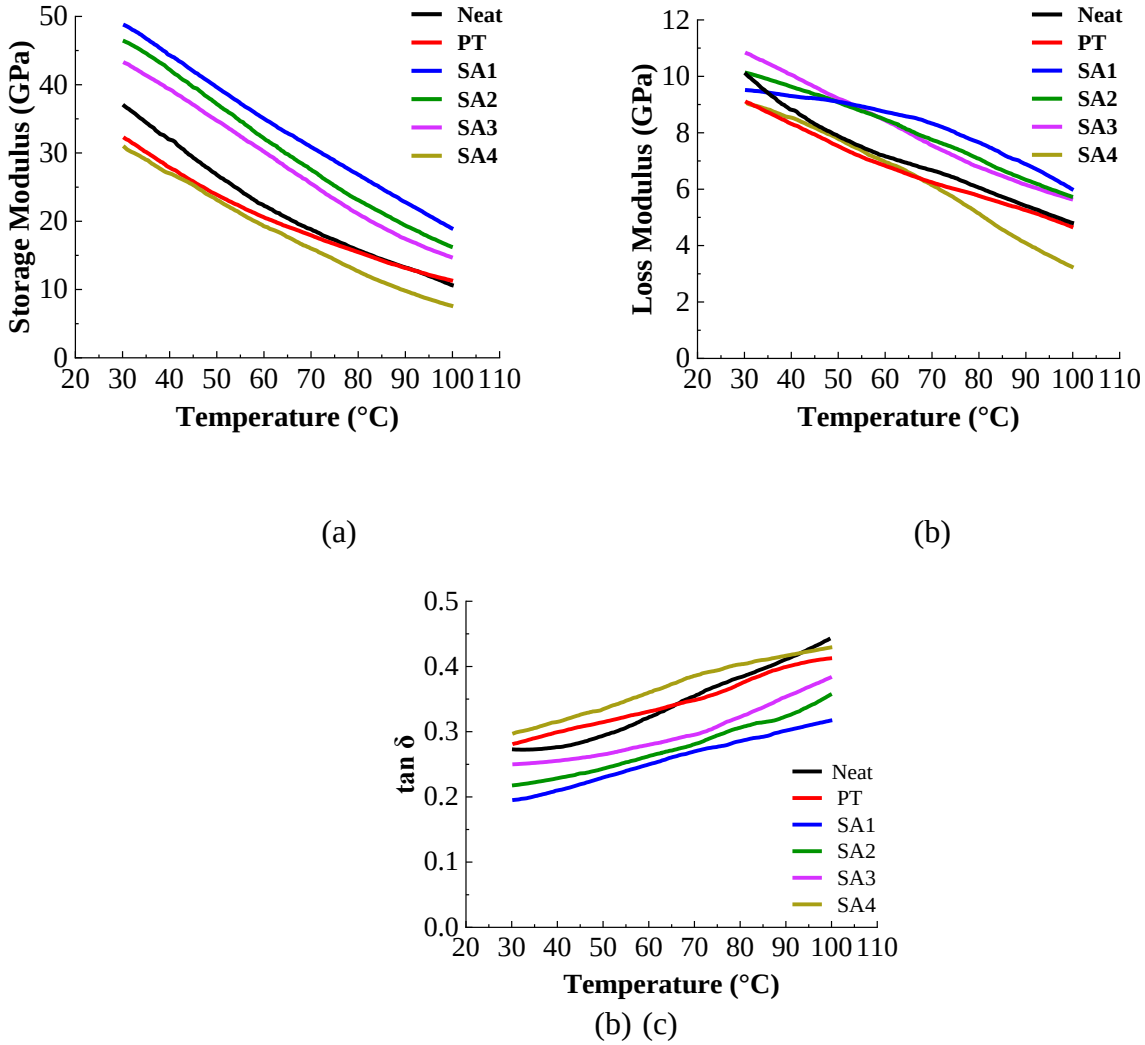

Figure 4.4. DMA temperature sweeps of the neat Spectra® yarn, plasma treated (PT) yarn, and PT yarn/PU/IF-WS_2 composites SA1-SA4: (a) storage modulus; (b) loss modulus; (c) tan delta.

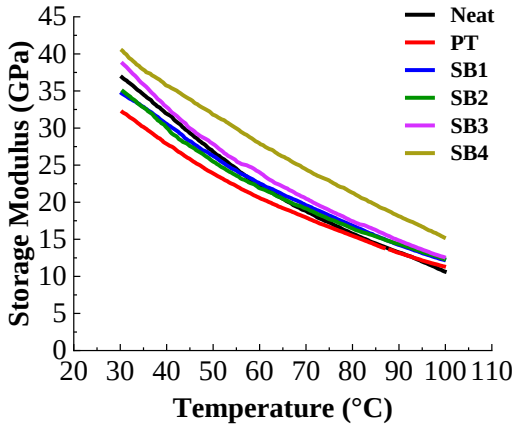

(a)

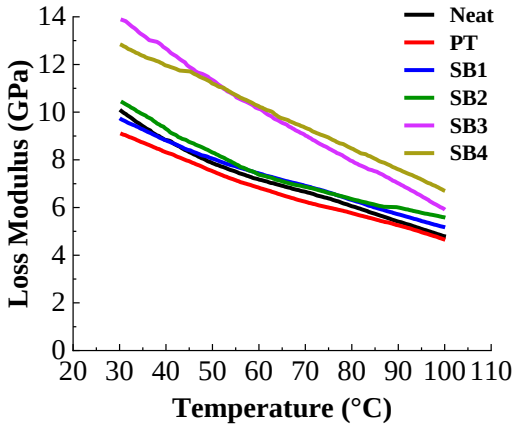

(b)

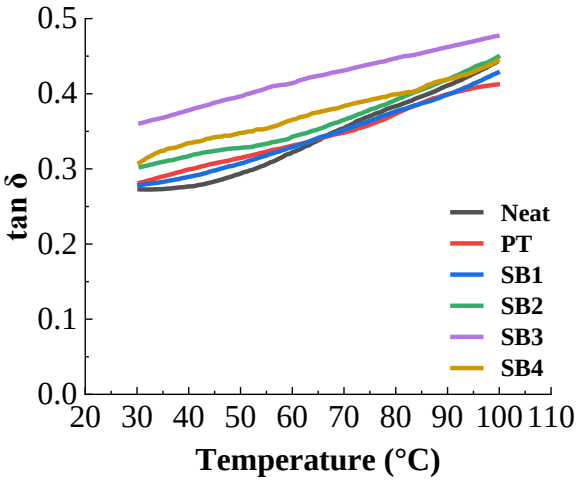

(c)

Figure 4.5. DMA temperature sweeps of the neat Spectra® yarn, plasma treated (PT) yarn, and PT yarn/PU/IF-WS_2 nanocomposites SB1-SB4: (a) storage modulus; (b) loss modulus; (c) tan delta.

Table 4.4. Summary of storage and loss moduli of the plasma treated (PT) yarn and PT yarn/ PU/IF-WS_2 nanocomposites at 30°C.

	PT	SA1	SA2	SA3	SA4	SB1	SB2	SB3	SB4
Storage Modulus (GPa)	32.29	49.06	46.69	43.26	31.89	34.65	34.68	38.65	41.85
Loss Modulus (GPa)	8.96	9.89	10.13	10.68	8.97	9.83	10.81	13.73	13.47

4.3.5. Mechanical properties

The tensile tests were conducted for the neat Spectra® yarn, PT yarn, and modified/coated yarns. As suggested by the ASTM 2256 standard, 12.5 twists were applied to each glued sample before testing to prevent yarn slippage under tension. From the test results, total energy to break and toughness were calculated for the pristine Spectra® yarn, plasma treated yarn, and fabricated composite samples (SA1-4, SB1-4). As shown in Figure 4.6 plasma treatment had no significant effect on the mechanical properties (energy to break and toughness) of Spectra yarns. This result agrees with the intact fiber surfaces after plasma treatment.

However, a one-way Anova test shows the energy to break values for composites SA1-SA4 and SB1-SB4 were significantly different (α=0.05, F ratio: 3.8570, p-value: 0.0025). The maximum average value was obtained from specimen SA3 with significant increase (α=0.05) in the energy to break by 26.7% and 29.9% compared to the neat yarn (F ratio: 8.1938, P-value: 0.0187) and PT yarn (F ratio: 5.0623, P-value: 0.0482), respectively. The gravimetrical toughness of the composites – total energy absorbed per unit weight of materials before rupturing, shows a similar trend to the energy-to-break values due to the small range of add-on amount. Similarly, the Anova analysis result indicates a significant difference in the toughness among coated samples (α=0.05, F ratio: 2.7409, P-value: 0.0195). SA3 of PUA and SB1 of PUB are the two samples with the highest toughness value from each PU group. The average toughness improved by 11.4% (SA3) and 9.7% (SB1) in comparison to neat yarn and 14.2% (SA3) and 12.4% (SB1) compared to PT yarn. The collective data shows the effectiveness of plasma pre-treatment and nanocomposite coatings on enhancement of tensile energy absorption of the Spectra® yarns while retaining their lightweight qualities.

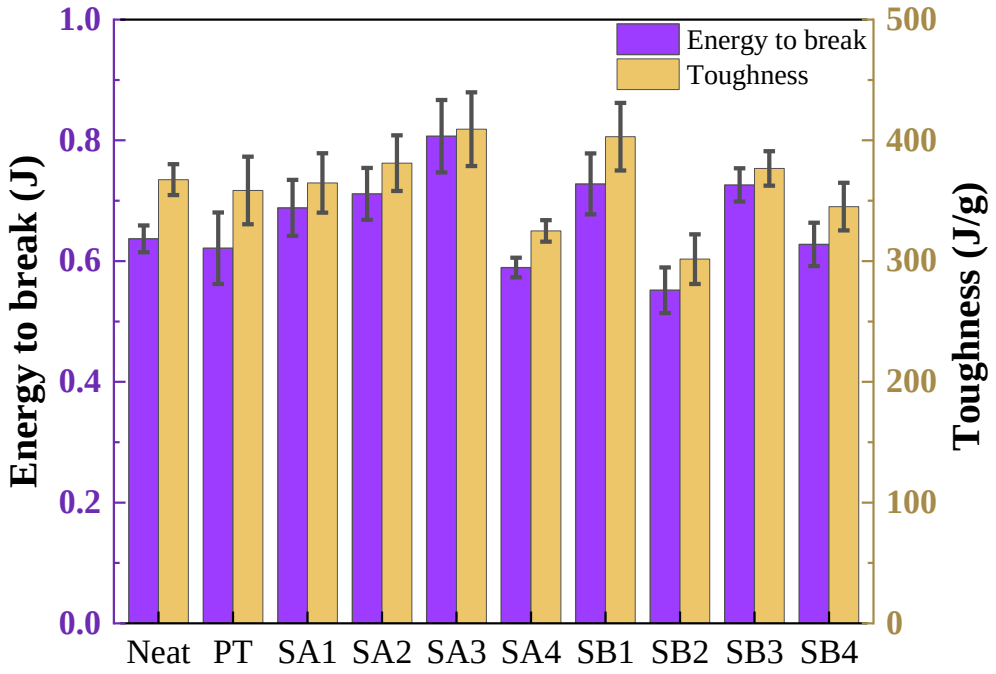

Figure 4.6. The total energy to break and toughness (mean and SE) of the neat Spectra® yarn, plasma treated (PT) yarn, and PT yarn/PU/IF-WS_2 nanocomposites (SA1-SA4, SB1-SB4).

4.3.6. Coating wash durability

All the fabricated composites were washed as per AATCC method 61 to simulate the home laundry procedure for their potential applications in protective garments and textiles. The sample weight for each composite was measured before and after washing to calculate an estimated percentage of retained weight. As presented in Figure 4.7, the weight retentions of the tested composites were significantly different at a 95% confidence level (F ratio: 11.6246, P-value: <.0001). The weight retention averages for the SA samples were all larger than those of the SB specimens. The retention of coatings on SA1-SA4 were 62.1% - 92.0% on average, while the coatings on SB1-SB4 remained only 10.3% - 42.3% after washing. Figure 4.8 exhibits the images

of unwashed (a, c) and washed (b, d) composite yarns. The color change of the samples after washing matches the weight retention result. The samples SA1-SA4 maintained most of their colors obtained from IF-WS_2 reinforced PUA after washing. However, specimens SB1-SB4 lost most of their coatings and showed similar white colors to uncoated yarns after washing. This shows the advantages of the self-crosslinking property that PUA has over PUB, which greatly strengthens the durability of the coating. The self-crosslinking mechanism reported in the literature is elucidated in Figure 4.9. This process occurs upon the removal of water in PUA, ketone groups (C=O) react with amine groups (-NH_2) to form imine (C=N) groups that crosslink molecular chains [51][52]. Through this process, PUA forms water-resistant and durable thermoset films on Spectra® fiber surfaces leading to better weight retention of PUA/IF-WS_2 coating even after washing. In contrast, waterborne PUB forms thermoplastic films without crosslinks on the fiber surfaces, making it more susceptible to damage by water swelling and agitation during washing. The lack of crosslinks for SB1-SB4 (PUB) samples results in a much lower water durability and weight retention of the coatings. SA3 had the highest average weight retention (92%) after washing among all samples. It is significantly higher than it for all SB samples (SB1-SB4) according to the conducted Tukey HSD test. This high wash durability was also confirmed from the sample appearance, the replicates of sample SA3 greatly maintained their light grey colors and united-filament structures after washing. Figure 4.10 shows surface morphologies of unwashed and washed SA3 samples, and no obvious loss of the nanocomposite coating was observed on the washed sample, its fiber shape and appearance were well retained compared to the unwashed sample.

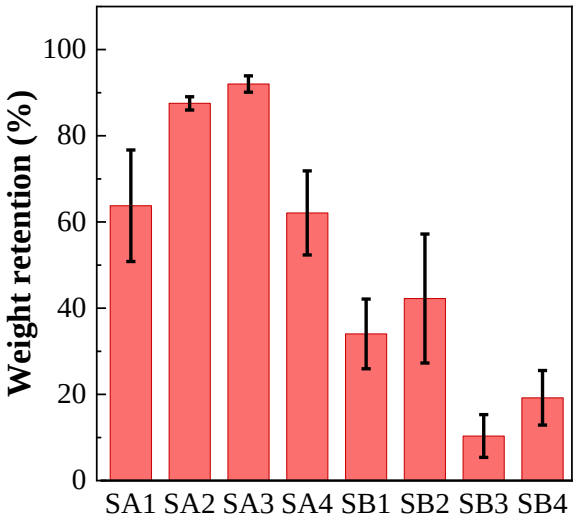

Figure 4.7. Coating weight retention percentages (mean and SE) of the plasma pre-treated Spectra® yarn/PU/IF-WS_2 nanocomposites after washing.

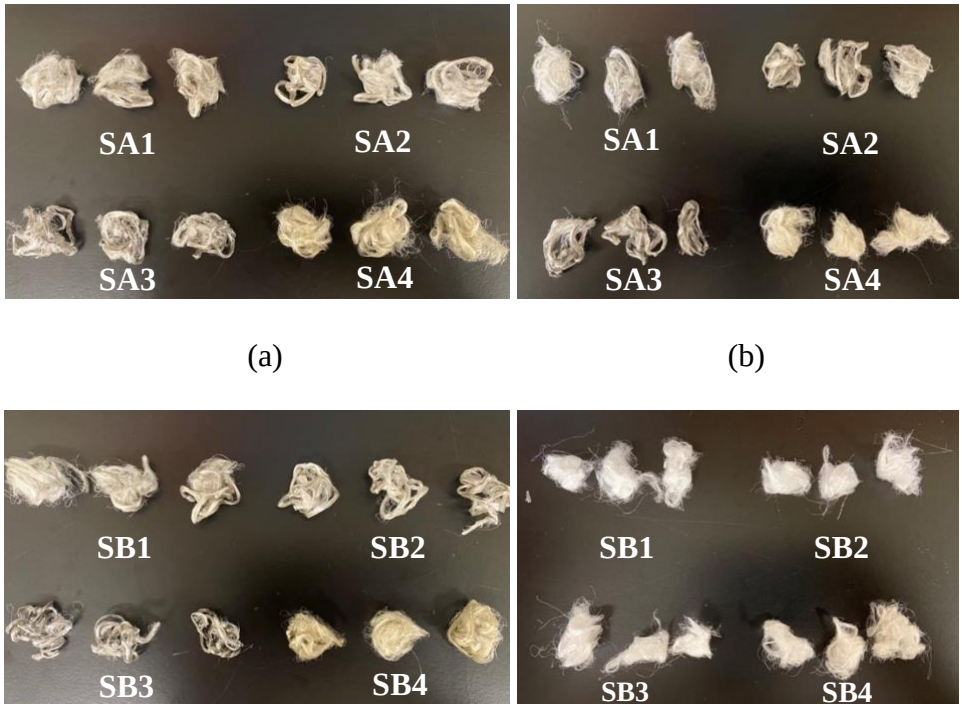

Figure 4.8. Photographs of plasma pre-treated Spectra®/PU/IF-WS_2 samples: (a) unwashed SA1-SA4; (b) washed SA1-SA4; (c) unwashed SB1-SB4; (d) washed SB1-SB4.

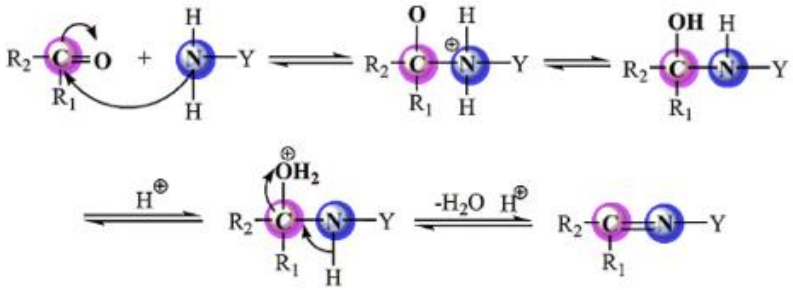

Figure 4.9. Self-crosslinking reaction mechanism for PUA [51][52].

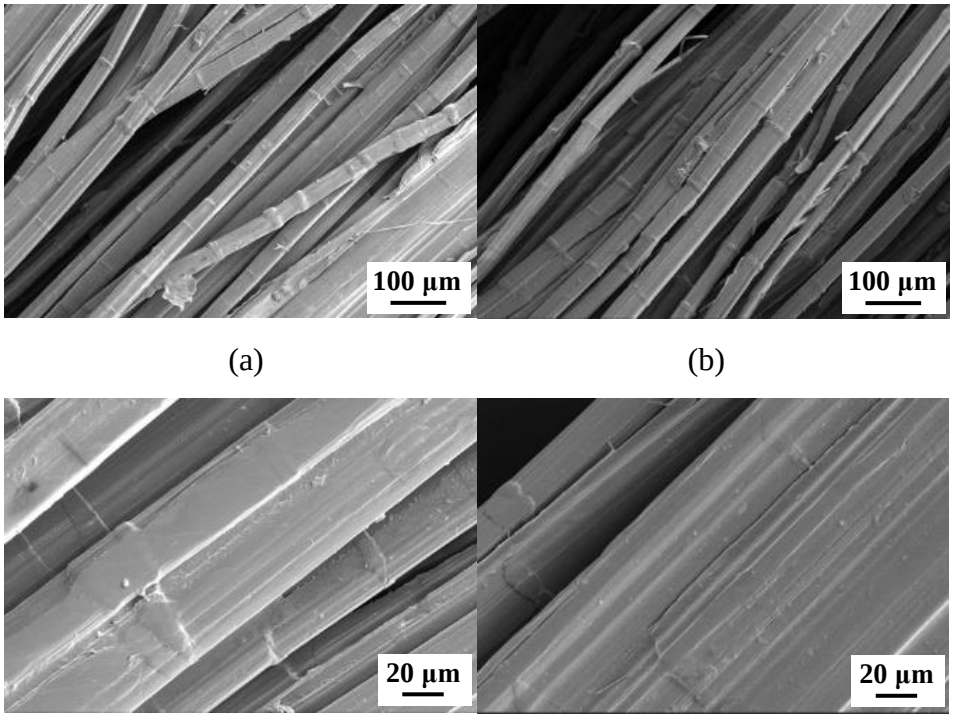

(a) (b)

(c) (d)

Figure 4.10. Surface appearances of the unwashed and washed SA3.

4.3.7. Effect of plasma pre-treatment on SA3

Composite SA3 exhibited the highest tensile energy absorption, toughness, and water durability among all fabricated composites. Thus, in this section, the effect of plasma pre-treatment on specimen SA3 was investigated. Its counterpart SA3-U ('U' to denote 'untreated') was fabricated as a control using the same PUA/IF-WS_2 coating component for untreated Spectra® yarn. The mechanical properties, viscoelastic properties, wash durability, and surface

morphologies of both specimens were tested and observed. Table 4.5 shows the mechanical properties of SA3-U and SA3 from tensile tests, During the test, 12.5 twists were applied to each sample before testing. Whereas Table 4.6 lists the mechanical properties of these specimens and neat yarns tested with no yarn twists applied. Also included in the table are the weight retention percentages of the coatings on nanocomposites SA3-U and SA3 after washing. By comparing the mechanical property results of SA3-U and SA3, it was found that the toughness and energy to break values showed no significant differences between the twisted and untwisted samples. However, applying the yarn twists significantly increased the breaking extension for both SA3-U (F ratio: 27.5042, P-value= 0.0004) and SA3 specimens (F ratio: 35.4744, P-value= 0.0002) at 95% confidence level. In addition, the maximum load of sample SA3 with twists showed a significant decrease (α=0.05, F ratio: 7.3070, P-value: 0.0243). To match the untwisted neat yarn condition, the mechanical property results tested with untwisted yarns were further analyzed. SA3 (treated) achieved significantly higher toughness (F ratio: 6.2823, P-value: 0.0311), energy to break (F ratio: 9.8663, P-value: 0.0105), and maximum load (F ratio: 6.1193, P-value: 0.0329) at 95% confidence level, compared to nanocomposite SA3-U (untreated). The applied plasma pre-treatment significantly improved these mechanical properties of SA3 by 21.2% (toughness), 16.2% (energy-to-break), and 9.9% (maximum load).

Meanwhile, the coating weight retention of composite SA3 after washing was improved by 9.7% to that of the counterpart SA3-U (α=0.05, F ratio: 8.8374, P-value: 0.0410). This revealed the plasma pre-treatment indeed enhanced the mechanical properties and coating durability of the composite by inducing oxygen-containing groups to the fiber surfaces and enhancing adhesion interaction between the Spectra® fibers and PUA matrix. Overall, in comparison to neat Spectra® yarn, the PT yarns/PUA/IF-WS_2 composite SA3 showed significantly higher toughness (31.6%),

energy to break (50.9%), and maximum load (33.3%). The corresponding Anova test results at 95% confidence level are (1) F ratio: 6.4254, P-value: 0.039, (2) F ratio: 13.6722, P-value: 0.0077, and (3) F ratio: 40.3593, P-value: 0.0004, respectively.

To determine the influence of plasma pre-treatment on the viscoelasticity of the composite, DMA tests were carried out on the pair of samples (SA3-U and SA3). As depicted in Figure 4.11, both storage modulus and loss modulus showed similar decreasing trends upon heating for nanocomposites SA3-U and SA3. However, in the tested temperature range, both moduli of sample SA3 were higher than those of sample SA3-U. This indicates the positive effect of plasma pre-treatment on the reinforcement of PUA/IF-WS_2 on high-performance Spectra® fibers, resulting in the improved abilities to store (elasticity) and dissipate (viscosity) dynamic energy for composite SA3. At 30°C, its storage and loss moduli rose by 30.0% and 25.8%, respectively, compared with those of specimen SA3-U. Figure 4.12 shows the coating appearance on both SA3-U and SA3 samples. A significant amount of PU clusters is observed on the untreated SA3 sample. The coating uniformity of PU matrix on plasma pre-treated SA3 is much higher that on the SA3-U specimen due to the increased wettability of UHMWPE fibers after plasma treatment, which leads to better spreading and bonding of waterborne PU on fiber surface.

Table 4.5. Mechanical properties (mean and SE) of specimens SA3-U and SA3 measured with 12.5 twists.

	Toughness (J/g)	Energy to break (J)	Maximum load (N)	Elongation at break (%)
SA3-U	362 ± 25	0.73 ± 0.05	497 ± 19	4.36 ± 0.09
SA3	409 ± 31	0.81 ± 0.06	509 ± 15	4.78 ± 0.08

Table 4.6. Mechanical properties (mean and SE) of SA3-U, SA3, and neat yarn measured with no twists along with the coating weight retention of SA3-U and SA3.

	Toughness (J/g)	Energy to break (J)	Maximum load (N)	Elongation at break (%)	Weight Retention after washing (%)
SA3-U	364 ± 13	0.74 ± 0.03	513 ± 15	3.72 ± 0.08	83.9 ± 1.9
SA3	441 ± 21	0.86 ± 0.04	564 ± 14	3.82 ± 0.13	92.0 ± 1.9
Neat yarn	335 ± 44	0.57 ± 0.08	423 ± 14	3.50 ± 0.48	-

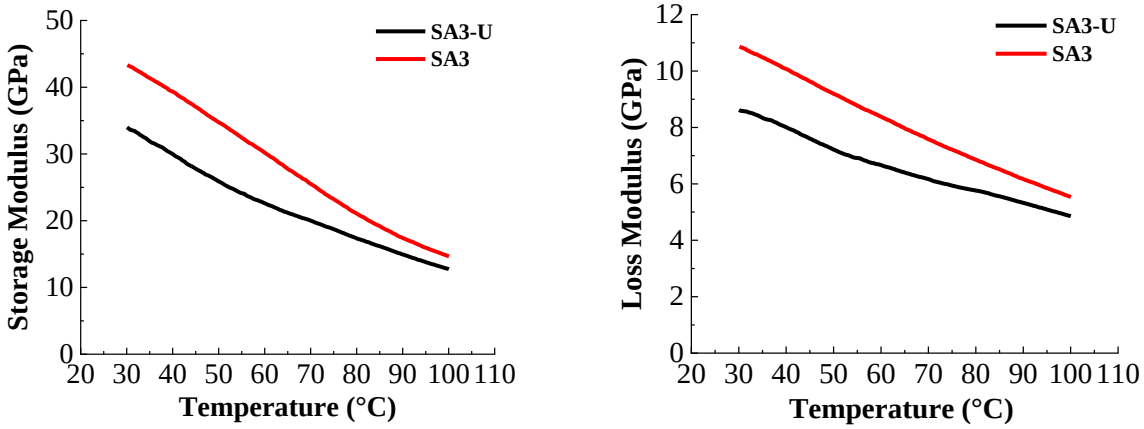

(a) (b)

Figure 4.11. DMA results of SA3-U and SA3 nanocomposites: (a) storage modulus; (b) loss modulus.

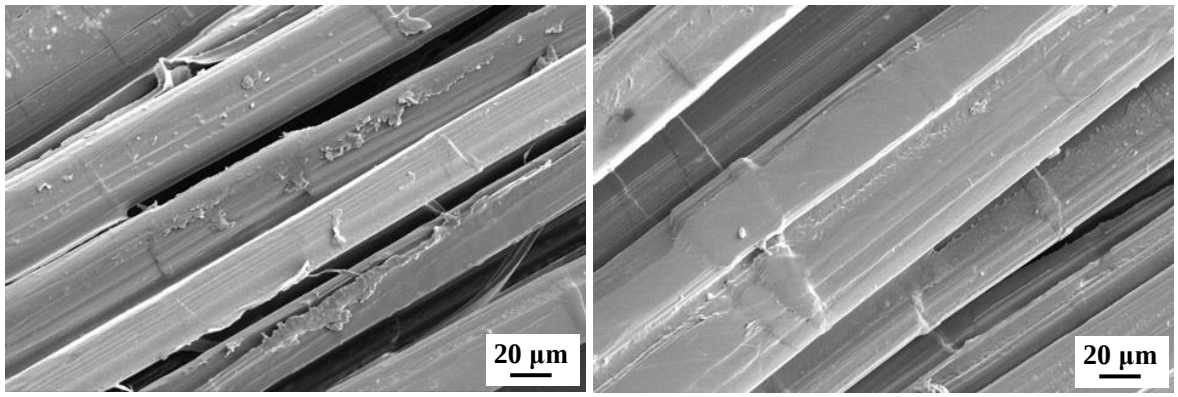

Figure 4.12. SEM photographs showing the surface features of the SA3-U and SA3 samples.

4.4. Summary

The poor interfacial adhesion between UHMWPE fibers and polymer matrices restricted the application of UHMWPE fibers in fiber-based polymer composites for protective gear. In this work, Spectra® multifilament yarns were modified using plasma pre-treatment. ATR-FTIR analysis showed that different oxygen-containing active groups (-OH, C=O, C-O) were introduced onto the plasma treated (PT) fiber surface. All fabricated nanocomposites, except SA4, showed improved storage and loss moduli to varying extents, compared to that of the PT yarn. Tensile test results revealed that the coating significantly affected the energy to break and toughness of the nanocomposites. Among all specimens, SA3 (coating components: 15% PUA, 6% IF-WS_2, water medium) achieved the highest energy-to-break and toughness on average. The PUA/IF-WS_2 coatings exhibited higher wash durability than the PUB/IF-WS_2 coatings on Spectra® yarns due to the high water-resistance and self-crosslinking function of the PUA product. The maximum coating weight retention after washing was also obtained for SA3 (92%).

The sample made with plasma-treated yarns, SA3, exhibited higher toughness (21.2%), energy-to-break (16.2%), and weight retention after washing (9.7%) than that of untreated SA3-U. Pretreating the Spectra® fibers with plasma discharge enhances the energy storage and dissipation capabilities of the nanocomposite. Overall, the toughness, energy to break values, and maximum load of nanocomposite SA3 (7.9 wt% PUA and 4.2 wt% IF-WS_2 on the yarn by calculation) significantly improved by 31.6%, 50.9%, and 33.3%, respectively, compared with the pristine yarn. Nanocomposite SA3 shows promising enhancements in mechanical properties and viscoelasticity while retaining the low weight of UHMWPE fibers and high coating durability for composites.

4.5. References

[1] Y. chen Xie, H. Zhang, W. Zhu, and G. yan Huang, "Effects of textile structure and projectile geometry on ballistic performance of UHMWPE textiles," *Compos. Struct.*, 2022.

[2] F. Zulkifli, J. Stolk, U. Heisserer, A. T. M. Yong, Z. Li, and X. M. Hu, "Strategic positioning of carbon fiber layers in an UHMWPE ballistic hybrid composite panel," *Int. J. Impact Eng.*, 2019.

[3] X. Jin, W. Wang, C. Xiao, T. Lin, L. Bian, and P. Hauser, "Improvement of coating durability, interfacial adhesion and compressive strength of UHMWPE fiber/epoxy composites through plasma pre-treatment and polypyrrole coating," *Compos. Sci. Technol.*, 2016.

[4] R. Zhang *et al.*, "Enhanced ballistic resistance of multilayered cross-ply UHMWPE laminated plates," *Int. J. Impact Eng.*, 2022.

[5] H. Wang, P. J. Hazell, K. Shankar, E. V. Morozov, and J. P. Escobedo, "Impact behaviour of Dyneema® fabric-reinforced composites with different resin matrices," *Polym. Test.*, 2017.

[6] S. Liu, J. Wang, Y. Wang, and Y. Wang, "Improving the ballistic performance of ultra high molecular weight polyethylene fiber reinforced composites using conch particles," *Mater. Des.*, vol. 31, no. 4, pp. 1711–1715, 2010.

[7] S. Clifton, B. H. S. Thimmappa, R. Selvam, and B. Shivamurthy, "Polymer nanocomposites for high-velocity impact applications-A review," *Compos. Commun.*, vol. 17, no. August 2019, pp. 72–86, 2020.

[8] J. G. H. Bouwmeester, R. Marissen, and O. K. Bergsma, "Carbon/Dyneema® intralaminar hybrids: New strategy to increase impact resistance or decrease mass of carbon fiber composites," in *ICAS Secretariat - 26th Congress of International Council of the Aeronautical Sciences 2008, ICAS 2008*, 2008.

[9] Z. Zheng, X. Tang, M. Shi, and G. Zhou, "Surface Modification of Uitrahigh-Molecular-Weight Polyethylene Fibers," *J. Polym. Sci. Part B Polym. Phys.*, 2004.

[10] X. Zhang, Y. Wang, C. Lu, and S. Cheng, "Interfacial adhesion study on UHMWPE fiber-Reinforced composites," *Polym. Bull.*, 2011.

[11] S. P. Lin, J. L. Han, J. T. Yeh, F. C. Chang, and K. H. Hsieh, "Surface modification and physical properties of various UHMWPE-fiber-reinforced modified epoxy composites," *J. Appl. Polym. Sci.*, 2007.

[12] M. S. Silverstein, O. Breuer, and H. Dodiuk, "Surface modification of UHMWPE fibers," *J. Appl. Polym. Sci.*, 1994.

[13] R. He, F. Niu, and Q. Chang, "The effect of plasma treatment on the mechanical behavior of UHMWPE fiber–reinforced thermoplastic HDPE composite," *Surf. Interface Anal.*, 2018.

[14] S. I. Moon and J. Jang, “Factors affecting the interfacial adhesion of ultrahigh-modulus polyethylene fibre-vinylester composites using gas plasma treatment,” *J. Mater. Sci.*, 1998.

[15] S. Teodoru, Y. Kusano, N. Rozlosnik, and P. K. Michelsen, “Continuous plasma treatment of ultra-high-molecular-weight polyethylene (UHMWPE) fibres for adhesion improvement,” in *Plasma Processes and Polymers*, 2009.

[16] K. Sakurai, Y. Kondo, K. Miyazaki, T. Okamoto, S. Irie, and T. Sasaki, “Ultrahigh-molecular-weight-polyethylene-fiber surface treatment by electron-beam-irradiation-induced graft polymerization and its effect on adhesion in a styrene-butadiene rubber matrix,” *J. Polym. Sci. Part B Polym. Phys.*, 2004.

[17] M. J. Martínez-Morlanes, P. Castell, V. Martínez-Nogués, M. T. Martinez, P. J. Alonso, and J. A. Puértolas, “Effects of gamma-irradiation on UHMWPE/MWNT nanocomposites,” *Compos. Sci. Technol.*, 2011.

[18] J. Wang, G. Liang, W. Zhao, S. Lü, and Z. Zhang, “Studies on surface modification of UHMWPE fibers via UV initiated grafting,” *Appl. Surf. Sci.*, 2006.

[19] Z. Zheng, X. Wang, X. Huang, M. Shi, and G. Zhou, “Chemical modification combined with corona treatment of UHMWPE fibers and their adhesion to vinylester resin,” *J. Adhes. Sci. Technol.*, 2006.

[20] S. Chhetri and H. Bougherara, “A comprehensive review on surface modification of UHMWPE fiber and interfacial properties,” *Compos. Part A Appl. Sci. Manuf.*, 2021.

[21] J. L. Holloway, A. M. Lowman, M. R. VanLandingham, and G. R. Palmese, “Chemical grafting for improved interfacial shear strength in UHMWPE/PVA-hydrogel fiber-based composites used as soft fibrous tissue replacements,” *Compos. Sci. Technol.*, 2013.

[22] I. Enomoto, K. Mishima, T. Kobayashi, and S. Soeda, “Functionalization of PE nonwoven fabric by plasma treatment to improve dyeing affinity,” *J. Photopolym. Sci. Technol.*, 2010.

[23] R. Oosterom, T. J. Ahmed, J. A. Poulis, and H. E. N. Bersee, “Adhesion performance of UHMWPE after different surface modification techniques,” *Med. Eng. Phys.*, 2006.

[24] F. P. M. Mercx, “Improved adhesive properties of high-modulus polyethylene structures: 3. Air- and ammonia-plasma treatment,” *Polymer (Guildf).*, 1994.

[25] B. Tissington, G. Pollard, and I. M. Ward, “A study of the effects of oxygen plasma treatment on the adhesion behaviour of polyethylene fibres,” *Compos. Sci. Technol.*, 1992.

[26] S. I. Moon and J. Jang, “The effect of the oxygen-plasma treatment of UHMWPE fiber on the transverse properties of UHMWPE-fiber/vinylester composites,” *Compos. Sci. Technol.*, 1999.

[27] S. M. M. Spyrides, F. S. Alencastro, E. F. Guimaraes, F. L. Bastian, and R. A. Simao, “Mechanism of oxygen and argon low pressure plasma etching on polyethylene (UHMWPE),” *Surf. Coatings Technol.*, 2019.

[28] C. Y. Huang, J. Y. Wu, C. S. Tsai, K. H. Hsieh, J. T. Yeh, and K. N. Chen, “Effects of argon plasma treatment on the adhesion property of ultra high molecular weight polyethylene

(UHMWPE) textile," *Surf. Coatings Technol.*, 2013.

[29] J. Li, J. Cui, J. Yang, Y. Li, H. Qiu, and J. Yang, "Reinforcement of graphene and its derivatives on the anticorrosive properties of waterborne polyurethane coatings," *Compos. Sci. Technol.*, 2016.

[30] G. Christopher, M. A. Kulandainathan, and G. Harichandran, "Biopolymers nanocomposite for material protection: Enhancement of corrosion protection using waterborne polyurethane nanocomposite coatings," *Prog. Org. Coatings*, 2016.

[31] C. Wang *et al.*, "Study on the corrosion resistance of sulfonated graphene/aluminum phosphate composites in waterborne polyurethane coatings," *Corros. Rev.*, 2021.

[32] M. Fazeli, X. Liu, and C. Rudd, "The effect of waterborne polyurethane coating on the mechanical properties of epoxy-based composite containing recycled carbon fibres," *Surfaces and Interfaces*, vol. 29, no. December 2021, p. 101684, 2021.

[33] H. C. Kuan, C. C. M. Ma, W. P. Chang, S. M. Yuen, H. H. Wu, and T. M. Lee, "Synthesis, thermal, mechanical and rheological properties of multiwall carbon nanotube/waterborne polyurethane nanocomposite," *Compos. Sci. Technol.*, 2005.

[34] B. K. Kim, J. W. Seo, and H. M. Jeong, "Morphology and properties of waterborne polyurethane/clay nanocomposites," *Eur. Polym. J.*, 2003.

[35] X. Cao, H. Dong, and C. M. Li, "New nanocomposite materials reinforced with flax cellulose nanocrystals in waterborne polyurethane," *Biomacromolecules*, 2007.

[36] J. Bergström, *Mechanics of Solid Polymers: Theory and Computational Modeling*. 2015.

[37] M. S. Kim, K. M. Ryu, S. H. Lee, Y. C. Choi, and Y. G. Jeong, "Influences of cellulose nanofibril on microstructures and physical properties of waterborne polyurethane-based nanocomposite films," *Carbohydr. Polym.*, 2019.

[38] D. M. Simić, D. B. Stojanović, S. J. Brzić, L. Totovski, P. S. Uskoković, and R. R. Aleksić, "Aramid hybrid composite laminates reinforced with inorganic fullerene-like tungsten disulfide nanoparticles," *Compos. Part B Eng.*, 2017.

[39] A. Mojtabaei *et al.*, "Influence of fullerene-like tungsten disulfide (IF-WS2) nanoparticles on thermal and dynamic mechanical properties of PP/EVA blends: Correlation with microstructure," *Compos. Part B Eng.*, 2017.

[40] D. M. Simić *et al.*, "Impact resistant hybrid composites reinforced with inorganic nanoparticles and nanotubes of WS2," *Compos. Part B Eng.*, 2019.

[41] V. Obradović, D. Simić, M. Zrilić, D. B. Stojanović, and P. S. Uskoković, "Novel Hybrid Nanostructures of Carbon Nanotube/Fullerene-like Tungsten Disulfide as Reinforcement for Aramid Fabric Composites," *Fibers Polym.*, 2021.

[42] M. Marjanović *et al.*, "Inorganic fullerene-like nanoparticles and nanotubes of tungsten disulfide as reinforcement of carbon-epoxy composites," *Fullerenes Nanotub. Carbon Nanostructures*, 2021.

[43] M. Naffakh, A. M. Díez-Pascual, C. Marco, G. J. Ellis, and M. A. Gómez-Fatou,

"Opportunities and challenges in the use of inorganic fullerene-like nanoparticles to produce advanced polymer nanocomposites," *Progress in Polymer Science*. 2013.

[44] W. E. Morton and J. W. S. Hearle, *Physical Properties of Textile Fibres: Fourth Edition*. 2008.

[45] H. Kim and S. J. Kim, "High toughness of bio-inspired multistrand coiled carbon nanotube yarn," *Carbon N. Y.*, 2018.

[46] W. Li, R. Li, C. Li, Z. R. Chen, and L. Zhang, "Mechanical properties of surface-modified ultra-high molecular weight polyethylene fiber reinforced natural rubber composites," *Polym. Compos.*, 2017.

[47] C. Li, Y. Shi, R. Zhang, G. Wang, and J. Jia, "Effect of surface modifications on the properties of UHMWPE fibres and their composites," *E-Polymers*, 2019.

[48] G. Zhang, O. R. Ghita, and K. E. Evans, "Dynamic thermo-mechanical and impact properties of helical auxetic yarns," *Compos. Part B Eng.*, 2016.

[49] D. Simić *et al.*, "Inorganic fullerene-like IF-WS2/PVB nanocomposites of improved thermo-mechanical and tribological properties," *Mater. Chem. Phys.*, 2016.

[50] T. Dayyoub *et al.*, "The structure and mechanical properties of the UHMWPE films modified by the mixture of graphene nanoplates with polyaniline," *Polymers (Basel).*, 2019.

[51] Y. Sun, C. Liu, Y. Hong, R. Liu, and X. Zhou, "Synthesis and application of self-crosslinking and flame retardant waterborne polyurethane as fabric coating agent," *Prog. Org. Coatings*, 2019.

[52] A. Harmsen, "(SELF) CROSSLINKABLE URETHANES AND URETHANE / ACRYLICS," no. January, 2016.

CHAPTER 5

Durable polyurethane/tungsten disulfide nanocoating on plasma-pretreated UHMWPE fabrics for improved mechanical and viscoelastic properties[4]

[4] Wu, S., Shaw, T.S., Bhat, G.S., and Gibbs, A.R. To be submitted to *Composites Science and Technology*.

Abstract

The influence of plasma pre-treatment and polyurethane (PU)/inorganic fullerene-like tungsten disulfide (IF-WS_2) coatings on the physical, mechanical, and viscoelastic properties of ultra-high-molecular-weight polyethylene (UHMWPE) fabrics is investigated. The UHMWPE fabrics are plasma pre-treated before various PU/IF-WS_2 dip coatings. Subsequently, the chemical structure, water contact angle, and surface morphology of plasma treated fabrics were evaluated and compared with those of the pristine fabric. The fabricated composites were subjected to dynamic mechanical analysis, tensile test, and wash durability test, and the properties are directly compared with that of the pristine fabric. The optimal composite is compared with its untreated & coated counterpart. It is found the plasma treatment induces polar groups on the fabric, slightly reduces its storage/loss modulus, and increases its elongation. After nanocomposite coatings, with less than 6% add-on the storage and loss moduli of the fabrics increase up to 694% and 757% respectively, at 30 ℃ over pristine fabrics. The gravimetric toughness of the coated fabrics improves from 67.1 J/g (pristine) up to 116.0 J/g, a maximum 73% increase. Plasma pre-treatment contributes to higher enhancement for both mechanical and viscoelastic performances of the optimal composite. Meanwhile, high wash durability (weight retention up to 98.8%) of the coatings is achieved for the composites with promising comprehensive property enhancement.

Keywords:

UHMWPE fabric, plasma pre-treatment, dip coating, dynamic modulus analysis, tensile test

5.1. Introduction

UHMWPE fabric has become one of the most popular high-performance fabrics employed in ballistic protection, aerospace, and defense applications owing to its very low density, startling mechanical properties, and high impact strength [1–4]. It can be used for flexible ballistic vests, structural fabrics in helmets and military vehicles, marine structures, etc [5,6]. Due to the increasing international conflicts and escalating demand for advanced ballistic materials, UHMWPE fabrics-reinforced polymer matrix composites (PMCs) have been extensively studied for further performance enhancement [7]. However, UHMWPE fiber shows low surface energy, smooth surface, and non-polar nature, which leads to low wettability and poor interfacial adhesion to polymer matrices [8–10]. These are detrimental in the endeavor to fabricate advanced composites and limit its application. Plasma treatment has been used as an efficient approach to improve the surface activity of UHMWPE fabrics owing to its advantages of high treating accuracy, easy up-scaling, and reduced impact on textural characteristics of materials [11–13]. After plasma treatment, various effects on UHMWPE fibers were found in previous studies such as induced oxygen-containing moieties, increased surface energy, micro-pores, and/or roughened fiber surface, which result in improved fiber/matrix interfacial adhesion [14–18].

Nanomaterials are often incorporated in polymer matrices as reinforcing nanofillers due to their outstanding energy absorption ability and high surface-to-volume ratios. Inorganic fullerene-like tungsten disulfide (IF-WS_2), which possesses unique morphology and spheric fullerene-like structure, has been reported to have high elasticity and superior shock resistance (higher than even that of carbon nanotubes) [19]. It is considered a potential material to improve the mechanical, thermal and tribological properties of polymer composites. IF-WS_2 has been employed as reinforcing fillers in matrices or composites of nylon-6 [20], polypropylene [21], poly(phenylene

sulphide) [22], poly(ether ether ketone) [23], epoxy [24], phenolic/poly (vinyl butyral)/aramid fabric [19], and PTFE/Kevlar fabric [25]. In this work, IF-WS_2 is used due to its low cost, exceptional impact resistance, and great energy absorption/dissipation capability. Waterborne polyurethanes (PUs) are applied as the polymer matrix owing to their balanced flexibility and mechanical properties as well as reduced environmental impact [26–28]. According to the thermal properties, polyurethane can be divided into thermoset and thermoplastic types. While thermoplastic PU reshapes upon sufficient heating, the molecular chains of thermoset PU crosslinks during the curing process and show no deformation process at elevated temperatures [29].

This paper considers incorporating water-based PU matrix and WS_2 nanoparticles on plasma pre-treated UHMWPE for developing lightweight advanced UHMWPE composites. Improved comprehensive properties are expected for the composites including enhanced mechanical and viscoelastic performances as well as high coating durability. This approach reduces volatile organic compounds (VOCs) discharge from the PMCs and requires low cost. The dip coating method is adopted to obtain low add-on amounts and maintain flexibility for impregnated fabrics. However, no studies have been found to directly investigate the effects of PU/WS_2 coatings on the physical, mechanical, and viscoelastic properties of plasma pre-treated UHMWPE fabrics. This work appears to be critical in filling the research gap and exploring the proposed approach systematically. In this study, the UHMWPE fabrics are plasma pre-treated and then dip-coated with varying PU/WS_2 dispersions. Two levels of PU type, PU amount, WS_2 amount, and dispersion mediums are involved. The effects of plasma treatment on the molecular structure, wettability, and surface morphology are studied using Fourier-transform infrared spectroscopy, water contact angle, and scanning electron microscopy. The influences of various

coatings on the viscoelastic characteristics, mechanical properties, and coating wash durability are investigated using dynamic mechanical analysis, tensile test, and weight retention after washing. Besides, this paper reports the impact of plasma pre-treatment on the performance of the optimal PU/WS_2/UHMWPE composite.

5.2. Materials and Methods

5.2.1. Materials and processing

UHMWPE fabrics (Spectra®, 1/1 plain weave, 38cm × 38cm) were obtained from Honeywell International Inc. Table 5.1 lists the physical properties of the UHMWPE fabrics and corresponding test conditions. Water-based polyurethane products PUA (Aptalon™ M8100) and PUB (Permax™ 202) were supplied by Lubrizol Corp. Thermoset PUA, produced by reacting isocyanates and polyamide polyols, possesses a self-crosslinking function upon curing. Whereas thermoplastic PUB, made from isocyanates and polyether polyols, shows higher flexibility and no self-crosslinking capability. The solid contents of PUA and PUB are 37 wt% and 41 wt%, respectively. IF-WS_2 aqueous suspension (IW-4000, measured solid content: 48.8 wt%) was provided by Nanotech Industrial Solutions Inc. The WS_2 nanoparticles have an average size of 80nm and exhibit fullerene-like spherical shapes and concentrically layered structure [30].

Table 5.1. Physical properties and test conditions for the UHMWPE fabrics.

Properties	Area density (g/m^2)	Fabric count (threads per cm)	Thickness (mm)	Fiber diameter (μm)
Averages	230	8.3×8.3	0.53	45
Test Conditions	3 replicates (38cm × 38cm)	3 areas	15 areas	20 fibers

The UHMWPE fabrics were plasma pre-treated on one side in N_2/O_2 (80%/20%) with assistance from Pillar Technologies, Inc. The power of 350 W and treating width of 0.3556m were applied. The fabrics were treated with a moving speed of 163.509 m/s. The UHMWPE fabrics (plasma-pretreated or untreated) were cut into small samples (about 9.5cm ×19cm) using an electric rotary fabric cutter (Allstar AS-100K). These samples were coated with PU/WS_2 nanofluids using 2-dip-2-nip method. When preparing a PU/WS2 nanofluid, a designed amount of WS_2 was added to water or water/ethanol medium, the mixture was sonicated for 30 min using a Kendal ultrasonic bath. Then PU dispersion was added into the mixture followed by sonication homogenization for another 30 min. During the coating process, each sample was dipped in prepared nanofluid for 1 min, nipped between the pressure rollers as shown in Figure 5.1. This process was repeated once, and the coated fabric was oven-dried at 100°C for 30 min. 8 replicates were prepared for each coating condition.

Table 5.2 shows the components of coating fluids in solid contents and abbreviates of corresponding PU/WS_2/UHMWPE composites. The composites A1-A4 and B1-B4 were fabricated with plasma pre-treated UHMWPE fabrics while composite A3-U was prepared with untreated fabrics as the control for composite A3.

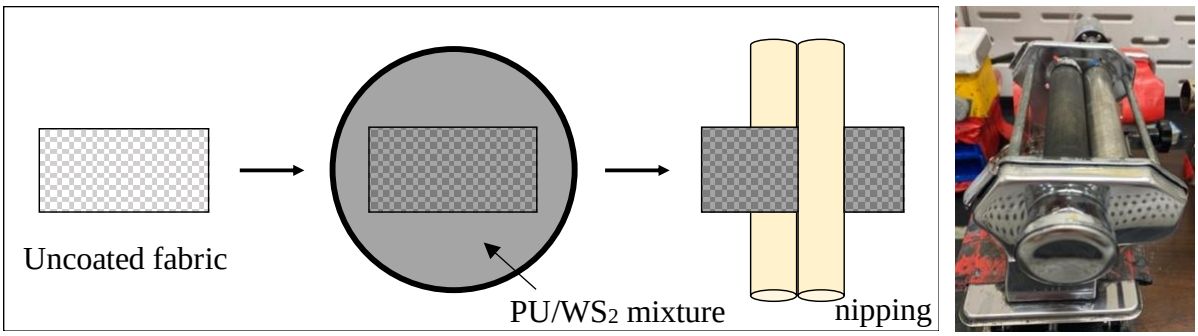

(a) (b)

Figure 5.1. Impregnation coating of PU/WS_2 on UHMWPE fabrics: (a) diagram; (b) padding setup connected with a motor.

Table 5.2. Abbreviates and coating fluid components for PU/WS_2 coated (pre-treated and untreated- "U") UHMWPE fabrics.

	PUA (%)	PUB (%)	WS_2 (%)	Medium
A1	3.7	-	1.0	W
A2	5.6	-	1.0	W
A3; A3-U	5.6	-	2.9	W
A4	0.9	-	1.0	WE
B1	-	3.7	1.0	W
B2	-	5.6	1.0	W
B3	-	5.6	2.9	W
B4	-	0.9	1.0	WE

Note: W: water; WE: water: ethanol (wt. 1:5)

5.2.2. Characterization

5.2.2.1. Fourier-transform infrared spectroscopy

The functional groups of untreated and plasma treated UHMWPE fabrics were detected using a Fourier transform infrared spectrometer (FT-IR) (ThermoFisher Nicolet 6700). The spectrums of absorbance in the range of 750 cm^{-1} to 4000 cm^{-1} were obtained.

5.2.2.2. Water contact angle

A microscope included lab setup (Figure 5.2) and AmScope analysis software were used to observe and measure the water contact angle for neat and plasma treated UHMWPE fabrics. At least three measurements were conducted at varying areas on each specimen.

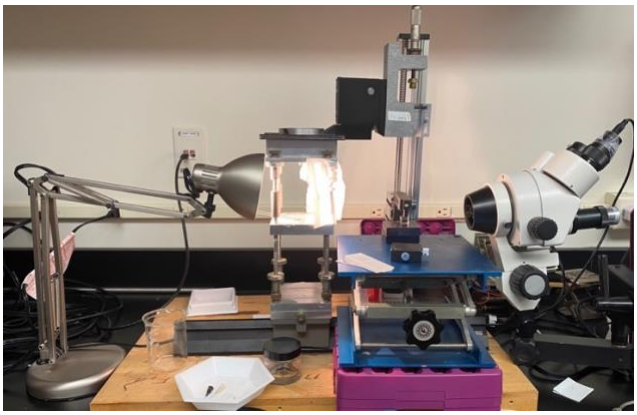

Figure 5.2. The lab setup for measuring water contact angles on UHMWPE fabrics.

5.2.2.3. Scanning electronic microscopy

A scanning electronic microscope (FE-SEM Thermo Fisher Teneo) was used to observe the surface appearances of untreated and plasma treated UHMWPE fabrics as well as their PUA/WS_2 coated counterparts. The magnifications of 100, 350, 500, 2000, and 5000 were applied.

5.2.2.4. Add-on and appearance

UHMWPE fabrics were weighed before and after nanocomposite coatings to determine the PU/WS_2 add-on percentage for each sample. The weights of 8 replicates were tested. Photographs of the coated specimens were taken in a Macbeth SpectraLight II light booth using daylight illumination.

5.2.2.5. Dynamic mechanical analysis

Viscoelastic properties of neat, plasma treated, and coated specimens were measured using a dynamic mechanical analysis (DMA) instrument (PerkinElmer DMA 8000). All samples with the size of 9 mm × 22 mm were tested in tension mode with frequency of 1 Hz, force multiplier of 1.2, and strain of 0.005 mm. Temperature sweeps in the range from 25 °C to 100 °C were conducted at a heating rate of 3 °C/min. In addition, frequency sweeps from 0.1 Hz to 10Hz at 25°C were carried out on selected composites, the frequency was set to increase logarithmically at

ten points per decade. When clamping the samples, double-sided tapes were applied to the clamps to prevent fabric slippage during testing. Sample thickness was measured using a caliper.

5.2.2.6. Mechanical properties

Mechanical properties of neat, plasma treated, and coated UHMWPE fabrics were tested using a universal testing machine (Instron 4411) according to the modified ASTM D5035 standard. The gauge length and extension rate applied were 75mm and 100mm/min, respectively. It is highly challenging to test the tensile strength of UHMWPE fabrics due to their extremely high tensile strength and smooth surface, which cause easy yarn or fabric slippage under force. In this work, a unique sample preparation method was used with reduced fabric width and fixation cardboards. Fabrics strips (16mm ×175mm) were cut using a rotary fabric cutter. Before testing, each sample was prepared as shown in Figure 5.3. Approximately 4 yarns were raveled from each length side leaving 5 central testing yarns, 25mm of yarns were also removed from the top and bottom of the fabric. The width and thickness of each sample were measured at three locations using a caliper and a ProGage thickness tester, respectively. The averages were used for further calculations. Both ends of the specimen were then glued symmetrically on cardboards (30mm × 50mm) leaving 75mm of the tested length using Elmer's Clear Glue. 2mm of the cardboards from the inner edges was left unglued to prevent jaw breaks. The yarns on the ends were split and spread on the cardboards with glue for a stronger bonding. The prepared samples were air dried overnight before the tensile test. Mechanical properties including maximum load and elongation at break were collected. The total energy absorption and volumetric toughness (VT) were calculated by integrating load-elongation and stress-strain curves, respectively [31]. Gravimetric toughness (GT) was calculated using the length, width, thickness, and weight of samples [32]. Means of three replicates are reported.

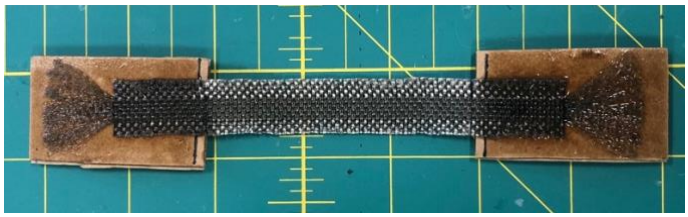

Figure 5.3. A prepared PU/WS2/UHMWPE sample for tensile test.

5.2.2.7. Wash durability

Wash durability of composites was tested according to the weight retention amount after standard washing. Three replicates (50mm× 100 mm) of coated dry fabrics were weighed and washed as per AATCC Test Method 61. 10 steel balls and 0.37% of AATCC detergent of total volume were added in a canister with each fabric, the washing procedure was conducted in an Atlas Launder-ometer at 40 °C for 45min. The washed samples were oven dried at 60°C overnight and weighed to estimate the weight retention percentage (R/%) of the coatings using equation (5.1).

$$R = \frac{W_a - \frac{W_b}{1 + A/100}}{W_b - \frac{W_b}{1 + A/100}} \times 100 \qquad (5.1)$$

Where W_b and W_a are the sample weights before and after washing, respectively; A is the coating add-on percent for the sample.

5.3. Results and Discussion

5.3.1. Chemical structures

Figure 5.4 shows the FT-IR spectrums of pristine (a) and plasma treated (b) UHMWPE fabrics. The characteristic peaks of UHMWPE fiber can be observed in both spectrums at 2916, 2849, 1473, and 727 cm^{-1}. These peaks are attributed to -CH_2 stretching (2916 cm^{-1}, 2849 cm^{-1}), -

CH_2 deformation, and -CH_2 rocking vibrations [33,34]. In comparison, new absorption peaks are exhibited in the plasma modified fabric at about 3250 and 1720 cm^{-1}, which are assigned to -OH and C=O stretching vibrations, respectively [35]. The new peaks with low intensity indicate a small amount of oxygen-based polar groups (-OH and -C=O) appear on the surface of modified UHMWPE fabrics, and the treatment conditions were strictly controlled to apply a limited modification.

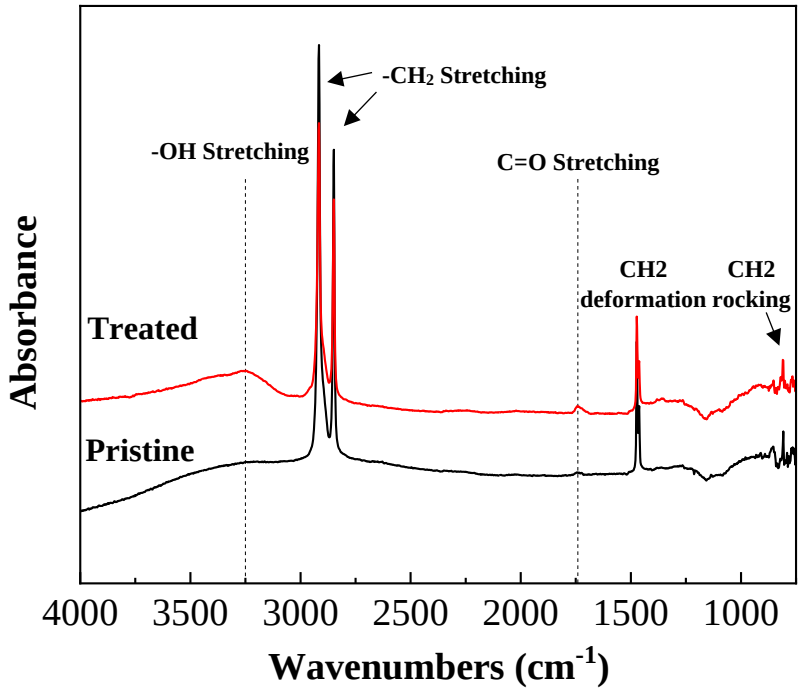

Figure 5.4. FT-IR Spectra of pristine and plasma treated UHMWPE fabrics.

5.3.2. Hydrophilic property

Water contact angles of the pristine and plasma treated UHMWPE fabric surfaces were measured to evaluate their hydrophilic properties. Figure 5.5 shows the water contact angles and appearance of water droplets on pristine and plasma pre-treated UHMWPE fabrics with varying

time: 0min, 3min, and 6 min. With plasma treatment, the water contact angle of UHMWPE fabrics drops significantly from 105.2° ± 1.4° to 81.1° ± 2.1° (P-value =0.0002) with a decrease of 22.9% on average over pristine fabrics. Along with the FT-IR result, it suggests that plasma pre-treatment improves the surface hydrophilicity of the UHMWPE fabrics by inducing oxygen-containing polar groups.

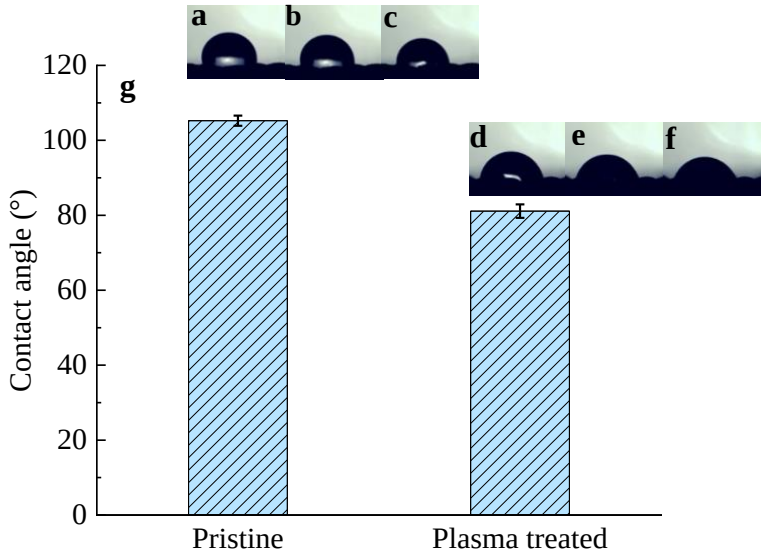

Figure 5.5. Water contact angles of UHMWPE fabrics: (a-c) pristine, after 0, 3, and 6 min; (d-f) plasma treated, after 0, 3, 6 min; (g) contact angles measured at 0 min.

5.3.3. Surface morphology

Figure 5.6 represents the SEM micrographs of (a) pristine and (b) surface modified UHMWPE fabrics. From both micrographs, cross-sectional small cracks on the smooth surfaces can be observed, which are formed from manufacturing. No significant changes or damages in surface morphology are shown in the yarns from the plasma treated fabric, which reflects the well-controlled plasma treatment on the fabrics and gentle treatment conditions.

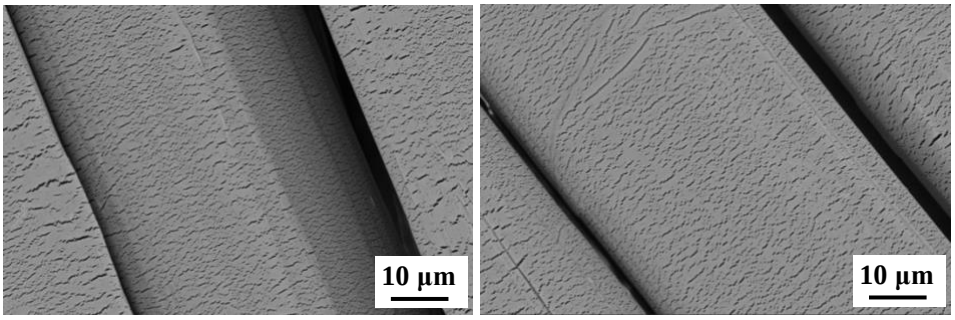

(a) (b)

Figure 5.6. SEM micrographs of (a) pristine and (b) plasma treated UHMWPE fabrics.

5.3.4. Physical properties

As shown in Table 5.3, through the two-dip-two-nip coating process, a small range of PU/WS_2 add-on amount (1.46 wt. % - 5.96 wt%) is obtained on treated UHMWPE fabrics A1-A4 and B1-B4. This is achieved by keeping the coating process and nipping pressure constant. It is observed that specimen B2 obtains a significantly higher coating amount over specimen B1 due to the increasing PU solid content (5.6% over 3.7%) in its coating fluid. In comparison to samples A2 and B2, samples A3 and B3 show rising add-on amounts, respectively, owing to their higher WS_2 solid contents (2.9% over 1.0%) in coating mixtures. The lower add-on percentages of composites A4 and B4 are ascribed to the lower solubility of PU in ethanol/water mixture over water and reduced PU addition in both dispersions. As expected, comparable add-on amounts are achieved for most pairs of A and B samples using the same PU and WS_2 amounts in fluids, e.g., A1-B1. For direct comparison, the tensile energy absorption capacity in section 3.6 was normalized by sample weight (gravimetric toughness). Figure 5.7 represents the optical images of the specimens A1-A4 and B1-B4. As observed, all fabrics are coated uniformly with light- or dark-brown shades from incorporated WS_2 particles. All specimens, except A3 and B3, show similar colors, while fabrics A3 and B3 exhibit darker colors due to their higher WS_2 amounts used.

Table 5.3. Add-on amounts (mean ± SE) for all pre-treated and PU/WS_2 coated UHMWPE fabrics.

Sample	A1	A2	A3	A4	B1	B2	B3	B4
Add-on (%)	2.62 ± 0.10	2.94 ± 0.06	5.36 ± 0.18	1.46 ± 0.11	2.96 ± 0.07	4.68 ± 0.12	5.94 ± 0.11	2.07 ± 0.17

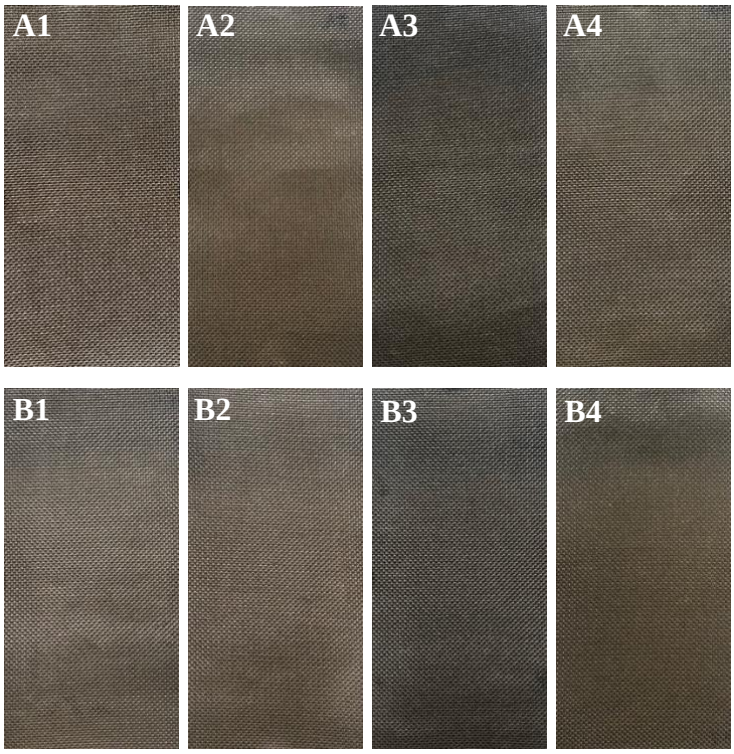

Figure 5.7. The appearance of plasma pre-treated and PU/WS_2 coated UHMWPE fabrics A1-A4 and B1-B4.

5.3.5. Viscoelastic properties

DMA temperature sweeps were conducted on neat, plasma treated, and all treated/coated UHMWPE specimens (A1-A4 and B1-B4). As depicted in Figures 5.8 (a) and (c), the samples exhibit decreasing trends in storage modulus, while their loss modulus in Figures 5.8 (b) and (d) first increases and then decreases. Storage modulus is associated with the elasticity and stiffness of a material and is proportional to the energy stored by the material during a loading cycle, while loss modulus indicates the viscosity and energy dissipated by the tested sample. They can be used

to predict the impact behaviors of materials at the intrinsic level [36]. With plasma treatment, both storage and loss moduli of the UHMWPE fabric drops slightly in the tested temperature range, in comparison to the neat fabric. Both storage and loss moduli of samples A1-A4 can be arranged in a descending order as A3>A4>A2>A1. Samples A2-A4 show enhanced storage and loss moduli over neat and plasma treated samples, while their tan δ (damping factor) slightly decrease due to the larger increase in storage modulus than in loss modulus. Similarly, the viscoelastic properties of specimens B1-B4 can be observed as B1>B3>B2>B4, and all four samples show increasing storage and loss moduli to different extents, compared to neat and plasma treated controls. Both the PU/WS_2 coatings and the combination of plasma treatment and the coatings improve the energy absorption and dissipation abilities of the UHMWPE fabrics. Tan δ of SB3 sample at the tested temperature range and SB1 sample at temperature higher than ~80 °C increased indicating their enhanced damping ability compared to both neat and plasma treated yarns.

As summarized in Table 5.4, compared with the neat control, the storage and loss moduli of the composites A1-A4 increase up to 402% and 343% at 30°C, respectively. The maximum moduli were obtained from specimen A3. When PUB is incorporated, storage and loss moduli of the composites B1-B4 increase up to 694% (from B1) and 757% (from B3), respectively. These results indicate that although the plasma treatment lowers the viscoelastic characteristics of UHMWPE fabrics, all final PU/WS_2 coated fabrics, except sample A1, exhibit higher elasticity and viscosity than the neat fabric to varying extents. Also, at the temperatures above 95°C, the storage modulus and/or loss modulus of the neat, plasma treated, and B3 specimens increase due to the shape memory effect (SME) of UHMWPE fibers. Upon heating, sample temperature rises with the energy absorbed which activates the SME, then UHMWPE fibers in the sample tends to

return to their original form before orientation leading to an increase in their cross sections. This effect ultimately results in rising storage and/or loss moduli [37,38].

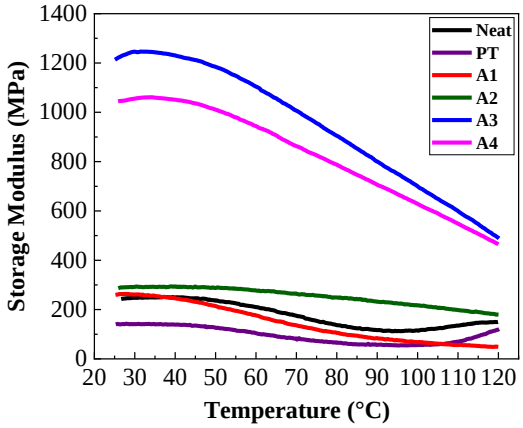

(a)

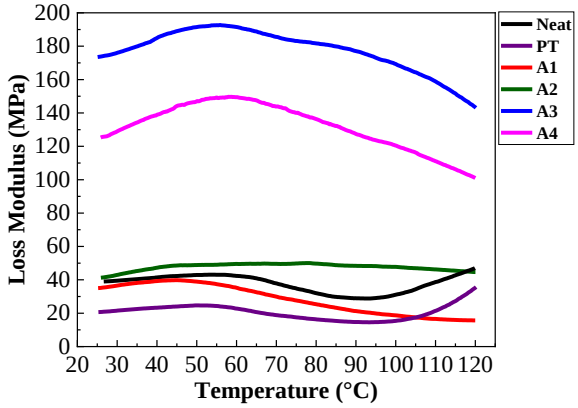

(b)

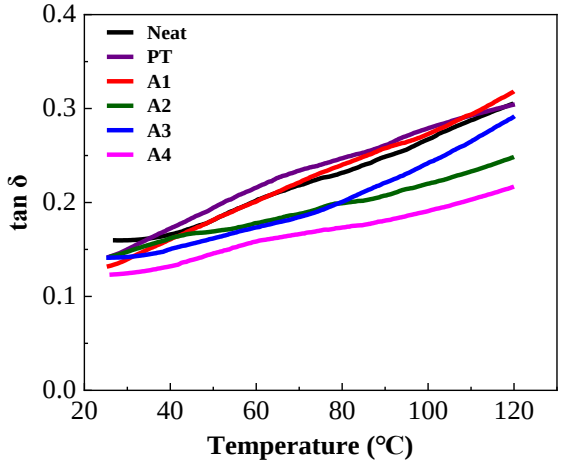

(c)

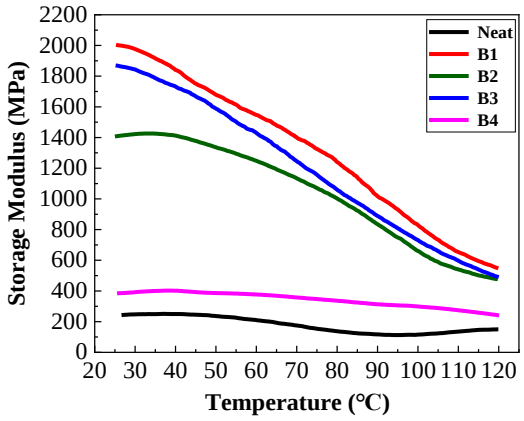

(d)

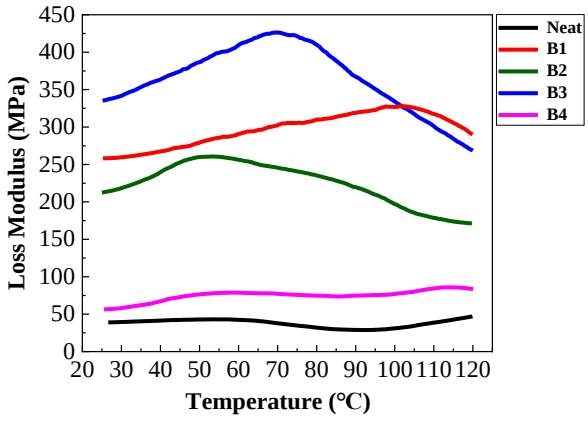

(e)

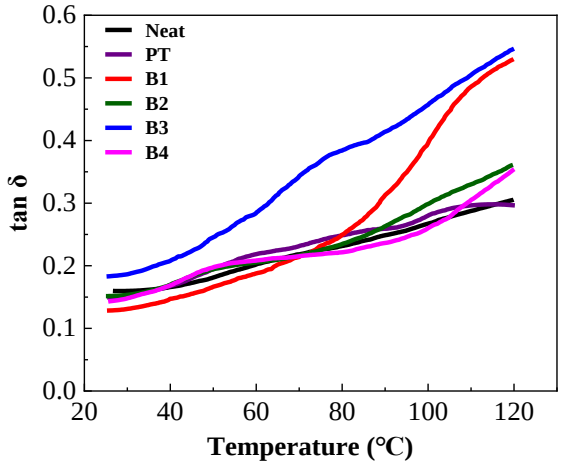

(f)

Figure 5.8. The DMA results for the control and PU/WS_2 coated UHMWPE fabrics: (a) storage modulus, (b) loss modulus, and (c) tan δ of the neat, plasma treated (PT), and A1-A4 samples; (d) storage modulus, (e) loss modulus, and (f) tan δ of the neat and B1-B4 samples.

Table 5.4. DMA results for neat, plasma treated (PT), A1-A4, and B1-B4 specimens collected at 30 °C.

	Neat	PT	A1	A2	A3	A4	B1	B2	B3	B4
Storage Modulus (MPa)	247.7	140.6	261.0	293.0	1243.6	1059.2	1967.3	1420.9	1800.1	393.2
Loss Modulus (MPa)	39.4	21.3	36.8	42.5	174.3	128.2	258.9	216.8	337.2	58.2

5.3.6. Mechanical properties

In section 3.5, coated specimens including A2-A4 and B1-B4 have shown enhanced viscoelastic properties over neat fabrics to different degrees. In this section, tensile tests were carried out on the same specimens i.e., neat, plasma treated, and PU/WS_2 coated A1-A4 and B1-B4 fabrics. The effects of plasma treatment and nanofiller-reinforced PU coating on their mechanical performance are studied. The results show the comparison of the average (a) maximum load, (b) elongation at break, (c) volumetric toughness, and (d) gravimetric toughness of the specimens. In the case of the maximum load of samples shown in Figure 5.9 (a), Anova analysis indicates the results from the tested groups are significantly different at α=0.05 (P-value<0.0001). Tukey test is further applied for multiple comparisons. It is found the maximum load values between the plasma treated and neat fabrics are not significantly different. Samples A2 and B1-3 show significantly lower maximum load than the neat fabric due to the incorporation of polyurethane matrix, which has lower tensile strength than UHMWPE materials resulting in reduced composite strength (rule of mixtures) [39]. The maximum load of specimen A1 is significantly higher than B1 despite the same PU/WS_2 ratio in their coating fluids and comparable addon% obtained, this indicates the higher tensile strength of PUA than PUB material. Figure 5.9

(b) represents the elongation at break values for these samples. They are significantly different for at least one pair of samples (α=0.05, P-value<0.0001). Tukey test reveals the plasma treatment significantly increased (86%) the elongation at break value for the UHMWPE fabrics due to the reduced modulus and maintained maximum load. Besides, PU/WS_2/UHMWPE composites A1-A4 and B1-B3 also show significantly higher elongation values than the neat fabric due to the combined effects of plasma treatment and nano-reinforced elastomer coatings. The elongation of composites A3 and A4 increases by 18% and 27% over the PT fabric; and 120% and 137%, over the neat fabric, respectively. Composite A3 shows 8% higher elongation than A4 even with a lower coating amount and PU addition. This is attributed to the better dispersion uniformity and stability of WS_2 nanoparticles in ethanol/water mixture than those in water. Dispersing homogeneity of nanomaterials on fiber/fabric substrates can largely impact their reinforcement on mechanical characteristics of fabricated nanocomposites [40]. Figure 5.9 (c) shows the volumetric toughness of the specimens, which was calculated by integrating the stress-to-strain curves. It represents the amount of energy per unit volume a tested fabric can absorb before rupture. Similarly, the gravimetric toughness, which is converted from VT, equals the amount of energy per unit mass a tensile sample can absorb before fracture (Figure 5.9 (d)). Both VT and GT for the tested specimens are significantly different (α=0.05, both P-values <0.0001). The multiple comparison results reveal the VT and GT between neat fabrics and plasma treated fabrics are not significantly different. This indicates the plasma treatment has no significant impact on the toughness/energy absorption capability of the UHMWPE fabric although it decreases the average maximum load and increases the elongation at break. Composites A3 and A4 show comparable VT and GT values, which are significantly higher (A3: 38% and 49%; A4: 49% and 73%) than the neat fabric. It means both composites absorb more energy per unit volume and per unit mass before rupture than

neat fabrics. It can also be interpreted as (1) with the same amount of energy absorbed during tensile tests, the composites A3 and A4 will be 28% and 33% smaller in volume or 33% and 42% lighter, respectively, than neat UHMWPE fabrics; or (2) with the same volume or weight as neat fabrics, the composites A3 and A4 possess 38% and 49% (same volume) or 49% and 73% (same weight) higher tensile energy absorption capacity, respectively.

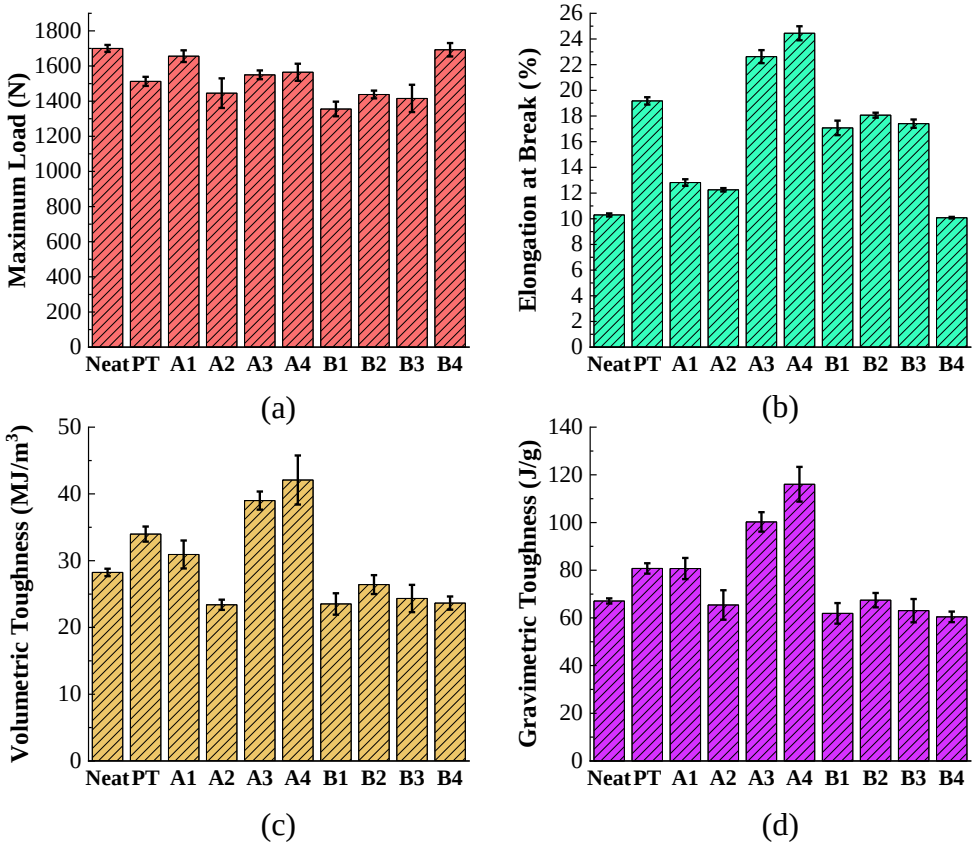

Figure 5.9. Mechanical properties (mean and SE) of the neat, plasma treated (PT), and PU/WS_2 coated UHMWPE fabrics: (a) maximum load; (b) elongation at break; (c) volumetric toughness; (d) gravimetric toughness.

5.3.7. Wash durability

For protective garment end uses, the wash durability of the coatings on fabrics appears to be critical. Figure 5.10 represents the weight retention of coatings of the eight groups of specimens.

The average values are significantly different at a 95% confidence level (P-value<-0.0001). After washing, the coating on the PUA based composites (A1-A4) retains 92.2% - 98.8%, while it on PUB based composites (B1-B4) keep 60.1- 93.3%. Due to the presence of a self-crosslinking function for PUA, the A1-A4 specimens show higher coating weight retention (up to 60.2%) than their counterparts. With crosslinks formed between molecular chains, the water-based PU turns into tough thermoset PU with high wash durability. Due to the ethanol/water mixture used, the B4 composite obtained better wash durability than the B1-B3 composites. The A3 and A4 specimens, which have enhanced storage modulus, loss modulus, VT, and GT, also show high weight retention of the coatings after wash, which are 98.8% and 97.3% on average, respectively. Their high wash durability can be confirmed by the color of the water after the wash procedure and the color difference between the unwashed and washed fabrics in Figure 5.11 The color for specimens A3 and A4 remained clear with some detergent bubbles and the colors of washed A3 and A4 fabrics are similar to those of the unwashed fabrics. In contrast, the water of specimen B3 showed a dark brown color due to the dispersion of a large amount of WS_2 particles that were washed off from the fabric. An obvious color fading is observed on the washed B3 sample in comparison to its unwashed counterpart, which is attributed to the loss of the PU/WS_2 coating.

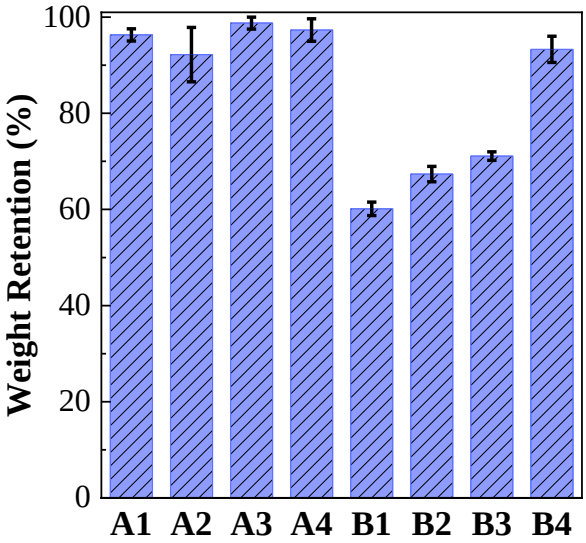

Figure 5.10. Weight retention (Mean and SE) of the plasma pretreated and PU/WS_2 coated UHMWPE fabrics.

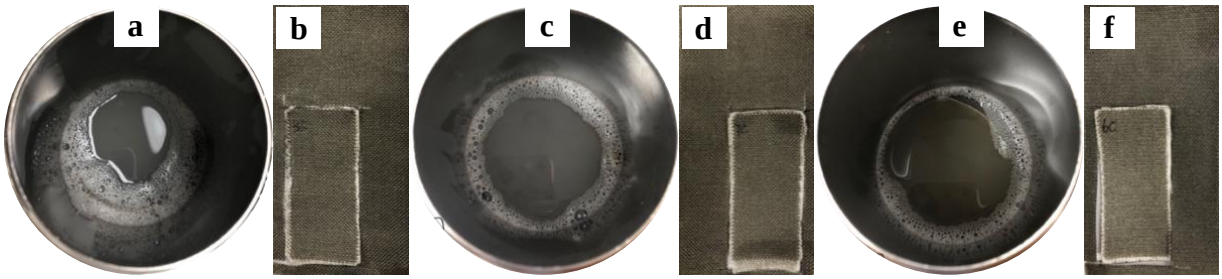

Figure 5.11. The appearance of washing water, unwashed sample, and washed sample: (a-b) A3; (c-d) A4; (e-f) B3.

5.3.8. Effects of plasma pre-treatment on the composites

As shown in sections 3.5 and 3.6, specimen A3, which was coated with a pre-treated UHMWPE fabric, achieves the highest viscoelastic properties and largely improved tensile toughness. To investigate the effects of plasma treatment on mechanical performance and wash durability of the composite, specimen A3-U was fabricated with untreated UHMWPE fabrics. The

add-on amounts for A3 and A3-U are 5.36 ± 0.18% and 5.66 ± 0.20%, respectively, which are not statistically different (p-value=0.2870). Table 5.5 compares their mechanical properties obtained from tensile tests, i.e., maximum load, elongation at break, total energy absorbed, and toughness. Also compared in the table are the coating weight retention % for the composites A3 and A3-U after washing, differences between all outcomes, and Anova P-values. The results indicate that the plasma pre-treatment decreases the average maximum load of the composite A3, however the difference is not statistically significant. Meanwhile, the elongation at break, total energy absorbed, volumetric toughness, gravimetric toughness, and weight retention of A3 are all significantly higher than those of A3-U, which show an improvement of 105.5%, 58.9%, 48.3%, 61.0%, and 6.7%, respectively. The enhanced mechanical properties and wash durability of the coating are ascribed to the plasma treatment, which introduces polar groups on UHMWPE fabrics and increases their surface wettability. The property enhancement reflects the improved interfacial adhesion between the polyurethane matrix and the UHMWPE fiber surface.

Table 5.5. Mechanical properties, weight retention, and statistical analysis for the composites A3-U and A3.

Properties	A3-U	A3	P-value
Maximum load (N)	1643 ± 33	1550 ± 25	0.0679
Elongation at break (%)	11.0 ± 0.3	22.6 ± 0.5	< 0.0001
Total energy absorbed (J)	5.6 ± 0.4	8.9 ± 0.4	0.0013
Volumetric toughness (MJ/m3)	26.3 ± 1.9	39.0 ± 1.4	0.0024
Gravimetric toughness (J/g)	62.3 ± 4.0	100.3 ± 4.1	0.0013
Weight retention (%)	92.6 ± 0.8	98.8 ± 1.2	0.0142

Figure 5.12 represents the DMA results for both composites A3-U and A3 from the temperature sweeps. Specimen A3 shows superior storage modulus and loss modulus over A3-U

for the tested temperature range. At 30℃, the storage moduli of A3-U and A3 are 267.3 MPa and 1243.6 MPa respectively resulting in an improvement of 365.2% for A3-U. In the case of loss modulus, A3 also shows an increase of 342.4% over A3-U with values of 174.3 MPa and 39.4MPa. With the greater improvement in storage modulus, the tan δ (loss modulus/storage modulus) of A3 sample decreases slightly compared to that of A3-U. The damping abilities of both samples improve as the temperature increases. Apart from typical temperature sweeps, frequency sweeps from 0.1 HZ to 10 Hz at 25℃ were also conducted on neat, A3-U, and A3 specimens. Figure 5.13 plots their storage modulus, loss modulus, and tan δ along with varying frequency. The storage modulus curves show slow rises with increasing frequency, while the loss modulus slightly decreases, which leads to the decline of tan δ values with higher frequency. It is observed the composite A3-U, without plasma pre-treatment, showed no obvious and consistent improvements in the outcomes over neat fabrics. While composite A3 exhibits significant increases in both moduli and tan δ over the neat sample or its counterpart A3-U.

Table 5.6 collects the storage modulus, loss modulus, and tan δ of the specimens from frequency sweeps at 10 Hz. As observed, without plasma pre-treatment, composite A3-U shows improved tan δ (0.17) compared to the neat fabric (0.11) due to its slightly higher loss modulus and lower storage modulus. Tan δ, also called the damping coefficient, reflects the energy dissipation potential of a material. It decreases for all three samples at a higher frequency due to the nature of their flexible textile substrates. The increased tan δ of composite A3-U indicates its better energy dissipation capability over neat UHMWPE fabrics. In the case of composite A3, the storage and loss moduli at 10 Hz reach 136.3 MPa and 22.8 MPa, which show an increase of 239.9% and 240.3%, respectively, over its counterpart A3-U. This suggests that the plasma pre-treatment on UHMWPE fabrics greatly enhances the elasticity (energy storage) and viscosity

(energy dissipation) of the PUA/WS_2 incorporated UHMWPE composites. In comparison to the neat fabric, PUA/WS_2 coated fabric A3 shows significantly higher storage, loss moduli, and tan δ, which are improved by 209.1%, 365.3%, and 54.5%, respectively. The enhanced viscoelastic properties are attributed to the combination of surface modification of UHMWPE by plasma treatment and PU/WS_2 nanocomposite coating. The former improves the wettability and surface activity of UHMWPE fabrics leading to better fiber/matrix interfacial adhesion, while the latter contributes to higher energy absorption and dissipation capacities due to the following mechanisms: (1) PU polymer failure, (2) fiber/matrix adhesion failure, and (3) nanoparticles energy absorption and dissipation.

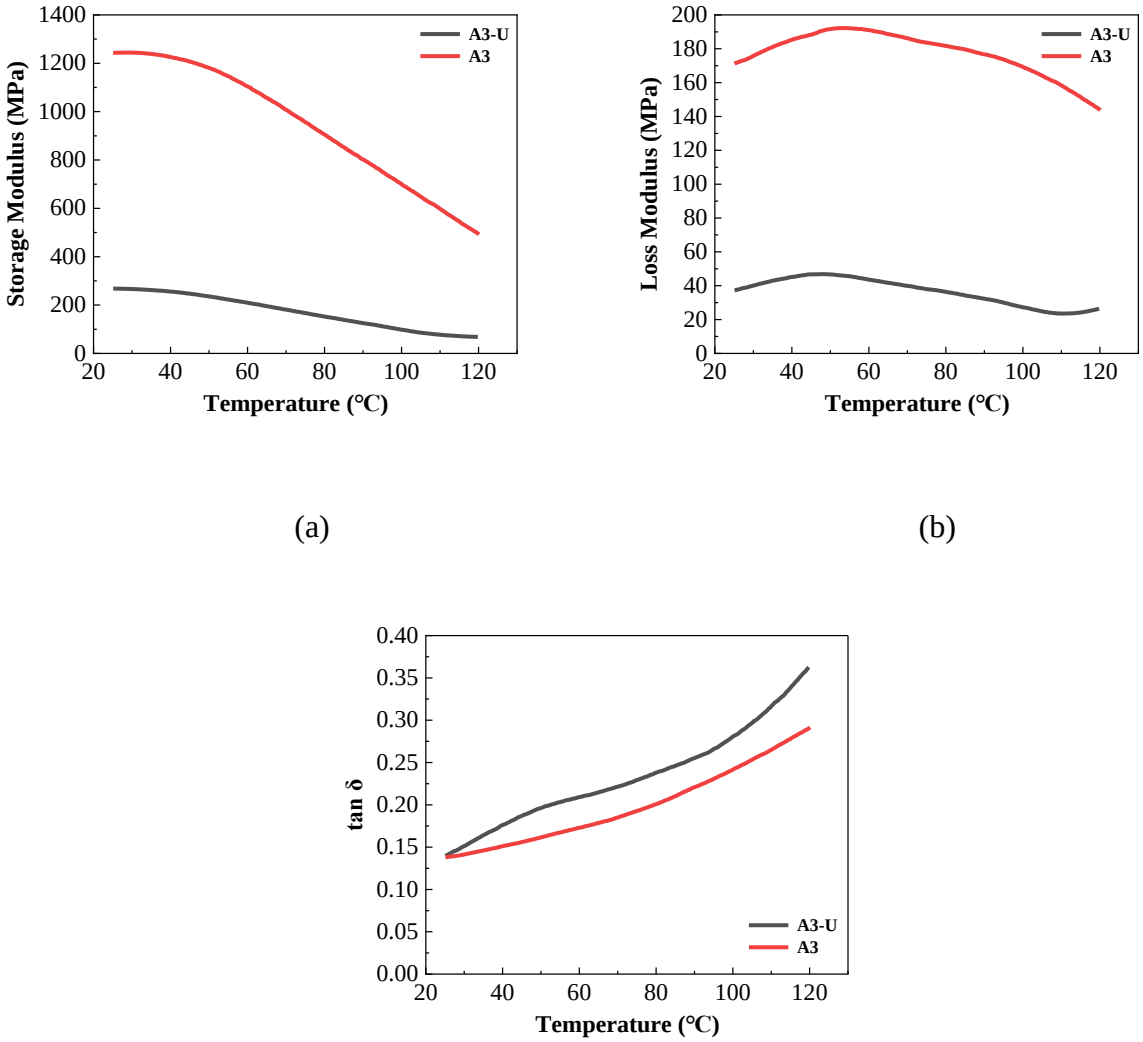

Figure 5.12. DMA temperature sweeps for PUA/WS_2/UHMWPE composites A3-U and A3: (a) storage modulus; (b) loss modulus; (c) tan δ.

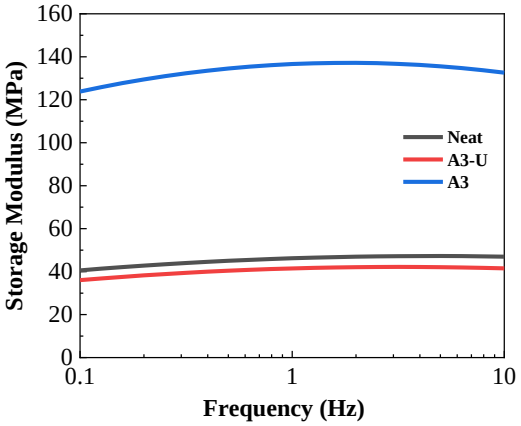

(a)

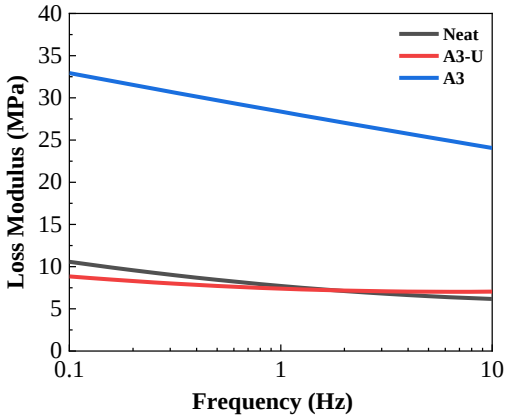

(b)

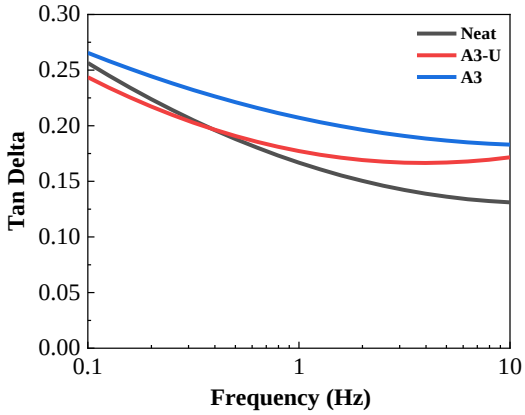

(c)

Figure 5.13. DMA frequency sweeps for the neat, A3-U and A3 specimens: (a) storage modulus; (b) loss modulus; (c) tan δ .

Table 5.6. DMA results collected from frequency sweeps at 10 Hz for the neat UHMWPE, A3-U, and A3 specimens.

	Storage Modulus (MPa)	Loss Modulus (MPa)	Tan Delta
Neat	47.0	6.2	0.13
A3-U	41.5	7.0	0.17
A3	132.6	24.0	0.18

Scanning electron microscopy was used to observe the surface morphologies of the specimens at different magnifications 100×, 350/500×, 2000×, and 5000×. Figure 5.14 (a-d), (e-h), and (i-l) present the SEM images of the neat UHMWPE, A3-U, and A3 specimens, respectively. The 1/1 plain-weave structure and fiber features shown in the neat fabric (a) are clearly observed from specimens A3-U (e) and A3 (i) due to their low add-on amounts (5.36% and 5.66%). After coating, some of the gaps between fibers are filled with PU/WS_2 material and surface roughness increases slightly for specimens A3-U and A3. While fiber surfaces in the neat fabric are clean and smooth as observed in Figure 14 (b-d), coated sample A3-U shows thin PU polymer films on fiber surfaces and some interlacing/overlapping edges bonding adjacent fibers, and a small amount of WS_2 particles embedded in PU films are seen on fiber surfaces (Figure 5.14 (f-h)). Similarly, on sample A3, thin PU films are formed on fiber surfaces, nevertheless, with a better uniformity. An increasing amount of WS_2 particles are observed on fiber surfaces of sample A3 compared to that of A3-U despite same WS_2 amount added in both coating fluids (Figure 5.14 (j-l)). These differences in surface features between the composites A3-U and A3 indicate improved wettability and surface activity of the UHMWPE fabric after plasma pre-treatment. This leads to an even spread of the PU on UHMWPE fibers and stronger interfacial adhesion between the UHMWPE fibers and PU films holding more WS_2 particles. Stronger bonding between adjacent fibers and higher load transfer efficiency can be achieved. Along with the energy absorption and dissipation contribution from additional adhered WS_2 particles, the mechanical and viscoelastic properties of composite A3 are enhanced compared to that of A3-U.

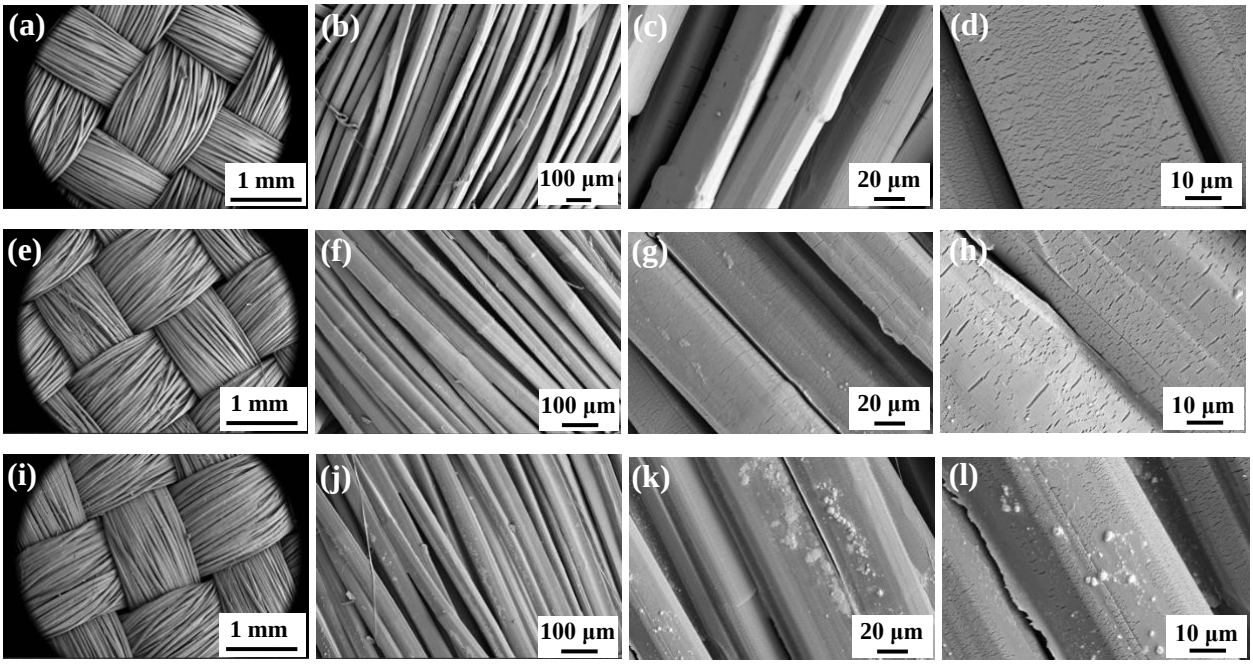

Figure 5.14. SEM images for the specimens at varying magnifications: (a-d) neat UHMWPE fabric; (e-h) coated fabric A3-U; and (i-l) coated fabric A3.

5.4. Summary

The effects of plasma pre-treatment and polyurethane (PU)/tungsten disulfide (WS_2) coatings on the performances of UHMWPE woven fabrics have been investigated experimentally in this work. The direct influence of plasma treatment on the fabrics is studied using FT-IR, water contact angle, and SEM. Several coating components have been used which involve two levels of PU type, PU amount, WS_2 amount, and the dispersion medium. Various properties for the coated fabrics have been tested or observed i.e., add-on amounts, coating uniformity, viscoelastic properties, mechanical properties, and wash durability. The conclusions can be summarized as follows:

- The plasma pre-treatment induced a small number of polar groups including -OH and C=O on the UHMWPE fabrics which significantly decrease the water contact angle of the fabrics

from 105.2° ± 1.4° to 81.1° ± 2.1°. With well-controlled treating conditions, the surface morphology of the plasma treated UHMWPE fabrics shows no obvious changes to the fiber surface and no significant effect on the toughness of the fabric. However, the plasma treatment slightly decreases the storage and loss moduli of the fabric, while it increases its elongation at break.

- The add-on amounts for the PU/WS_2 coated UHMWPE fabrics are maintained at a low range of 1.46 wt% - 5.96 wt%. At 30 ℃, the storage and loss moduli of specimens A2-A4 are improved up to 402% and 343% compared to the neat fabric (maximum obtained from A3, in which 5.6% PUA and 2.9% WS_2 were used in water). In the case of specimens B1-B4, the same properties increase up to 694% and 757%, respectively. Meanwhile, the volumetric toughness (VT) of A3 and A4 is enhanced by 38% and 49%, while the gravimetric toughness (GT) of A3 and A4 is 49% and 73% higher than the neat fabric, respectively. The elongation of A3 and A4 are 120% and 137% higher than that of the neat fabric. These improvements are attributed to enhanced UHMWPE fiber/PU film interfacial adhesion and nano-reinforced elastomeric coatings.
- The weight retention of PUA based WS_2/UHMWPE composites after washing is overall higher than that of PUB based composites due to the self-crosslinking function of PUA, leading to their great potential in particular end-uses such as ballistic vests and protective gloves.
- The plasma pre-treatment indeed improves the performance of the coated fabrics. It results in an increase of 105.5%, 58.9%, 48.3%, 61.0%, and 6.7% for the elongation at break, total energy absorbed, VT, GT, and weight retention of composite A3 (3.5 wt% PU and 1.9 wt% WS_2 on the fabric by calculation). And the storage and loss moduli are increased with

varying temperature or frequency compared to untreated counterpart A3-U. At 10 Hz, an improvement of 209.1%, 365.3%, and 54.5% is achieved for the storage modulus, loss modulus, and tan δ of composite A3 over the neat sample.

- Overall, plasma pre-treated and PUA/WS_2 coated UHMWPE fabrics A3 and A4 show promising mechanical, viscoelastic, and wash durability properties. With further research, they may be used for flexible and lightweight ballistic and energy absorption materials.

5.5. Reference

[1] Bhatnagar A. Lightweight Ballistic Composites: Military and Law-Enforcement Applications: Second Edition. 2016. https://doi.org/10.1016/C2014-0-03657-X.

[2] Zhang D, Sun Y, Chen L, Zhang S, Pan N. Influence of fabric structure and thickness on the ballistic impact behavior of Ultrahigh molecular weight polyethylene composite laminate. Mater Des 2014;54:315–22. https://doi.org/10.1016/j.matdes.2013.08.074.

[3] Meng L, Li W, Ma R, Huang M, Wang J, Luo Y, et al. Long UHMWPE fibers reinforced rigid polyurethane composites: An investigation in mechanical properties. Eur Polym J 2018. https://doi.org/10.1016/j.eurpolymj.2018.05.021.

[4] Zhang TG, Satapathy SS, Vargas-Gonzalez LR, Walsh SM. Ballistic impact response of Ultra-High-Molecular-Weight Polyethylene (UHMWPE). Compos Struct 2015;133:191–201. https://doi.org/10.1016/j.compstruct.2015.06.081.

[5] Liu S, Wang J, Wang Y, Wang Y. Improving the ballistic performance of ultra high molecular weight polyethylene fiber reinforced composites using conch particles. Mater Des 2010;31:1711–5. https://doi.org/10.1016/j.matdes.2009.01.044.

[6] Nguyen LH, Ryan S, Cimpoeru SJ, Mouritz AP, Orifici AC. The effect of target thickness on the ballistic performance of ultra high molecular weight polyethylene composite. Int J Impact Eng 2015;75:174–83. https://doi.org/10.1016/j.ijimpeng.2014.07.008.

[7] Firouzi D, Mudzi P, Ching CY, Farncombe TH, Ravi Selvaganapathy P. Use of pressure sensitive adhesives to create flexible ballistic composite laminates from UHMWPE fabric. Compos Struct 2022;287. https://doi.org/10.1016/j.compstruct.2022.115362.

[8] Chhetri S, Bougherara H. A comprehensive review on surface modification of UHMWPE fiber and interfacial properties. Compos Part A Appl Sci Manuf 2021. https://doi.org/10.1016/j.compositesa.2020.106146.

[9] Kharitonov AP, Maksimkin A V., Mostovaya KS, Kaloshkin SD, Gorshenkov M V., D'yachkova TP, et al. Reinforcement of bulk ultrahigh molecular weight polyethylene by fluorinated carbon nanotubes insertion followed by hot pressing and orientation stretching. Compos Sci Technol 2015. https://doi.org/10.1016/j.compscitech.2015.10.009.

[10] Zhang X, Wang Y, Lu C, Cheng S. Interfacial adhesion study on UHMWPE fiber-Reinforced composites. Polym Bull 2011. https://doi.org/10.1007/s00289-011-0491-2.

[11] Teodoru S, Kusano Y, Rozlosnik N, Michelsen PK. Continuous plasma treatment of ultra-high-molecular-weight polyethylene (UHMWPE) fibres for adhesion improvement. Plasma Process. Polym., 2009. https://doi.org/10.1002/ppap.200930906.

[12] He R, Niu F, Chang Q. The effect of plasma treatment on the mechanical behavior of UHMWPE fiber–reinforced thermoplastic HDPE composite. Surf Interface Anal 2018. https://doi.org/10.1002/sia.6337.

[13] Tissington B, Pollard G, Ward IM. A study of the effects of oxygen plasma treatment on the adhesion behaviour of polyethylene fibres. Compos Sci Technol 1992. https://doi.org/10.1016/0266-3538(92)90011-Q.

[14] Lee SG, Kang TJ, Yoon TH. Enhanced interfacial adhesion of ultra-high molecular weight polyethylene (UHMWPE) fibers by oxygen plasma treatment. J Adhes Sci Technol 1998. https://doi.org/10.1163/156856198X00263.

[15] Gao S, Zeng Y. Surface modification of ultrahigh molecular weight polyethylene fibers by plasma treatment. I. Improving surface adhesion. J Appl Polym Sci 1993. https://doi.org/10.1002/app.1993.070471116.

[16] Gao S, Zeng Y. Surface modification of ultrahigh molecular weight polyethylene fibers by plasma treatment. II. Mechanism of surface modification. J Appl Polym Sci 1993. https://doi.org/10.1002/app.1993.070471202.

[17] Wu JY, Lin SK, Tsai CS, Huang CY, Yeh JT, Chen KN. Effects of surface modification by argon plasma on peel strength of woven-type ultrahigh-molecular-weight polyethylene. Jpn J Appl Phys 2010. https://doi.org/10.1143/JJAP.49.08JA01.

[18] Zhang Y, Shi F, He J, Wu H, Qiu Y. Surface characterization of oxygen plasma treated nano-SiO2 sol-gel coating UHMWPE filaments. Mater. Sci. Forum, 2010. https://doi.org/10.4028/www.scientific.net/MSF.658.117.

[19] Simić DM, Stojanović DB, Brzić SJ, Totovski L, Uskoković PS, Aleksić RR. Aramid hybrid composite laminates reinforced with inorganic fullerene-like tungsten disulfide nanoparticles. Compos Part B Eng 2017. https://doi.org/10.1016/j.compositesb.2017.05.002.

[20] Naffakh M, Marco C, Gómez MA, Jiménez I. Novel melt-processable nylon-6/inorganic fullerene-like WS2 nanocomposites for critical applications. Mater Chem Phys 2011. https://doi.org/10.1016/j.matchemphys.2011.05.018.

[21] Naffakh M, Martín Z, Fanegas N, Marco C, Gómez MA, Jiménez I. Influence of inorganic fullerene-like WS2 nanoparticles on the thermal behavior of isotactic polypropylene. J Polym Sci Part B Polym Phys 2007. https://doi.org/10.1002/polb.21231.

[22] Díez-Pascual AM, Naffakh M, Marco C, Ellis G. Mechanical and electrical properties of carbon nanotube/poly(phenylene sulphide) composites incorporating polyetherimide and inorganic fullerene-like nanoparticles. Compos Part A Appl Sci Manuf 2012. https://doi.org/10.1016/j.compositesa.2011.12.026.

[23] Naffakh M, Díez-Pascual AM, Marco C, Gómez MA, Jiménez I. Novel melt-processable poly(ether ether ketone)(PEEK)/inorganic fullerene-like WS2 nanoparticles for critical

applications. J Phys Chem B 2010. https://doi.org/10.1021/jp105340g.

[24] Shneider M, Dodiuk H, Tenne R, Kenig S. Nanoinduced morphology and enhanced properties of epoxy containing tungsten disulfide nanoparticles. Polym Eng Sci 2013. https://doi.org/10.1002/pen.23517.

[25] Naffakh M, Díez-Pascual AM, Marco C, Ellis G. Morphology and thermal properties of novel poly(phenylene sulfide) hybrid nanocomposites based on single-walled carbon nanotubes and inorganic fullerene-like WS 2 nanoparticles. J Mater Chem 2012. https://doi.org/10.1039/c1jm12543e.

[26] Li J, Cui J, Yang J, Li Y, Qiu H, Yang J. Reinforcement of graphene and its derivatives on the anticorrosive properties of waterborne polyurethane coatings. Compos Sci Technol 2016. https://doi.org/10.1016/j.compscitech.2016.04.017.

[27] Zhang P, Lu Y, Fan M, Jiang P, Bao Y, Gao X, et al. Role of cellulose-based composite materials in synergistic reinforcement of environmentally friendly waterborne polyurethane. Prog Org Coatings 2020. https://doi.org/10.1016/j.porgcoat.2020.105811.

[28] Santamaria-Echart A, Ugarte L, García-Astrain C, Arbelaiz A, Corcuera MA, Eceiza A. Cellulose nanocrystals reinforced environmentally-friendly waterborne polyurethane nanocomposites. Carbohydr Polym 2016. https://doi.org/10.1016/j.carbpol.2016.06.069.

[29] Bergström J. Mechanics of Solid Polymers: Theory and Computational Modeling. 2015. https://doi.org/10.1016/C2013-0-15493-1.

[30] Mojtabaei A, Otadi M, Goodarzi V, Khonakdar HA, Jafari SH, Reuter U, et al. Influence of fullerene-like tungsten disulfide (IF-WS2) nanoparticles on thermal and dynamic mechanical properties of PP/EVA blends: Correlation with microstructure. Compos Part B Eng 2017. https://doi.org/10.1016/j.compositesb.2016.12.006.

[31] Morton WE, Hearle JWS. Physical Properties of Textile Fibres: Fourth Edition. 2008. https://doi.org/10.1533/9781845694425.

[32] Kim H, Kim SJ. High toughness of bio-inspired multistrand coiled carbon nanotube yarn. Carbon N Y 2018. https://doi.org/10.1016/j.carbon.2018.01.048.

[33] Li W, Li R, Li C, Chen ZR, Zhang L. Mechanical properties of surface-modified ultra-high molecular weight polyethylene fiber reinforced natural rubber composites. Polym Compos 2017. https://doi.org/10.1002/pc.23685.

[34] Meng L, Li W, Ma R, Huang M, Cao Y, Wang J. Mechanical properties of rigid polyurethane composites reinforced with surface treated ultrahigh molecular weight polyethylene fibers. Polym Adv Technol 2018. https://doi.org/10.1002/pat.4193.

[35] Li C, Shi Y, Zhang R, Wang G, Jia J. Effect of surface modifications on the properties of UHMWPE fibres and their composites. E-Polymers 2019. https://doi.org/10.1515/epoly-2019-0006.

[36] Sharma S, Dhakate SR, Majumdar A, Singh BP. Improved static and dynamic mechanical properties of multiscale bucky paper interleaved Kevlar fiber composites. Carbon N Y 2019. https://doi.org/10.1016/j.carbon.2019.06.055.

[37] Dayyoub T, Maksimkin A V., Kaloshkin S, Kolesnikov E, Chukov D, Dyachkova TP, et al. The structure and mechanical properties of the UHMWPE films modified by the mixture of

graphene nanoplates with polyaniline. Polymers (Basel) 2019. https://doi.org/10.3390/polym11010023.

[38] Maksimkin A, Kaloshkin S, Zadorozhnyy M, Tcherdyntsev V. Comparison of shape memory effect in UHMWPE for bulk and fiber state. J Alloys Compd 2014. https://doi.org/10.1016/j.jallcom.2012.12.014.

[39] Nurazzi NM, Asyraf MRM, Khalina A, Abdullah N, Aisyah HA, Rafiqah SA, et al. A review on natural fiber reinforced polymer composite for bullet proof and ballistic applications. Polymers (Basel) 2021. https://doi.org/10.3390/polym13040646.

[40] Abtew MA, Boussu F, Bruniaux P, Loghin C, Cristian I. Ballistic impact mechanisms – A review on textiles and fibre-reinforced composites impact responses. Compos Struct 2019;223. https://doi.org/10.1016/j.compstruct.2019.110966.

CHAPTER 6

Effects of fabrication parameters on mechanical properties and wash durability of nanocomposite coated UHMWPE yarns[5]

[5] Wu, S., Gibbs, A.R., Mandal, A., Bhat, G. S., Hagiya. Y. D. and Shaw. T. S. To be submitted to *Composite Structures.*

Abstract

Fiber-based nanocomposites are extensively studied for defense and aerospace applications due to their low density and high strength. In this work, ultra-high-molecular-weight polyethylene (UHMWPE) yarns were continuously coated with polyurethane (PU) matrix dispersed with inorganic fullerene-like tungsten disulfide (IF-WS_2) nanoparticles. The effects of six fabrication parameters on the tensile toughness and coating weight retention after wash were investigated using factorial designs. Neither the dispersing medium nor curing time showed a significant impact on the outcomes. A higher PU addition or curing temperature was found to significantly decrease toughness and increase weight retention of the yarn composites. A higher IF-WS_2 or stabilizer amount first increased and then decreased the toughness of coated yarns, whereas it lowered the coating wash durability due to reduced PU film integrity. Additionally, the influence of graphene nanoplatelets (GNP) addition was studied with optimized parameters, which showed no significant effects on the outcomes. At the optimal condition (1 wt% solid IF-WS_2, 10 wt% PU, 5 wt% stabilizer, 120℃/30min for curing), the maximum load, tensile energy absorption, and toughness of the composite yarn were enhanced by 31.9%, 66.7%, and 43.3% over that of neat yarns, respectively. 94.1% of the coating was retained on the composite yarn after washing.

Keywords: UHMWPE fiber; Nanocomposite coating; Fabrication parameter; Factorial design; Mechanical property

6.1. Introduction

Ultra-high-molecular-weight polyethylene (UHMWPE) fiber is one of the most common fiber materials used in protective gears, such as soft body armors, due to its good flexibility, high specific strength and high specific modulus [1][2][3][4]. However, enhanced materials with lighter weight and higher performance are always in high demand due to the emergence of advanced firearms and ammunition. To strengthen UHMWPE fibers while retaining sufficient flexibility and lightweight, a promising approach is developing fiber-based nanocomposites by incorporating nanofiller reinforced polymer matrices [5][6]. This is due to the benefits of nanomaterials such as high mechanical properties, low density, high surface area-to-weight ratios, and high energy absorption capacity [7]. Whereas polymer matrices provide addition energy absorption and bonding strength with nanomaterials and fiber substrates. Inorganic fullerene-like tungsten disulfide (IF-WS_2) nanoparticle is a 1D nanomaterial with particle diameter within 100nm. It possesses a unique inorganic molecular structure and hollow fullerene-like quasi-spherical shape, which contribute to its low friction coefficient, high elasticity, high stiffness, and outstanding shock resistance [8][9][10]. Meanwhile, it is chemically inert, non-toxic, and much more cost-effective and efficient than carbon nanotubes (CNTs), carbon nanofibers, and nanoclay [11][12]. IF-WS_2 nanoparticles have been incorporated with various polymer matrices such as poly(vinyl butyral), isotactic polypropylene, poly(phenylene sulfide), epoxy for improved mechanical, tribological, and thermal properties [13][14][15][16]. Different from IF-WS_2, graphene nanoplatelets (GNPs) are 2D carbon nanomaterials with the thickness on a nanoscale. Due to their high strength, Young's modulus and thermal conductivity, GNPs have been used in different composite systems such as polymethyl methacrylate matrix, hybrid carbon/glass fiber/epoxy, basalt/epoxy to improve mechanical, thermal, and tribological performances [17][18][19][20]. In

this work, it is used as a comparison to IF-WS_2. In recent years, waterborne polyurethane has attracted increasing interest in the coating, composite, and adhesive applications due to its environmentally friendly, easy-to-disperse, high stability, and balanced strength and flexibility properties [21][22][23]. To achieve the reinforcement of polymer nanocomposite on fiber/fabric substrates, it is critical to consider the effects of various fabrication parameters, for instance, polymer matrix factors (type, concentration), nanofiller factors (type, size, amount, distribution uniformity), fabrication method, and dry/cure procedure (temperature, time) [24][25][26][27][28][29]. For instance, Rangaswamy et al. studied the effects of MWCNT nanofiller amount, compression pressure, compression time, and mold temperature on the mechanical and tribological properties of multiwall carbon nanotube (MWCNT)/epoxy/glass/Kevlar composites fabricated by compression molding. It was found that 0.6% MWCNTs led to higher mechanical strength and hardness for the composites than 0.3% and 0.9% addition. All three fabrication parameters showed significant effects on composite tensile and bending strength, while the compression pressure had the maximum effect [30]. EhiImoisili et. al. optimized the fabrication factors for MWCNT/epoxy/plantain fiber composites for high impact strength using response surface methodology. The factors include MWCNT content, potassium permanganate (KMnO4) treatment time for enhancing fiber/matrix adhesion, and fiber content. The impact strength obtained at optimal condition (1.23% MWCNT, 2.60 min treatment time, 13.50 wt% fiber content) was 46.62 J/m, which increased by 58.16% over the neat epoxy system [31]. Adamua et al. investigated the effects of clay loading, PVA amount, NaOH amount, and modification time on the modulus of elasticity (MOE) and modulus of rupture (MOR) of nanoclay/ polyvinyl alcohol/ bamboo fiber composites. The optimal MOE (15.08 GPa) and MOR

(96.88MPa) were obtained at the optimal condition of 5 wt% clay loading, 1 wt% PVA, no NaOH, and 15min for modification [32].

However, a systematic study on the effects of fabrication parameters on the mechanical properties and wash durability of IF-WS_2 or GNP reinforced PU/UHMWPE composite fibers has not been reported. To understand the potential of these composite materials in high strength and energy absorption applications, the completion of this research is critical. In this work, a continuous dip coating method is used to incorporate the PU/nanofiller on UHMWPE fibers due to its easy-to-operate, feasibility for low add-on and even coating, and low material consumption advantages. The effects of various fabrication factors are studied including PU amount, nanofiller amount, stabilizer amount, medium type, curing temperature, and curing time. A fractional factorial design and full factorial design are adopted to screen and optimize factors and levels. Toughness and coating weight retention after washing are selected as response variables due to the potential application of the composites in lightweight protective garments. Other mechanical properties such as maximum load, elongation at break, and total tensile energy absorption are also analyzed to better understand the effect mechanisms.

6.2. Materials and Methods

6.2.1. Materials

UHMWPE fibers used in this study were in the form of continuous and untwisted multifilament yarns-Spectra ® 1600 (Honeywell International, Inc.). The measured linear density (*D*) of the yarn is 1557 denier. Polyurethane aqueous dispersion-Aptalon™ M8100 (Lubrizol Corp., solid content: 37 wt%, pH: 7.5-8.5) was applied as the elastomeric polymer matrix. It contains unique polyamide polyols and diisocyanate monomers possessing self-crosslinking

function upon curing. IF-WS_2 nanoparticle (aqueous suspension IW-4000, Nanotech Industrial Solutions, Inc.) was employed as a reinforcing nanomaterial. Its solid content was measured as 48.8 wt%. The size of the fullerene-like spherical nanoparticles ranges from 20nm to 80nm. More detailed information about the IF-WS_2 is given elsewhere [10]. The graphene nanoplatelets (powder, Sigma-Aldrich, Inc) possess an average surface area of 750 m^2/g, a thickness of a few nm, and a density of 0.2-0.4 g/cm^3. Acrylic rheology modifier-RHEOVIS AS 1125 (BASF SE) was applied as a stabilizer to improve the anti-setting property of WS_2 nanoparticles in an aqueous medium. Its solid content is about 25.8 wt% and its pH value is 2.3-3.3. As an alkali swellable emulsion, it swells to thicken water-based dispersions upon neutralization [33]. Ethanol was used with deionized (DI) water to disperse WS_2 nanoparticles in selected designs.

6.2.2. Design of experiments

6.2.2.1. Factional factorial design (2^{6-2})

A factional factorial design was adopted to study the main and interaction effects of selected coating variables on mechanical properties and wash durability of PU/WS_2 coated UHMWPE yarns with reduced experiments. Six factors (A-F) with two levels (– / +) were included i.e., curing time, curing temperature, PU amount, medium, WS_2 amount, and stabilizer amount. The PU and WS_2 dispersion additions were calculated based on total fluid weight. The stabilizer amount was calculated with respect to the WS_2 dispersion amount used. 16 experimental conditions shown in Table 6.1 were generated to reduce experimental runs while maximizing collected information. The generators E=AB and F=ACD were selected based on preliminary knowledge of the significance of the two-factor interactions (2fi), and the goal was to reduce aliased 2fi (e.g., AF=CD). Two statistical assumptions were made: (1) main effects are more likely to be significant than 2fi or higher fi, and (2) 3fi or higher fi are negligible compared to main

effects and 2fi. Based on these assumptions, the effects of all main factors and 2fi including BC, BD, BF, CE, DE, and EF can be evaluated using the design.

The six factors were studied to screen significant coating variables for improving gravimetric toughness (tensile energy absorbed per unit mass) and wash durability of the coatings. The curing times were selected to ensure sufficient curing/crosslinking reaction while preventing yarn damage due to long-time heating. The curing temperatures were chosen to avoid the formation of brittle PU films at low temperature and UHMWPE fiber melting at 144–152 °C [34]. PU matrix was used to disperse WS_2 nanofillers on UHMWPE yarns, the levels of both PU and WS_2 amounts were determined based on preliminary tests. The waterborne PU and WS_2 nanoparticles show improved dispersibility and stability in water and ethanol, respectively. Hence, the effects of both water and water/ethanol mixture on the mechanical properties and coating durability of the composites were studied. As reported, the distribution uniformity of nanoparticles on textile substrates may largely affect the mechanical properties of reinforced composites, thus, the factor of stabilizer amount with two levels was included [25].

The responses investigated on composite yarns fabricated using each experimental condition were the add-on amount, tensile maximum load, elongation at break, total energy absorbed before rupture, gravimetric toughness, and coating weight retention after wash. All 16 experiments were conducted in a random order to avoid bias because of uncontrollable factors.

Table 6.1. The 2^{6-2} fractional factorial design.

Experimental Condition	A	B	C	D	E=AB	F=ACD
	Curing time (min)	Curing Temper -ature (℃)	PU amount (wt%)	Dispersion medium	WS_2 amount (wt%)	Stabilizer amount (wt%)
1	– (30)	– (100)	– (2.5)	– (water)	+ (6)	– (0)
2	+ (50)	– (100)	– (2.5)	– (water)	– (2)	+ (3.5)
3	– (30)	+ (120)	– (2.5)	– (water)	– (2)	– (0)
4	+ (50)	+ (120)	– (2.5)	– (water)	+ (6)	+ (3.5)
5	– (30)	– (100)	+ (10)	– (water)	+ (6)	+ (3.5)
6	+ (50)	– (100)	+ (10)	– (water)	– (2)	– (0)
7	– (30)	+ (120)	+ (10)	– (water)	– (2)	+ (3.5)
8	+ (50)	+ (120)	+ (10)	– (water)	+ (6)	– (0)
9	– (30)	– (100)	– (2.5)	+ (mix)	+ (6)	+ (3.5)
10	+ (50)	– (100)	– (2.5)	+ (mix)	– (2)	– (0)
11	– (30)	+ (120)	– (2.5)	+ (mix)	– (2)	+ (3.5)
12	+ (50)	+ (120)	– (2.5)	+ (mix)	+ (6)	– (0)
13	– (30)	– (100)	+ (10)	+ (mix)	+ (6)	– (0)
14	+ (50)	– (100)	+ (10)	+ (mix)	– (2)	+ (3.5)
15	– (30)	+ (120)	+ (10)	+ (mix)	– (2)	– (0)
16	+ (50)	+ (120)	+ (10)	+ (mix)	+ (6)	+ (3.5)

Note: mix – water/ethanol mixture (ethanol in medium = 80 wt%)

6.2.2.2. Full factorial design ($3^2 2^1$)

Based on the initial results from the first design, a full factorial design was established with three factors A-C and 3, 3, and 2 levels, which are WS_2 amount (2/6/10 wt%), PU amount (10/30/50 wt%), and temperature (100/120℃). The fixed factors during the fabrication include curing time (30 min), stabilizer amount (3.5 wt%), and dispersion medium (water). 18 experimental conditions were generated as shown in Table 6.2. With the full factorial design, all main effects (A, B, C), 2fi (AB, AC, BC), and 3fi (ABC) were studied on the mechanical properties and wash durability of coated yarns. The order of the experiments was randomized.

Table 6.2. The $3^2 2^1$ full factorial design.

Experimental Condition	A	B	C
	WS_2 amount (wt%)	PU Amount (wt%)	Temperature (°C)
1	2	10	100
2	2	30	100
3	2	50	100
4	6	10	100
5	6	30	100
6	6	50	100
7	10	10	100
8	10	30	100
9	10	50	100
10	2	10	120
11	2	30	120
12	2	50	120
13	6	10	120
14	6	30	120
15	6	50	120
16	10	10	120
17	10	30	120
18	10	50	120

Based on the results, three one-factor designs were added. The effects of WS_2 suspension amount were further investigated with levels of 0.5, 1.0, 2.0, 6.0, 10.0 wt%, which contain solid WS_2 amounts of 0.2, 0.5, 1.0, 2.9, 4.9wt%, respectively, for direct comparison with GNPs powder addition. In the coating mixtures, 10 wt% PU and 3.5 wt% stabilizer was used. The impact of stabilizer amount was also studied with levels of 0, 0.035, 0.07 (3.5 wt% based on WS_2 liquid amount), 3.0, 5.0, 7.0, and 9.0 wt%, with respect to total liquid weight. The PU and WS_2 dispersion amounts were kept constant at 10 wt% and 2.0 wt%. Besides, PU/GNPs/UHMWPE composite yarns were fabricated with GNPs (0, 0.2, 0.5, 1.0, 2.9, 4.9, 6.8, and 8.8wt%), 10 wt% PU, and 5 wt% stabilizer, regarding total liquid weight. The effect of GNPs amount on composite performances was studied. The JMP and RStudio software was used to perform statistical analysis (ANOVA) on collected data from all designs [35].

6.2.3 Preparation for PU/WS_2 coated UHMWPE yarns

PU/WS_2 coating nanofluids were prepared in the medium of either water or water/ethanol mixture (ethanol in total: 80 wt%). When preparing a coating liquid, designed amounts of WS_2 suspension and stabilizer if any are added into the selected medium followed by homogenization for 30 min using a Kendal ultrasonic bath. Then weighed PU dispersion is mixed with the nanofluid for another 30 min using sonication. The same procedure was applied to prepare aqueous GNP/PU mixtures as per designed experimental conditions. UHMWPE yarns were continuously coated with prepared PU/WS_2 or PU/GNP dispersions at a constant speed using a lab assembled setup (Figure 6.1). Where the yarn is stretched, dipped coated in prepared fluid, nipped between two rollers with constant pressure, dried in the furnace at a measured temperature of 196 ± 7°C, and wound up on a 3D printed rod. The coated yarns were then rewound on a customized heat-resistant aluminum rack and cured in a lab oven at the designed condition.

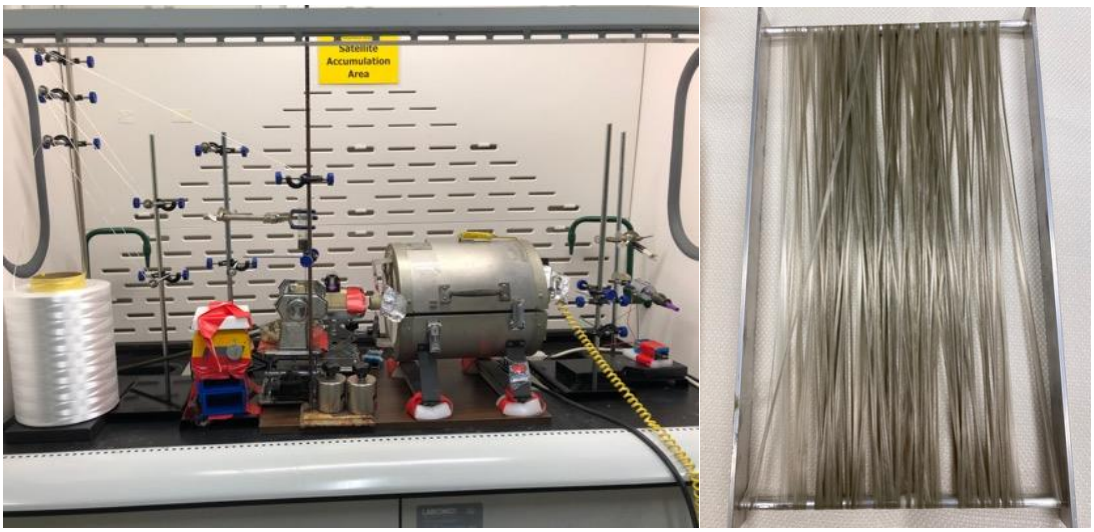

(a) (b)

Figure 6.1. Continuous yarn dip-coating (a) image of the lab-assembled setup; (b) a PU/WS_2 coated yarn wound on a customized aluminum frame.

6.2.4. Characterizations

The add-on amounts for coated yarns were estimated according to the cut length (300mm), weights of yarns, and the linear density of the pristine yarn. Results from at least 7 replicates were presented. Tensile tests were conducted on pristine and coated yarns as per ASTM 2256 standard using a CRE tensile tester (Intron 4400 R). The gauge length of 100 mm and a crosshead speed of 100mm/min were applied due to the low strain rate of UHMWPE fibers. Capstan grips and cardboard gluing method were adopted to prevent yarn slippage under tension. Both ends of each yarn were glued on cardboard with constant thickness followed by air drying overnight. After tensile tests, the maximum load and elongation at break were collected. Total energy absorbed before rupture (energy to break) (J) of yarn was calculated by integrating the load-displacement curve. The gravimetric toughness T (J/g), or normalized energy to break was converted from the energy to break, linear density, and tested length of yarn (Equation 6.1) [36]. At least 3 replicates were tested. The standard wash procedure from AATCC test method 61 was adopted for PU/WS_2 coated yarns (length of 300 mm), the coating weight retention after wash R (%) was estimated using the pristine linear density, yarn length, and yarn weights before and after wash (Equation 6.2). Three replicates were used. Scanning electronic microscopy (FE-SEM Thermo Fisher Teneo) was applied to observe the coating appearance on the fabric surface. The settings include 5kV acceleration voltage and magnification of ×1500 and ×2500.

$$\mathrm{T}\,(J/g) = (9000 \times E)/(D \times l_1) \qquad (6.1)$$

Where, *T*, *E*, *D*, and l_1 are the gravimetric toughness, energy to break, pristine yarn linear density in denier, and yarn tested length, respectively.

$$R(\%) = \frac{W_a \times 9000 - Dl_2}{W_b \times 9000 - Dl_2} \times 100 \qquad (6.2)$$

Where, R, W_a, W_b, D, and l_2 are the coating weight retention, yarn weight after wash, yarn weight before wash, pristine yarn linear density in denier, and yarn cut length, respectively.

6.3. Results and Discussion

6.3.1. Effect of twists on mechanical properties

During the tensile test, applying yarn twists on UHMWPE yarns may largely reduce yarn slippage probability under stress due to increasing yarn roughness and surface friction. However, it may also affect the mechanical and energy absorption properties of the UHMWPE yarns. To choose a proper tensile testing method for the UHMWPE and composite yarns, both non-twist and twist (12.5 twists, 3.2 twists per inch, calculated as per ASTM 2256) approaches were applied to the coated yarns, their mechanical properties and total energy absorption were collected, the mean values and 95% confidence intervals (CIs) for each outcome were plotted in Figure 6.2. Each pair of non-overlapped CIs indicates a significant difference in the outcome between untwisted and twisted yarns. As observed, applying twists decreases the mean maximum load for all coated yarns, the difference is significant for the yarns coated with the following conditions: 3, 8, 10, 11, 13, 15, and 16 (Figure 6.2 (a)). This phenomenon has been reported in other types of yarns or fiber-based polymer composites [37][38][39]. It can be explained by the torsional or off-axis deformation and PU polymer cracking induced by the twists. When no twists are applied, most fibers in the yarns are aligned with the force direction leading to high breaking force. In contrast, a twisted yarn breaks when the weakest part of the yarn fails, which only contains fibers close to the axis resulting in lower yarn strength. From Figure 6.2 (b), the yarn twist is found to increase the average elongation to break for all nanocomposite yarns, whereas a significant difference is seen from the samples coated using the following conditions: 2, 4, 5, 6, 7, 8, 9, 12, 13, 14, and 16. This extended

fracture elongation is attributed to the yarn contraction effect and spinning tension caused by twists, both increasing the extension limit of the composite yarns [40][41]. In the case of energy absorption and gravimetric toughness as shown in Figure 6.2 (c-d), twisted composite yarns (3, 8, and 10) give significantly lower averages than their untwisted counterparts. Thus, the tensile data collected with no yarn twists was chosen in this research to be consistent with the untwisted neat yarns and avoid any effects or bias caused by applied yarn twists.

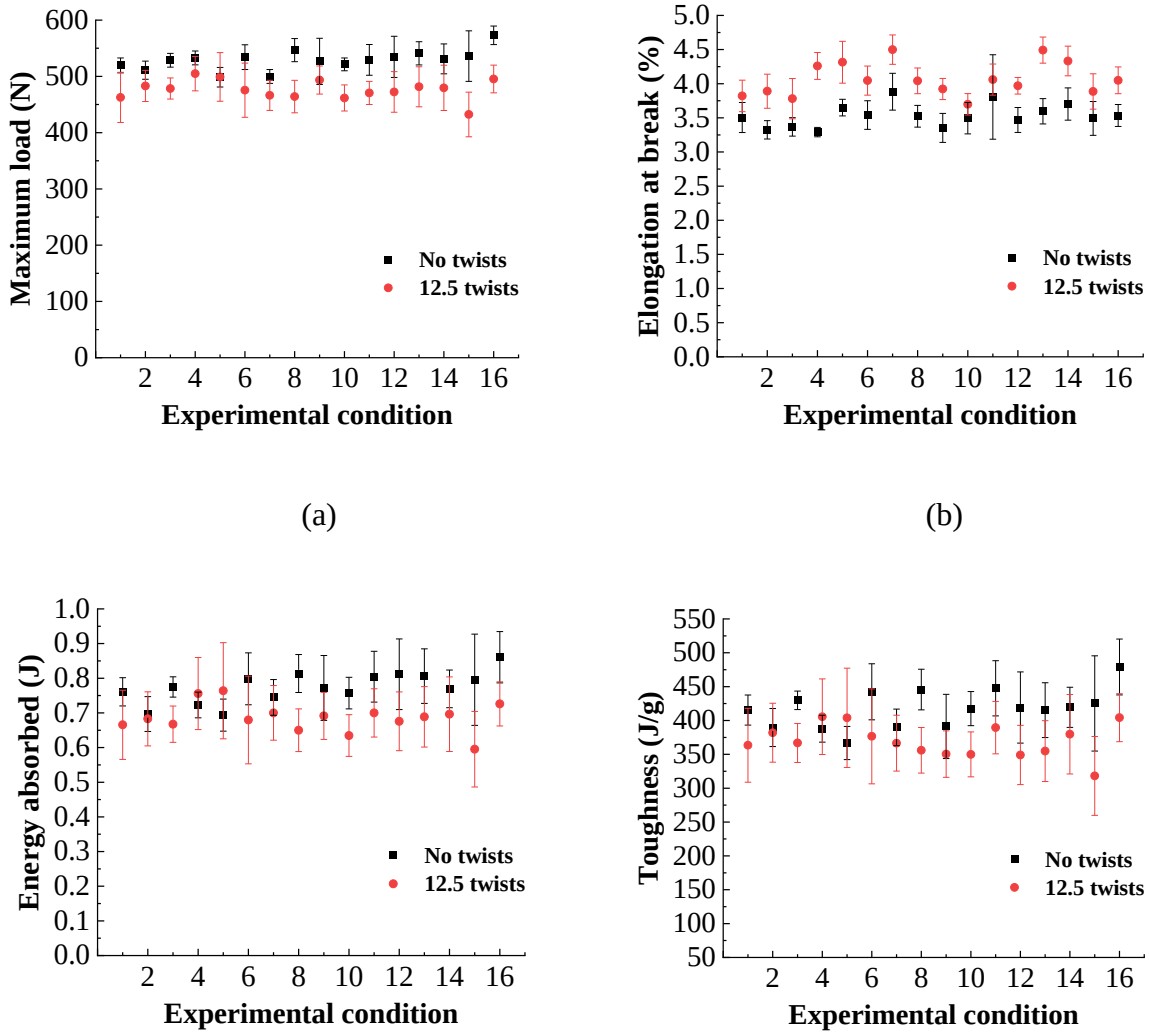

Figure 6.2. Means and 95% confidence intervals (CIs) for the mechanical properties and energy absorption of the PU/WS_2 coated UHMWPE yarns from the fractional factorial design: (a) maximum load; (b) elongation at break; (c) energy absorbed; (d) gravimetric toughness.

6.3.2. Screen of fabrication factors

Table 6.3 lists the add-on amounts for all 16 groups of PU/WS_2/UHMWPE yarns, which were fabricated as per the fractional factorial design. The coating amounts are in a small range of 3.2% - 13.8% with low variations. In lightweight protective and high-performance areas, it is critical to control material weight increase while attempting to enhance their mechanical and

energy absorption performances. Hence, gravimetric toughness (energy absorption normalized by weight) of the specimens was used as one of the outcomes to generate statistical inference for screening fabrication factors. Meanwhile, the wash durability of the coatings was studied due to the potential use of these composite yarns in protective garments. Weight retention of the coatings in percentage was calculated according to the weight change of the composite yarns after wash, the results were included as the second outcome. The goal of this section is to find factors that significantly affect gravimetric toughness and weight retention of coated yarns and collect information for further study. Table 6.4 presents the P-values of the six main factor effects and all unaliased 2-factor interaction effects obtained from ANOVA tests on both outcomes. Significant effects are identified with bold P-values at $\alpha = 0.05$. In the case of gravimetric toughness, only the effect of curing temperature appears to be significant based on the levels selected with P-value = 0.039. Weight retention of the coatings is significantly affected by the curing temperature (P-value = 0.029), PU amount (P-value < 0.001), and 2fi interactions between (1) curing temperature and stabilizer amount (P-value = 0.022), (2) medium and WS_2 amount (P-value < 0.001), and (3) WS_2 amount and stabilizer amount (P-value = 0.047).

Table 6.3. Add-on amounts (mean and SE) for the PU/IF-WS_2 coated UHMWPE yarns from the fractional factorial design.

Condition	1	2	3	4	5	6	7	8
Add-on (%)	5.7±1.0	3.2±0.4	5.0±0.6	7.5±0.9	9.1±0.7	4.1±0.7	10.2±0.4	5.3±0.9
Condition	9	10	11	12	13	14	15	16
Add-on (%)	13.8±2.0	4.6±1.1	3.7±0.6	11.7±0.3	12.0±0.9	5.8±1.0	8.0±0.8	3.6±0.9

Table 6.4. ANOVA P-values for the main effects and unaliased 2-factor interaction effects on analyzed properties.

P-value	Toughness (J/g)	Weight retention (%)
Curing Time (CTI)	0.135	0.698
Curing Temperature (CTE)	**0.039**	**0.029**
PU Amount (PA)	0.286	**<0.001**
Medium (MD)	0.067	0.368
WS2 Amount (WA)	0.608	0.881
Stabilizer Amount (SA)	0.084	0.599
CTE × PA	0.751	0.881
CTE × MD	0.268	0.155
CTE × SA	0.178	**0.022**
PA × WA	0.208	0.389
MD × WA	0.699	**<0.001**
WA × SA	0.979	**0.047**

Figure 6.3 shows the main and 2-factor interaction effect plots of all significant effects with means of gravimetric toughness and weight retention of the yarns at each level. Figure 6.3 (a) depicts the mean toughness for the composite yarns slightly increases from 407.2 J/g to 428.0 J/g (5.1%) at a higher curing temperature (120℃ over 100℃). Other factors such as PU and WS_2 amounts exhibit no significant impacts on the toughness results possibly due to the narrow level selection. In terms of coating weight retention after wash, Figure 6.3 (b-c) shows applying a higher curing temperature or PU amount (10% vs 2.5%) increases the mean of the weight retention percentage. PU amount has a larger main effect over curing temperature as observed from the difference of means between the two levels. Figure 6.3 (d) presents the 2fi effect plot of curing temperature and stabilizer amount for weight retention. High mean values are obtained from the fabrication condition of either 120℃ & 0 wt% stabilizer or 100℃ & 3.5 wt% stabilizer. Similarly, Figure 6.3 (e) exhibits the interaction plot of medium type and WS_2 amount, a high mean of weight retention is shown in the condition of mixed medium with 6 wt% WS_2 or water medium with 2 wt% WS_2. Figure 6.3 (f) shows the interaction plot of WS_2 amount and stabilizer amount, the

conditions of 6 wt% WS_2 with 3.5 wt% stabilizer and 2 wt% WS_2 & 0 wt% stabilizer leads to a higher mean of coating weight retention. A significant interaction effect between the two factors can be observed from all three interaction plots.

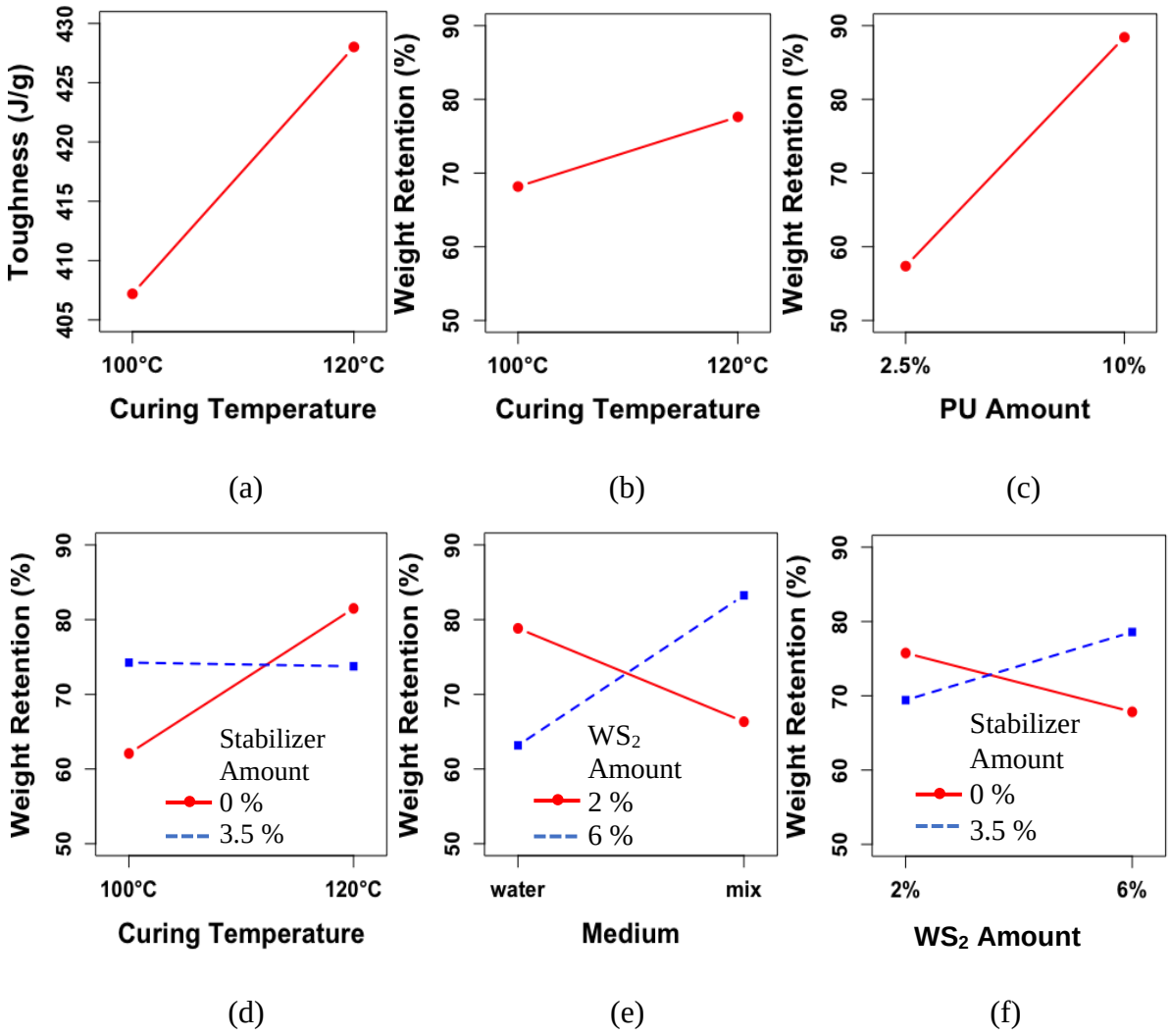

Figure 6.3. Effect plots for the means of (a) toughness and (b-f) weight retention: (a) curing temperature; (b) curing temperature; (c) PU amount; (d) curing temperature with stabilizer amount; (e) medium with WS_2 amount; (f) WS_2 amount with stabilizer amount.

6.3.3. Optimization of fabrication factors and levels

6.3.3.1. Add-on

Based on the previous results obtained, the effects of three factors (PU amount, WS_2 amount, and curing temperature) were further studied using a $3^2 2^1$ full factorial design. The PU and WS_2 amounts were expanded into three levels, which are 10%, 30%, and 50% for PU amount and 2%, 6%, and 10% for WS_2 amount. Both levels of curing temperature (100℃ and 120℃) were included to better understand its main and interaction effects. Water medium was used as the dispersion medium for all sample preparation since the medium factor had no significant main effects on either the toughness or wash durability of the coatings. Besides, adding ethanol lowers the dispersibility of the PU material in the medium increasing preparation difficulty for the coating fluids. Curing time was kept constant at 30min to reduce energy and time consumptions due to its insignificant impacts on both outcomes. A 3.5% stabilizer was used for fabricating all composite yarns. The coated yarns were coated with 5.6% to 59.7% add-on on average, a wider range is obtained than it from the fractional factorial design due to the higher PU and WS_2 amounts selected in the levels (Table 6.5). An increasing trend for the add-on % can be observed with a higher amount of PU usage, i.e., conditions 1-3; 4-6; 7-9; 10-12; 13-15; 16-18.

Table 6.5. Add-on amounts (mean and SE) for the PU/IF-WS_2 coated UHMWPE yarns from the full factorial design.

Condition	1	2	3	4	5	6
Add-on (%)	5.6±1.2	21.2±2.4	26.5±0.7	10.9±1.5	27.5±1.5	42.7±2.1
Condition	7	8	9	10	11	12
Add-on (%)	16.1±0.8	22.3±1.1	41.6±1.2	13.5±1.1	23.8±0.7	58.5±3.7
Condition	13	14	15	16	17	18
Add-on (%)	11.0±1.0	19.6±1.0	59.7±1.9	14.0±0.8	29.0±1.2	39.1±2.5

6.3.3.2. Tensile properties

Table 6.6 lists the ANOVA P-values for effects of the three main factors and all interactions on mechanical and energy absorption properties including maximum load, elongation at break, energy absorbed, and toughness. The P-values for the significant effects at 95% confidence level were marked in bold. The p-values reveal the maximum load is significantly affected by the curing temperature, 2fi effect between WS_2 amount and curing temperature, and 3fi effect among WS_2 amount, PU amount, and curing temperature. While elongation at break is significantly affected by the PU amount and curing temperature. Total energy absorbed is significantly impacted by the PU amount and WS_2 amount & curing temperature interaction. Whereas toughness significantly depends on the PU amount, curing temperature, and 2fi effects of WS_2 amount & curing temperature as well as PU amount & curing temperature.

Table 6.6. ANOVA P-values for all main effects and interaction effects on mechanical properties and energy absorption capacity.

Effect	Maximum Load (N)	Elongation at break (%)	Energy absorbed (J)	Toughness (J/g)
WS_2 Amount (WA)	0.446	0.740	0.358	0.125
PU Amount (PA)	0.640	**<0.001**	**0.001**	**<0.001**
Curing Temperature (CTE)	**0.008**	**<0.001**	0.659	**0.039**
WA × PA	0.825	0.386	0.465	0.721
WA × CTE	**<0.001**	0.427	**0.000**	**0.002**
PA × CTE	0.251	0.817	0.169	**0.015**
WA × PA × CTE	**0.001**	0.404	0.056	0.814

Figure 6.4 shows the significant main and interaction effect plots for the mean of maximum load. The y-axis scale was kept constant for easy comparison among different plots. Figure 6.4 (a) depicts raising the curing temperature from 100℃ to 120℃ slightly decreases the mean of maximum load by 3.4%. Figure 6.4 (b) indicates the mean of maximum load increases (up to 6.4%) with a higher WS_2 amount when 100℃ curing temperature is used. Whereas at 120℃, the mean

value decreases (up to 7.9%) with a higher WS_2 amount. Figure 6.4 (c-d) shows the 3-factor interaction plots with maximum load, different trends for the mean values can be observed with increasing PU amount, curing temperature, and WS_2 amount. The plots are not nearly parallel indicating the significance of the three-factor interaction effect. When 50 wt% PU is used, the maximum load of composite yarns shows a significant increase (up to 16.2%) with a rising amount of WS_2 at a curing temperature of 100℃; however, it shows a shape decrease (up to 19.4%) with a higher amount of WS_2 at curing temperature of 120℃. The maximum mean of the outcome (589.8N) is obtained for the composite yarn that was fabricated using 10 wt% WS_2, 50 wt% PU, and 100℃ curing temperature. It increases by 24.3% over the lowest mean of maximum load (474.5N) for the yarn coated using 10 % WS_2, 50 % PU, and 120℃ curing temperature.

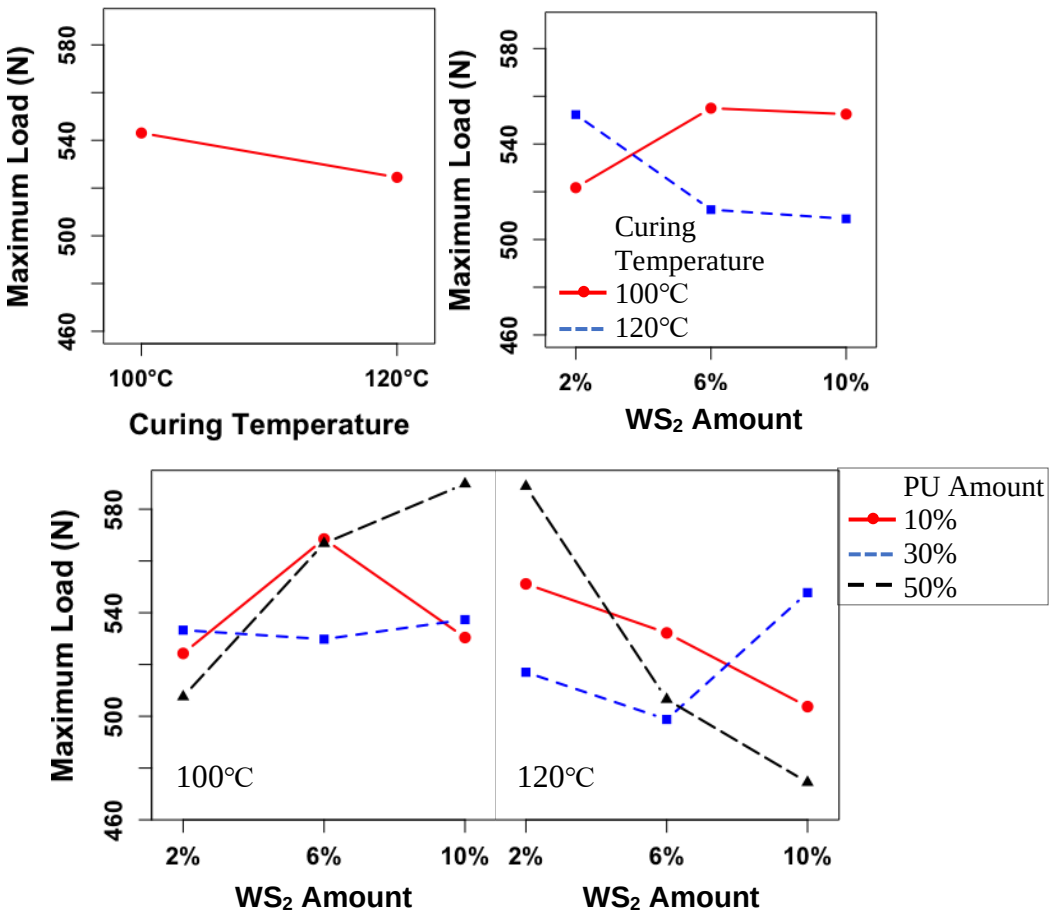

Figure 6.4. Effect plots for the means of maximum load: (a) PU amount; (b) interaction of WS_2 amount and curing temperature; (c) interaction of WS_2 amount, PU amount, and curing temperature.

Figure 6.5 presents the main effect plots of PU amount and curing temperature for the mean of elongation at break values. As expected, increasing PU amount leads to higher mean values of elongation at break for the coated yarns due to the high elongation of elastomeric PU material. Compared to 10% PU, 50% PU results in 17.1% higher elongation at break for the coated yarn. Besides, the higher curing temperature (120℃ vs 100℃) leads to 7.5% increase in the mean elongation at break due to the toughener PU films formed at a higher temperature.

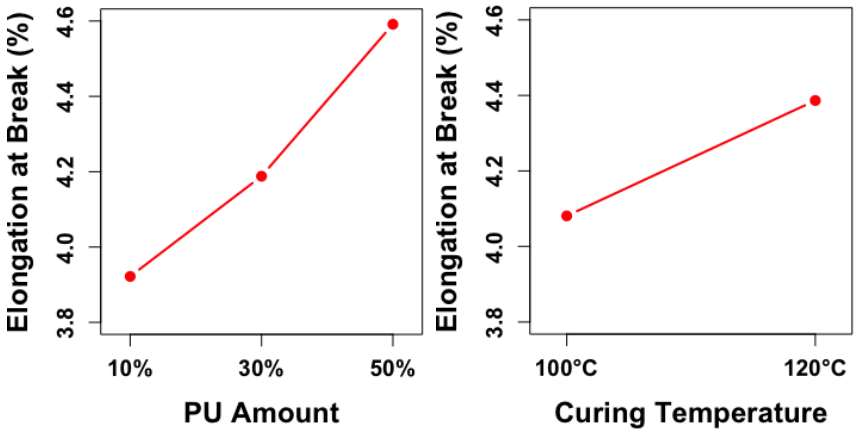

Figure 6.5. Effect plots for the means of elongation at break: (a) PU amount; (b) curing temperature.

Figure 6.6 shows the main plot of PU amount and interaction plot of WS_2 amount and curing temperature regarding total energy absorbed by the composite yarns before rupture. Figure 6.6 (a) illustrates the rising trend of mean energy absorption values of samples fabricated with an increasing amount of PU material. The mean of energy absorption increases by 10.6% for the yarns using 50 % PU over 10 % PU. This is mainly due to the energy absorption contribution from the additional PU matrix through ductile breakage, matrix failure, and fiber/matrix debonding. Figure

6.6 (b) indicates a higher WS_2 amount tends to increase the energy absorption of specimens when the curing process is carried out at 100℃. An improvement of 14.0% is obtained with 10% WS_2 amount over 2% WS_2. However, the total energy absorption declines with increasing WS_2 addition when the specimens are cured at 120℃. At which, the mean value reduces by 16.7% at 2% WS_2 addition compared to 10% WS_2.

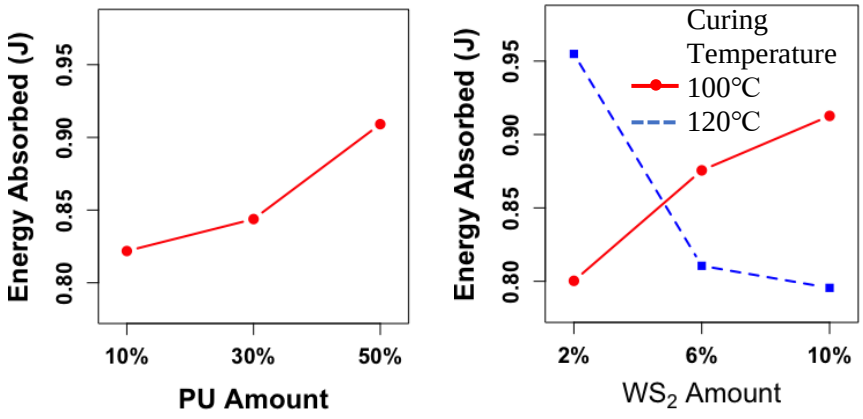

Figure 6.6. Effect plots for the means of energy absorbed: (a) PU amount; (b) interaction of WS_2 amount and curing temperature.

Figure 6.7 presents main and interaction effect plots of PU amount, curing temperature, and WS_2 amount for the mean of toughness. It is found increasing PU amount and curing temperature both decrease the toughness of the PU/WS_2 coated UHMWPE yarns (Figure 6.7 (a-b)). The decreasing trend for a higher PU amount appears to be highly linear in the tested range. The means toughness of the composites at 10 % and 50 % PU addition are 424.8 J/g and 394.6 J/g, respectively. The lower PU addition (10 %) leads to an improvement of 17.0% over the higher amount (50 %). Although increasing PU addition enhances the elongation at break and energy absorption of the samples, the coating add-on also significantly increases, which leads to lower energy absorption per unit weight of the materials. In this full factorial design, only water medium

was used, applying a higher curing temperature (120℃) slightly reduces the mean toughness of the samples by 5.5% due to the heating damage to the fibers. Figure 6.7 (c) shows the interaction effect plot between WS_2 amount and curing temperature for toughness. Increasing the WS_2 amount with 100℃ curing temperature slightly rises the sample toughness by 5.0%, while it largely decreases the mean toughness of samples by 13.8% with 120℃ curing temperature. This interaction trend agrees with the energy absorption interaction plot. High toughness is obtained under two conditions: (1) 2 % WS_2 and 120℃ for curing, (2) 10 % WS_2 and 100℃ for curing. Figure 6.7 (d) plots the interaction of PU amount and curing temperature for the mean toughness of specimens. Increasing PU amount lowers the mean toughness for both curing temperatures up to 7.7% (100℃) and 21.8% (120℃). When 10% and 30% PU are used, both curing temperatures lead to comparable toughness outcomes. When 50% PU is used, the lower curing temperature (100℃) results in 16% higher mean toughness than its counterpart. These confirm the significant interaction effect of PU amount and curing temperature on toughness. Based on the effect plots on the toughness, the coating condition should be chosen from the two following options to maximize the composite toughness within the studied levels: (1) 100℃, 10%PU, 10%WS_2, (2) 120℃, 10%PU, 2%WS_2.

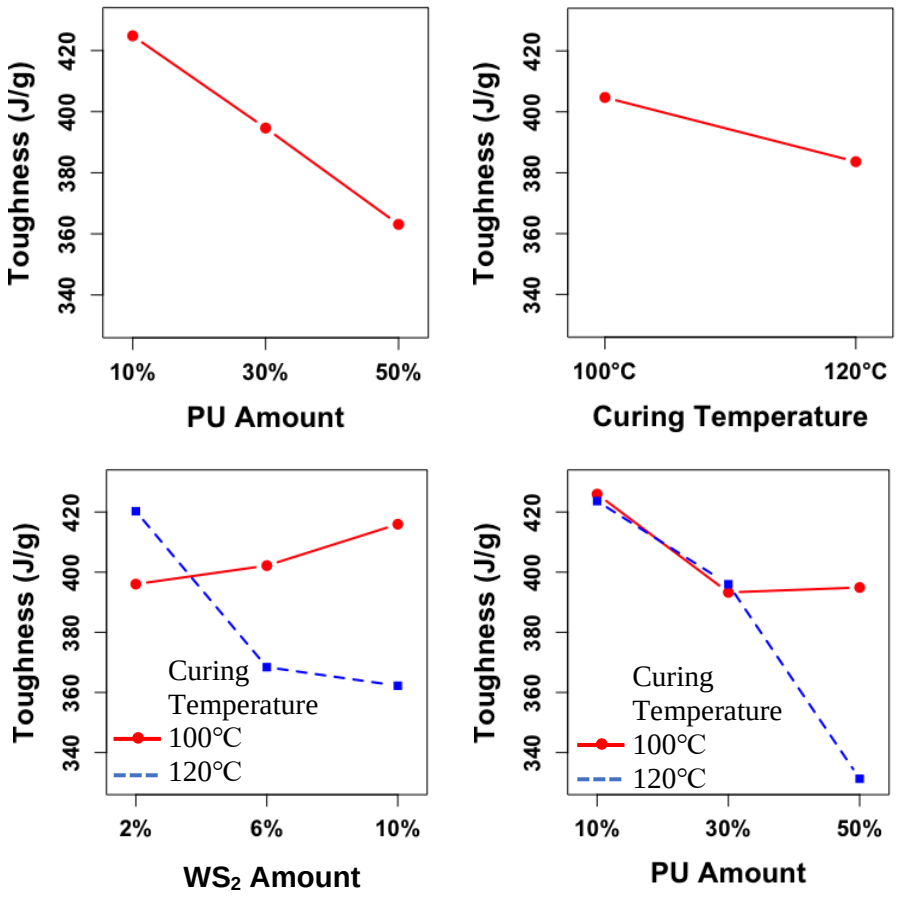

Figure 6.7. Effect plots for the means of toughness: (a) PU amount; (b) curing temperature; (c) interaction of WS_2 amount and curing temperature; (d) interaction of PU amount and curing temperature.

6.3.3.3. Wash durability

The PU/WS_2 coated yarns were subjected to a standard wash, and the coating weight retention was calculated from the weight changes and plotted in Figure 6.8. The mean of weight retention shows an increasing trend with higher PU addition. This is because more PU material contributes to higher integrity of the PU films and larger interfacial bonding areas between the PU films and UHMWPE fibers, which leads to higher coating wash durability. This effect can be observed from the surface morphology of three groups of yarns in Figure 6.9. These yarns were coated with varying PU amounts (10%, 30%, 50%) and 2% WS_2, then cured at 120°C. With an

increasing PU amount, reduced PU debris, rough film edges, and film cracks were formed. Besides, rising curing temperature from 100℃ to 120℃ increases the mean weight retention for all coated yarns. The weight retention averages are in the ranges of 67.5% - 96.3% and 91.0% - 99.7% when the samples are cured at 100℃ and 120℃, respectively. This is attributed to the better film formation of the PU material at 120℃ since the applied PU is more likely to form brittle films rather than tough and intact films at lower curing temperatures upon water removal. In the case of WS_2 amount, no obvious trend in the weight retention is seen with an increasing WS_2 addition for the studied levels. These effects are confirmed by the ANOVA P-values shown in Table 6.7. At a 95% confidence level, both PU amount and curing temperature have significant impacts on sample weight retention, the corresponding P-values are <0.001 and 0.001, respectively. The 2fi effect between PU amount and curing temperature is also significant with P-value = 0.022. Figure 6.10 presents the main and interaction plots of the significant effects. Figure 6.10 (a-b) shows increasing PU amount (from 10% to 30%) improves the mean of weight retention percentage from 83.5% to 97.0%, whereas applying a higher curing temperature (from 100℃ to 120℃) increases the mean value from 87.7% to 96.6%. Figure 6.10 (c) depicts the curing temperature of 120℃ gives higher means of weight retention along all PU levels. When 100℃ curing temperature is applied, 50% PU leads to the highest mean of weight retention (95.3%), whereas at 120℃, 30% PU gives the highest mean value (99.0%).

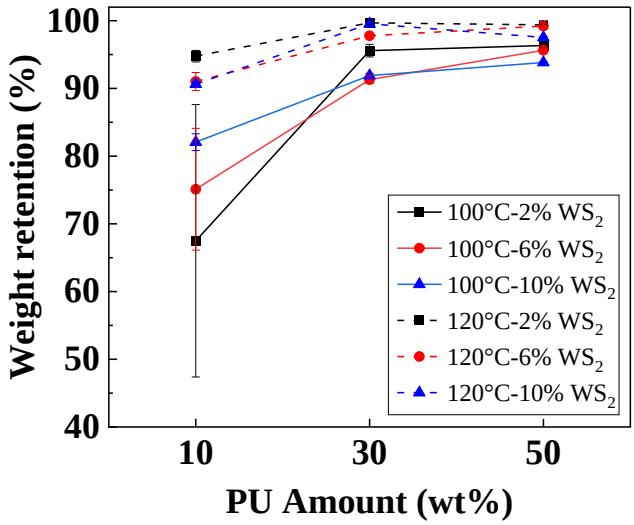

Figure 6.8. Weight retention of the PU/WS_2 coating on UHMWPE yarns after wash with different fabrication conditions.

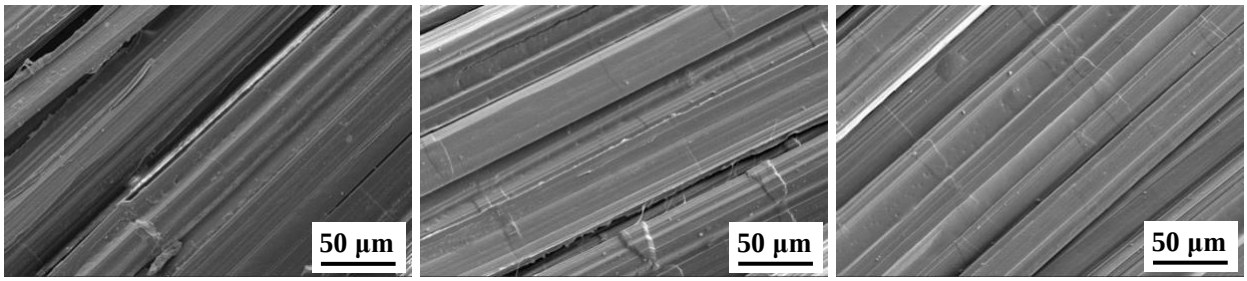

Figure 6.9. SEM images of the PU/WS_2 coated UHMWPE yarns with 2% WS_2 and varying PU amounts: (1) 10%; (2) 30%; (3) 50%.

Table 6.7. ANOVA P-values for all main effects and interaction effects on coating weight retention of the composite yarns after wash.

Effect	Weight retention
WS_2 Amount	0.899
PU Amount	**<0.001**
Curing Temperature (CT)	**0.001**
WS_2 × PU	0.306
WS_2 × CT	0.411
PU × CT	**0.022**
WS_2 × PU × CT	0.182

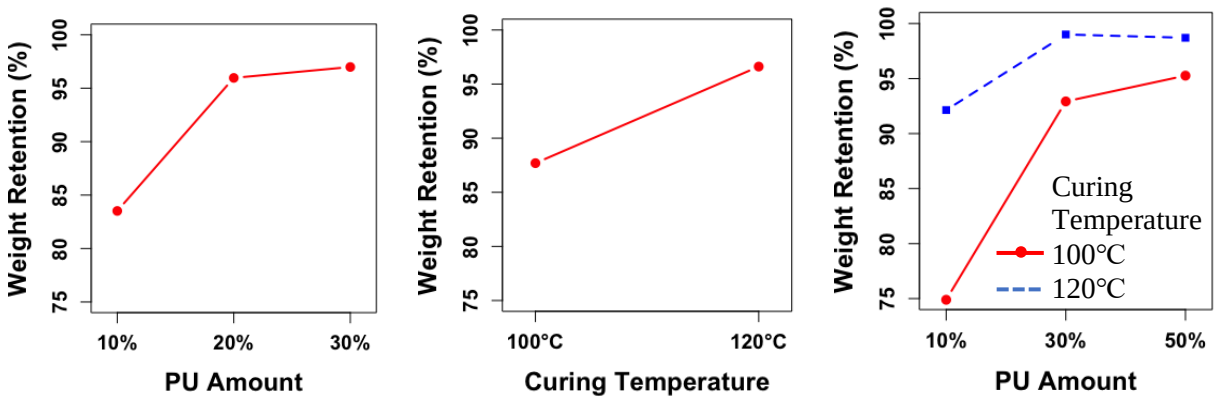

Figure 6.10. Effect plots for the means of weight retention: (a) PU amount; (b) curing temperature; (c) interaction of PU amount and curing temperature.

Although increasing PU amount improves the coating wash durability, it also dramatically decreases the toughness of coated yarns due to the weight increase. Thus, it was maintained at 10% to prioritize its toughness impact for later designs. The higher curing temperature (120°C) was adopted to ensure high weight retention of the coatings. When 120°C is used for curing, the toughness of the samples increases with lower WS_2 amounts as previously analyzed. To check the effect of the WS_2 amount less than 2 % under this condition, lower levels of WS_2 amount are needed.

6.3.3.4. Effects of WS_2 amount on PU/WS_2/UHMWPE yarns

To study the effects of WS_2 amount, two more levels of WS_2 addition (0.5 wt% and 1 wt%) were added. The PU amount and curing temperature were kept at 10 wt% and 120°C. Figure 6.11 plots the mechanical properties, energy absorption, and weight retention of the specimens fabricated with five levels of WS_2 amount (0.5%, 1%, 2%, 6%, 10%). The average add-on amounts of coated yarns are in the range of 11.0-14.0%. One-way ANOVA result shows the elongation at break values of the composites are significanly different with various WS_2 levels (α=0.05, P-

value=0.0301). Figure 6.11(a) shows the average elongation values increase with a higher amount of WS_2. Similar elongation values of the specimens are obtained with 2%, 6%, and 10% WS_2, which are 4.0%, 4.0%, and 4.1%, respectively. They are 12.3%, 12.2%, and 13.2% higher than that of the specimen fabricated with 0.5% WS_2. WS_2 amount shows no significant effects on the maximum load and energy absorption of the specimens, therefore the plots are not presented here. Figure 6.11(b) exhibits the toughness and weight retention of the specimens with varying WS_2 amount. Significant effects of WS_2 amount on both both toughness and weight retention are found with corresponding P-values of 0.0355 and 0.0001. When the WS_2 amount increases, the mean toughness first increases due to the primary nanoparticle reinforcement, then it decreases owing to its major negative impact on PU film integrity. The highest mean toughness (454.4 J/g) is obtained from the samples fabricated with 2 wt% WS_2. Meanwhile, adding more WS_2 negatively affects sample weight retention after wash due to the lower integrity of formed PU films. However, all weight retention averages are in a high range of 91%-100%. At 2% WS_2, the weight retention of the sample coating reaches 94.8%, which indicates a high wash durability of the specific coating.

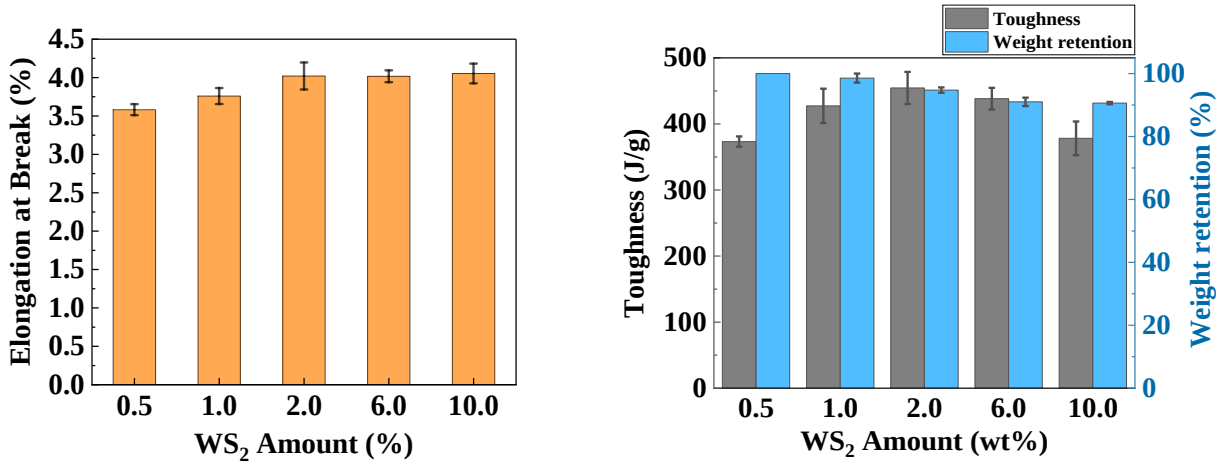

Figure 6.11. The properties of PU/WS_2 coated UHMWPE yarns with varying WS_2 amounts: (a) elongation at break; (b) toughness and weight retention.

6.3.3.5. Effects of stabilizer amount on PU/WS_2/UHMWPE yarns

In the fractional factorial design, two levels of stabilizer were studied: 0% and 3.5% with respect to WS_2 amount, which is 0% and 0.07% regarding the total fluid weight. In this section, the levels of stabilizer amount were expanded by adding 0.035%, 3%, 5%, 7%, and 9%, their effects on the mechanical and energy absorption properties of samples were studied. Other fabrication conditions including 10% PU, 2% WS_2, and 120℃ for curing were used. The mean add-on amounts of the coated samples are in the range of 13.2% - 20.0%. Figure 6.12 presents the elongation at break, energy absorbed, toughness, and weight retention of the composite specimens. The maximum load of the specimens show no significant difference for varying stabilizer additions and is not presented. It is found the stabilizer amount significantly affects both elongation at break (P-value < 0.0001) and total energy absorption (P-value < 0.0001). Both outcomes show a similar increasing and decreasing trend with a higher stabilizer amount (Figure 6.12 (a-b)). This is because adding more stabilizer improves the dispersing uniformity and stability of WS_2 nanoparticles in the aqueous environment and on the fiber surface. This leads to an evener distribution of load or energy within the PU matrix and on coated fibers increasing the breaking elongation and energy absorption capacity. However, adding the stabilizer (a rheology modifier) over its optimal amount may cause difficulty in proper mixing of the PU and WS_2 materials due to the high viscocity of the liquid. This eventually decreases the presented performance of specimens. When 7% of stabilizer is used, the sample obtains the highest elongation at break and energy absorption on average, which are significantly higher (32.3% and 32.0%) than those from 0 wt% of stabilizer (Tukey's test), respectively. When 5% of stabilizer is used, the sample exihibits 21.3% and 31.6% higher elongation at break and total energy absorption over the sample prepared with 0 wt% sabilizer. Similarly, the ANOVA test shows the stabilizer amount significantly affects the

toughness (P-value < 0.0001) and coating weight retention (P-value = 0.0022) of the specimens. Figure 6.12 (c) shows the toughness average inclines with a higher amount of stabilizer and then declines. The toughness reaches to the highest average (480.2 J/g) at 5% stabilizer amount. It is significantly higher (34.6%) than that of the specimen with 0 wt% stabilizer. Adding 5% stabilizer largely increases the dispersion uniformity of WS_2 nanoparticles in the PU films formed on fiber surface in comparison to no stabilizer (Figure 6.13). In the case of weight retention, adding more stabilizer tends to decrease the average coating weight retention after washing for the samples, however, the means of the groups with 0%, 0.035%, 0.07%, 3% and 5% stabilizer are not significantly different. When 5% stabilizer is used, 94.1% of the coating on the sample was retained.

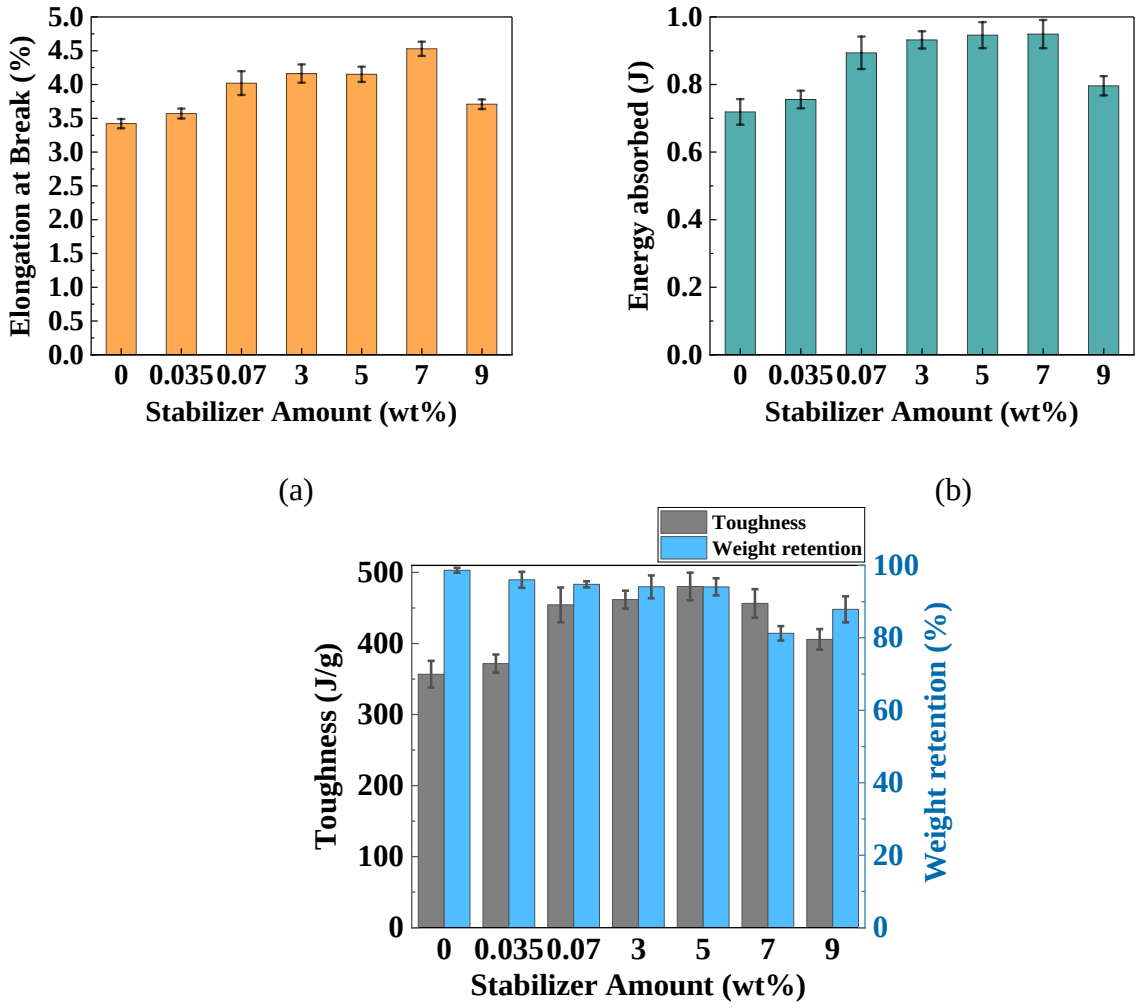

Figure. 6.12. The properties of PU/WS_2 coated UHMWPE yarns with varying stabilizer amounts: (a) elongation at break; (b) energy absorbed; (c) toughness and weight retention.

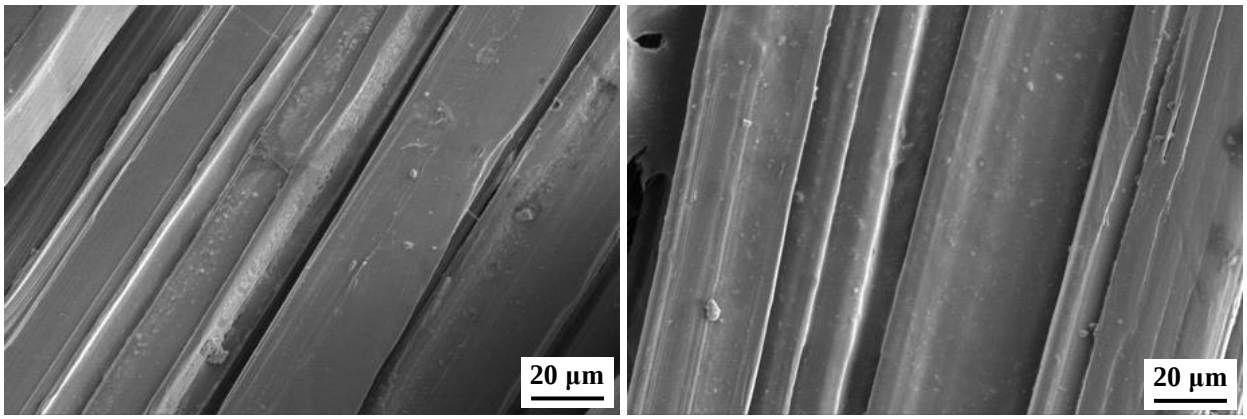

Figure 6.13. SEM images of PU/WS_2 coated yarn surfaces: (a) no stabilizer; (b) 5% stabilizer.

6.3.3.6. Effects of GNP amount on PU/GNP/UHMWPE yarns

The graphene nanoplatelets powder was used as another reinforcing nanomaterial, its effect on PU coated UHMWPE yarns was studied and compared with the WS_2 based composites. Different levels of GNP solid amount were included: 0, 0.2, 0.5, 1.0, 2.9, 4.9, 6.8, and 8.8%. Other optimized conditions were applied, i.e., 10% PU, 120℃ curing temperature, 5% stabilizer, 30min curing time, and water medium. An add-on amount of 6.8% - 13.3% was obtained for the composites. Figure 6.14 depicts the toughness and weight retention of the PU/GNP coated UHMWPE yarns. The mean toughness and weight retention are in the range of 410.5 J/g - 500.6 J/g and 83.3% - 96.2%, respectively. One-way ANOVA result indicates GNP amount has no significant effect on either outcome. Similarly, no significant effects of GNP addition were detected on the maximum load, elongation at break, and energy absorption of the specimens, which are not shown. However, when 2.9% of GNPs is used, the mean toughness of the coated sample is the highest among all GNP levels, and it is significantly higher than that of neat UHMWPE yarns (P-value = 0.0140).

Table 6.8 summarizes the mechanical properties, energy absorption, and weight retention results for the neat UHMWPE yarn, 10%PU/1.0% solid WS_2/UHMWPE yarn, and 10%PU/2.9% GNP/UHMWPE yarn. Both composite yarns were fabricated using the same condition: 5% stabilizer, water medium, 120℃ curing temperature, and 30min curing time. Compared to the neat yarn, the 1.0% solid WS_2/10%PU/UHMWPE yarn shows significantly higher maximum load (P-value = 0.0005), tensile energy absorption (P-value = 0.0011), and toughness (P-value=0.0072), which improve by 31.9%, 66.7%, and 43.3%, respectively. Its increase in toughness indicates the composite absorbed 43.3% higher tensile energy per unit weight over the neat yarn, or 30.2% less weight of the composite is required than the neat yarn to absorb the same amount of energy before

rupture. In the case of the 2.9%GNP/10%PU/UHMWPE yarn, it also exhibits significantly higher maximum load (P-value= 0.0009), tensile energy absorption (P-value= 0.0057), and toughness (P-value= 0.0140) over the neat sample. Improvements of 30.5%, 63.1%, and 49.6% are achieved, respectively. This means 49.6% higher energy absorption per unit weight or 33.1% less weight for the same energy absorption capacity of the neat yarn. However, since the properties of both WS_2 and GNP reinforced optimal composites are comparable, the WS_2 nanomaterial is preferred to the GNPs due to its much lower cost and smaller addition amount required.

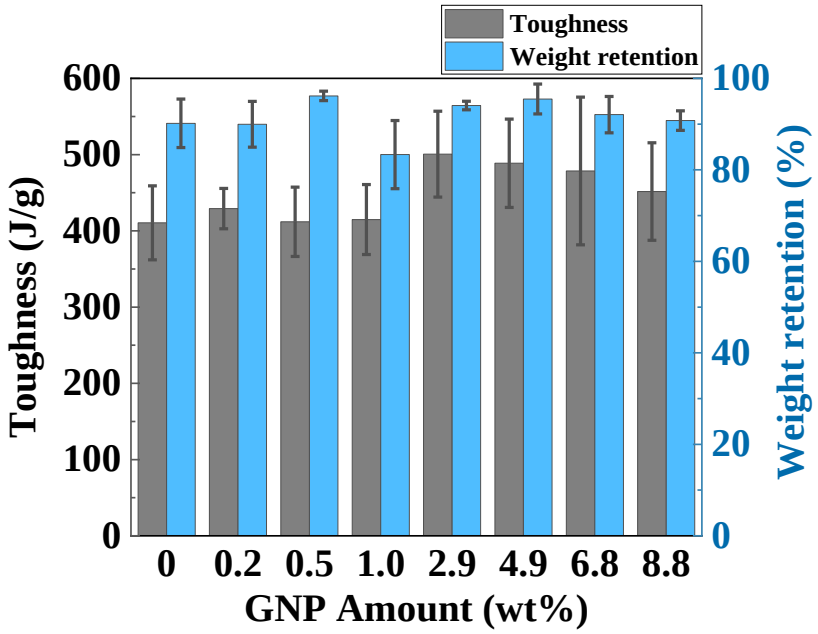

Figure 6.14. Toughness and weight retention of PU/GNP coated UHMWPE yarns using varying GNP amounts.

Table 6.8. Properties (mean and SE) for the neat UHMWPE yarn and optimized PU/nanomaterial/UHMWPE yarns.

Properties	Maximum load (N)	Elongation at break (%)	Energy absorbed (J)	Toughness (J/g)	Weight retention (%)
Neat	423 ± 14	3.47 ± 0.48	0.57 ± 0.08	335 ± 44	-
1.0% WS_2/PU coated	558 ± 14	4.15 ± 0.11	0.95 ± 0.04	480 ± 20	94.1 ± 2.4
2.9%GNP/PU coated	552 ± 15	3.78 ± 0.16	0.93 ± 0.05	501 ± 29	94.1 ± 0.9

6.4. Summary

Fiber-based nanocomposites have been researched in different areas such as aerospace and defense due to their high strength-to-weight ratios. During fabrication, various factors may affect their mechanical properties, for instance, matrix type and concentration, nanofiller type, size, concentration, and distribution uniformity, as well as fabrication method. In this work, waterborne polyurethane and tungsten disulfide nanoparticles were incorporated with UHMWPE yarns through a continuous dip-coating method. Fiber-based nanocomposite yarns were fabricated. The effects of several coating factors on mechanical properties and coating weight retention after wash for the specimens are studied. These factors include the PU amount, WS_2 amount, stabilizer amount, curing temperature, curing time, and medium type.

The curing time and medium type have no significant effects on sample toughness and coating weight retention. Increasing the PU amount and curing temperature decreases the toughness of coated yarns prepared using a water medium due to the high weight addition and heat damage to fibers, respectively. In contrast, the weight retention of sample coating after wash shows an increasing trend with a higher PU addition and curing temperature due to larger bonding areas between PU matrix and UHMWPE fibers and tougher PU films formed on the fiber surface, respectively.

Increasing the WS_2 amount first increases and then decreases the yarn toughness, whereas it lowers the wash durability of coated yarns. Adding the stabilizer leads to an even distribution of WS_2 nanoparticles within the PU matrix and on coated fibers increasing breaking elongation and energy absorption capacity of the specimens. No significant effects of GNP amount are found on the mechanical properties and wash durability of the GNP/PU coated UHMWPE yarns.

Compared to neat yarns, the optimal composite yarn was fabricated with conditions: 1 wt% solid IF-WS_2,10 wt% PU, 5 wt% stabilizer, and 120℃ for curing. The actual IF-WS_2 and PU amounts on the yarn are calculated as 2.2 wt% and 8.5 wt%, respectively. Compared to neat yarns, this optimal yarn shows 31.9% higher maximum load, 66.7% higher tensile energy absorption, and 43.3% higher toughness. The composite yarn made with 2.9 wt% solid GNP and 10 wt% PU in the dispersion (2.9 wt% GNP + 3.6 wt% PU on the yarn by calculation) achieved 30.5%, 63.1%, and 49.6% improvements for the same outcomes. The coating weight on both specimens retained 94.1% after wash.

6.5. Reference

[1] Crouch IG. Body armour – New materials, new systems. Def Technol 2019. https://doi.org/10.1016/j.dt.2019.02.002.

[2] Peinado J, Jiao-Wang L, Olmedo Á, Santiuste C. Influence of stacking sequence on the impact behaviour of UHMWPE soft armor panels. Compos Struct 2022;286. https://doi.org/10.1016/j.compstruct.2022.115365.

[3] Xie Y chen, Zhang H, Zhu W, Huang G yan. Effects of textile structure and projectile geometry on ballistic performance of UHMWPE textiles. Compos Struct 2022. https://doi.org/10.1016/j.compstruct.2021.114785.

[4] Wang K, Shen L, Lu R, Yang Z, Qin Z. Journal of Industrial and Engineering Chemistry Remarkably improved interfacial adhesion of UHMWPE fibers reinforced composite by constructing a three-dimensional stacked nanoparticles structure at interphase 2022.

[5] Rahman M, Hosur M, Zainuddin S, Vaidya U, Tauhid A, Kumar A, et al. Effects of amino-functionalized MWCNTs on ballistic impact performance of E-glass/epoxy composites using a spherical projectile. Int J Impact Eng 2013;57:108–18. https://doi.org/10.1016/j.ijimpeng.2013.01.011.

[6] Domun N, Kaboglu C, Paton KR, Dear JP, Liu J, Blackman BRK, et al. Ballistic impact behaviour of glass fibre reinforced polymer composite with 1D/2D nanomodified epoxy matrices. Compos Part B Eng 2019. https://doi.org/10.1016/j.compositesb.2019.03.024.

[7] Domun N, Paton KR, Hadavinia H, Sainsbury T, Zhang T, Mohamud H. Enhancement of fracture toughness of epoxy nanocomposites by combining nanotubes and nanosheets as fillers. Materials (Basel) 2017. https://doi.org/10.3390/ma10101179.

[8] Díez-Pascual AM, Naffakh M, Gómez-Fatou MA. Mechanical and electrical properties of novel poly(ether ether ketone)/carbon nanotube/inorganic fullerene-like WS2 hybrid nanocomposites: Experimental measurements and theoretical predictions. Mater Chem

Phys 2011. https://doi.org/10.1016/j.matchemphys.2011.06.019.

[9] Simić DM, Stojanović DB, Brzić SJ, Totovski L, Uskoković PS, Aleksić RR. Aramid hybrid composite laminates reinforced with inorganic fullerene-like tungsten disulfide nanoparticles. Compos Part B Eng 2017. https://doi.org/10.1016/j.compositesb.2017.05.002.

[10] Mojtabaei A, Otadi M, Goodarzi V, Khonakdar HA, Jafari SH, Reuter U, et al. Influence of fullerene-like tungsten disulfide (IF-WS2) nanoparticles on thermal and dynamic mechanical properties of PP/EVA blends: Correlation with microstructure. Compos Part B Eng 2017. https://doi.org/10.1016/j.compositesb.2016.12.006.

[11] Naffakh M, Díez-Pascual AM, Marco C, Ellis GJ, Gómez-Fatou MA. Opportunities and challenges in the use of inorganic fullerene-like nanoparticles to produce advanced polymer nanocomposites. Prog Polym Sci 2013. https://doi.org/10.1016/j.progpolymsci.2013.04.001.

[12] Díez-Pascual AM, Naffakh M, Marco C, Ellis G. Mechanical and electrical properties of carbon nanotube/poly(phenylene sulphide) composites incorporating polyetherimide and inorganic fullerene-like nanoparticles. Compos Part A Appl Sci Manuf 2012. https://doi.org/10.1016/j.compositesa.2011.12.026.

[13] Simić D, Stojanović DB, Kojović A, Dimić M, Totovski L, Uskoković PS, et al. Inorganic fullerene-like IF-WS2/PVB nanocomposites of improved thermo-mechanical and tribological properties. Mater Chem Phys 2016. https://doi.org/10.1016/j.matchemphys.2016.09.060.

[14] Díez-Pascual AM, Naffakh M. Mechanical and thermal behaviour of isotactic polypropylene reinforced with inorganic fullerene-like WS2 nanoparticles: Effect of filler loading and temperature. Mater Chem Phys 2013. https://doi.org/10.1016/j.matchemphys.2013.06.039.

[15] Naffakh M, Marco C, Gómez MA, Gómez-Herrero J, Jiménez I. Use of inorganic fullerene-like WS2 to produce new high-performance polyphenylene sulfide nanocomposites: Role of the nanoparticle concentration. J Phys Chem B 2009. https://doi.org/10.1021/jp902700x.

[16] Shneider M, Dodiuk H, Tenne R, Kenig S. Nanoinduced morphology and enhanced properties of epoxy containing tungsten disulfide nanoparticles. Polym Eng Sci 2013. https://doi.org/10.1002/pen.23517.

[17] Pan Y, Yang B, Jia N, Yu Y, Xu X, Wang Y, et al. Enhanced thermally conductive and thermomechanical properties of polymethyl methacrylate (PMMA)/graphene nanoplatelets (GNPs) nanocomposites for radiator of electronic components. Polym Test 2021. https://doi.org/10.1016/j.polymertesting.2021.107237.

[18] Iqbal AA, Sakib N, Iqbal AKMP, Nuruzzaman DM. Graphene-based nanocomposites and their fabrication, mechanical properties and applications. Materialia 2020. https://doi.org/10.1016/j.mtla.2020.100815.

[19] Abu-Okail M, Alsaleh NA, Farouk WM, Elsheikh A, Abu-Oqail A, Abdelraouf YA, et al. Effect of dispersion of alumina nanoparticles and graphene nanoplatelets on microstructural and mechanical characteristics of hybrid carbon/glass fibers reinforced polymer composite. J Mater Res Technol 2021. https://doi.org/10.1016/j.jmrt.2021.07.158.

[20] Sukur EF, Onal G. Graphene nanoplatelet modified basalt/epoxy multi-scale composites with improved tribological performance. Wear 2020. https://doi.org/10.1016/j.wear.2020.203481.

[21] Wu Z, Cao S, Sun Q, Zhong F, Zhang M, Duan H. Mechanical, thermal and gas sensing properties of flexible multi-walled carbon nanotubes/waterborne polyurethane composite film. Compos Sci Technol 2021. https://doi.org/10.1016/j.compscitech.2021.109040.

[22] Zhao H, Li K, Wu W, Li Q, Jiang Y, Cheng B, et al. Journal of Industrial and Engineering Chemistry Microstructure and viscoelastic behavior of waterborne polyurethane / cellulose nanofiber nanocomposite 2022.

[23] Du W, Jin Y, Lai S, Shi L, Shen Y, Pan J. Urethane-silica functionalized graphene oxide for enhancing mechanical property and fire safety of waterborne polyurethane composites. Appl Surf Sci 2019. https://doi.org/10.1016/j.apsusc.2019.06.227.

[24] Clifton S, Thimmappa BHS, Selvam R, Shivamurthy B. Polymer nanocomposites for high-velocity impact applications-A review. Compos Commun 2020;17:72–86. https://doi.org/10.1016/j.coco.2019.11.013.

[25] Abtew MA, Boussu F, Bruniaux P, Loghin C, Cristian I. Ballistic impact mechanisms – A review on textiles and fibre-reinforced composites impact responses. Compos Struct 2019. https://doi.org/10.1016/j.compstruct.2019.110966.

[26] Khodadadi A, Liaghat G, Vahid S, Sabet AR, Hadavinia H. Ballistic performance of Kevlar fabric impregnated with nanosilica/PEG shear thickening fluid. Compos Part B Eng 2019. https://doi.org/10.1016/j.compositesb.2018.12.121.

[27] Benzait Z, Trabzon L. A review of recent research on materials used in polymer–matrix composites for body armor application. J Compos Mater 2018;52:3241–63. https://doi.org/10.1177/0021998318764002.

[28] Laha A, Majumdar A. Shear thickening fluids using silica-halloysite nanotubes to improve the impact resistance of p-aramid fabrics. Appl Clay Sci 2016. https://doi.org/10.1016/j.clay.2016.07.017.

[29] Staudinger U, Thoma P, Lüttich F, Janke A, Kobsch O, Gordan OD, et al. Properties of thin layers of electrically conductive polymer/MWCNT composites prepared by spray coating. Compos Sci Technol 2017. https://doi.org/10.1016/j.compscitech.2016.11.015.

[30] Rangaswamy H, M HH, Gowdru Chandrashekarappa MP, Pimenov DY, Giasin K, Wojciechowski S. Experimental investigation and optimization of compression moulding parameters for MWCNT/glass/kevlar/epoxy composites on mechanical and tribological properties. J Mater Res Technol 2021. https://doi.org/10.1016/j.jmrt.2021.08.037.

[31] Imoisili PE, Jen TC. Modelling and optimization of the impact strength of plantain (Musa paradisiacal) fibre/MWCNT hybrid nanocomposite using response surface methodology. J Mater Res Technol 2021. https://doi.org/10.1016/j.jmrt.2021.05.101.

[32] Adamu M, Rahman MR, Hamdan S. Formulation optimization and characterization of bamboo/polyvinyl alcohol/clay nanocomposite by response surface methodology. Compos Part B Eng 2019. https://doi.org/10.1016/j.compositesb.2019.107297.

[33] Shay GD. Alkali-Swellable and Alkali-Soluble Thickener Technology, 1989. https://doi.org/10.1021/ba-1989-0223.ch025.

[34] Tam T, Bhatnagar A. High-performance ballistic fibers and tapes. Light. Ballist. Compos. Mil. Law-Enforcement Appl. Second Ed., 2016. https://doi.org/10.1016/B978-0-08-100406-7.00001-5.

[35] Oliveira L, Santos JC, Panzera TH, Freire RTS, Vieira LMG, Scarpa F. Evaluation of hybrid-short-coir-fibre-reinforced composites via full factorial design. Compos Struct 2018. https://doi.org/10.1016/j.compstruct.2018.01.088.

[36] Morton WE, Hearle JWS. Physical Properties of Textile Fibres: Fourth Edition. 2008. https://doi.org/10.1533/9781845694425.

[37] Goutianos S, Peijs T. The optimisation of flax fibre yarns for the development of high-performance natural fibre composites. Adv Compos Lett 2003. https://doi.org/10.1177/096369350301200602.

[38] Shah DU, Schubel PJ, Clifford MJ. Modelling the effect of yarn twist on the tensile strength of unidirectional plant fibre yarn composites. J Compos Mater 2013. https://doi.org/10.1177/0021998312440737.

[39] Khanum R, Ahmed F, Mahabubuzzaman AKM, Ehsan MN, Asaduzzaman AM. Consequence of Twist on Yarn Properties in Textiles. Online) J Innov Dev Strateg 2011.

[40] Platt MM. Mechanics of Elastic Performance of Textile Materials: III. Some Aspects of Stress Analysis of Textile Structures— Continuous-Filament Yarns. Text Res J 1950. https://doi.org/10.1177/004051755002000101.

[41] Yao W-H, Yeh J-T, Chou W-L, Shu Y-C. A study on preparation and mechanical properties of UHMWPE/nylon composite covered yarn. Second Int. Conf. Smart Mater. Nanotechnol. Eng., 2009. https://doi.org/10.1117/12.840350.

CHAPTER 7

Effects of inorganic fullerene-like tungsten disulfide and graphene nanoplatelets on waterborne polyurethane films[6]

[6] Wu, S., Shaw, T. S., and Bhat, G. S. To be submitted to *Progress in Organic Coatings*.

Abstract

Nanocomposite films were prepared with waterborne polyurethane (PU) and inorganic fullerene-like tungsten disulfide (IF-WS_2) or graphene nanoplatelets (GNPs) using the casting method. The appearance, mechanical properties, tensile energy absorption, viscoelasticity, and thermal transition of the PU and nanocomposite films were investigated. The results indicated that PU/IF-WS_2 films achieved up to 48.0%, 115.5%, and 48.3% higher maximum load, total tensile energy absorption, and specific energy absorption, respectively compared to the PU film. It was attributed to good film formation and uniform nanoparticle distribution. The storage modulus, loss modulus, and damping ratio of the IF-WS_2 reinforced PU films increased up to 107.9%, 171.8%, and 90.4%, respectively, over those of the pure PU film, which is due to the energy storage and dissipation distribution of IF-WS_2 nanoparticles. PU/GNP films showed relatively lower mechanical and viscoelastic properties over PU films due to the micro pores and the GNP agglomerates formed on the film surface. At the same nanofiller additions, PU/IF-WS_2 nanocomposite films showed much higher mechanical properties than the PU/GNP films. Adding IF-WS_2 slightly decreased the glass transition temperature (T_g) of PU films, whereas incorporating GNPs showed no significant effect on the T_g of the films.

Keywords: Waterborne polyurethane; Inorganic fullerene-like tungsten disulfide; Nanocomposite film; Mechanical property; Viscoelasticity

7.1. Introduction

Polyurethane (PU) polymer has been used in various industrial applications including protective coatings, defense coatings, adhesives (sealants and sealers), automotives, textiles, leather, etc. owing to its versatile properties, high flexibility, excellent abrasion resistance, and good mechanical properties [1][2][3]. Unlike conventional solvent-based PU, waterborne PU (WPU) can be dispersed and prepared in an aqueous environment, which leads to less emission of volatile organic compounds (VOCs) and hazardous air pollutants (HAPs) [4]. Due to increasingly strict environmental regulation, waterborne PU becomes one of the highly favored alternatives to conventional PU products for various applications due to its environmentally friendly, nontoxic, and nonflammable characteristics [5][6][7]. WPU is often modified by incorporating nanomaterials including MWCNTs, nano SiO_2, nano TiO_2, attapulgite, cellulose nanowhiskers, nanocrystalline cellulose, etc. The purposes are to tailor their performances regarding mechanical, thermal, rheological, hydrophobic, flame retardant, and anticorrosive properties for diversified applications [8][9][10][11][12]. For instance, Kuan et al. synthesized modified-MWCNTs reinforced WPU nanocomposites. The modified-MWCNTs increased the tensile stress, tensile modulus, degradation temperature, and melt viscosity of the WPU [13]. Wu et al. cast thermoset nanocomposite films with WPU and cellulose nanowhiskers (CNWs). In comparison to pristine WPU films, the WPU/CNW films exhibited increased glass transition temperature (T_g), Young's modulus, and tensile strength and decreased thermal stability [14]. They also prepared WPU films with modified nano SiO_2 and found out that adding modified SiO_2 could increase the water contact angle, T_g, 50% weight loss temperature, and weight residuals of the nanocomposite films [15]. Yin et al. synthesized nanoTiO_2 dispersed WPU emulsions and cast thermoset WPU/TiO_2 composite films on Teflon plates. The effect of nano TiO_2 addition on WPU films was investigated. The

results suggested the incorporated nano TiO_2 improved the tensile strength, thermal stability, light-shielding property, and flame retardancy of the WPU films [16].

Inorganic fullerene-like tungsten disulfide (IF-WS_2) nanoparticles are composed of inorganic elements but have a similar spherical structure to fullerene (C_{60}). This unique structure endows them with high modulus, high impact resistance, good shock absorption ability, and excellent tribology property such as ultra-low friction [17][18][19][20][21]. Due to their exceptional properties, non-toxicity, and low cost, IF-WS_2 has drawn considerable attention in developing polymer nanocomposites with isotactic polypropylene, poly(ether ether ketone), poly(phenylene sulphide), poly(vinyl butyral), etc. for enhanced mechanical, thermal, tribological, and rheological properties [22][23][24][25][26][27][28][29][30]. Haba et al. dispersed IF-WS_2 powder in epoxy resin and prepared epoxy/IF-WS_2 nanocomposite plates with a steel mold. Increased fracture toughness was obtained for the nanocomposite likely due to shear fracture and increase in fracture surface area [31]. Mojtabaei et al. investigated the effect of IF-WS_2 nanoparticles on dynamic mechanical and thermal properties of polypropylene (PP)/ethylene vinyl acetate (EVA) blends. It was found the IF-WS_2 addition improved the loss modulus and thermal stability of the composite blend [32]. Naffakh et al incorporated IF-WS_2 nanoparticles with polyphenylene sulfide polymer, and the fabricated nanocomposites achieved improved mechanical properties over the pristine polymer [33]. Guo et al. mixed IF-WS_2 and polyvinylidene fluoride (PVDF) in N, N-dimethylformamide (DMF) solvent and cast the nanocomposites films on the glass substrate and characterized them. The results indicated the IF-WS_2 reinforced PVDF films achieved enhanced tensile strength, elongation, and energy storage performances [34].

GNP is a thin stack of graphene which is a 2D nanomaterial with carbon atoms located in a hexagonal lattice [35]. It possesses unique properties including large surface area, very high

aspect ratio, high ultimate strength, and high elastic modulus, which make it a promising reinforcing candidate in polymer matrices [36]. However, very limited papers reported the application of GNPs in WPU matrices. Amri et al. cast nanocomposite films with GNPs, cellulose nanofibers (CNFs), and WPU. The GNPs were first dispersed in acetone and then mixed with WPU/CNFs in the preparation. It was found that at a fixed CNFs level, adding GNPs could enhance the mechanical, thermal, and hydrophobic performances of the WPU films [37]. Due to sp2 hybridized carbons in its structure, GNP also show good electrical and thermal conductivity. Kim et al. studied the effect of adding GNPs on the electrical properties of cast WPU films for electrical heating textiles application. The results suggested increasing the GNPs amount improved the electrical performance of the composite films. Moreover, GNPs have been used to reinforce organic solvent-based polyurethane for enhanced stiffness, tensile strength, thermal stability, thermal conductivity, and flame retardancy [38][39][40].

Due to mentioned properties of IF-WS_2 and GNPs, it is generally assumed that incorporating these nanofillers in WPU could improve its mechanical properties and specific energy absorption. However, the reinforcing effects of individual IF-WS_2 and GNPs components on the WPU matrix have not been reported in the literature. Thus, to fill the research gap, WPU and WPU/nanofiller films were prepared using water-based casting method in this work, and were investigated using tensile test, dynamic mechanical analysis (DMA), differential scanning calorimetry (DSC), and scanning electron microscope (SEM), respectively.

7.2. Materials and Methods

7.2.1. Materials

Aqueous polyurethane (Aptalon™ M 8100) having a milky white color was provided by Lubrizol, Corp., USA. It has 41 wt% solid content, viscosity < 500, pH 7.5 - 8.5, and self-crosslinking property with its unique polyamide polyol type used [41]. Inorganic fullerene-like tungsten disulfide dispersion (IF-WS_2) (IW-4000) was obtained from Nanotech Industrial Solutions, Inc., USA. The dark-brown dispersion contains cage-structured IF-WS_2 nanoparticles with an average size of 80nm, it is often used as a lubricant additive due to its low friction [42][32]. IF-WS_2 solid content was measured as 48.8 wt%. Graphene nanoplates (GNPs) (powder, surface area: 750m^2/g, thickness < 10nm, density: 0.2-0.4 g/cm^3) were purchased from MilliporeSigma, USA. Figure 7.1 (a-b) and (c-d) exhibit the bright field-scanning transmission electron microscopy (BF-STEM) images obtained for the GNPs and IF-WS_2 nanoparticles, respectively. Kapton® polyimide sheets (254×178×0.05mm) were purchased from Push Plastic, USA. Polyimide exhibits exceptional thermal stability > 500℃, it can stand high temperature during the curing process of PU films [43]. The sheets have transparent release liner backings, which were used for casting and releasing PU and PU/IF-WS_2 films. Aluminum plates (254×102×0.8mm) were purchased from K&S Precision Metals, USA, and they were applied to back Kapton® sheets due to their high-temperature stability and stiffness.

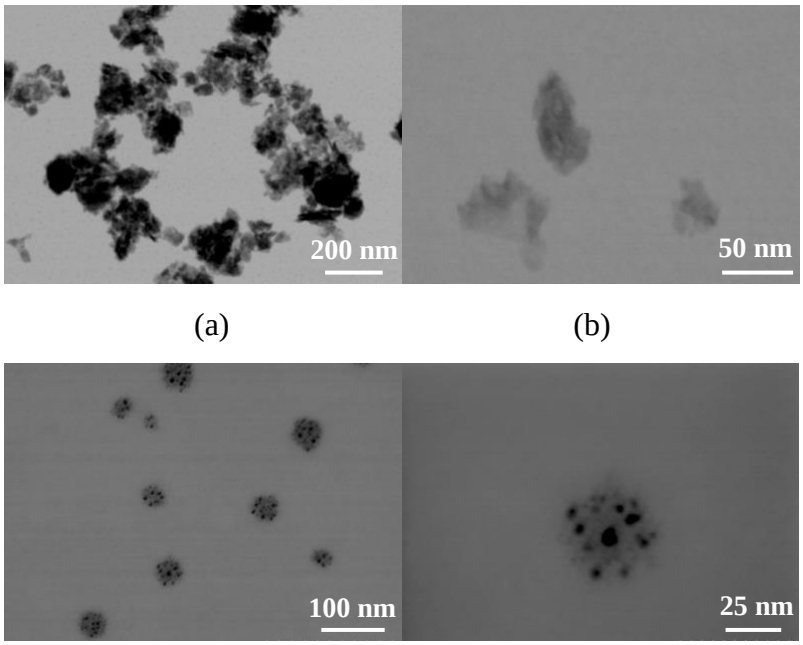

Figure 7.1. BF-STEM images of the nanomaterials: (a-b) GNP nanosheets; (c-d) IF-WS_2 nanoparticles.

7.2.2. Film preparation

Table 7.1 lists the PU/WS_2 and PU/GNP fluid compositions used to prepare the PU and nanocomposite films, different levels of nanofiller addition regarding PU solid weight were selected. When the GNP amount is higher than 11.9 wt%, the cast films are too brittle to be removed from Kapton® sheets, therefore higher GNP levels were not included. The coating fluids were prepared by adding IF-WS_2 or GNPs into PU dispersion as per the calculated amount in a 50mL centrifuge tube, followed by 30 min sonication using an ultrasonic bath (Kendal). Due to the difficulty to cast PU films with low-viscosity dispersions, the mixed dispersion was transferred into a 50ml beaker and heated at 90°C for 45 min on a hotplate (VWR® Advanced) to evaporate a proper amount of water. Spontaneously, the dispersion was mixed using a magnetic stirrer at 500rpm to maintain its homogeneity during heating. With the prepared dispersions, PU and PU/IF-WS_2 films were cast on Kapton® sheets backed with aluminum plates using a micrometric film

applicator (Elcometer 3570). The casting thickness was set at 400 μm. The plates with cast films were dried and cured in an oven at 120°C for 30min and then removed from Kapton® sheets. Figure 7.2 shows a cast PU film before and after removal from the Kapton® sheet.

Table 7.1. Abbreviates of fabricated films and corresponding compositions of casting fluids.

Sample	PU liquid (g)	WS_2 liquid (g)	GNP powder (g)	WS_2 liquid with respect to PU liquid (wt%)	Nanoparticle to PU solid weight ratio
PU	30.0	0	-	0	0:100
PW3	28.6	1.4	-	5	6.0:100
PW4	27.3	2.7	-	10	11.9:100
PW5	25.0	5.0	-	20	23.8:100
PW6	18.7	11.3	-	60	71.3:100
PW7	15.0	15.0	-	100	118.9:100
PG1	29.9	-	0.2	-	1.2:100
PG2	29.6	-	0.4	-	3.6:100
PG3	29.3	-	0.7	-	6.0:100
PG4	28.6	-	1.4	-	11.9:100

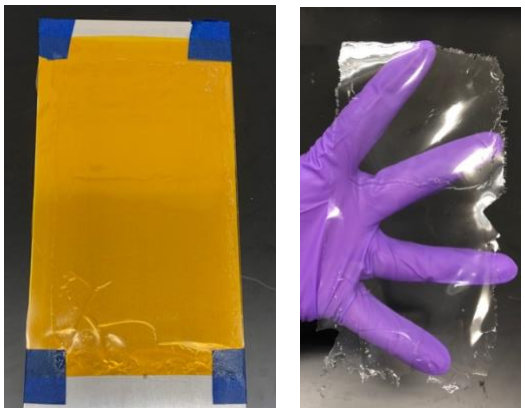

Figure 7.2. A cast and cured PU film: (a) on a Kapton sheet backed with an aluminum plate; (b) after removal.

7.2.3. Characterizations

7.2.3.1. Tensile properties and energy absorption

The tensile properties of the PU and nanocomposite films were tested using a tensile tester (Instron 4411) according to the ASTM D412 standard [44]. Tensile test strips (5mm × 70mm) were cut from the PU, PU/IF-WS_2, and PU/GNP films (thickness: 0.1-0.3 mm) and weighed for calculating film areal density. The sample strips were tested with a crosshead speed of 100 mm/min. Maximum load and elongation at break values were recorded. Total energy absorbed by a sample before fracture was obtained by integrating the load-displacement curve. And the specific energy absorption was calculated by dividing the total energy absorption by the areal density of the sample. Average values of at least 8 replicates were reported.

7.2.3.2. Dynamic mechanical analysis

Dynamic mechanical analysis (DMA) was employed to investigate the effect of nanofiller amounts on the elastic and viscous properties of the PU film. A DMA instrument (PerkinElmer DMA 8000) was used to conduct the test at tenson mode for pure PU and nanocomposite films. Prior to the test, film samples (5mm × 20mm) were cut, the thickness of each film was measured at two locations and the average was taken for the DMA test. During sample clamping, the double-sided tape was used on each film end to prevent sample slippage. Temperature sweeps were applied from 30°C to 120°C at a 3°C/min heating rate, 1Hz frequency, and 0.005mm strain. Figure 7.3 shows the tensile (left) and DMA (right) test samples from a nanocomposite film.

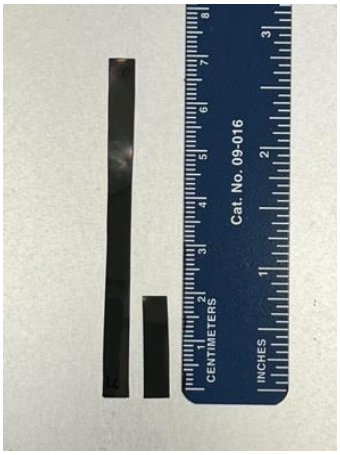

Figure 7.3. Image of a tensile test sample (left) and a DMA test sample (right).

7.2.3.3. Differential scanning calorimetry

A differential scanning calorimeter (DSC) (PerkinElmer DSC 8000) was used to study the thermal properties of the PU and nanocomposite films. A heating rate of 30°C/min was applied between -20°C to 100°C in the presence of inert gas N_2 (gas flow of 20 mL min−1). The relationship between thermal energy and sample temperature was plotted. Glass transition temperature of each sample was detected.

7.2.3.4. Scanning electron microscopy

The surface morphologies and microstructures of the PU and nanocomposite films were observed using a scanning electron microscope (SEM) (Thermo Fisher Scientific Teneo FE). Approximately 15 nm of gold coating was applied to the samples to prevent charging during SEM observation. The acceleration voltage was set at 5 kV. Images were taken with magnifications of ×50 and ×5000.

7.3. Results and Discussion

7.3.1. Film appearance

Figure 7.4. presents the images of cut specimens from the PU and PU/IF-WS_2 films cast with varying amounts of IF-WS_2 nanoparticles. It is observed that high uniformity of IF-WS_2 nanoparticles is achieved for all IF-WS_2 reinforced PU films, which shows even black colors for the films PW3, PW4, PW5, PW6, and PW7, whereas the pure PU film exhibits a transparent and clear appearance. It is also seen that all the nanocomposite films show highly smooth and flat surfaces on the macro scale indicating that the IF-WS_2 nanoparticles are mostly embedded in the PU matrix. Figure 7.5 shows the appearance of the PU film and PU/GNP films incorporated with varying GNP amounts. Uniform grey to black colors can be observed in the composite films. Compared to IF-PU/WS_2 films, the PU/GNP films show rough surfaces with raised granules that are evenly distributed. Among four films, the PG3 film shows the highest smoothness and lowest visible granule formation.

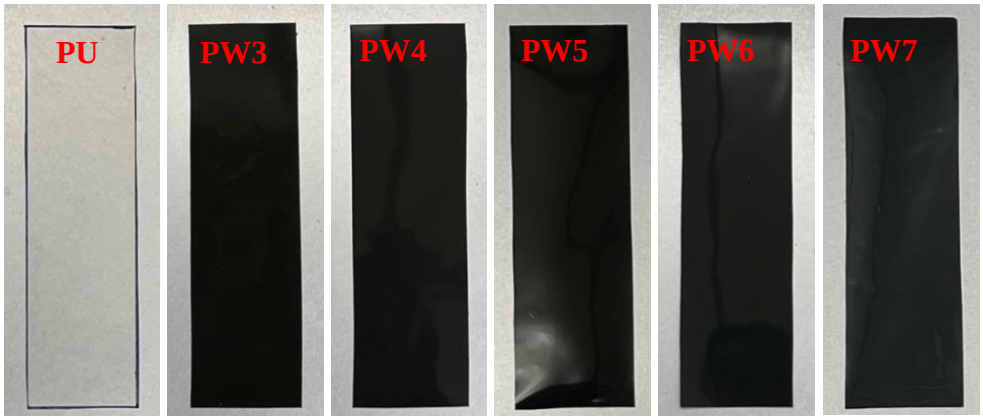

Figure 7.4. Images of the PU and PU/IF-WS_2 nanocomposite films.

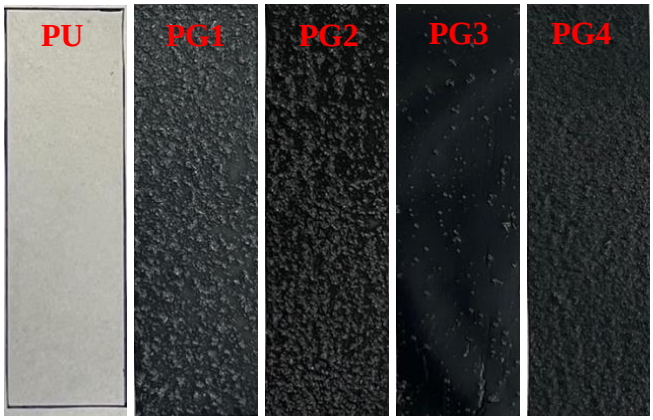

Figure 7.5. Images of the PU and PU/GNP nanocomposite films.

7.3.2. Tensile properties

Tensile tests were conducted on the pure PU film (PU), and IF-WS_2 dispersed PU films (PW3, PW4, PW5, PW6, and PW7) to study the effects of WS_2 addition on their mechanical properties and energy absorption capacity. Figure 7.6 represents their corresponding maximum load, elongation at break, total energy absorbed before rupture, and specific energy absorption. One-way analysis-of-variance (ANOVA) and Tukey's test are used for the statistical analysis. Figure 7.6 (a) represents the maximum load of the tested films and their corresponding IF-WS_2 additions. It is evident that the mean values of the films are significantly different (P-value < 0.0001). When the IF-WS_2 amount increases in the tested levels, the maximum load of the PU/IF-WS_2 films first increases and then decreases. The average values of PW4 and PW5 films reach 20.0 N and 22.4 N, which are significantly improved by 32.0% and 48.0%, respectively, over that of the pure PU film. The tensile strength enhancement can be attributed to the reinforcement of high-strength IF-WS_2 particles that are uniformly distributed in the PU films. However, an excess amount of IF-WS_2 particles leads to decrease in maximum load due to the unbalanced PU/IF-WS_2 ratio, and largely affects the integrity of PU films. Figure 7.6 (b) shows the elongation at break of the same samples, and the average values vary with different IF-WS_2 amounts. High elongation-

at-break values are obtained from the PW4, PW5, and PW6 films. However, the ANOVA results indicate that IF-WS_2 amount has no significant effect on the elongation at break of the cast PU/IF-WS_2 films at a 95% confidence level (P-value = 0.0817). Figures 7.6 (c) and (d) exhibit similar trends for the total energy absorbed (EA) and specific energy absorption (SEA) for the PU films reinforced with an increasing amount of IF-WS_2. The mean values are significantly different among tested films for both EA and SEA at α=0.05, the corresponding P-values are 0.0194 and 0.0470. It means the IF-WS_2 addition amount significantly affects the energy absorption and specific energy absorption capacities of cast PU/IF-WS_2 films. When 6.0 wt% IF-WS_2 is used, both EA and SEA averages of the PW3 films decline due to the limited IF-WS_2 impact with low addition and reduced PU integrity with embedded IF-WS_2 nanoparticles. With 11.9, 23.8, and 71.3 wt% IF-WS_2 addition, the nanocomposite films (PW4, PW5, and PW6) show increased mean EA values (0.24 J, 0.23 J, and 0.20 J), which are 115.5%, 105.2%, and 78.5% higher than that of the PU film. With further increase in IF-WS_2 addition, the PW7 nanocomposite film, however, exhibits a much lower EA value, which may be ascribed to the overload of IF-WS_2 nanoparticles and insufficient PU bonding with nanoparticles. The specific energy absorption, which is total energy absorption normalized by areal density, declines for the PW5, PW6 and PW7 films with an increasing IF-WS_2 amount. The SEA averages for the PW4 and PW5 specimens are 22.4 J*cm^2/g and 18.8 J*cm^2/g, which show improvements of 48.3% and 24.0% over the PU film, respectively. The mechanical and energy absorption results indicate the IF-WS_2 reinforcement at low addition (11.9 wt% and 23.8 wt%) improves the tensile strength of the PU films and their tensile energy absorption capacity based on the same areal density.

Similarly, Figure 7.7 presents the same outcomes for the PU and PU/GNP films. The corresponding y-axis scales from the PU/IF-WS_2 figures are used for direct comparison between

IF-WS_2 and GNP incorporated films. Figure 7.7(a) exhibits the maximum load and GNP addition amount for the PU and nanocomposite films. All PU/GNP nanocomposite films show decreased (33.1%-81.9%) maximum load compared to the PU film. A significant effect of GNP amount on the maximum load is observed. Increasing GNP amount tends to decrease, increase, and then decrease the maximum load of the films. The order of the mean values for the composite films can be observed as PG3>PG1>PG2>PG4. The PG3 film shows the highest maximum load, which agrees with its highest smoothness and fewest granules in the film. Figure 7.7(b-d) present the elongation at break, EA, and SEA of the films. In contrast to the PU/IF-WS_2 films, all cast PU/GNP films with varying GNPs amounts show significantly lower elongation at break, EA, and SEA than the PU film. Compared to PW3 and PW4 films, GNP dispersed PU films - PG3 and PG4 obtained much lower mechanical properties and energy absorption capacities with the same amount of nanofillers due to the hydrophobicity and low dispersibility of GNPs in an aqueous environment. These observed trends are the result of the changes in morphology and corresponding changes in failure mechanisms, the data has to be interpreted carefully in drawing any conclusions. One observation that is clear is that adding nanoparticles makes the films very brittle.

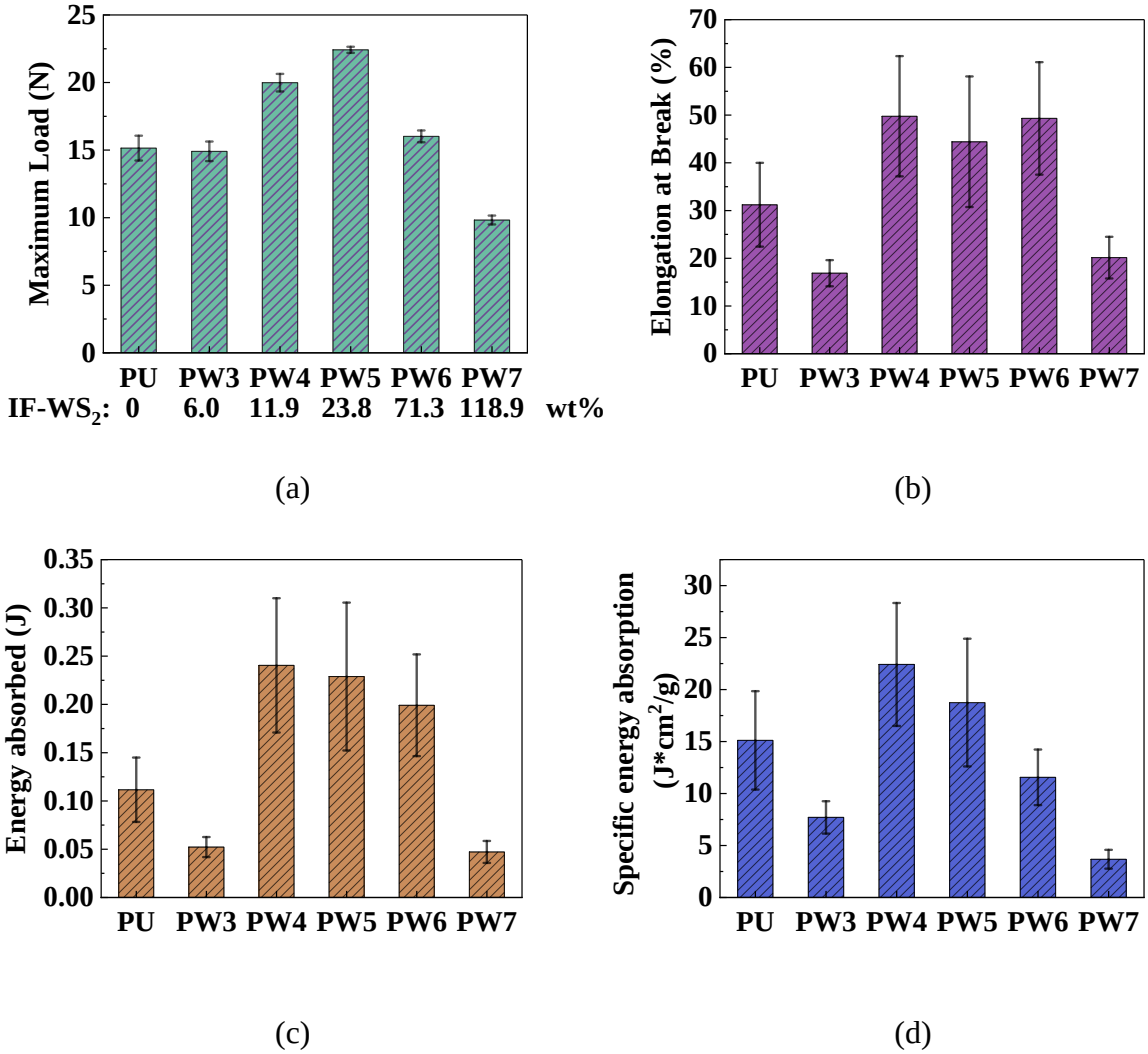

Figure 7.6. Tensile and energy absorption properties (mean and SE) of the PU/IF-WS_2 films fabricated with varying amount of IF-WS_2: (a) maximum Load; (b) elongation at break; (c) energy absorbed; (d) specific energy absorption.

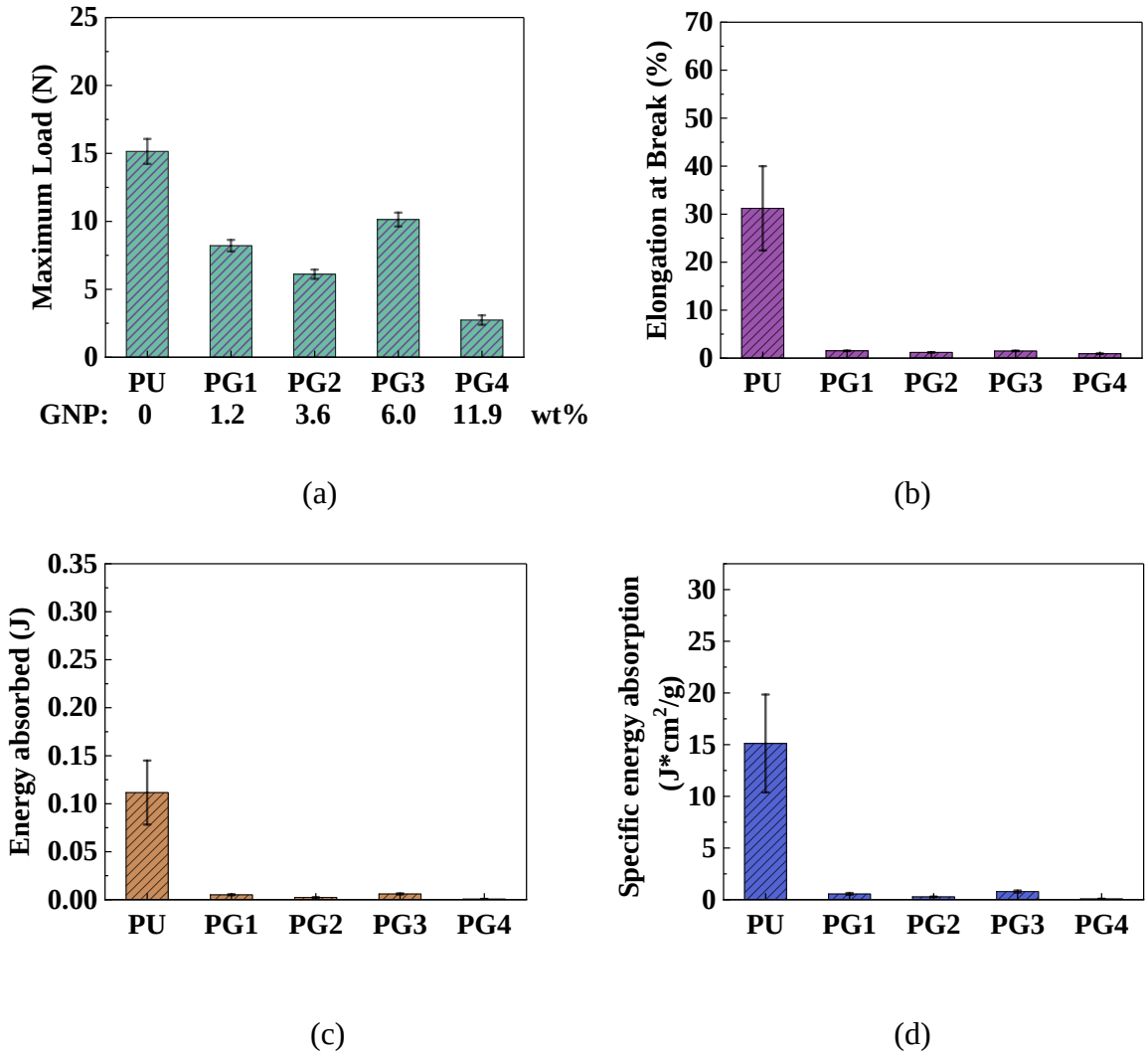

Figure 7.7. Tensile and energy absorption properties (mean and SE) of the PU/GNP films fabricated with varying amounts of GNPs: (a) maximum Load; (b) elongation at break; (c) energy absorbed; (d) specific energy absorption.

7.3.3. Viscoelastic Properties

Plots of storage modulus and loss modulus for the PU and PU/IF-WS_2 films are shown in Figure 7.8. Also shown in the figure are the tan δ curves for the neat, PW6, and PW7 samples. The storage and loss moduli show a decreasing trend with increasing temperature from 30°C to 120°C due to the heating and softening effect. The storage modulus and loss modulus of the PU control film is about 2.4 GPa and 0.3 Gpa at 30°C, respectively. With an increasing IF-WS_2 amount, both moduli of the nanocomposite films first decrease (PW3), then increase (PW4, PW5, PW6), and

finally decrease again for PW7 film. This trend agrees with the tensile energy absorption and specific energy absorption data. The result is most likely due to the balance between IF-WS_2 energy absorption/dissipation contribution and its negative impact on the integrity/formation of PU films, which affect the energy storage and dissipation abilities of the overall films. When the IF-WS_2 amount is above its optimal amount, the excess nanoparticles largely impact the formation of PU films leading to decreased viscoelastic properties for the nanocomposite films. The maximum storage and loss moduli are obtained from the PW6 film followed by the PW7 film. The tan δ of both films is higher than that of the pure PU film within the tested temperature range suggesting both IF-WS_2 incorporated films (PW6 and PW7) show improved damping ability. The two peaks at about 50°C and 95°C of the pure PU film correspond to the T_g of the soft segment and hard segment, respectively. Adding IF-WS_2 in the PW6 film decreases the T_g of its soft segment (to about 41°C) and increases the T_g of hard segment (to about 110°C) resulting in better phase separation. While the T_g of the PW7 film is not observed due to the applied temperature range and/or high IF-WS_2 & low PU contents in the film.

Meanwhile, Figure 7.9 depicts the storage and loss moduli of fabricated PU and PU/GNP films. Also included in the figure is the tan δ curves for the pure PU, PG2 and PG4 samples. All films show an overall decreasing trend for both moduli with increasing temperature. The descending order of the moduli for PU/GNP films is PG4>PG2>PG3>PG1. Increasing GNP amount tends to improve the dynamic mechanical properties of most nanocomposite films. However, compared to the pure PU film, all cast PU/GNP films exhibit lower storage and loss moduli at a temperature below ~45°C, while the outcomes of PG4 films are slightly higher at a temperature above ~45°C. No significant increase is observed for the tan δ values of both PG2 and PG4 films over the PU film. The T_g of the soft segment of the films shows no obvious trends with

higher GNPs addition, while the T_g of the hard segment decreases for PG2 (to ~ 77°C). This indicates the added GNPs largely lower the crosslinking of PU polymer chains in the hard segments and increase the movability of the chains. In the PG4 film, the T_g for the segments is not clearly shown due to its low PU content.

Both moduli and damping ratios (loss to storage modulus, tan δ) of the PU and PU/nanofiller films at 30°C are summarized in Table 7.2. The storage modulus, loss modulus, and damping ratio of the PW6 film reach 4.928 GPa, 0.742 GPa, and 0.151, which show an improvement of 107.9%, 171.8%, and 31.3% respectively, over the PU film. And the same outcomes of the PW7 film are 2.788 GPa, 0.612GPa, and 0.219, which increase by 17.6%, 124.2%, and 90.4%, respectively over the PU film. This indicates both PW6 and PW7 films possess significantly better energy storage, energy dissipation, and damping properties than the PU film. Their enhanced viscoelastic performances are ascribed to the presence of IF-WS_2 nanoparticles which have excellent shock-absorbing ability. However, the high IF-WS_2 addition in PW7 film leads to its dramatic decline in tensile strength and tensile energy absorption capacity due to the overload of IF-WS_2 nanoparticles and low PU matrix bonding resulting in brittle films. The PW4 film, which has the maximum EA and SEA during tensile tests, shows slightly lower storage and loss moduli over the pure PU film.

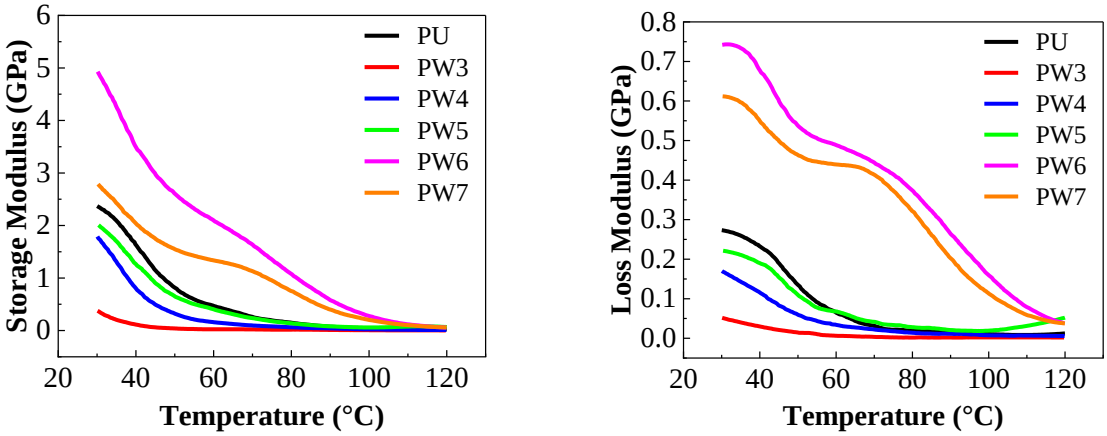

(a)

(b)

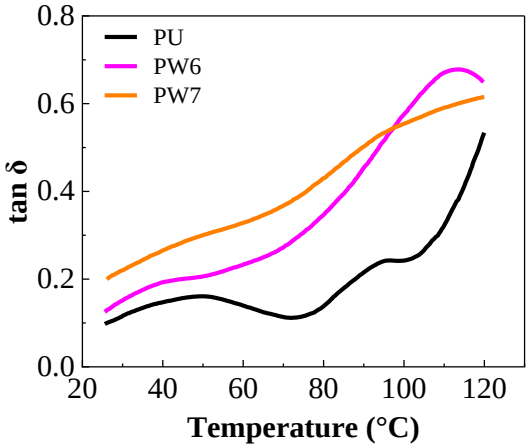

(c)

Figure 7.8. DMA results for the PU and PU/IF-WS_2 films: (a) storage modulus; (b) loss modulus; (c) tan δ.

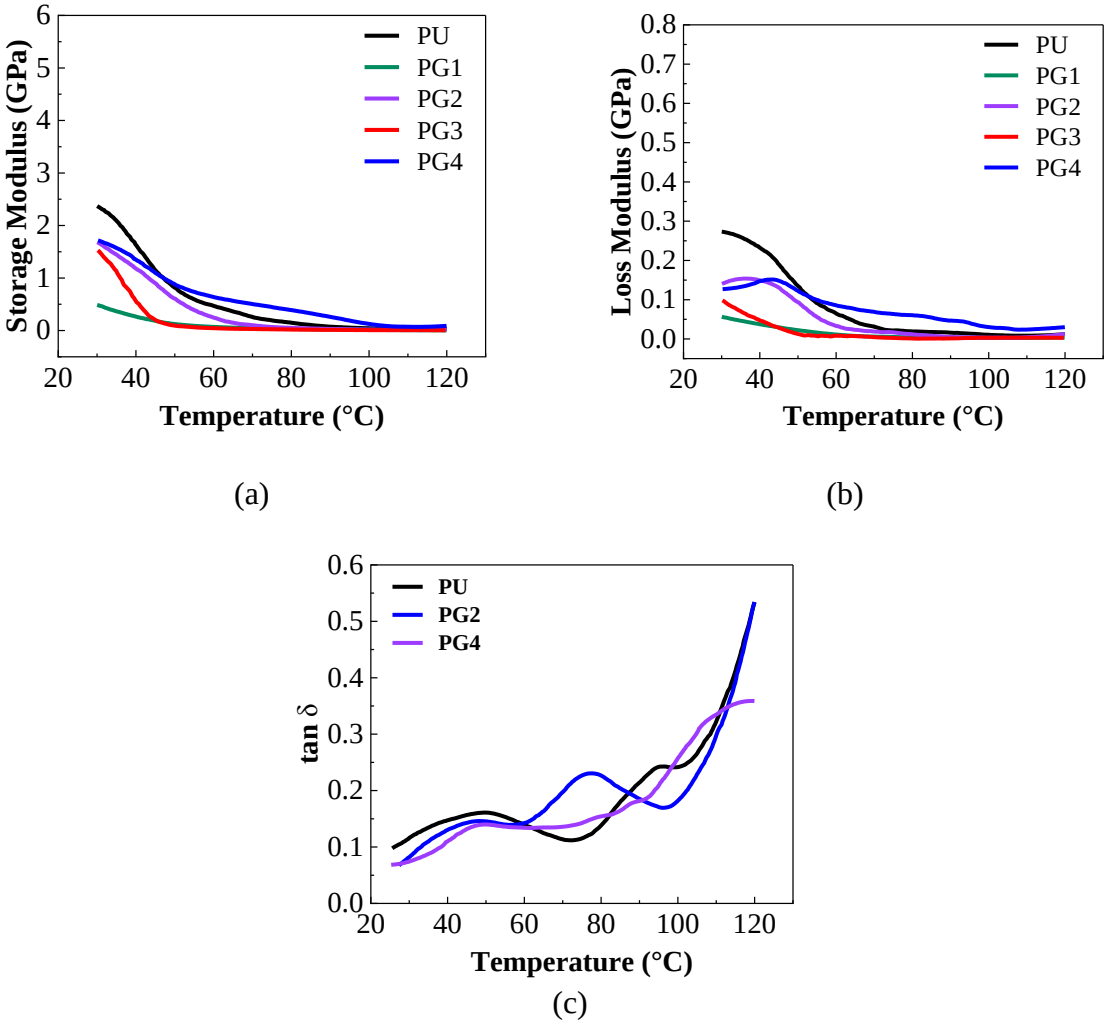

Figure 7.9. DMA results for the PU and PU/GNP films: (a) storage modulus; (b) loss modulus; (c) tan δ.

Table 7.2. DMA analysis data of the PU, PU/IF-WS_2 and PU/GNP films collected at 30°C.

Sample	Storage Modulus (GPa)	Loss Modulus (GPa)	Loss/Storage Ratio
PU	2.370	0.273	0.115
PW3	0.376	0.052	0.138
PW4	1.791	0.170	0.095
PW5	2.008	0.221	0.110
PW6	4.928	0.742	0.151
PW7	2.788	0.612	0.220
PG1	0.484	0.056	0.116
PG2	1.666	0.140	0.084
PG3	1.569	0.098	0.062
PG4	1.722	0.127	0.074

7.3.4. DSC analysis

Figure 7.10 depicts the endothermic behavior of the PU and nanocomposite films from -20°C to 100°C. A high heating rate (30°C /min) was applied to detect the glass transition temperature (T_g) of the films. The DSC curves from the second heating are presented. The figure compares the pure PU film with IF-WS_2 and GNP dispersed films with increasing nanofiller amount. The T_g of soft segments from all cast films is shown between 30 and 50°C, while the T_g from hard segments is not detected using DSC. A decreasing trend in T_g is observed from the IF-WS_2 incorporated PU films with increasing nanoparticle amounts, whereas in the PU/GNP films, no significant changes in T_g are observed with varying nanofiller amounts. This agrees with the results obtained using DMA. The decrease in T_g for PU/ IF-WS_2 films can be related to the changes in free volume (varying mobility) of polymer chains due to the dispersed small particles between PU polymer chains. The particles space the chains apart and act as plasticizers. Meanwhile, the IF-

WS_2 defects and/or impurity in IF-WS_2 suspension may also interfere with the self-crosslinking process of PU increasing polymer chain mobility. The T_g of soft segments for all PU and nanocomposite films are acquired and listed in Table 7.3. It lowers from 41.7°C to 34.1°C (18.2%) by adding up to 118.9% of IF-WS_2. For the PW4 and PW6 films, it decreases to 40.8°C (2.2%) and 37.7°C (9.6%), respectively. Whereas for the PU/GNP films, the T_g difference is not significant to draw any solid conclusions.

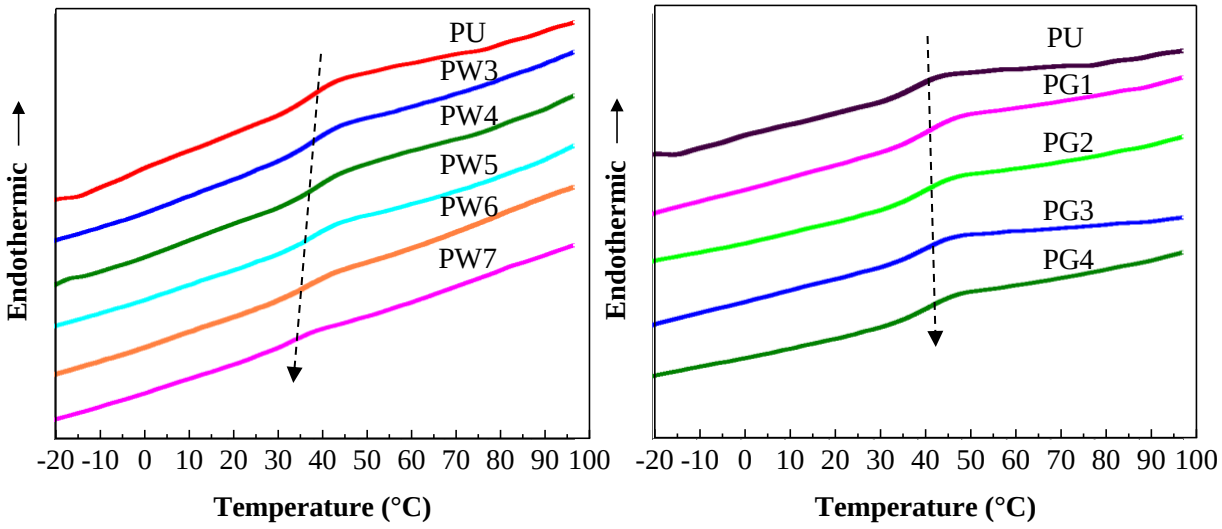

(a) (b)

Figure 7.10. The DSC thermograms of the pure PU and PU nanocomposite films: (a) PU and IF-WS_2 dispersed PU films (PW3-PW7). (b) PU and GNP dispersed PU films (PG1-PW4).

Table 7.3. Glass transition temperatures of the PU and PU nanocomposite films.

Films with IF-WS_2	T_g (°C)	Films with GNPs	T_g (°C)
PU	41.7	PU	41.7
PW3	41.2	PG1	42.7
PW4	40.8	PG2	42.9
PW5	39.9	PG3	42.9
PW6	37.7	PG4	43.2
PW7	34.1		

7.3.5. Surface morphology

Figure 7.11 shows the SEM images of the cast films, where the surface morphologies of PU and nanocomposite films are identified. The pure PU film (PU) formed a smooth, uniform, and flat surface (Figure 7.11 a). With 6.0 wt% of IF-WS_2 used, a small number of IF-WS_2 nanoparticles are observed on the surface of PW3 film. However, nanoscale dense voids/dents were formed on the film surface resulting in a drastic decrease in its surface smoothness, compared to the pure PU film (Figure 7.11 b). With 11.9 wt% of IF-WS_2, the nanocomposite film (PW4) was formed with nanoparticles that were evenly dispersed and embedded in the PU polymer. Film integrity and smoothness are mostly maintained (Figure 7.11 c). Further increasing IF-WS_2 addition leads to more nanoparticles embedded and partially exposed on the surface layers of PW5, PW6, and PW7 films, respectively. These nanoparticles increase the surface roughness and negatively affect the integrity of the films (Figure 7.11 d-f). In the PW6 film, some nanoparticle agglomerates were formed in microscale circles and were evenly distributed. At the highest IF-WS_2 amount, the PW7 film shows the largest surface roughness and exposed nanoparticle amount, as the IF-WS_2 particle becomes the major component of the film rather than PU polymer.

Figure 7.12 presents the SEM images of fabricated PU/GNP nanocomposite films at two magnifications: ×50 and ×5000. In all four films, different numbers of microscale pores with varying sizes were observed, which is the main reason for their low mechanical properties and tensile energy absorption. The PG1 film formed small pores that were evenly distributed with high density, these pores prevent formation of continuous PU matrix, and dramatically lower the strength of the films (Figure 7.12 a). Due to the hydrophobicity of GNP powder and its low compatibility with waterborne PU dispersion, adding GNPs largely affects the formation of PU films and reduces their maximum load and elongation at break. Compared to the PG1 film, pores

with a lower density are found on the PG2 film. However, the average size of the pores is much larger than it is on the PG1 film, which leads to further decrease in mechanical properties (Figure 7.12 b). The PG3 film formed the lowest number of micro pores due to sufficient GNP film contribution, showing the best film formation and highest maximum load among all specimens (Figure 7.12 c). With further increase in GNPs amount, micro pores with the highest density and large size were formed on PG4 due to the overload of GNPs, which leads to reduction in mechanical performance (Figure 7.12 d). Besides, the PU/GNP films show an increasing amount of GNP agglomerates on the film surface with a higher GNP addition (Figure 7.12 e-h). These agglomerates with a higher density and larger sizes negatively affect the mechanical properties of the films to a greater extent. The PG3 film shows GNP agglomerates with a high density but small sizes, which limited their impact on the film performance. Overall, both micro pores and GNP agglomerates on film surfaces influence the mechanical properties and tensile energy absorption capacities of the GNP dispersed PU films.

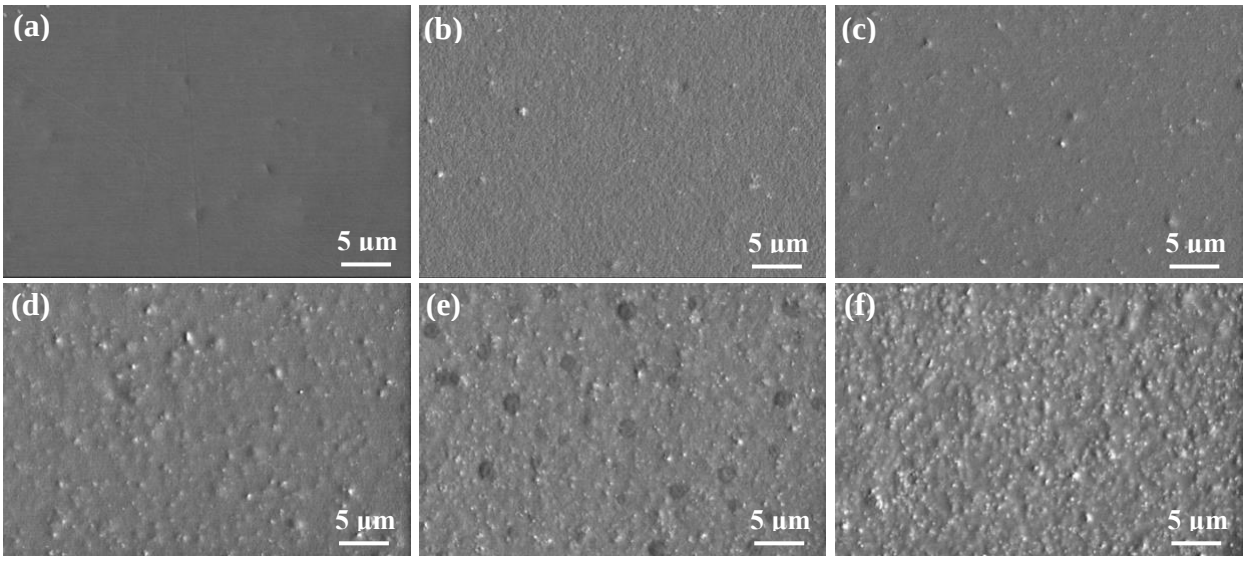

Figure 7.11. SEM images for the fabricated PU and PU/IF-WS_2 films: (a) PU; (b) PW3; (c) PW4; (d) PW5; (e) PW6; (f) PW7.

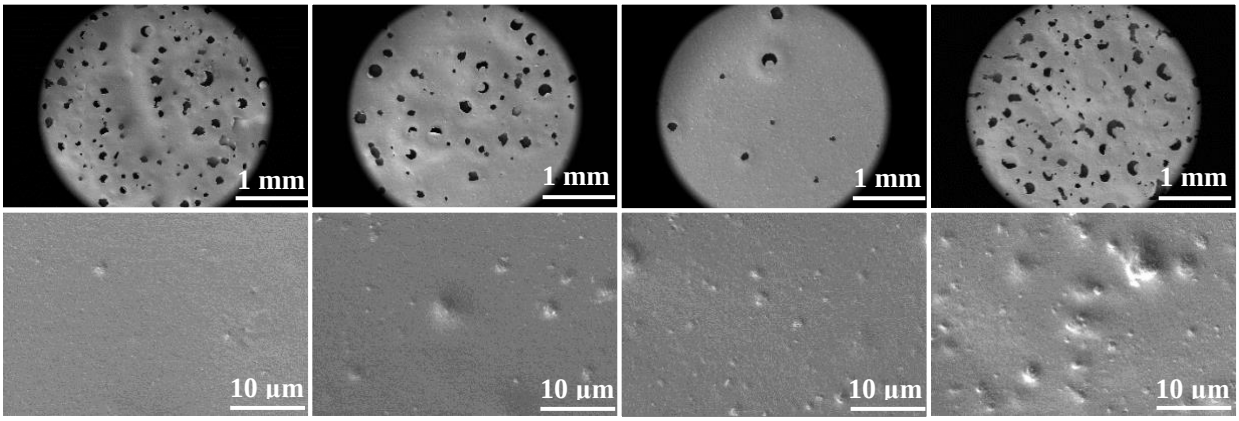

Figure 7.12. SEM images for the fabricated PU/GNP films: (a) PG1, ×50; (b) PG2, ×50; (c) PG3, × 50; (d) PG4, ×50; (e) PG1, ×5000; (f) PG2, ×5000; (g) PG3, × 5000; (h) PG4, ×5000.

7.4. Summary

IF-WS_2 nanoparticles and GNPs dispersed polyurethane thin films were prepared using the casting method. The effects of nanofiller addition on film appearance, mechanical properties, tensile energy absorption, and viscoelastic properties were studied. On the macro-scale, the PU/IF-WS_2 films showed smooth surface and uniform distribution of nanoparticles, whereas PU/GNP films exhibited rough surface with small granules. Adding water-based IF-WS_2 nanoparticles improved the maximum load, total energy absorption, and specific energy absorption of the PU films up to 48.0%, 115.5%, and 48.3%, respectively. The storage modulus, loss modulus, and damping ratio of the PU/IF-WS_2 films increased up to 107.9%, 171.8%, and 90.4% over the PU film, respectively. Incorporating GNP powders negatively impacted the mechanical and viscoelastic properties of the PU films due to the formation of micro pores and GNP agglomerates. The mixed IF-WS_2 nanoparticles and GNPs slightly increased and decreased T_g of the PU films, respectively. The former could be ascribed to the low shear strength and high tribology properties of IF-WS_2, and the latter could be due to the increased friction between PU molecular chains. This study helps understand the effects of incorporating IF-WS_2 and GNP on the mechanical properties,

tensile energy absorption, and viscoelastic properties of PU films and demonstrates the preparation of water-based nanocomposite (PU/IF-WS_2) coatings for high strength and energy absorption applications, especially the complexities due to formation of different morphologies.

7.5. References

[1] Erdodi G, Bird J, Skoff I, Pourahmady N, Materials LA. NOVEL WATER-BORNE [1] Cheng Z, Li Q, Yan Z, Liao G, Zhang B, Yu Y, et al. Design and synthesis of novel aminosiloxane crosslinked linseed oil-based waterborne polyurethane composites and its physicochemical properties. Prog Org Coatings 2019. https://doi.org/10.1016/j.porgcoat.2018.11.020.

[2] Mills DJ, Jamali SS, Paprocka K. Investigation into the effect of nano-silica on the protective properties of polyurethane coatings. Surf Coatings Technol 2012. https://doi.org/10.1016/j.surfcoat.2012.08.056.

[3] Meera KMS, Sankar RM, Jaisankar SN, Mandal AB. Physicochemical studies on polyurethane/siloxane cross-linked films for hydrophobic surfaces by the sol-gel process. J Phys Chem B 2013. https://doi.org/10.1021/jp3097346.

[4] Santamaria-Echart A, Fernandes I, Barreiro F, Corcuera MA, Eceiza A. Advances in waterborne polyurethane and polyurethane-urea dispersions and their eco-friendly derivatives: A review. Polymers (Basel) 2021. https://doi.org/10.3390/polym13030409.

[5] Chen JJ, Zhu CF, Deng HT, Qin ZN, Bai YQ. Preparation and characterization of the waterborne polyurethane modified with nanosilica. J Polym Res 2009. https://doi.org/10.1007/s10965-008-9238-7.

[6] Sardon H, Irusta L, Fernández-Berridi MJ, Lansalot M, Bourgeat-Lami E. Synthesis of room temperature self-curable waterborne hybrid polyurethanes functionalized with (3-aminopropyl)triethoxysilane (APTES). Polymer (Guildf) 2010. https://doi.org/10.1016/j.polymer.2010.08.035.

[7] Yin X, Pang H, Luo Y, Zhang B. Eco-friendly functional two-component flame-retardant waterborne polyurethane coatings: A review. Polym Chem 2021. https://doi.org/10.1039/d1py00920f.

[8] Zhou S, Wu L, Sun J, Shen W. The change of the properties of acrylic-based polyurethane via addition of nano-silica. Prog Org Coatings 2002. https://doi.org/10.1016/S0300-9440(02)00085-1.

[9] Pan H, Chen D. Preparation and characterization of waterborne polyurethane/attapulgite nanocomposites. Eur Polym J 2007. https://doi.org/10.1016/j.eurpolymj.2007.06.031.

[10] Fu C, Hu X, Yang Z, Shen L, Zheng Z. Preparation and properties of waterborne bio-based polyurethane/siloxane cross-linked films by an in situ sol-gel process. Prog Org Coatings 2015. https://doi.org/10.1016/j.porgcoat.2015.02.008.

[11] Seeni Meera KM, Murali Sankar R, Paul J, Jaisankar SN, Mandal AB. The influence of

applied silica nanoparticles on a bio-renewable castor oil based polyurethane nanocomposite and its physicochemical properties. Phys Chem Chem Phys 2014. https://doi.org/10.1039/c4cp00516c.

[12] Abd El-Fattah M, Hasan AMA, Keshawy M, El Saeed AM, Aboelenien OM. Nanocrystalline cellulose as an eco-friendly reinforcing additive to polyurethane coating for augmented anticorrosive behavior. Carbohydr Polym 2018. https://doi.org/10.1016/j.carbpol.2017.12.084.

[13] Kuan HC, Ma CCM, Chang WP, Yuen SM, Wu HH, Lee TM. Synthesis, thermal, mechanical and rheological properties of multiwall carbon nanotube/waterborne polyurethane nanocomposite. Compos Sci Technol 2005. https://doi.org/10.1016/j.compscitech.2005.02.017.

[14] Wu GM, Chen J, Huo SP, Liu GF, Kong ZW. Thermoset nanocomposites from two-component waterborne polyurethanes and cellulose whiskers. Carbohydr Polym 2014. https://doi.org/10.1016/j.carbpol.2014.01.095.

[15] Wu G, Liu D, Chen J, Liu G, Kong Z. Preparation and properties of super hydrophobic films from siloxane-modified two-component waterborne polyurethane and hydrophobic nano SiO2. Prog Org Coatings 2019. https://doi.org/10.1016/j.porgcoat.2018.06.016.

[16] Yin X, Dong C, Chai C, Luo Y. Thermostability and flame retardance of green functional two-component waterborne polyurethane coatings with nanoparticles. Prog Org Coatings 2018. https://doi.org/10.1016/j.porgcoat.2018.01.027.

[17] Zhu YQ, Sekine T, Van Li H, Fay MW, Zhao YM, Poa CHP, et al. Shock-absorbing and failure mechanisms of WS2 and MoS 2 nanoparticles with fullerene-like structures under shock wave pressure. J Am Chem Soc 2005. https://doi.org/10.1021/ja054715j.

[18] Joly-Pottuz L, Martin JM, Dassenoy F, Belin M, Montagnac G, Reynard B, et al. Pressure-induced exfoliation of inorganic fullerene-like WS 2 particles in a Hertzian contact. J Appl Phys 2006. https://doi.org/10.1063/1.2165404.

[19] Haba D, Brunner AJ, Barbezat M, Spetter D, Tremel W, Pinter G. Correlation of epoxy material properties with the toughening effect of fullerene-like WS2 nanoparticles. Eur Polym J 2016. https://doi.org/10.1016/j.eurpolymj.2016.09.022.

[20] Yang H, Liu S, Li J, Li M, Peng G, Zou G. Synthesis of inorganic fullerene-like WS2 nanoparticles and their lubricating performance. Nanotechnology 2006. https://doi.org/10.1088/0957-4484/17/5/058.

[21] Tevet O, Goldbart O, Cohen SR, Rosentsveig R, Popovitz-Biro R, Wagner HD, et al. Nanocompression of individual multilayered polyhedral nanoparticles. Nanotechnology 2010. https://doi.org/10.1088/0957-4484/21/36/365705.

[22] Naffakh M, Díez-Pascual AM, Marco C, Ellis G. Novel polypropylene/inorganic fullerene-like WS2 nanocomposites containing a β-nucleating agent: Mechanical, tribological and rheological properties. Mater Chem Phys 2014. https://doi.org/10.1016/j.matchemphys.2013.12.020.

[23] Díez-Pascual AM, Naffakh M. Mechanical and thermal behaviour of isotactic polypropylene reinforced with inorganic fullerene-like WS2 nanoparticles: Effect of filler loading and temperature. Mater Chem Phys 2013.

https://doi.org/10.1016/j.matchemphys.2013.06.039.

[24] Naffakh M, Martín Z, Fanegas N, Marco C, Gómez MA, Jiménez I. Influence of inorganic fullerene-like WS2 nanoparticles on the thermal behavior of isotactic polypropylene. J Polym Sci Part B Polym Phys 2007. https://doi.org/10.1002/polb.21231.

[25] Kalin M, Zalaznik M, Novak S. Wear and friction behaviour of poly-ether-ether-ketone (PEEK) filled with graphene, WS2 and CNT nanoparticles. Wear 2015. https://doi.org/10.1016/j.wear.2014.12.036.

[26] Golbang A, Harkin-Jones E, Wegrzyn M, Campbell G, Archer E, McIlhagger A. Production and characterization of PEEK/IF-WS2 nanocomposites for additive manufacturing: Simultaneous improvement in processing characteristics and material properties. Addit Manuf 2020. https://doi.org/10.1016/j.addma.2019.100920.

[27] Naffakh M, Díez-Pascual AM, Gómez-Fatou MA. New hybrid nanocomposites containing carbon nanotubes, inorganic fullerene-like WS2 nanoparticles and poly(ether ether ketone) (PEEK). J Mater Chem 2011. https://doi.org/10.1039/c1jm10441a.

[28] Díez-Pascual AM, Naffakh M, Marco C, Ellis G. Rheological and tribological properties of carbon nanotube/thermoplastic nanocomposites incorporating inorganic fullerene-like WS2 nanoparticles. J Phys Chem B 2012. https://doi.org/10.1021/jp3035314.

[29] Simić D, Stojanović DB, Kojović A, Dimić M, Totovski L, Uskoković PS, et al. Inorganic fullerene-like IF-WS2/PVB nanocomposites of improved thermo-mechanical and tribological properties. Mater Chem Phys 2016. https://doi.org/10.1016/j.matchemphys.2016.09.060.

[30] Sethulekshmi AS, Jayan JS, Saritha A, Joseph K. Insights into the reinforcibility and multifarious role of WS2 in polymer matrix. J Alloys Compd 2021. https://doi.org/10.1016/j.jallcom.2021.160107.

[31] Haba D, Brunner AJ, Pinter G. Dispersion of fullerene-like WS2 nanoparticles within epoxy and the resulting fracture mechanics. Compos Sci Technol 2015. https://doi.org/10.1016/j.compscitech.2015.09.013.

[32] Mojtabaei A, Otadi M, Goodarzi V, Khonakdar HA, Jafari SH, Reuter U, et al. Influence of fullerene-like tungsten disulfide (IF-WS2) nanoparticles on thermal and dynamic mechanical properties of PP/EVA blends: Correlation with microstructure. Compos Part B Eng 2017. https://doi.org/10.1016/j.compositesb.2016.12.006.

[33] Naffakh M, Marco C, Gómez MA, Gómez-Herrero J, Jiménez I. Use of inorganic fullerene-like WS2 to produce new high-performance polyphenylene sulfide nanocomposites: Role of the nanoparticle concentration. J Phys Chem B 2009. https://doi.org/10.1021/jp902700x.

[34] Guo D, Cai K, Deng P, Si G, Sun L, Chen F, et al. Structure tailorable triple-phase and pure double-polar-phase flexible IF-WS2@poly(vinylidene fluoride) nanocomposites with enhanced electrical and mechanical properties. J Mater 2020. https://doi.org/10.1016/j.jmat.2020.04.004.

[35] Phiri J, Gane P, Maloney TC. General overview of graphene: Production, properties and application in polymer composites. Mater Sci Eng B Solid-State Mater Adv Technol 2017. https://doi.org/10.1016/j.mseb.2016.10.004.

[36] Papageorgiou DG, Kinloch IA, Young RJ. Mechanical properties of graphene and

graphene-based nanocomposites. Prog Mater Sci 2017. https://doi.org/10.1016/j.pmatsci.2017.07.004.

[37] Amri MR, Yasin FM, Abdullah LC, Al-Edrus SSO, Mohamad SF. Ternary nanocomposite system composing of graphene nanoplatelet, cellulose nanofiber and jatropha oil based waterborne polyurethane: Characterizations, mechanical, thermal properties and conductivity. Polymers (Basel) 2021. https://doi.org/10.3390/polym13213740.

[38] Quan H, Zhang B qing, Zhao Q, Yuen RKK, Li RKY. Facile preparation and thermal degradation studies of graphite nanoplatelets (GNPs) filled thermoplastic polyurethane (TPU) nanocomposites. Compos Part A Appl Sci Manuf 2009. https://doi.org/10.1016/j.compositesa.2009.06.012.

[39] Navidfar A, Trabzon L. Graphene type dependence of carbon nanotubes/graphene nanoplatelets polyurethane hybrid nanocomposites: Micromechanical modeling and mechanical properties. Compos Part B Eng 2019. https://doi.org/10.1016/j.compositesb.2019.107337.

[40] Wu X, Wang Y, Wang H, Zheng B, Wu Y, Xue R, et al. Semi-quantitative orientation control of graphite nanoplatelets in GNP/PU nanocomposite via balancing the effects of gravity and micro-flow field and application in manufacturing heat spreader substrate with excellent thermal conductivity. Compos Part A Appl Sci Manuf 2021. https://doi.org/10.1016/j.compositesa.2021.106657.

[41] Erdodi G, Bird J, Skoff I, Pourahmady N, Materials LA. NOVEL WATER-BORNE URETHANE / UREA COPOLYMERS MADE FROM TELECHELIC POLYAMIDE OLIGOMERS n.d.

[42] Xu F, Kobayashi T, Yang Z, Sekine T, Chang H, Wang N, et al. How the Toughest Inorganic Fullerene Cages Absorb Shockwave Pressures in a Protective Nanocomposite: Experimental Evidence from Two in Situ Investigations. ACS Nano 2017. https://doi.org/10.1021/acsnano.7b02943.

[43] McKeen LW. Film Properties of Plastics and Elastomers: Fourth Edition. 2017.

[44] Wu G min, Liu G feng, Chen J, Kong Z wu. Preparation and properties of thermoset composite films from two-component waterborne polyurethane with low loading level nanofibrillated cellulose. Prog Org Coatings 2017. https://doi.org/10.1016/j.porgcoat.2016.10.031.

CHAPTER 8

Conclusions and Recommendations

8.1. Overall Summary

In this study, PU/IF-WS_2 reinforced UHMWPE filament yarns and fabrics were developed with significantly enhanced mechanical properties and viscoelastic performances for potential ballistic and high-performance applications.

Individual UHMWPE filament yarn coating was conducted with thermoplastic PU and IF-WS_2 nanoparticles (chapter three). The effect of dispersing medium including water, water/ethanol mixture, and ethanol on the nanoparticle stability was studied. Varying PU and IF-WS_2 amounts were applied for the yarn coating using different mediums. Also investigated were the mechanical properties, distribution of PU and IF-WS_2 nanoparticles, and failure mechanisms of the neat and coated yarns. The results indicate IF-WS_2 nanoparticles show uniform distribution and good stability for all three medium systems up to one day. The order of stability in the mediums is ethanol>water/ethanol>water. However, waterborne PU has poor solubility in pure ethanol making pure ethanol unsuitable for further use. Adding ethanol negatively affects distribution uniformity of the PU and IF-WS_2 on fiber surface. Comparable mechanical properties are obtained for the optimal PU/IF-WS_2/UHMWPE composite yarns prepared in three mediums. Incorporating PU/IF-WS_2 on UHMWPE fibers leads to changes in failure mechanisms including matrix failure, fiber/matrix debonding, and fiber ductile breakage as reported in the literature [1][2].

The effects of plasma pre-treatment and PU/IF-WS_2 continuous coating on mechanical and viscoelastic performances of UHMWPE yarns (chapter four) and fabrics (chapter five) were investigated. A lab-scale coating line was set up for continuous yarn coating with high efficiency. Neat and plasma pretreated yarns and fabrics were coated with PU/IF-WS_2 dispersions at various compositions. The results showed the maximum load, energy to break, and toughness the SA3 nanocomposite yarn (coating condition: plasma pre-treated, 15% PU, 6% IF-WS_2, water medium) with an improvement by 33.3%, 50.9%, and 31.6%, respectively over neat yarns. Plasma treatment induces oxygen-containing groups (-OH, C=O, C-O) on fiber surface and improves the energy-to-break, toughness, and coating weight retention after washing. Thermoset PUA leads to better wash durability for the composite yarns than thermoplastic PUB. The weight retention of plasma treated and PU/IF-WS_2 coated UHMWPE yarns can reach to 92%. After plasma treatment, fabric samples show increase in wettability based on the decrease in water contact angle. The combined effects of plasma treatment and PU/IF-WS_2 coating contributes to maximum increases in the storage modulus, loss modulus, elongation at break, and gravimetric toughness, 694%, 757%, 137%, and 73%, respectively, for the UHMWPE fabrics. Meanwhile, good wash durability (weight retention after washing up to 98.8%) is obtained for the fabricated composites.

Moreover, factorial designs were applied to systematically study the effects of fabrication parameter on the PU/IF-WS_2/UHMWPE yarns (chapter six). Studied factors include thermoset PU amount, IF-WS_2 amount, dispersing medium, stabilizer amount, curing temperature, and curing time. In addition, the effect of GNPs amount was also studied and compared with IF-WS_2. Toughness and weight retention were used as the response variables. A higher PU amount or curing temperature leads to lower toughness (J/g) due to the large weight addition or heat damage, respectively. It increases the wash durability due to higher integrity of PU films or tougher films

are formed. Adding stabilizer improves nanoparticles distribution uniformity contributing to increase in composite toughness. Increasing IF-WS_2 amount first increases and then decreases the toughness, but slightly decreases sample wash durability due to its negative impact on film formation [3]. The optimized fabrication condition is 1 wt% solid IF-WS_2, 10 wt% PU, 5 wt% stabilizer, and 120℃ for curing, at which, high weight retention after wash (94.1%) and improvements in maximum load (31.9%), tensile energy absorption (66.7%), and toughness (43.3%) are achieved for the yarns. However, GNPs did not show significant effect on the outcomes, although the sample with 2.9% GNPs showed 30.5%, 63.1%, and 49.6% higher maximum load, energy absorption, and toughness, respectively, over neat yarns.

PU/IF-WS_2 and PU/GNP thin films were prepared to study the mechanisms of the nanofillers on the polymer matrix (chapter seven). The effects of different levels of IF-WS_2 and GNP amount on mechanical properties, viscoelastic performances, thermal transition, appearance, and surface morphologies of PU films were studied. IF-WS_2 show homogeneous distribution on the PU film and has limited impact on the film formation due to its water-based form. Smooth and flat PU/IF-WS_2 films are formed under most of the conditions. Increasing IF-WS_2 amount first decreases, then increases, and then decreases the mechanical and viscoelastic properties. This trend is consistent with the effect of IF-WS_2 on individually coated yarns. The observed trend can be explained by the nanoparticle effect on film formation and the balance between IF-WS_2 reinforcement and PU film integrity. IF-WS_2 addition improves the maximum load, energy absorption, specific energy absorption, storage modulus, loss modulus, and damping ratio of the films. High IF-WS_2 addition leads to stiff but brittle films while low IF-WS_2 addition results in composite films with high mechanical properties but lower stiffness. Adding IF-WS_2 decreases T_g of the PU films due to possible free volume changes and defects/impurities. Incorporating GNPs

however lowers mechanical performance and viscoelasticity of the films due to their significant effect on PU film formation. In macroscale, GNPs dispersed PU films show rough surface with dense granules. In microscale, small pores and GNPs agglomerates are formed on the films due to the superior hydrophobicity of the GNP and its low compatibility with waterborne PU.

This study provides a clear insight into the mechanisms of the nanoparticle effects and some important factors for preparing nanocomposite coating including matrix formation, nanoparticle distribution uniformity, and matrix/filler compatibility. Importance of surface modification of nonwetting fibers was clearly demonstrated to achieve improvement in property enhancement as well as durability of the coatings.

8.2. Recommendations for Future Work

The fundamental mechanical properties and reinforcing mechanisms of the nanocomposite coated UHMWPE filament yarns and fabrics were studied in this work. The developed yarn and fabric composites show promising properties and a good potential for ballistic and high-performance end uses, such as lightweight soft armors. However, additional aspects of the work can be investigated in future research.

- UHMWPE coated filament yarns can be woven into fabrics, the mechanical and ballistic performances can be evaluated. Both yarn coating and fabric coating approaches can be compared based on the impact resistance and impact energy absorption capacity of the fabric composites
- Optimization of the nanocomposite coating on UHMWPE fabrics can be conducted using both dip and spray coating methods based on mechanical properties including tensile

strength, elongation, and modulus. The optimized condition can be applied on plasma treated fabrics and further evaluation can be conducted using ballistic tests

- To evaluate ballistic performance of developed fabric composites, actual ballistic testing needs to be conducted. Multi-layered (8-10 layers) flexible composite panels can be prepared with sewed edges, and high-velocity ballistic tests can be conducted on composite panels. The initial velocity and residual velocity of the impact bullet after penetration can be captured using a high-speed camera and used to calculate energy absorbed by composite materials. Other ballistic performances such as ballistic limit (V50) and back face signature (non-penetrating) can also be included depending on facility and material availability. Bullet and sample deformation can be qualitatively compared and analyzed to understand the failure mechanisms.

8.3. References

[1] Cui J, Wang S, Wang S, Li G, Wang P, Liang C. The effects of strain rates on mechanical properties and failure behavior of long glass fiber reinforced thermoplastic composites. Polymers (Basel) 2019. https://doi.org/10.3390/polym11122019.

[2] Yang L, Yan Y, Liu Y, Ran Z. Microscopic failure mechanisms of fiber-reinforced polymer composites under transverse tension and compression. Compos Sci Technol 2012. https://doi.org/10.1016/j.compscitech.2012.08.001.

[3] Mohammadalipour M, Masoomi M, Ahmadi M, Kazemi Z. The effect of simultaneous fiber surface treatment and matrix modification on mechanical properties of unidirectional ultra-high molecular weight polyethylene fiber/epoxy/nanoclay nanocomposites. J Compos Mater 2018. https://doi.org/10.1177/0021998318755542.